INFORMATION TO USERS

This manuscript has been reproduced from the microfilm master. UMI films the text directly from the original or copy submitted. Thus, some thesis and dissertation copies are in typewriter face, while others may be from any type of computer printer.

The quality of this reproduction is dependent upon the quality of the copy submitted. Broken or indistinct print, colored or poor quality illustrations and photographs, print bleedthrough, substandard margins, and improper alignment can adversely affect reproduction.

In the unlikely event that the author did not send UMI a complete manuscript and there are missing pages, these will be noted. Also, if unauthorized copyright material had to be removed, a note will indicate the deletion.

Oversize materials (e.g., maps, drawings, charts) are reproduced by sectioning the original, beginning at the upper left-hand corner and continuing from left to right in equal sections with small overlaps. Each original is also photographed in one exposure and is included in reduced form at the back of the book.

Photographs included in the original manuscript have been reproduced xerographically in this copy. Higher quality 6" x 9" black and white photographic prints are available for any photographs or illustrations appearing in this copy for an additional charge. Contact UMI directly to order.

UMI

A Bell & Howell Information Company
300 North Zeeb Road, Ann Arbor MI 48106-1346 USA
313/761-4700 800/521-0600

ELASTIC PLASTIC ANALYSIS

OF SEMI-RIGID INDUSTRIAL FRAMES

BY

Mahmoud Hassan El-Boghdadi

A Dissertation Presented to the

FACULTY OF THE COLLEGE OF GRADUATE STUDIES

KING FAHD UNIVERSITY OF PETROLEUM & MINERALS

DHAHRAN, SAUDI ARABIA

In Partial Fulfillment of the
Requirements for the Degree of

DOCTOR OF PHILOSOPHY

In

CIVIL ENGINEERING

June, 1998

KING FAHD UNIVERSITY OF PETROLEUM & MINERALS
DHAHRAN 31261, SAUDI ARABIA

COLLEGE OF GRADUATE STUDIES

This dissertation, written by **Mahmoud Hassan El-Boghdadi** under the direction of his Dissertation Advisor and approved by his Dissertation Committee, has been presented to and accepted by the Dean of the College of Graduate Studies, in partial fulfillment of the requirements for the degree of **DOCTOR OF PHILOSOPHY in CIVIL ENGINEERING (Structures)**

Dissertation Committee

Dr. Abul Kalam Azad (Chairman)

Dr. Al-Farabi M. Sharif (Co-Chairman)

Dr. Mohammed. H. Baluch (Member)

Dr. Ali H. Al-Gadhib (Member)

Dr. Saeid A. Al-Ghamdi (Member)

Anwar Khalil Sheikh
Dr. Anwar K. Sheikh (Member)

Dr. Sahl N. Abduljauwad
Department Chairman

Dr. Abdullah M. Al-Shehri
Dean, College of Graduate Studies

11/19/98
Date: June 1998

بسم الله الرحمن الرحيم

This dissertation is dedicated

to

my mother, father, brother and sister

my wife, daughter and son

ACKNOWLEDGMENT

Firstly, I thank ALLAH, All Praise is for Him, for bestowing me with the strength and health to complete this work.

Acknowledgment is due to King Fahd University of Petroleum and Minerals for the opportunity given to me to pursue graduate study.

I would like to offer my indebtedness and sincere appreciation to my advisor and committee chairman Dr. A. K. Azad, who has been a constant source of help and encouragement during my thesis work. I greatly appreciate the invaluable suggestions and co-operation extended by Dr. Al-Farabi S. who served as a co-chairman of my dissertation committee. I acknowledge, with deep gratitude and appreciation the guidance given to me by Dr. M. H. Baluch. I am also indebted to Dr. A. H. Al-Ghadib for his help. Special thanks are also due to Dr. S. A. Al-Ghamdi for his effort in reviewing the dissertation, helpful remarks and constructive comments. I am also grateful to Dr. A. K. Sheikh for his valuable comments.

I am grateful to the chairman, Civil Engineering Department, Dr. S. N. Abduljauwad and the graduate advisor Dr. H. N. Al-Ghamdi for providing every facility and help throughout this research.

Thanks also are due to Al-Zamil Steel Company for its generous help in providing and fabricating the material required for the experimental work.

I would like to express my thanks to the extensive computer facilities provided by the Information and Technology Center at KFUPM. Thanks are also due to all the technical personnel in the research laboratories who assisted greatly in the experimental part of the research.

I owe my parents, wife, daughter and son an expression of gratitude for their prayers, sacrifices, patience, support, understanding and encouragement which make this work possible.

Lastly, but not the least, I am thankful to all faculty, colleagues and friends who made my study at the university a memorable and valuable experience.

TABLE OF CONTENTS

LIST OF TABLES

LIST OF FIGURES

DISSERTATION ABSTRACT

NAME OF STUDENT : MAHMOUD HASSAN EL-BOGHDADI

TITLE OF STUDY : ELASTIC PLASTIC ANALYSIS OF SEMI-RIGID INDUSTRIAL FRAMES

MAJOR FIELD : CIVIL ENGINEERING

DATE OF DEGREE : JUNE 1998

The behavior of steel frames is highly influenced by the beam-column connections. In analysis and design, they are idealized as either rigid or pinned for simplicity and between these two extremities lie the actual behavior of steel frames connections which is semi-rigid. This classification is characterized by the nonlinear moment-rotation relationship which must be incorporated in the analysis. Cap-plate connection is widely used in industrial steel frames for its advantages over other types of building connections, but the response of such connection has not been theoretically and experimentally determined.

In this research, the behavior of cap-plate connections was studied by testing six different connections to obtain data for moment-rotation curves of such connections, to measure the forces in the tension bolts, and to measure the strain distribution at different cross-section along the beam at the connection. A computer program was developed for a refined analysis of industrial steel frames taking into consideration the nonlinearities resulting from the connection flexibility and second-order effects. A mathematical model for the connection moment-rotation curve is also proposed using the finite element method and the yield line method. A good agreement was found by comparing the proposed model results to the experimental results.

DOCTOR OF PHILOSOPHY DEGREE

KING FAHD UNIVERSITY OF PETROLEUM AND MINERALS

Dhahran, Saudi Arabia

JUNE 1998

خلاصة الرسالة

اسم الطالب : محمود حسن البغدادى

عنوان الدراسة : التحليل المرن اللدن للإطارات الصناعية الشبه جاسئة

التخصص : الهندسة المدنية

تاريخ الشهادة : يونيو ١٩٩٨

يتأثر سلوك الإطارات المعدنية بصورة واضحة بوصلة الكمرة مع العمود، و تصنف هذه الوصلة في التحليل و التصميم الإنشائي على أنها جاسئة أو مفصلية نظرا لسهولة هذا التصنيف، بينما يقع السلوك الفعلي لوصلات الإطارات المعدنية بين هذين الحدين و هو السلوك شبه الجاسئ الذي يتميز بالعلاقة الغير خطية لمنحنى العزم مع الدوران الواجب أخذها في الاعتبار عند القيام بالتحليل و التصميم الإنشائي، و تستخدم وصلة لوح قمة العمود بكثرة في الإطارات المعدنية الصناعية نظرا لأفضليتها عن وصلات المباني الأخرى، و قد اتضح من مراجعة الكتابات السابقة أن هذه الوصلة لم يتم دراستها نظريا و معمليا في السابق.

لذلك تمت دراسة سلوك وصلات ألواح قمة العمود عن طريق الاختبار المعملي لعدد ست وصلات مختلفة للحصول على بيانات منحنيات العزم مع الدوران لهذه الوصلات و قياس مقدار القوة في مسامير الشد لهذه الوصلة بالإضافة إلى قياس توزيع الانفعالات على مقاطع مختلفة للكمرة بطول الوصلة مع العمود. و تم إنشاء برنامج حاسب آلي لتحليل الإطارات المعدنية الصناعية مع الأخذ في الاعتبار التصرف الغير خطى الناتج عن مرونة الوصلة و التأثيرات الثانوية للقوى المحورية في أعضاء الإطار الإنشائي. و كذلك تم إنشاء نموذج رياضي لمنحنى العزم مع الدوران الخاص بالوصلة باستخدام طريقة العناصر المحددة و طريقة خط الخضوع. و قد وجد اتفاق جيد بمقارنة نتائج النموذج الرياضي المقترح مع النتائج العملية.

درجة الدكتوراه في الفلسفة

جامعة الملك فهد للبترول و المعادن

الظهران ، المملكة العربية السعودية

يونيو ١٩٩٨

CHAPTER 1

INTRODUCTION

1.1 GENERAL

In the design process of steel structures, the design of the main structural members (beams, columns and beam-columns) must take into account the end connections of these members. As the actual behavior of a member is dictated by the connection, the design of the connection must be made in accordance with the assumptions made in design. Most of structural failures show that connections are the origin rather than members of such failures. Therefore, the designer must consider the behavior of connection in both analysis and design.

In analysis and design of steel frames, connections are idealized as either rigid or pinned for simplicity. Between these two extremities lies the actual behavior of steel frame connections which is ***semi-rigid*** as concluded from experimental tests. To achieve this aim of using semi-rigid connection in analysis and design, a better understanding of the connection behavior and its effect on the whole structure from strength and stability points of view must be considered. A good classification,

labeling and modeling for different connection types is essential to help the designer in studying the performance of the structure as a whole.

The influence of end conditions on the bending moment distribution for a uniformly loaded beam is shown in Fig. 1.1. The mid span deflection, end rotations and moments are listed in Table 1.1 for comparison. Essentially all steel connections can be classified as semi-rigid. This classification is characterized by the moment-rotation relationship, where the rotation is defined as the relative angular change of the centerlines of the connected members as shown in Fig. 1.2.

The advantage of a design utilizing semi-rigid connection is that beam-moments are reduced leading to lighter beams in many cases [1] as shown in Fig. 1.1. Another possible source of economy lies in the columns where a better understanding of actual restraint conditions and end moments may well lead to more rationally based, less conservative methods of design [2]. But it must be noted that semi-rigid connections are not suited for every type of building since the structural stability is the main problem with steel frames. Thus, a proper consideration of the second-order effects in analysis is necessary to predict the actual behavior of frames. Also, from the design point of view, the use of limit state design is the best technique to use due to the high non-linearity of the system. However, the analysis of a frame with semi-rigid connections is difficult to perform unless the exact moment-rotation relation of such joints is known.

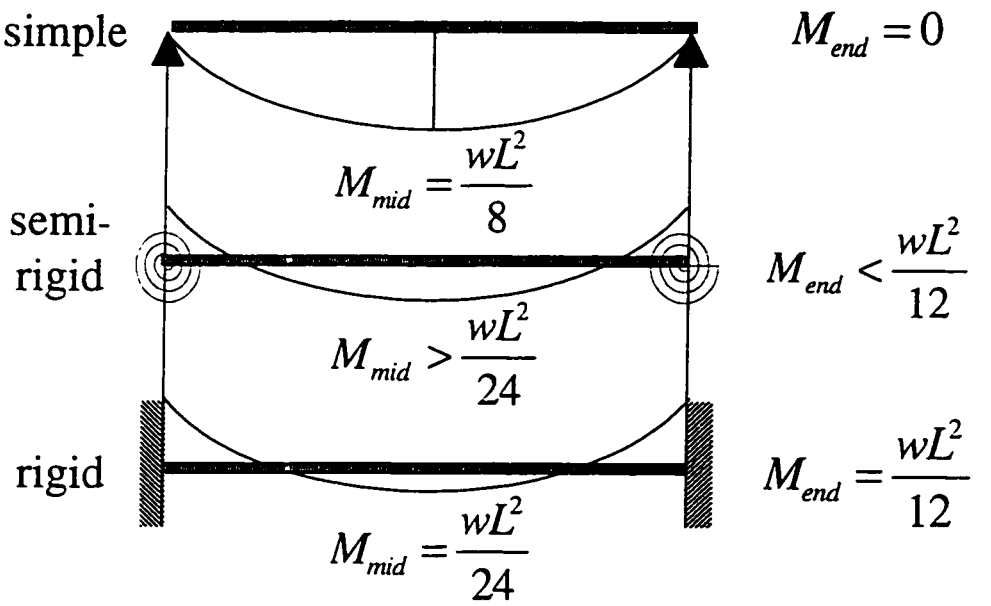

Figure 1.1 Pinned, Semi-Rigid and Rigid Connections

TABLE 1.1 Pinned, Semi-Rigid and Rigid Connections

Support Type	End-Support Moment	Mid-Span Moment	End-Support Rotation	Mid-Span Deflection
Simple	$M_{end} = 0$	$M_{mid} = \frac{wL^2}{8}$	$\theta = \frac{wL^3}{24EI}$	$\delta = \frac{5wL^4}{384EI}$
Semi-Rigid	$0 < M_{end} < \frac{wL^2}{12}$	$\frac{wL^2}{24} < M_{mid} < \frac{wL^2}{8}$	$0 < \theta < \frac{wL^3}{24EI}$	$\frac{wL^4}{384EI} < \delta < \frac{5wL^4}{384EI}$
Rigid	$M_{end} = \frac{wL^2}{12}$	$M_{mid} = \frac{wL^2}{24}$	$\theta = 0$	$\delta = \frac{wL^4}{384EI}$

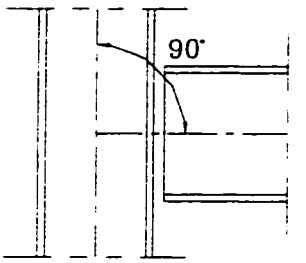

(a) Unloaded beam–column connection

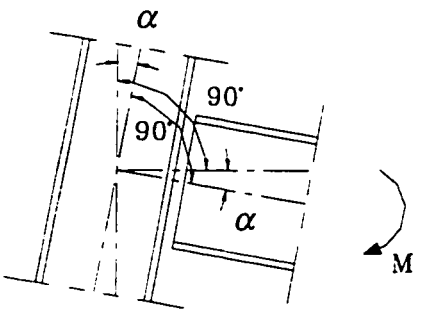

(b) Loaded rigid connection

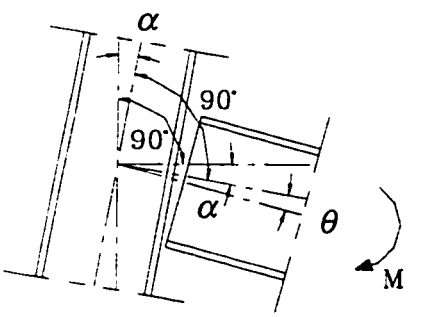

(c) Loaded semi–rigid connection

Figure 1.2 Rigid Versus Semi-Rigid Connections

Of various types of beam-column connections used in industrial frames, single or multiple bays, the cap plate connection shown in Fig. 1.3 is frequently used. It has two main advantages over the header plate connection shown in Fig. 1.4. Firstly, from the practical point of view, cap plate connection is easier for erection, as the beam rests directly on the column head. Secondly, no vertical shear from dead load and live load is transferred by bolts.

The nature of this connection in which only the bottom flange of beam is connected to the column invariably introduces greater flexibility at the joint than the conventional moment connection in which beam is connected to the side of the column. Also, because of the discontinuity at the beam-column joint, this type of connection is a typical case of a semi-rigid connection which allows appreciable amount of rotation even at the service load level.

Almost all of the experimental investigations available in literature have been conducted using the header plate connections as well as traditional building connections. No test data has been reported in the literature for the cap plate type connection. Thus the experimental data provided in this work would serve as the newly added information for the behavior of cap plate type semi-rigid connections commonly employed in industrial steel buildings.

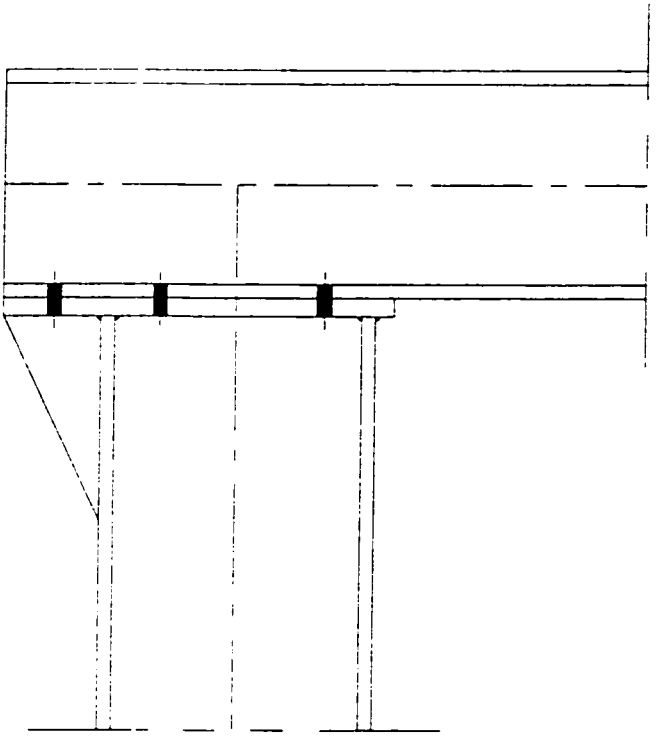

Figure 1.3 Cap Plate Connection

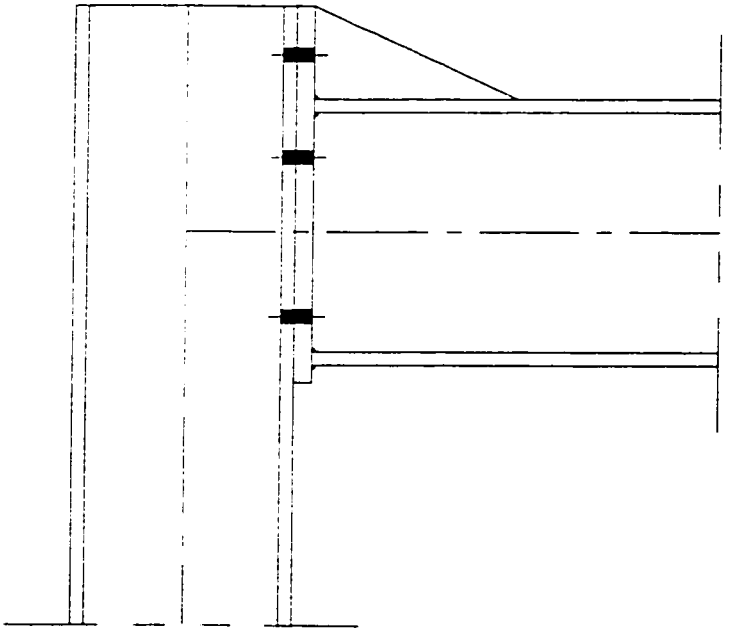

Figure 1.4 Header Plate Connection

1.2 OBJECTIVES OF THE RESEARCH

The main objective of this research is to study the actual behavior of cap plate connections, which are widely used in industrial steel frames and to incorporate the effect of the joint behavior in the analysis and design of such frames. In this respect, it is necessary to undertake a series of experiments using cap plate type connections to obtain a realistic moment-rotation response.

The primary objectives of this study are:

1. To test several connections with different beam sizes (moment capacity), different plate thickness and different bolt diameters to obtain data for moment-rotation curves for such type of connection. These experiments will provide an insight into the behavior of such connections, the failure mode, bolt forces and the stress distribution in the beam.

2. To develop a moment-rotation model for this type of connection using the experimental data obtained from this study.

3. To develop a computer program for a refined analysis of industrial steel frames taking into consideration the effect of connection flexibility, the effect of axial deformation and the P-delta effect.

4. To conclude with some recommendations for design of this type of connection.

1.3 SCOPE OF WORK

The behavior of industrial frames is highly influenced by the beam-column connection. Some of the end connections used are truly semi-rigid. The analysis of such frames, whether elastic or inelastic, can only be performed with accuracy, if the joint behavior is incorporated in the analysis.

At the beginning, a literature review is presented to show the available tests conducted on different types of connection, followed by the available models in the literature that capture the nonlinear response of the connections. Various techniques used in monitoring the connection behavior during the tests are also highlighted.

A computer program is developed to analyze industrial steel frames taking into account the nonlinearity of the connection as well as secondary effects of axial deformations and second-order (P-Delta) effect.

For the experimental program, a test setup is designed, fabricated and installed in a reaction floor lab to conduct full scale tests on cap plate connections. Six separate cap plate connections tests were undertaken using different beam sizes, plate thicknesses and bolt diameters. From these tests, the moment-rotation curves are plotted, the tensile force in bolts are determined and the beam strain distribution at different cross-sections are measured at the connection location.

Based on the test results, an applicable mathematical form of the moment-rotation relationship has been developed for such joints. A comparison of the proposed model results to the experimental results is also given.

CHAPTER 2

LITERATURE REVIEW

2.1 GENERAL

In this chapter, the classification of steel structure connections in accordance with the American and the European design codes is first introduced, followed by different types of steel connections which had been tested previously with their main characteristics. Based on experimental results, the models developed in the past to represent the connection behavior are listed. Measuring techniques used to monitor the connection rotation during tests are also given with the main connection data bases. Methods to analyze semi-rigid frames are finally introduced at the end of the chapter.

2.2 CLASSIFICATION OF CONNECTIONS

2.2.1 American Specification

One of the most widely used design rules are those of the American Institute of Steel Construction (AISC) [3, 4]. Steel construction is classified into various types depending on the amount of restraint developed by the connections.

In the Allowable Stress Design Specification (ASD) [3], the types of construction are divided into three basic categories:

- ***Type 1***, commonly designated as "rigid frame" (continuous frame), assumes that beam-to-column connections have sufficient rigidity to hold virtually unchanged the original angles between intersecting members.

- ***Type 2***, commonly designated as "simple framing" (unrestrained, free-ended), assumes that, insofar as gravity loading is concerned, ends of beams and girders are connected for shear only and are free to rotate under gravity load.

- ***Type 3***, commonly designated as "semi-rigid framing" (partially restrained), assumes that the connections of beams and girders possess a dependable and known moment capacity intermediate in degree between the rigidity of Type 1 and the flexibility of Type 2.

In the Load and Resistance Factor Design Specification (LRFD) [4], only two categories define the types of construction:

- ***Type FR*** (fully-restrained), commonly designated as "rigid-frame" (continuous frame), assumes that beam-to-column connections have sufficient rigidity to hold the original angles between intersecting members virtually unchanged.

- ***Type PR*** (partially-restrained) assumes that the connections of beams and girders possess an insufficient rigidity between the intersecting members.

Figure 2.1 shows a diagram of the beam-line equation as well as the moment rotation behavior of typical connections of ASD Types 1, 2 and 3; and LRFD Types FR and PR [5]. The typical rigid connection (Type 1) would have to carry an end moment about 90% or more of M, where M is the fixed end moment of a uniformly loaded beam. The simple connection (Type 2) may have to resist only 20% or less of M, while the semi-rigid connection (Type 3) would be expected to resist some intermediate value at about 50% of the fixed end moment M.

2.2.1 European Specification

In the European Code for steel structures Eurocode 3 (1992), joints are classified either by their rigidity or strength [6]. A typical $M-\theta$ curve of a beam-column joint is shown in Fig. 2.2, where $M_{j.R}$ is the moment resistance of the joint, R_i is its initial rotational stiffness and θ_c is its rotational capacity. When the classification is by rigidity, the classification boundaries are determined by the joint initial rotational stiffness R_i as follows:

For braced frames:

- Connection is rigid if $R_i \geq \dfrac{8EI_b}{L_b}$
- Connection is semi-rigid if $\dfrac{0.5EI_b}{L_b} < R_i < \dfrac{8EI_b}{L_b}$

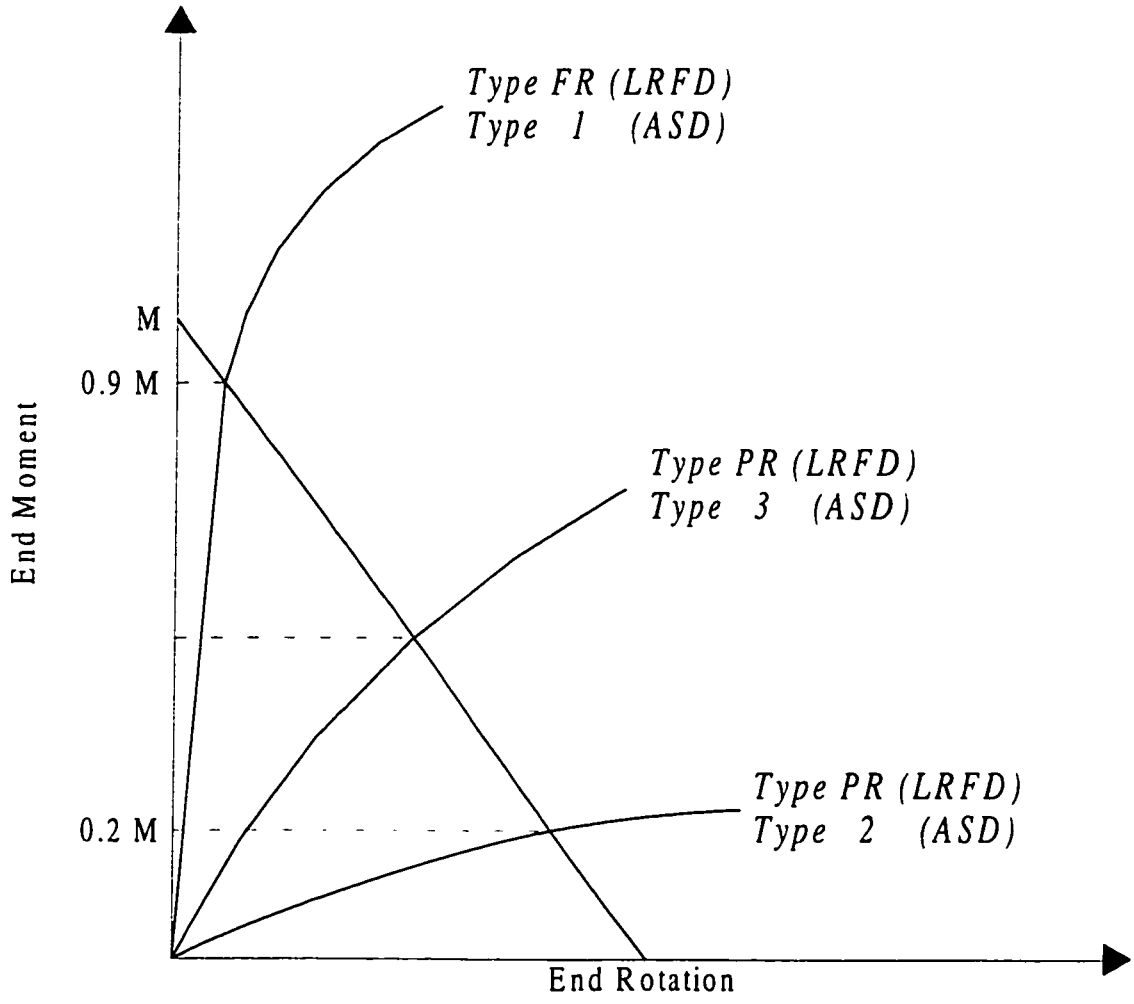

Figure 2.1 Moment-Rotation Characteristics of AISC Connection Types

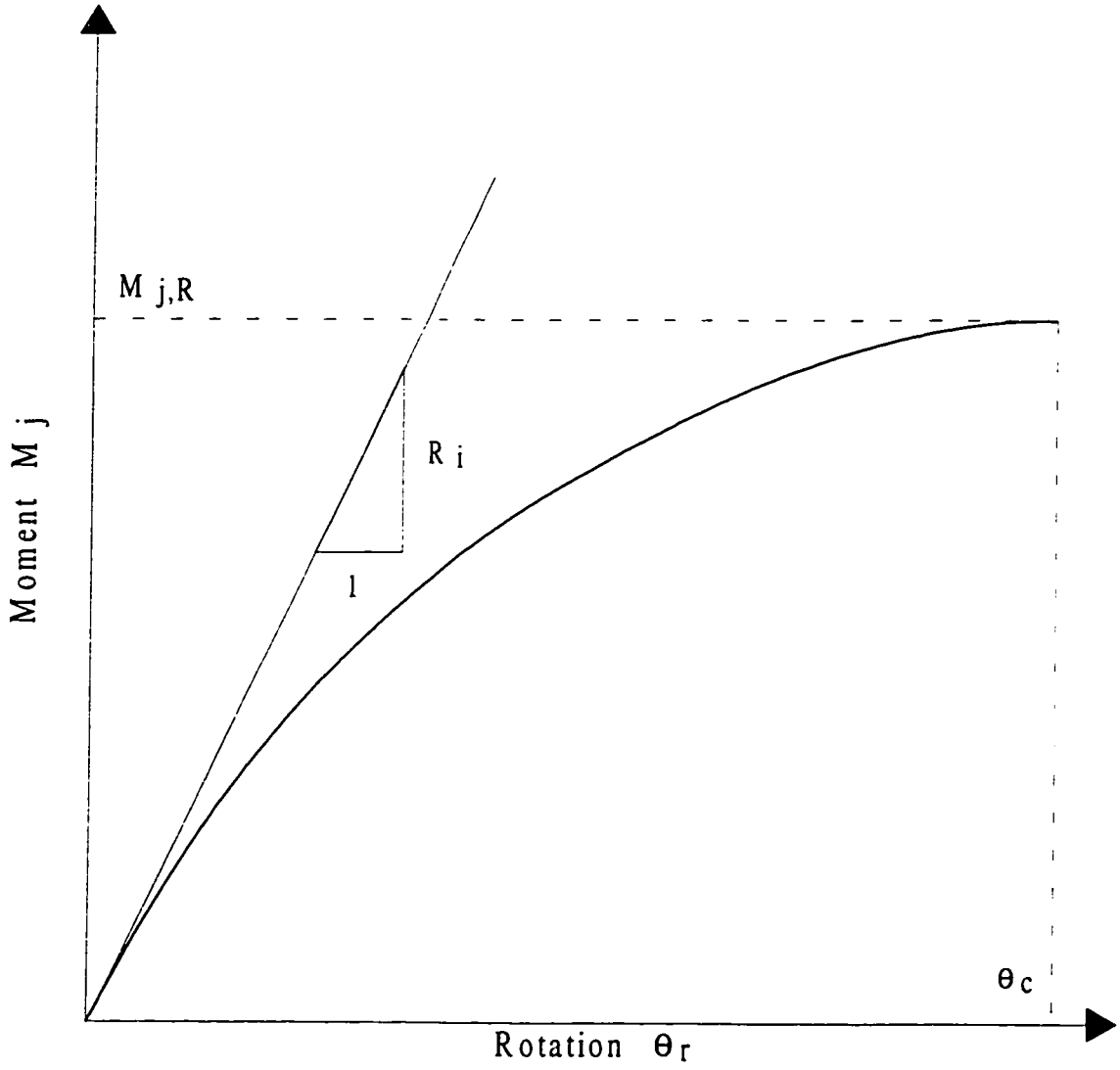

Figure 2.2 Typical Moment-Rotation Curve of a Beam Column Connection

- Connection is nominally pinned if $R_i \leq \frac{0.5EI_b}{L_b}$

For unbraced frames:

- Connection is rigid if $R_i \geq \frac{25EI_b}{L_b}$

- Connection is semi-rigid if $\frac{0.5EI_b}{L_b} < R_i < \frac{25EI_b}{L_b}$

- Connection is nominally pinned if $R_i \leq \frac{0.5EI_b}{L_b}$

If the classification is by strength, the classification limits are the value of the moment resistance, $M_{j.R}$, of the joint compared with the plastic moment resistance $M_{b.pl}$ and $M_{c.pl}$ of the beam and column members which it joins at intermediate column height:

- Connection has full strength if $M_{j.R} \geq M_{b.pl}$

  or $M_{j.R} \geq 2M_{c.pl}$

- Connection is nominally pinned if $M_{j.R} < 0.25$ times the moment resistance required for a full-strength joint

- Partial strength connection is in between these two limits

In semi-continuous design, both elastic (semi-rigid) and plastic (partial-strength) analysis can be used for moment-resisting frames but it is necessary to check the rotation capacity of the joints. As seen, Eurocode 3 (EC3) uses bi- or tri-linear alternative approximate curves in the derivation of moment-rotation characteristics provided that the approximate curve lies wholly below the more precise characteristic. Figure 2.3 shows the tri-linear curves representing the boundaries between different connection types for braced and unbraced frames [7]. The nondimensional parameters used in the classification are $m' = \frac{M_j}{M_p}$ and $\theta' = \frac{\theta_r}{(M_p L_b / EI_b)}$ where M_p is the member plastic moment in the absence of axial load.

Although several design codes of steel structures allow the use of semi-rigid joint action in the design, designers rarely employ this approach and prefer to use basic approaches of simple or continuous construction.

2.3 TYPES OF BUILDING CONNECTIONS

Different types of building beam-column connections were tested in the past to obtain their moment-rotation response [8]. They are classified and summarized in the following sections.

2.3.1 Single Web Angles Connections

The single web angle connections consist of an angle either bolted or welded to both the column flange and the beam web as shown in Fig. 2.4a. Tests conducted by

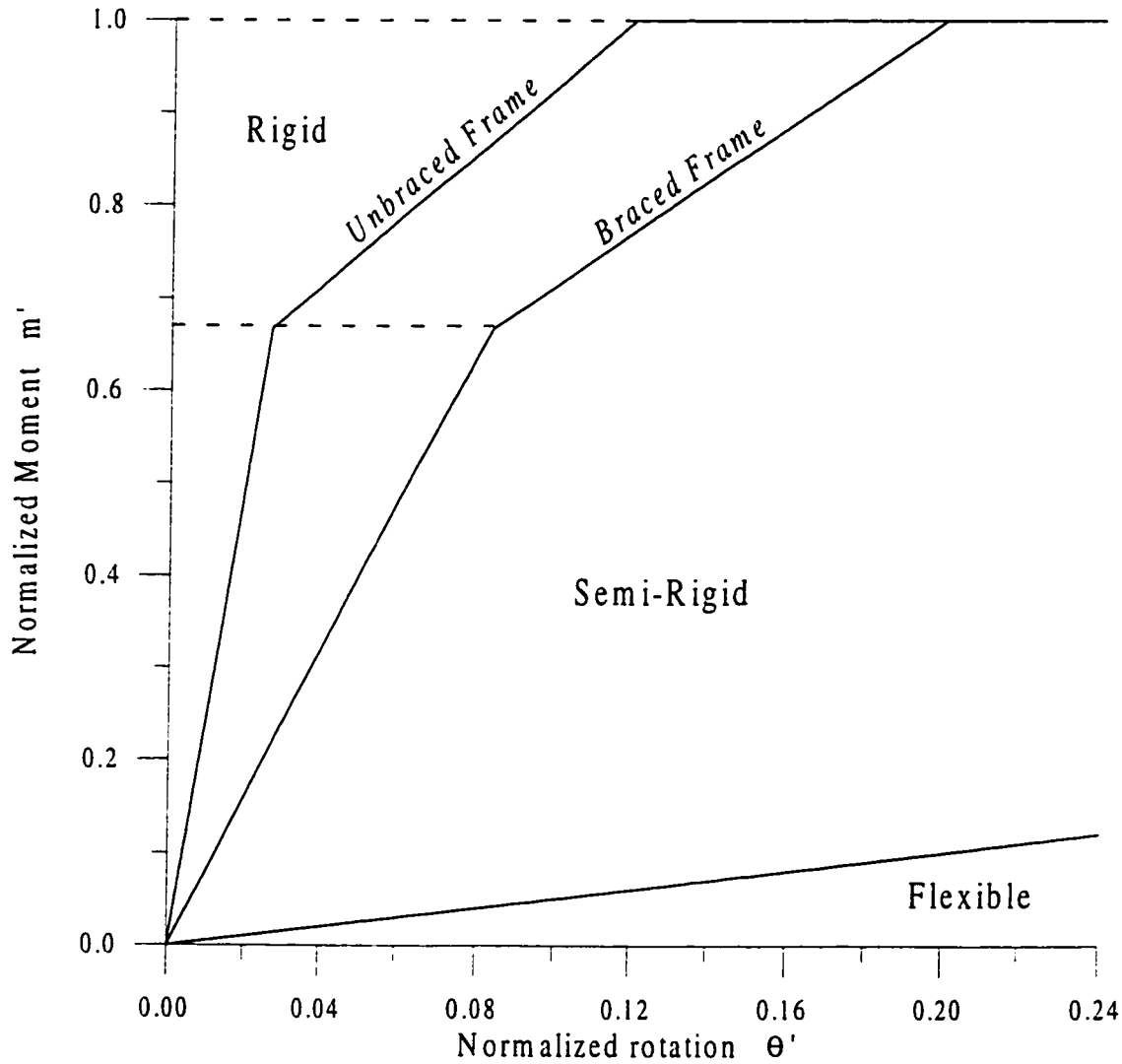

Figure 2.3 Classification of Connections According to Eurocode 3

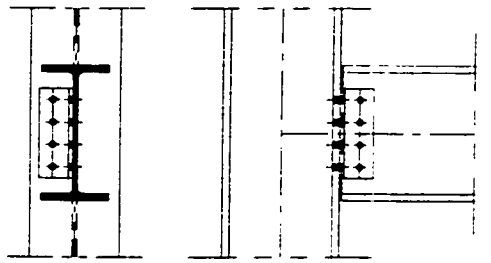

(a) Single Web Angle

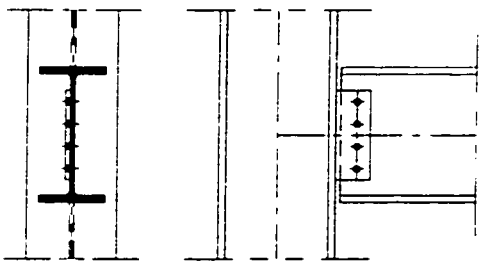

(b) Single Web Plate

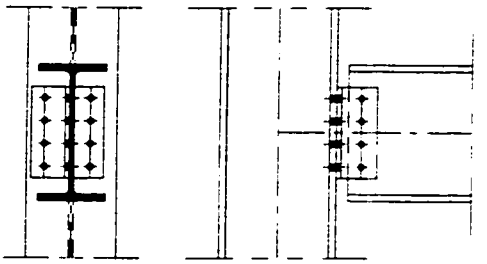

(c) T Shear

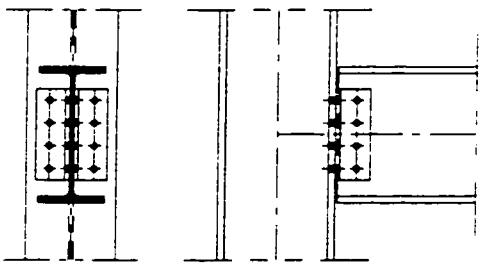

(d) Double Web Angles

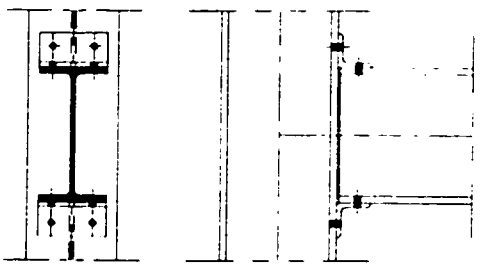

(e) Top and Seat Angles

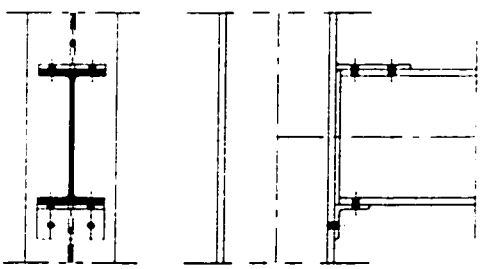

(f) Top Plate and Seat Angle

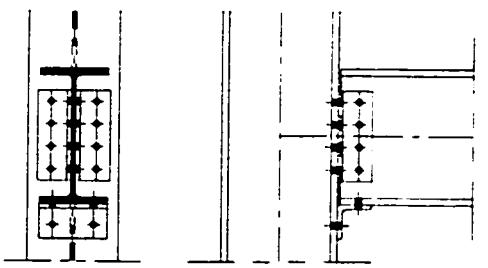

(g) Seat and Web Angles

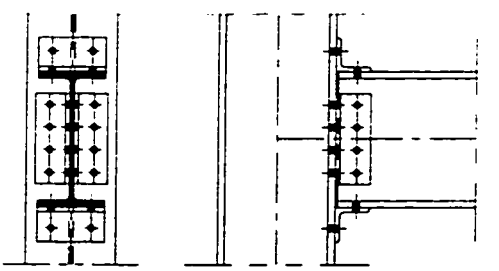

(h) Web and Flange Angles

Figure 2.4 Types of Building Beam-Column Connections

Lipson and Antonio [9] show that the increase of the number of bolts increases significantly both the connection stiffness and the moment capacity. And with less than six bolts, the connection functions essentially as a pin support.

2.3.2 Single Web Plate Connections

For single web plate connections, a plate is used instead of the web angle, which requires less material and minimizes the influence of eccentricity as shown in Fig. 2.4b. In general, single web plate connections have rigidity equal to or greater than the single web angle connections [10]. Tests were conducted on connections with finger-tight bolts and non-torqued bolts by Richard *et al.* [11]. Similar tests but with fully torqued bolts in round and slotted holes were performed by Richard *et al.* [12] and Hormby *et al.* [13] respectively. From these tests it was observed that connections with finger-tight bolts were very flexible since no clamping action was provided. Also, no difference was observed in the performance of the fully torqued bolts in either the round or slotted holes. Moore and Owens [14] tested the effect of the plate length on the behavior of such connections. They concluded that the short plate connections usually fail by bearing failure of either the plate or the beam web. Long plates have a tendency to twist and can be subjected to lateral torsional buckling.

2.3.3 Tee Shear Connections

A tee-framing shear connection consists of a steel tee section connecting the beam to the column as shown in Fig. 2.4c. The main role of this connection is to transfer the

beam shear to the column. The actual behavior of this type of connection is investigated by Astaneh and Nader [15] for tee connections that are bolted to the beam web and welded to the column. The tested tee connections were found to be very ductile and flexible enough to be considered as Type 2 (simple) connections. A design procedure for this type of connection was also proposed.

2.3.4 Double Web Angles Connections

Double web angle connections consist of two angles either bolted or welded to both the column flange and the beam web as shown in Fig. 2.4.d. Tests were conducted for bolted/bolted angles by Bose [16] and for bolted/welded angles by Bjorhovde [17]. The main sources of the flexibility of this type of connection is due to the deformation and yield of connecting angles as well as bolt slip. The connection stiffness can be increased by using heavier angles and increasing the number of bolts in a single row or using double row.

2.3.5 Top and Seat Angle Connections

This type of connection is illustrated in Fig. 2.4e where the beam is connected to the column by flange angles only. It is also known as flange angle connection. The AISC-ASD Specification [3] describes the seat angle to transfer vertical reaction only and to use the top angle for lateral stability. However, according to experimental results by Maxwell *et al.* [18], these connections are able to resist some end moments of the beam. Tests of Van Dalen and Godoy [19] showed the effect of composite action on

the stiffening and strengthening of connection. The connection stiffness can be increased by increasing the angle thickness and by placing first line of bolts on vertical leg of tension angle as close to root radius as possible. Furthermore, torqued bolts can be used to prevent bolt slip.

2.3.6 Top Plate and Seat Angle Connections

The top plate and seat angle connection shown in Fig. 2.4f is stiffer than top and seat angle connection. It is widely used for roofs and composite slabs, when the top angle is not recommended. Van Dalen and Godoy [19] studied the effect of composite action of the beam-slab on the moment-rotation curve of this connection.

2.3.7 Bottom Flange and Web Angles Connections

In this type of connection the beam is connected to the column by web angles and a seat angle only as shown in Fig. 2.4g. Few tests for this type of connection were conducted by Aggarwal [20].

2.3.8 Web and Flange Angles Connections

For this connection, the flanges and the web of the beam are connected with angles to the column flange as shown in Fig. 2.4h. Tests conducted by Zoetemeijer [21] showed a nonlinear behavior of the connection over the entire range of rotations. Altman *et al.* [22] showed that both initial stiffness and moment capacity were strongly influenced by the angles details.

2.3.9 Header End Plate Connections

The header plate connection shown in Fig. 2.4i consists of an end plate welded to the beam web and bolted to the column. The length of the header plate is usually less than the depth of the beam. Tests on this type of connection were conducted by Sommer [23] and Owens and Moore [24]. The header plate connection is used usually to transfer the reaction from the beam to the column.

2.3.10 Clipped End Plate Connections

For practical considerations, header end plate can not be erected safely if they are connected with a common set of bolts. An economical and safe solution is the use of clipped end plate connection which is shown in Fig. 2.4j. The connection is composed of an end plate, with a length less than the beam depth, welded to the beam web with a cut of the upper right-hand corner of the end plate made in the shop. Van Dalen and Mac Intyre [25] conducted several tests to get the moment-rotation behavior of such connection. Furthermore, they compared between clipped and unclipped end plate connections from the rotational point of view.

2.3.11 Header End Plate and Seat Angle Connections

The header end plate connections with seat angle shown in Fig. 2.4k was tested by Aggarwal [26]. Analytical model describing the moment-rotation curve of such connection was given by Abdalla and Chen [27].

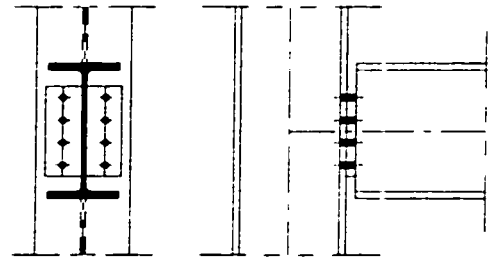

(i) Header End Plate

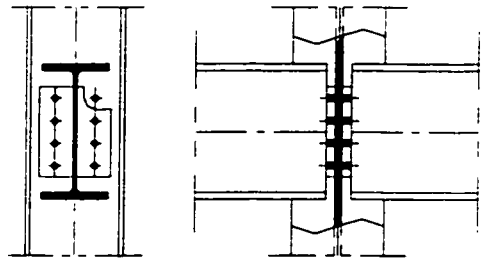

(j) Clipped End Plate

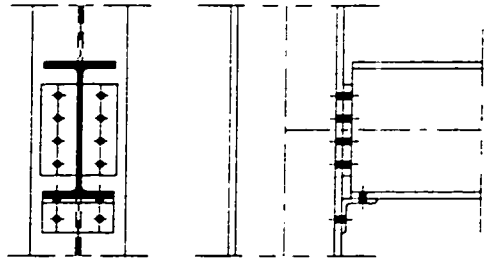

(k) Header Plate and Seat Angle

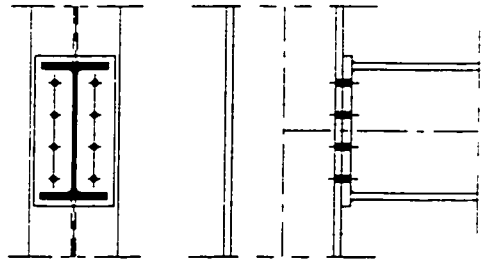

(l) Flush End Plate

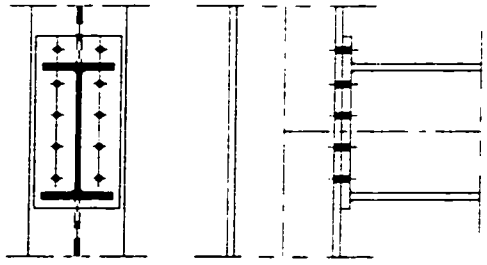

(m) Extended End Plate

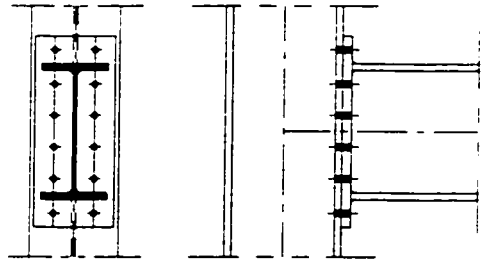

(n) Extended End Plate

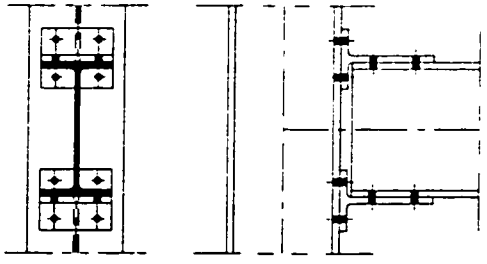

(o) Flanges T-Stubs

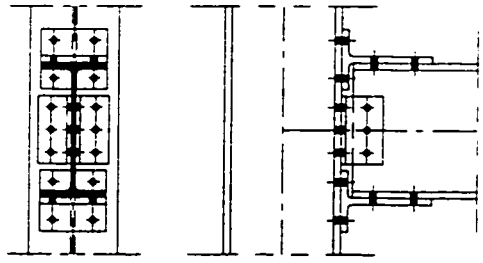

(p) Flanges T-Stubs and Web Angles

Figure 2.4 Types of Building Beam-Column Connections (cont.)

2.3.12 Flush End Plate Connections

The flush end plate connections are similar in shape to header plate connections but the length of the plate is equal to the beam depth as shown in Fig. 2.4l. This type of connection can resist moments more than the header plate connections. Jenkins *et al.* [28] conducted several tests and proposed a limit state design method for the flush end plate connection. The ductility, strength and stiffness of this type of connection were discussed by Bose *et al.* [1, 6] from their tests.

2.3.13 Extended End Plate Connections

The extended end plate connection consists of an end plate welded to the beam web and bolted to the column. The length of the end plate is bigger than the beam depth. It can be extended in the tension region only as shown in Fig. 2.4m or extended in tension and compression region as shown in Fig. 2.4n if the load is of reversed type. Bose and Hughes [1] studied the effect of end plate thickness on the ductility of the connection. Their test specimens had loading and geometric symmetry, so no effect of web panel shear deformation is taken into consideration. It was expected that the rotational stiffness was proportional to the square of the distance between the centers of compression and tension. Bose and Hughes [1] concluded that end plates which are excessively thick have a low rotational capacity which leads to a non-ductile failure. It has been suggested that any connection achieving 0.03 radian can confidently be regarded as ductile. If connection fails to achieve 0.02 radian rotation capacity, plastic design should not be employed. The end plate and bolts behavior is influenced by the

presence of flange column stiffeners. This is due to the effect of preventing excessive deformation in column flanges.

2.3.14 T-Stub Connections

Figure 2.4o shows the flanges T-stub connection which is more flexible than the flanges T-stub with web angles connection shown in Fig. 2.4p. Zoetemeijer [21] noticed that a significant slip occur at about 30 to 40% of the joint's moment capacity, leading to a plateau on the $M-\theta$ curve followed by a stiffening as the bolts came into bearing.

2.4 TECHNIQUES USED FOR MONITORING JOINT ROTATION

Moore and Owens [14] used a rotation device composed of a horizontal arm connected to a vertical pendulum by a thin metal strip. Four strain gauges in full bridge configuration were mounted on the metal strip. The horizontal arm was fixed to the beam (column). Rotation of the beam (column) caused the thin metal strip to bend as the weight remain vertical. As the device was quite delicate and subject to vibration, the output was taken from 50 readings then averaged.

Aggarwal and Coates [29] adopted an optical technique to measure the rotation of the beam-column connection. The system was composed of two separate mirrors fixed on the beam and column flanges close to the connection under investigation. Graph paper mounted on vertical boards served as sighting targets. A pair of theodolites was used to observe the reflected images of the graph papers. The

readings were taken during the test to calculate the connection rotation at each load increment. However, this method was incapable of automatic recording.

Jenkins *et al.* [28] measured the rotation of end plate connection using dial gauges attached to the specimen and bearing on extension arms to amplify the measured displacements during loading.

Bose and Hughes [1] monitored the rotation of the beam-column connection by two independent means using a pair of dial gauges as well as a pair of displacement transducers on both the beam and the column. The rotation of each element was calculated followed by the relative rotation between them.

2.5 CONNECTION BEHAVIOR

From experimental tests it was found that the moment-rotation curves are always non-linear. This nonlinearity arises from various sources such as for example: the type of connection, bolt deformation and local yielding of the connecting materials (plates, angles, tees, etc.) [8, 30]. A schematic comparison for the connection behavior of different types of connections is illustrated in Fig. 2.5. At any stage of load, the connection stiffness depends on the load path. During loading, the connection has a tangential stiffness R_t. But when unloading the connection, its stiffness becomes equal to initial slope R_i of the moment rotation curve as shown in Fig. 2.6.

The literature review shows that no experimental work has been carried out thus far using the cap-plate type beam-column joint. This is probably due to the fact

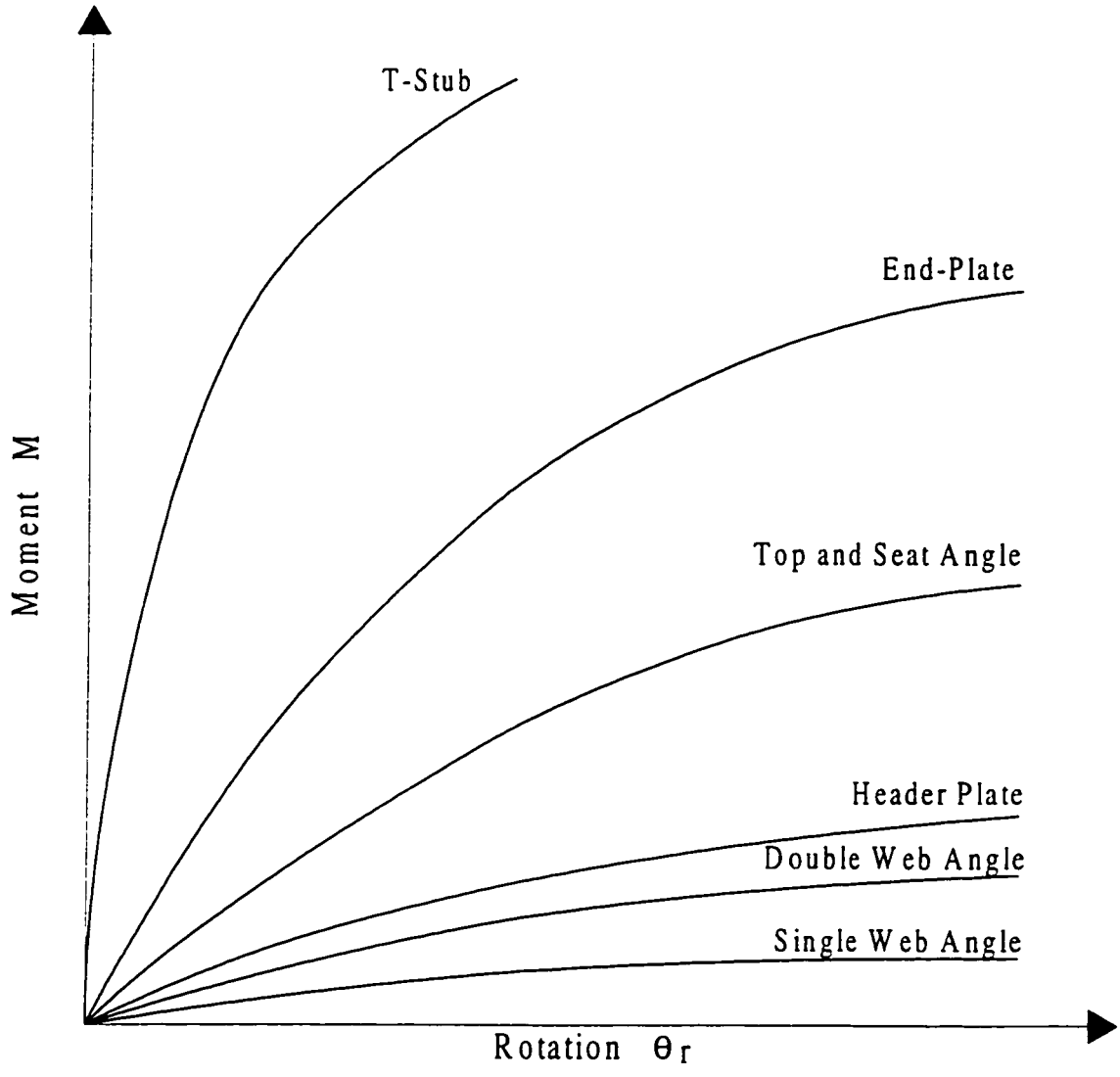

Figure 2.5 Comparison of Moment-Rotation Relation for Different Joints

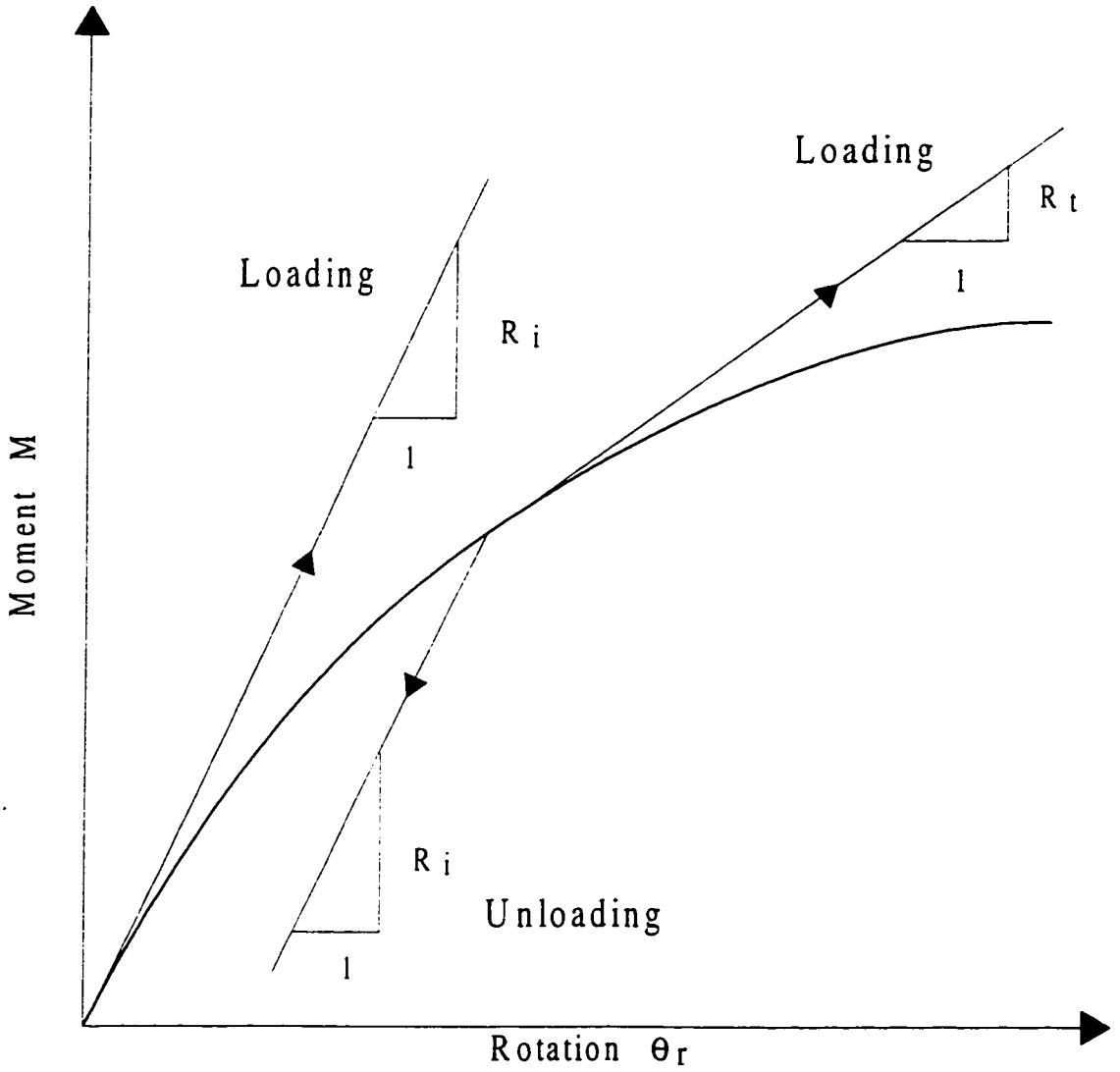

Figure 2.6 Loading and Unloading Paths of Semi-Rigid Connections

that cap-plate type connections are used only in single story industrial frames and researchers in the past have focused their attention on the connections used in common steel buildings.

2.6 MODELING OF CONNECTIONS

Various models were derived in different ways to represent the non-linear behavior of steel moment connections. They were based on several experimental tests. Each of these models has its advantages, disadvantages and limitations.

2.6.1 Linear Models

Linear models were developed by Rathbun [31], Monforton and Wu [32], Lightfoot and Le Messurier [33] and Jones *et al.* [34]. The connection behavior is represented in the linear model by the initial rotational stiffness R_i for the entire range of loading

$$R_i = \frac{M}{\theta_r} \tag{2.1}$$

where: M = the applied moment at the connection

θ_r = the relative rotation between the beam and the column

This model is easy to use in the analysis but is no longer valid as the moment increases beyond the service limit of the connection.

A better representation of the connection behavior is the bilinear model developed by Romstad and Subramanian [35] and Sugimoto and Chen [36]. The

model has a shallower second slope at a certain transition moment M_t to represent the reduced connection stiffness at higher rotations. To overcome the limitations of the previous models, the piecewise linear model (multilinear model) was proposed by Moncarz and Grestle [37] and Razzaq [38]. In the piecewise linear model, the nonlinear shape of the $M-\theta$ curve is approximated by a series of straight lines.

2.6.2 Polynomial Models

In this model, Frye and Morris [39] and Morris and Packer [40] represented the $M-\theta$ relationship by the odd-power polynomial function

$$\theta_r = C_1(KM)^1 + C_2(KM)^3 + C_3(KM)^5 \qquad (2.2)$$

where: K = parameter depending on the geometry of the connection

C_i = curve fitting constants to be determined by the method of least squares

The primary disadvantage of this model is that the first derivative of the function which indicates the connection stiffness may become negative at some values of M, which is physically impossible.

2.6.3 Cubic B-Spline Models

To avoid possible negative slope, the B-spline model is suggested by Jones *et al.* [41], where the test data are divided into a number of subsets, each spanning a small range of moment. The model has the form

$$\theta_r = \sum_{j=0}^{3} a_j M_j + \sum_{j=1}^{m} b_j \left(< M - M_j > \right)^3 \qquad (2.3)$$

where: m = number of knots (junctions of multi-part curve)

M_j = upper bound moment in the jth part of the curve

a_j and b_j = coefficients obtained by least-squares curve fitting

$< M - M_j >$ $= M - M_j$ for $(M - M_j) > 0$

$= 0$ for $(M - M_j) < 0$

The cubic B-spline function is used to fit each subset of data with enforcing of the continuity of the first and second derivatives at their intersections. But a large amount of data is required in the curve-fitting process.

2.6.4 Power Models

The simplest form of the power model is the two-parameter model developed by Krishnamurthy *et al.* [42], it has the form

$$\theta_r = aM^b \qquad (2.4)$$

where: a and b are parameters to be found from curve fitting

This model is not recommended if accurate results are desired.

Goldberg and Richard [43] introduced the three-parameter model which is a better alternative to represent the $M-\theta$ curve. Kishi and Chen [44] proposed a similar power model which has the form

$$\theta_r = \frac{|M|}{R_{ki}\left(1-\left|\frac{M}{M_u}\right|^n\right)^{\frac{1}{n}}} \tag{2.5}$$

where: R_{ki} = the initial connection stiffness

M_u = the ultimate moment capacity of the connection

n = a shape parameter

The shape parameter was used to adjust the curvature of the portion of the curve connecting the initial stiffness to the ultimate moment. To represent the nonlinear $M-\theta$ behavior of a variety of connections, the four-parameter model was introduced by Ang and Morris [45]. This parameter is a standardization constant K depending on the connection type and geometry.

2.6.5 Exponential Models

The multi-parameter exponential models were proposed by Lui and Chen [46] to give good curve-fitting to test data. Some parameters are determined analytically, whilst others are obtained empirically by curve-fitting to experimental data. It has the form

$$M = \sum_{j=1}^{m} C_j \left[1 - \exp\left(-\frac{|\theta_r|}{2j\alpha} \right) \right] + M_0 + R_{kf} |\theta_r| \qquad (2.6)$$

where: M_0 = starting value of connection moment to which the curve is fitted

R_{kf} = strain hardening stiffness of the connection

α = scaling factor

C_j = curve-fitting constants

Other modified exponential models were developed by Yee and Melchers [47], Wu and Chen [48] and Chen and Lui [30].

2.6.6 Finite Element Models

Chasten *et al.* [49] studied the effect of prying and shear in end-plate connection using the finite element program ADINA. The analytically predicted bolt forces were compared with the experimentally measured forces and good agreement was found. Bahaari and Sherbourne [50, 51, 52] employed the finite element modeling to evaluate analytically the stiffness and strength characteristics of steel bolted end-plate connections. In the analysis, the general-purpose finite element code ANSYS was used. Choi and Chung [53] employed the finite element methodology to investigate the behavior of the end-plate connections. They established a three-dimensional model with nonconforming 3-D elements to simulate the actual behavior of the connection.

2.7 CONNECTION DATA BASE

It is a collection of experimental tests for several types of beam-column connections collected over several years. They are compiled with the following details: (a) physical properties of connection elements as beam, column and connection dimensions; (b) material properties as type of steel used; (c) connection details; (d) moment-rotation data; (e) researcher name and date of experiment.

The main connection data bases are :

- Goverdhan data base (1983) at Vanderbilt University, Nashville, Tennessee [54]. Much of the available test data on moment-rotation characteristics were collected with a prediction equation for each curve.

- Nethercot data base (1985) at the University of Sheffield, U.K. [55]. A review of steel beam-to-column connection test data were presented and the corresponding curve representations were conducted by fitting the experimental results.

- Kishi-Chen data base (1986) at Purdue University, U.S.A. [56, 57]. Kishi and Chen developed the Steel Connection Data Bank (SCDB) based on the collected experimental test data. The SCDB program provides different functions, including routines for tabulating and plotting the experimental test data and determining the values of the proposed prediction equations for test data.

2.8 ANALYSIS OF RIGID AND SEMI-RIGID FRAMES

The first-order analysis of rigid plane frames using the direct stiffness method was formulated by Gutkowski [58], Wang [59], Chajes [60] and Weaver and Gere [61]. The second-order analysis and its effect on the stability of rigid plane frames was developed by Ghali [62], Chajes [63, 64], Chen and Lui [30, 65] by introducing the stability functions in the member stiffness matrix. A simplified method that accounted for the P-delta effects was developed by Gaiotti and Smith [66].

Frye and Morris [39] presented the first-order analysis of flexible frames. The connection nonlinearity was modeled by the odd-power polynomial model. Monforton and Wu [32] derived the relationship between forces and displacements at the end of members with elastically restrained ends, by modifying the ordinary stiffness matrices by a correction matrix whose elements are functions of two parameters designated as fixity factors.

Analytical procedures for the second-order analysis of plane framed structures considering the flexibility of beam-to-column connections were presented by Chen and Lui [30], Abu-Yasein and Fredrick [67] and Mourad [68]. Lui [69] proposed a method of second-order frame analysis using first-order structural analysis. The proposed method accounted for the P-delta effects by the use of fictitious or pseudo lateral loads. Practical methods for the analysis of plane frames taking into consideration the connection flexibility and the second-order effects were developed by Barakat and Chen [70] and Al-Mashary and Chen [71].

Li *et al.* [72] considered the beam-to-column connection as an independent multi-degree spring element which is free from both beams and columns. The effects of connection size and shear deformation in modeling of flexible connections were considered by Lo and Stiemer [73]. Ang and Morris [45] presented a procedure for analyzing three-dimensional rectangular frames with flexible connections. Rashed *et al.* [74] analyzed the stability of space steel frames with semi-rigid connections. Plastic analysis and design of semi-rigid frames was investigated by Galal [75], Patodi and Patel [76] and Liew *et al.* [77]. Scholz [78] suggested a plastic design approach of sway frames with semi-rigid connections using the allowable slenderness ratios to control overall and member stability.

CHAPTER 3

DEVELOPMENT OF STIFFNESS MATRICES AND METHOD OF ANALYSIS

3.1 GENERAL

A beam-column member in a plane frame is subjected to secondary moments due to the axial forces. Frames are classified as rigid, semi-rigid and simple depending upon the stiffness of the beam-column connection. The connection flexibility must be incorporated in the analysis, by considering its effect on the stiffness of the beam-column member. In this chapter, an introduction to the frame behavior is given. The stiffness matrix of plane framed structure is developed by idealizing the connection at the beam-column end as a nonlinear spring. Then, the method of solution of the nonlinear problem is presented.

3.1.1 Effective Length

In steel frames the behavior of a column is influenced by its end condition and whether the frame is braced or not. For braced frames lateral side sway is prevented

by the use of diagonal bracings or shear walls. Braced frames differ than unbraced frames in the effective length of columns kL. In the AISC specification [3], the effective length concept is used for estimating the interaction effects of the total frame on a column being considered.

For braced frames kL is less than or equal the actual length L. The effective column length coefficient k increases with decreasing stiffness of the beam and becomes unity with zero stiffness. For unbraced frames kL is greater than the actual length. The effective column length coefficient k increases with decreasing stiffness of the beam and tends to infinity as the beam stiffness approaches zero [79], that is why the LRFD specification [4] requires that k shall be determined by structural analysis and shall not be less than unity.

For design purpose, alignment charts for evaluating the effective length of columns are given [5, 79], and for simple cases, the Structural Stability Research Council *(SSRC) Guide* [80] may be used. Equations derived by Aristizabal-Ochao [81] may be used to predict the effective length for cases of unsymmetric geometry or loading.

3.1.2 Second Order Effects

Under given loads, simple and continuous beams are subjected only to primary deflections and primary moments which govern the design. For frames, secondary deflections and secondary moments are obtained in addition to primary ones. The

secondary effects result from the application of member axial forces on the primary deflections. This effect is mainly in columns rather than beams of a given frame. The design is based on the accumulative primary and secondary actions.

Second order effects are of two types [30] as shown in Fig. 3.1. The first is the $P-\delta$ effect which result from the application of the axial force on the deflected shape due to primary loads on a member with end translation prevented. This effect is also known as the member instability effect. The second is the $P-\Delta$ effect which result from the application of axial force on the member having end translation Δ. This effect will increase the drift Δ leading to further increase in moment. This effect is also known as the frame instability effect. To take into account the secondary effects, second order analysis must be used in an iterative process by applying the loads incrementally on the analyzed frame. The fundamental case of buckling of a prismatic member hinged at both ends is given by $P_{cr} = \frac{\pi^2 EI}{L^2}$ which is the critical buckling load of this member.

3.1.3 Rigid and Semi-Rigid Frames

For most of the structural analysis softwares, frames are assumed as rigid. In the analysis process of these frames, members are considered as rigidly connected with very stiff joints. The main characteristic of these joints is that the angle between the connected members remains the same before and after the application of the loads.

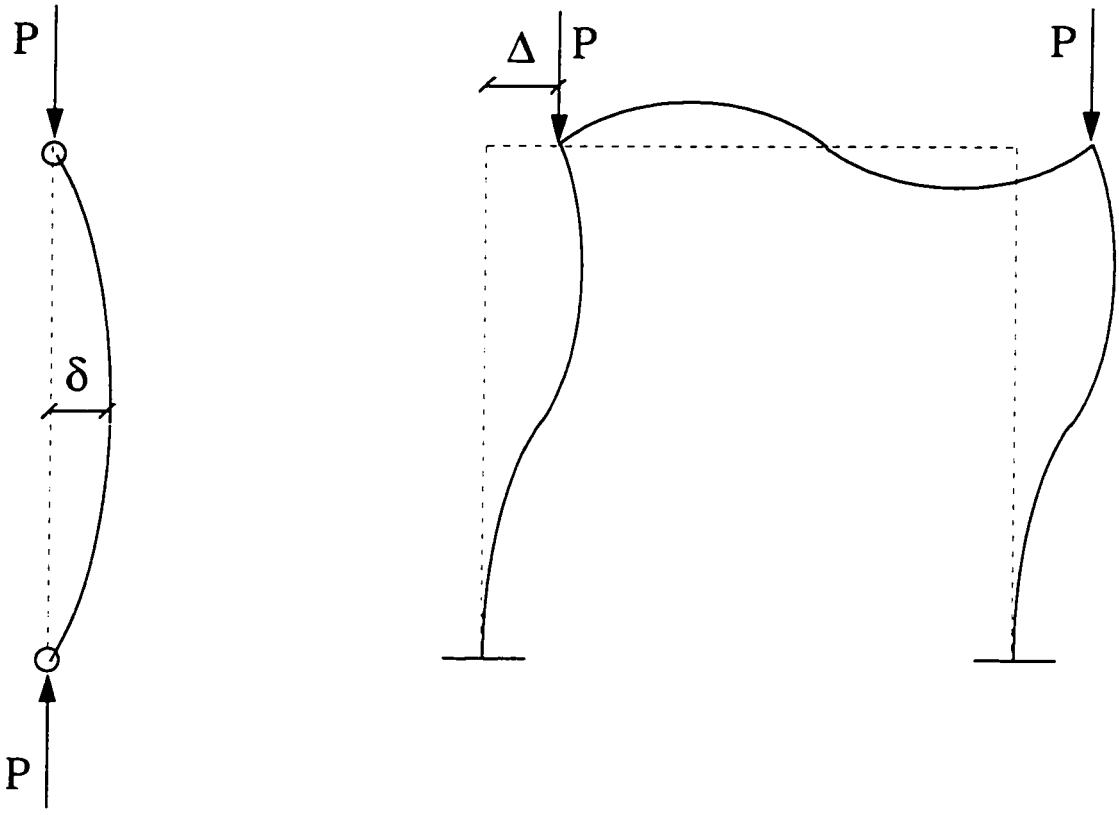

Figure 3.1 Second-Order Effects

More advanced softwares take into account the second-order effects leading to nonlinear analysis.

Neglecting connection flexibility in steel frames leads to an underestimation of lateral displacement and an overestimation of connection moments which consequently results in heavier connections and heavier columns. In semi-rigid frames analysis, the effect of joint flexibility is taken into consideration. The joint characteristics are defined by the nonlinear moment rotation relationship obtained from testing such joint. If second-order effects (i.e. $P-\Delta$, $P-\delta$ and connection flexibility) are also considered, the problem becomes highly nonlinear.

3.1.4 Failure Modes of Frames

The frame failure modes are either by frame instability due to buckling of members or by plastic collapse due to development of enough number of plastic hinges forming a mechanism.

3.1.4.1 Critical Buckling Load

The critical buckling load of a frame depends on the geometry, the applied load and the boundary conditions of the member. The critical buckling load cannot be derived for individual columns, especially for frames with sidesway, since columns and beams are coupled together and they influence each other. Then, the overall behavior of the frame must be considered to get its critical buckling load.

3.1.4.2 Plastic Mechanism

For simple and continuous beams the failure mechanism is attained when $M = M_p$ in the absence of an axial force, where $M_p = F_y Z_p$ is the fully plastic moment, F_y = material yield stress and Z_p = cross sectional plastic modulus [82]. In the absence of moments the plastic collapse is given by $N_p = F_y A$ where N_p is the fully plastic thrust and A = cross sectional area of the member [82].

For a frame with n number of degree of indeterminancy and a number of possible plastic hinges equal to N, a complete collapse mechanism is obtained only if $N = n+1$. Sometimes a partial mechanism is obtained if $n+1 > N$ leaving part of the structure unfailed and with some degree of redundancy [83]. The number of independent mechanisms N' is given by $N' = N - n$. Different modes of failure are shown in Fig. 3.2.

3.2 ASSUMPTIONS

The following assumptions are used in the derivation of the stiffness matrices of the beam-column members with prescribed end conditions: (a) members are prismatic and straight; (b) the material is homogeneous, linearly elastic; (c) deformations are small so that they do not significantly change the geometry of the structure during loading; (d) a connection at a member end, considered to be small compared to the member length, is modeled as a rotational spring with non-linear moment-rotation

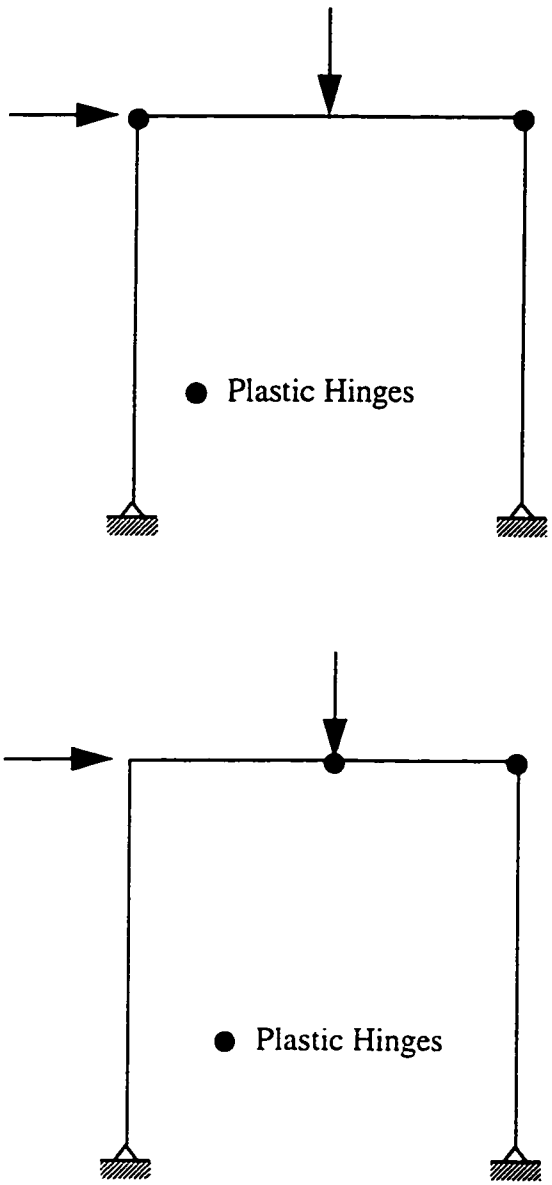

Figure 3.2 Frame Failure by Plastic Mechanism

characteristics; (e) the connections are fully capable of transmitting axial forces, shear forces and bending moments.

3.3 MEMBER STIFFNESS MATRICES

The stiffness of a beam-column member depends on its boundary conditions. There are eight possible combinations of end conditions as shown in Table 3.1. The member type having rotational springs at both ends was derived by Chen and Lui [30]. The case of one end hinged has been included to cater to the cases of a natural hinge or a plastic hinge being developed during the incremental loading. The stiffness matrix of each member type is derived and given in the following sections. The relation between different member types is introduced as a check for the derivation. These types are used latter in the development of a general computer program to solve the rigid and semi-rigid frames taking into consideration the second order effects as well as the nonlinearity of connections.

3.3.1 Type 1 (Fixed - Fixed)

Member Type 1 is the traditional beam-column member which is used in the analysis of rigid frames. For this type, both end connections are assumed to be rigid. The second order effects, due to the axial force P, are taken into consideration through the trigonometric and hyperbolic functions. Using the numbering system of Fig. 3.3, the stiffness matrix $[K_m]_1$ for member m (Type 1) is given as follows [30, 61, 62]:

TABLE 3.1 Different Types of Beam-Column Members

Member Type	End i	Member Shape	End j
1	Fixed	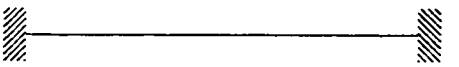	Fixed
2	Spring	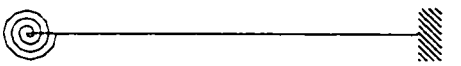	Fixed
3	Fixed	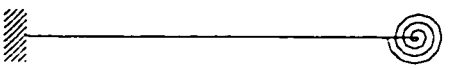	Spring
4	Hinged	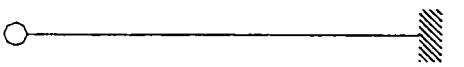	Fixed
5	Fixed	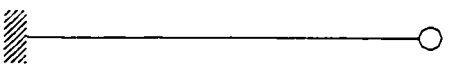	Hinged
6	Spring	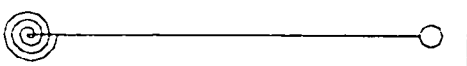	Hinged
7	Hinged		Spring
8	Hinged	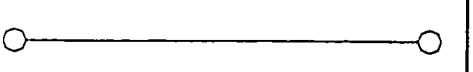	Hinged

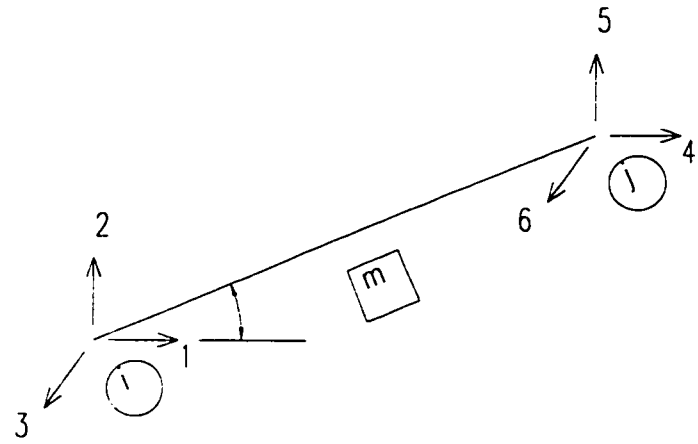

Numbering degrees of freedom in global axes

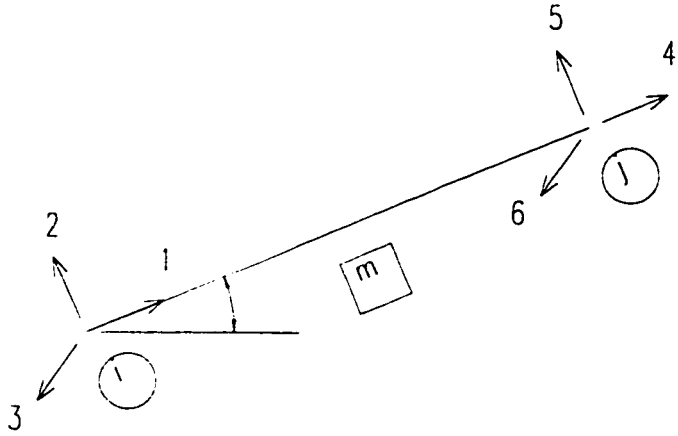

Numbering degrees of freedom in local axes

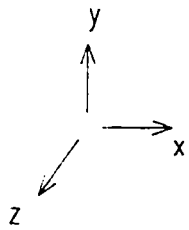

Figure 3.3 Numbering System

$$[K_m]_1 = \lambda \begin{bmatrix} \frac{AL^2}{I} & 0 & 0 & -\frac{AL^2}{I} & 0 & 0 \\ 0 & \left(\frac{\phi_1}{\phi_6}\right) & L\left(\frac{\phi_2}{\phi_6}\right) & 0 & -\left(\frac{\phi_1}{\phi_6}\right) & L\left(\frac{\phi_2}{\phi_6}\right) \\ 0 & L\left(\frac{\phi_2}{\phi_6}\right) & L^2\left(\frac{\phi_3}{\phi_6}\right) & 0 & -L\left(\frac{\phi_2}{\phi_6}\right) & L^2\left(\frac{\phi_4}{\phi_6}\right) \\ -\frac{AL^2}{I} & 0 & 0 & \frac{AL^2}{I} & 0 & 0 \\ 0 & -\left(\frac{\phi_1}{\phi_6}\right) & -L\left(\frac{\phi_2}{\phi_6}\right) & 0 & \left(\frac{\phi_1}{\phi_6}\right) & -L\left(\frac{\phi_2}{\phi_6}\right) \\ 0 & L\left(\frac{\phi_2}{\phi_6}\right) & L^2\left(\frac{\phi_4}{\phi_6}\right) & 0 & -L\left(\frac{\phi_2}{\phi_6}\right) & L^2\left(\frac{\phi_3}{\phi_6}\right) \end{bmatrix} \tag{3.1}$$

where:

A = cross-sectional area of beam-column member

$\lambda = \frac{EI}{L^3}$

E = Young's modulus of elasticity

I = moment of inertia of the beam-column member about the axis of bending

L = member length

$\phi_1,\ldots,\phi_6$ = functions of kL expressed in Table 3.2

$k = \sqrt{\frac{P}{EI}}$

TABLE 3.2 Trigonometric and Hyperbolic Functions

Function	If P is compressive	If P is tensile
ϕ_1	$(kL)^3 \sin kL$	$(kL)^3 \sinh kL$
ϕ_2	$(kL)^2(1-\cos kL)$	$(kL)^2(\cosh kL-1)$
ϕ_3	$(kL)(\sin kL - kL\cos kL)$	$(kL)(kL\cosh kL - \sinh kL)$
ϕ_4	$(kL)(kL-\sin kL)$	$(kL)(\sinh kL - kL)$
ϕ_5	$(kL)^4 \cos kL$	$(kL)^4 \cosh kL$
ϕ_6	$2-2\cos kL - kL\sin kL$	$2-2\cosh kL + kL\sinh kL$
ϕ_7	$(kL)^2$	$-(kL)^2$

As shown in Table 3.2, the functions ϕ_1 to ϕ_6 are trigonometric functions of kL when the axial force P is compressive and these functions become hyperbolic when P is a tensile force.

3.3.2 Type 2 (Spring - Fixed)

For member Type 2 (Table 3.1), the end i is supported by an elastic rotational spring of stiffness R_1 and the end j is fixed. Key steps of the procedure for the derivation of the elements in the stiffness matrix for member Type 2 are given in the following section.

3.3.2.1 Derivation

The beam-column member shown in Fig. 3.4 is subjected to an axial compressive force P and a unit vertical displacement ($\Delta = 1$) is applied at the end i. If the effects of shearing deformations and shortening of the member axis are neglected, the curvature of the axis of the member can be expressed using the elastic line method. The governing differential equation of the beam-column elastic line is given by

$$EIy'' = P(\Delta - y) - M_1 + \left(\frac{M_1 + M_2 - P\Delta}{L}\right)x \tag{3.2}$$

or

$$y'' + k^2 y = \left(\frac{P\Delta - M_1}{EI}\right) + \left(\frac{M_1 + M_2 - P\Delta}{LEI}\right)x \tag{3.3}$$

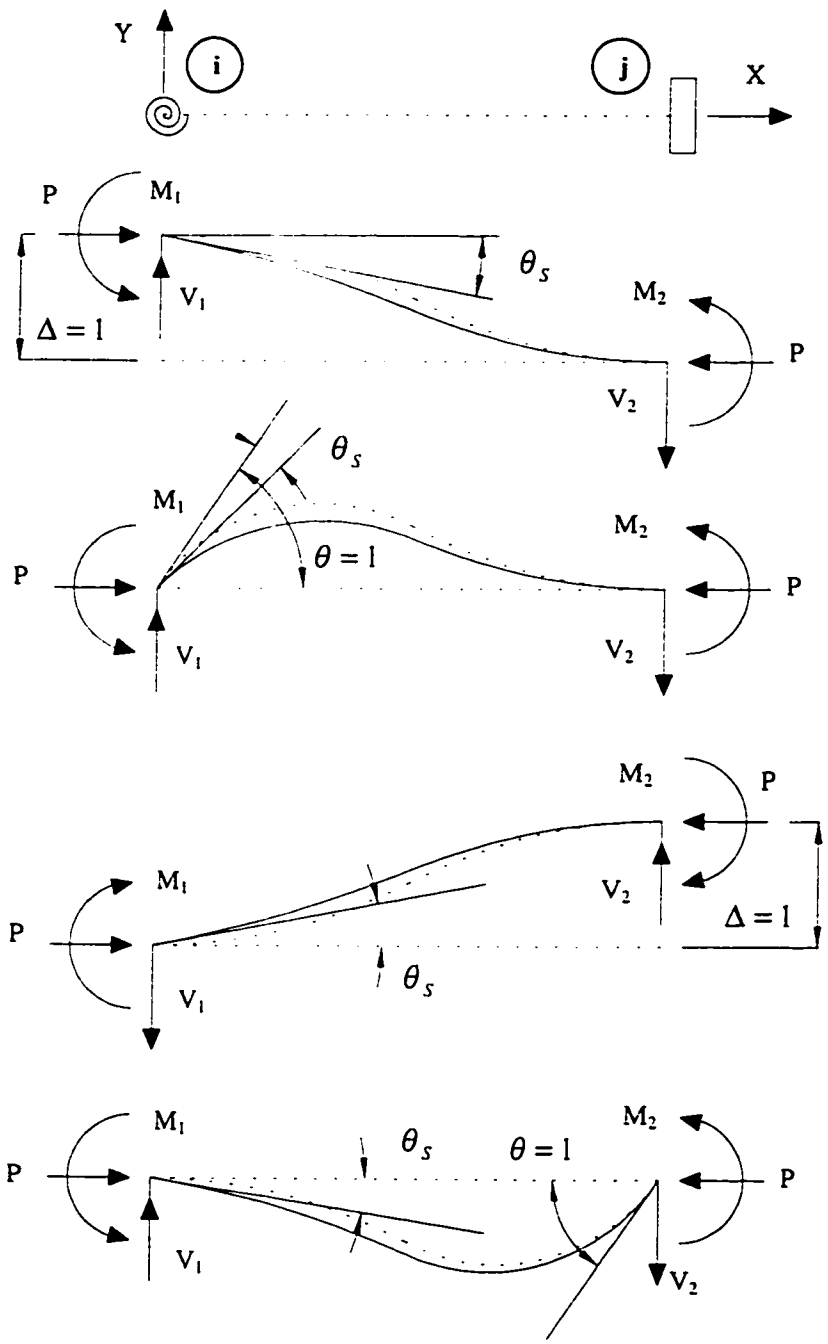

Figure 3.4 Unit Displacements and Rotations at the i and j Ends

where: $k = \sqrt{\frac{P}{EI}}$ (3.4)

and EI represents the flexural rigidity of the beam in the plane of bending.

The general solution for the elastic curve is given by

$$y = A\sin kx + B\cos kx + Cx + D \tag{3.5}$$

where A, B, C and D are constants to be determined for the specified boundary conditions.

Differentiating twice

$$y'' = -Ak^2 \sin kx - Bk^2 \cos kx \tag{3.6}$$

Substituting Eqs. (3.5) and (3.6) into Eq. (3.3), the two constants C and D are determined as

$$C = \left(\frac{M_1 + M_2 - P\Delta}{PL}\right) \tag{3.7}$$

$$D = \left(\frac{P\Delta - M_1}{P}\right) \tag{3.8}$$

Eq. (3.5) then becomes

$$y = A\sin kx + B\cos kx + \left(\frac{M_1 + M_2 - P\Delta}{PL}\right)x + \left(\frac{P\Delta - M_1}{P}\right) \tag{3.9}$$

and the slope at any point is given by differentiating Eq. (3.9) once

$$y' = Ak\cos kx - Bk\sin kx + \left(\frac{M_1 + M_2 - P\Delta}{PL}\right) \tag{3.10}$$

By substituting the following two boundary conditions

(a) at $x = 0$, $y = \Delta$ (3.11)

(b) at $x = 0$, $y' = -\theta_s = -\left(\frac{M_1}{R_1}\right)$ (3.12)

into Eqs. (3.9) and (3.10) respectively, the two constants A and B can be found as

$$A = \frac{1}{k}\left[\left(\frac{\Delta}{L}\right) - \left(\frac{M_1 + M_2}{PL}\right) - \left(\frac{M_1}{R_1}\right)\right] \tag{3.13}$$

$$B = \left(\frac{M_1}{P}\right) \tag{3.14}$$

where R_1 is the connection rotational stiffness

and Eq. (3.9) becomes

$$y = \frac{1}{k}\left[\left(\frac{\Delta}{L}\right) - \left(\frac{M_1 + M_2}{PL}\right) - \left(\frac{M_1}{R_1}\right)\right]\sin kx + \left(\frac{M_1}{P}\right)\cos kx + \left(\frac{M_1 + M_2 - P\Delta}{PL}\right)x + \left(\frac{P\Delta - M_1}{P}\right) \tag{3.15}$$

from the other two boundary conditions,

(c) at $x = L$, $y = 0$ (3.16)

(d) at $x = L$, $y' = 0$ (3.17)

the end moments M_1 and M_2 can be found after some mathematical manipulation

$$M_1 = \frac{EI}{L^2}\left[\frac{\phi_2}{\phi_6 + \left(\frac{EI}{L}\right)\left(\frac{1}{R_1}\right)\phi_3}\right] \tag{3.18}$$

and

$$M_2 = \frac{EI}{L^2}\left[\frac{\phi_2 + \left(\frac{EI}{L}\right)\left(\frac{1}{R_1}\right)\phi_1}{\phi_6 + \left(\frac{EI}{L}\right)\left(\frac{1}{R_1}\right)\phi_3}\right] \tag{3.19}$$

From equilibrium, the end shears can be calculated as

$$V_1 = V_2 = \frac{EI}{L^3}\left[\frac{\phi_1 + \left(\frac{EI}{L}\right)\left(\frac{1}{R_1}\right)\phi_5}{\phi_6 + \left(\frac{EI}{L}\right)\left(\frac{1}{R_1}\right)\phi_3}\right] \tag{3.20}$$

By applying a unit rotation at the end i, the following differential equation is given

$$EIy'' = \left(\frac{M_1 + M_2}{L}\right)x - M_1 - Py \tag{3.21}$$

The boundary conditions are

(a) at $x = 0$, $y = 0$ (3.22)

(b) at $x = 0$, $y' = 1 - \theta_x = 1 - \left(\frac{M_1}{R_1}\right)$ (3.23)

(c) at $x = L$, $y = 0$ (3.24)

(d) at $x = L$, $y' = 0$ (3.25)

The same procedure is applied and the end moments are given as

$$M_1 = \frac{EI}{L^2}\left[\frac{\phi_3}{\phi_6 + \left(\frac{EI}{L}\right)\left(\frac{1}{R_1}\right)\phi_3}\right] \tag{3.26}$$

and

$$M_2 = \frac{EI}{L^2}\left[\frac{\phi_4}{\phi_6 + \left(\frac{EI}{L}\right)\left(\frac{1}{R_1}\right)\phi_3}\right] \tag{3.27}$$

From equilibrium, the end shears can be calculated as

$$V_1 = V_2 = \frac{EI}{L^3}\left[\frac{\phi_2}{\phi_6 + \left(\frac{EI}{L}\right)\left(\frac{1}{R_1}\right)\phi_3}\right] \tag{3.28}$$

By applying unit displacements in the respective directions of the other degrees of freedom, the remaining elements in the member stiffness matrix can be derived. The full stiffness matrix $[K_m]_2$ for member Type 2 is given as

$$[K_m]_2 = \lambda \begin{bmatrix} \frac{AL^2}{I} & 0 & 0 & -\frac{AL^2}{I} & 0 & 0 \\ 0 & \left(\frac{\phi_1+\rho_1\phi_5}{\phi_6+\rho_1\phi_3}\right) & L\left(\frac{\phi_2}{\phi_6+\rho_1\phi_3}\right) & 0 & -\left(\frac{\phi_1+\rho_1\phi_5}{\phi_6+\rho_1\phi_3}\right) & L\left(\frac{\phi_2+\rho_1\phi_1}{\phi_6+\rho_1\phi_3}\right) \\ 0 & L\left(\frac{\phi_2}{\phi_6+\rho_1\phi_3}\right) & L^2\left(\frac{\phi_3}{\phi_6+\rho_1\phi_3}\right) & 0 & -L\left(\frac{\phi_2}{\phi_6+\rho_1\phi_3}\right) & L^2\left(\frac{\phi_4}{\phi_6+\rho_1\phi_3}\right) \\ -\frac{AL^2}{I} & 0 & 0 & \frac{AL^2}{I} & 0 & 0 \\ 0 & -\left(\frac{\phi_1+\rho_1\phi_5}{\phi_6+\rho_1\phi_3}\right) & -L\left(\frac{\phi_2}{\phi_6+\rho_1\phi_3}\right) & 0 & \left(\frac{\phi_1+\rho_1\phi_5}{\phi_6+\rho_1\phi_3}\right) & -L\left(\frac{\phi_2+\rho_1\phi_1}{\phi_6+\rho_1\phi_3}\right) \\ 0 & L\left(\frac{\phi_2+\rho_1\phi_1}{\phi_6+\rho_1\phi_3}\right) & L^2\left(\frac{\phi_4}{\phi_6+\rho_1\phi_3}\right) & 0 & -L\left(\frac{\phi_2+\rho_1\phi_1}{\phi_6+\rho_1\phi_3}\right) & L^2\left(\frac{\phi_3+\rho_1\phi_1}{\phi_6+\rho_1\phi_3}\right) \end{bmatrix} \tag{3.29}$$

where:

$$\rho_1 = \left(\frac{EI}{L}\right)\left(\frac{1}{R_1}\right) \tag{3.30}$$

The functions $\phi_1,\ldots,\phi_7$ are given in Table 3.2

The presence of the spring at the end i affects the stiffness elements for moments and shear in proportion to the value of ρ_1. The secondary order effects are built in the functions previously defined in Table 3.2. A comparison between Type 1 and Type 2 shows that Type 1 is a special case of Type 2. If the stiffness of the spring at the member end i is very high, R_1 approaches infinity and the end becomes

practically fixed. ρ_1 then approaches to zero, and the stiffness matrix $[K_m]_2$ of Type 2 reduces to the stiffness matrix $[K_m]_1$ of Type 1.

3.3.3 Type 3 (Fixed - Spring)

Member Type 3 is the opposite mirror of Type 2 as seen from their end conditions. Its boundary conditions are a fixed support at end *i* and an elastic rotational spring of stiffness R_2 at end *j*. Also, the moment and shear coefficients are affected by the value of ρ_2. But, it must be noted that these coefficients are not simply switched to obtain Type 3 from Type 2, as the sign of forces must be considered. For this member type, the stiffness matrix is given as

$$[K_m]_3 = \lambda \begin{bmatrix} \frac{AL^2}{I} & 0 & 0 & -\frac{AL^2}{I} & 0 & 0 \\ 0 & \left(\frac{\phi_1+\rho_2\phi_5}{\phi_6+\rho_2\phi_3}\right) & L\left(\frac{\phi_2+\rho_2\phi_1}{\phi_6+\rho_2\phi_3}\right) & 0 & -\left(\frac{\phi_1+\rho_2\phi_5}{\phi_6+\rho_2\phi_3}\right) & -L\left(\frac{\phi_2}{\phi_6+\rho_2\phi_3}\right) \\ 0 & L\left(\frac{\phi_2+\rho_2\phi_1}{\phi_6+\rho_2\phi_3}\right) & L^2\left(\frac{\phi_3+\rho_2\phi_1}{\phi_6+\rho_2\phi_3}\right) & 0 & -L\left(\frac{\phi_2+\rho_2\phi_1}{\phi_6+\rho_2\phi_3}\right) & L^2\left(\frac{\phi_4}{\phi_6+\rho_2\phi_3}\right) \\ -\frac{AL^2}{I} & 0 & 0 & \frac{AL^2}{I} & 0 & 0 \\ 0 & -\left(\frac{\phi_1+\rho_2\phi_5}{\phi_6+\rho_2\phi_3}\right) & -L\left(\frac{\phi_2+\rho_2\phi_1}{\phi_6+\rho_2\phi_3}\right) & 0 & \left(\frac{\phi_1+\rho_2\phi_5}{\phi_6+\rho_2\phi_3}\right) & -L\left(\frac{\phi_2}{\phi_6+\rho_2\phi_3}\right) \\ 0 & -L\left(\frac{\phi_2}{\phi_6+\rho_2\phi_1}\right) & L^2\left(\frac{\phi_4}{\phi_6+\rho_2\phi_3}\right) & 0 & -L\left(\frac{\phi_2}{\phi_6+\rho_2\phi_3}\right) & L^2\left(\frac{\phi_3}{\phi_6+\rho_2\phi_3}\right) \end{bmatrix} \tag{3.31}$$

where:

$$\rho_2 = \left(\frac{EI}{L}\right)\left(\frac{1}{R_2}\right) \tag{3.32}$$

3.3.4 Type 4 (Hinged - Fixed)

Member Type 4 has a true hinge at the end i and a fixed support at the other end. Also, Type 4 can be considered as a special case of Type 2. If the connection stiffness of Type 2 is so flexible to be considered practically as a hinge connection, then R_1 tends to zero as ρ_1 approaches infinity. As a result, Type 2 is reduced to Type 4 and the term ρ_1 will vanish. Thus, the stiffness matrix becomes

$$[K_m]_4 = \lambda \begin{bmatrix} \frac{AL^2}{I} & 0 & 0 & -\frac{AL^2}{I} & 0 & 0 \\ 0 & \left(\frac{\phi_5}{\phi_3}\right) & 0 & 0 & -\left(\frac{\phi_5}{\phi_3}\right) & L\left(\frac{\phi_1}{\phi_3}\right) \\ 0 & 0 & 0 & 0 & 0 & 0 \\ -\frac{AL^2}{I} & 0 & 0 & \frac{AL^2}{I} & 0 & 0 \\ 0 & -\left(\frac{\phi_5}{\phi_3}\right) & 0 & 0 & \left(\frac{\phi_5}{\phi_3}\right) & -L\left(\frac{\phi_1}{\phi_3}\right) \\ 0 & L\left(\frac{\phi_1}{\phi_3}\right) & 0 & 0 & -L\left(\frac{\phi_1}{\phi_3}\right) & L^2\left(\frac{\phi_1}{\phi_3}\right) \end{bmatrix} \tag{3.33}$$

Since a true hinge exists at the end i, it is noted that the coefficients of the third column and the third row equal to zero which are related to the moment at the end i (the true hinge).

3.3.5 Type 5 (Fixed - Hinged)

The member Type 5 is a mirror of member Type 4, but with a true hinge at the end j. Again it is a special case of Type 3 if the spring is very soft with no rotational stiffness. The stiffness matrix is given as

$$[K_m]_5 = \lambda \begin{bmatrix} \frac{AL^2}{I} & 0 & 0 & -\frac{AL^2}{I} & 0 & 0 \\ 0 & \left(\frac{\phi_5}{\phi_3}\right) & L\left(\frac{\phi_1}{\phi_3}\right) & 0 & -\left(\frac{\phi_5}{\phi_3}\right) & 0 \\ 0 & L\left(\frac{\phi_1}{\phi_3}\right) & L^2\left(\frac{\phi_1}{\phi_3}\right) & 0 & L\left(\frac{\phi_1}{\phi_3}\right) & 0 \\ -\frac{AL^2}{I} & 0 & 0 & \frac{AL^2}{I} & 0 & 0 \\ 0 & -\left(\frac{\phi_5}{\phi_3}\right) & -L\left(\frac{\phi_1}{\phi_3}\right) & 0 & \left(\frac{\phi_5}{\phi_3}\right) & 0 \\ 0 & 0 & 0 & 0 & 0 & 0 \end{bmatrix} \tag{3.34}$$

For this member type the elements of the sixth column and row are equal to zero.

3.3.6 Type 6 (Spring - Hinged)

For Type 6 the rotational spring exists at the end *i* and a true hinge is at the end *j*.

$$[K_m]_6 = \lambda \begin{bmatrix} \frac{AL^2}{I} & 0 & 0 & -\frac{AL^2}{I} & 0 & 0 \\ 0 & \left(\frac{\phi_5 - \rho_1\phi_1\phi_7}{\phi_3 + \rho_1\phi_1}\right) & L\left(\frac{\phi_1}{\phi_3 + \rho_1\phi_1}\right) & 0 & -\left(\frac{\phi_5 - \rho_1\phi_1\phi_7}{\phi_3 + \rho_1\phi_1}\right) & 0 \\ 0 & L\left(\frac{\phi_1}{\phi_3 + \rho_1\phi_1}\right) & L^2\left(\frac{\phi_1}{\phi_3 + \rho_1\phi_1}\right) & 0 & -L\left(\frac{\phi_1}{\phi_3 + \rho_1\phi_1}\right) & 0 \\ -\frac{AL^2}{I} & 0 & 0 & \frac{AL^2}{I} & 0 & 0 \\ 0 & -\left(\frac{\phi_5 - \rho_1\phi_1\phi_7}{\phi_3 + \rho_1\phi_1}\right) & -L\left(\frac{\phi_1}{\phi_3 + \rho_1\phi_1}\right) & 0 & \left(\frac{\phi_5 - \rho_1\phi_1\phi_7}{\phi_3 + \rho_1\phi_1}\right) & 0 \\ 0 & 0 & 0 & 0 & 0 & 0 \end{bmatrix} \tag{3.35}$$

Comparing Type 6 to Type 5, it can be noticed that giving the connection of Type 6 a high stiffness will transform it to Type 5 member (ρ_1 will be zero).

3.3.7 Type 7 (Hinged - Spring)

Type 7 represents a member with a true hinge at the end i and a spring at the end j. For this element the stiffness matrix is given as

$$[K_m]_7 = \lambda \begin{bmatrix} \frac{AL^2}{I} & 0 & 0 & -\frac{AL^2}{I} & 0 & 0 \\ 0 & \left(\frac{\phi_5 - \rho_2\phi_1\phi_7}{\phi_3 + \rho_2\phi_1}\right) & 0 & 0 & -\left(\frac{\phi_5 - \rho_2\phi_1\phi_7}{\phi_3 + \rho_2\phi_1}\right) & L\left(\frac{\phi_1}{\phi_3 + \rho_2\phi_1}\right) \\ 0 & 0 & 0 & 0 & 0 & 0 \\ -\frac{AL^2}{I} & 0 & 0 & \frac{AL^2}{I} & 0 & 0 \\ 0 & -\left(\frac{\phi_5 - \rho_2\phi_1\phi_7}{\phi_3 + \rho_2\phi_1}\right) & 0 & 0 & \left(\frac{\phi_5 - \rho_2\phi_1\phi_7}{\phi_3 + \rho_2\phi_1}\right) & -L\left(\frac{\phi_1}{\phi_3 + \rho_2\phi_1}\right) \\ 0 & L\left(\frac{\phi_1}{\phi_3 + \rho_2\phi_1}\right) & 0 & 0 & -L\left(\frac{\phi_1}{\phi_3 + \rho_2\phi_1}\right) & L^2\left(\frac{\phi_1}{\phi_3 + \rho_2\phi_1}\right) \end{bmatrix} \tag{3.36}$$

Again, the substitution of ρ_2 with zero in Type 7 results in Type 4 which illustrates the case of very stiff connection at the end j.

3.3.8 Type 8 (Hinged - Hinged)

Member Type 8 represents a link member with hinges at both ends. No resistance to moment exists for these members which leads to zero shear also.

$$[K_m]_8 = \lambda \begin{bmatrix} \frac{AL^2}{I} & 0 & 0 & -\frac{AL^2}{I} & 0 & 0 \\ 0 & 0 & 0 & 0 & 0 & 0 \\ 0 & 0 & 0 & 0 & 0 & 0 \\ -\frac{AL^2}{I} & 0 & 0 & \frac{AL^2}{I} & 0 & 0 \\ 0 & 0 & 0 & 0 & 0 & 0 \\ 0 & 0 & 0 & 0 & 0 & 0 \end{bmatrix} \tag{3.37}$$

It has to be noted that all the derived stiffness matrices $[K_m]$ are symmetric as expected.

3.4 STRUCTURAL STIFFNESS MATRIX

For a two-dimensional frame, a transformation is required to transform the member stiffness matrix from local axes to global axes. The structural (global) stiffness matrix is constructed by multiplying every member stiffness matrix by its rotation transformation matrix T_T which depends on the original orientation of the member [61] and it has the following form

$$[T_T]=\begin{bmatrix} T & 0 \\ 0 & T \end{bmatrix} \tag{3.38}$$

where

$$[T]=\begin{bmatrix} \cos\gamma & \sin\gamma & 0 \\ -\sin\gamma & \cos\gamma & 0 \\ 0 & 0 & 1 \end{bmatrix}=\begin{bmatrix} c & s & 0 \\ -s & c & 0 \\ 0 & 0 & 1 \end{bmatrix} \tag{3.39}$$

thus

$$[T_T]=\begin{bmatrix} c & s & 0 & 0 & 0 & 0 \\ -s & c & 0 & 0 & 0 & 0 \\ 0 & 0 & 1 & 0 & 0 & 0 \\ 0 & 0 & 0 & c & s & 0 \\ 0 & 0 & 0 & -s & c & 0 \\ 0 & 0 & 0 & 0 & 0 & 1 \end{bmatrix} \tag{3.40}$$

where:

γ = the angle between the local and global x-axis

s = $\sin\gamma$

c = $\cos\gamma$

And the member stiffness matrix in structural (global) axes $[K_{ms}]$ is given as:

$$[K_{ms}] = [T_T^T][K_m][T_T] \tag{3.41}$$

The overall stiffness matrix $[K]$ is constructed by assembling the structural stiffness matrices of the members of a discretized structure in their appropriate locations.

3.5 TRANSITION BETWEEN MEMBER TYPES

During the analysis the load is applied incrementally to consider the nonlinearity resulting from the spring connections as well as the second-order effects. At a high load level when the spring reaches its limiting moment capacity, the connection cannot resist any additional moment. The spring is transformed to an imaginary hinge in the next load step. Also, an internal hinge can develop at a nodal point due to yielding of the section. The yield criterion is based on the interaction between the total applied moment and the total applied axial force and is taken as [3]

$$\frac{P}{P_y} + \frac{M}{1.18M_p} \leq 1.0 \tag{3.42}$$

where

P = the axial force in the member

M = the bending moment

P_y = the plastic capacity of the member under axial force only = $F_y A$

M_p = the plastic moment of the member = $F_y Z_p$

The transition between different member types is indicated in Fig. 3.5.

3.6 MATHEMATICAL MODEL

From the experimental results, appropriate mathematical expression for the nonlinear moment-rotation response is developed for use in the analytical study. Such an expression is derived in Chapter 7 based on the best fitting without losing the characteristic shape of the moment-rotation plots.

3.7 METHOD OF ANALYSIS

The beams and columns of a single story, single bay frame are considered as laterally supported so as to preclude premature lateral buckling prior to collapse of the frame. Each member is represented as a beam-column member with its individual stiffness and the connections are idealized as special spring elements. The load is applied incrementally in steps up to the failure. The failure modes will be either by ***frame instability*** due to columns buckling or the formation of a mechanism which will lead

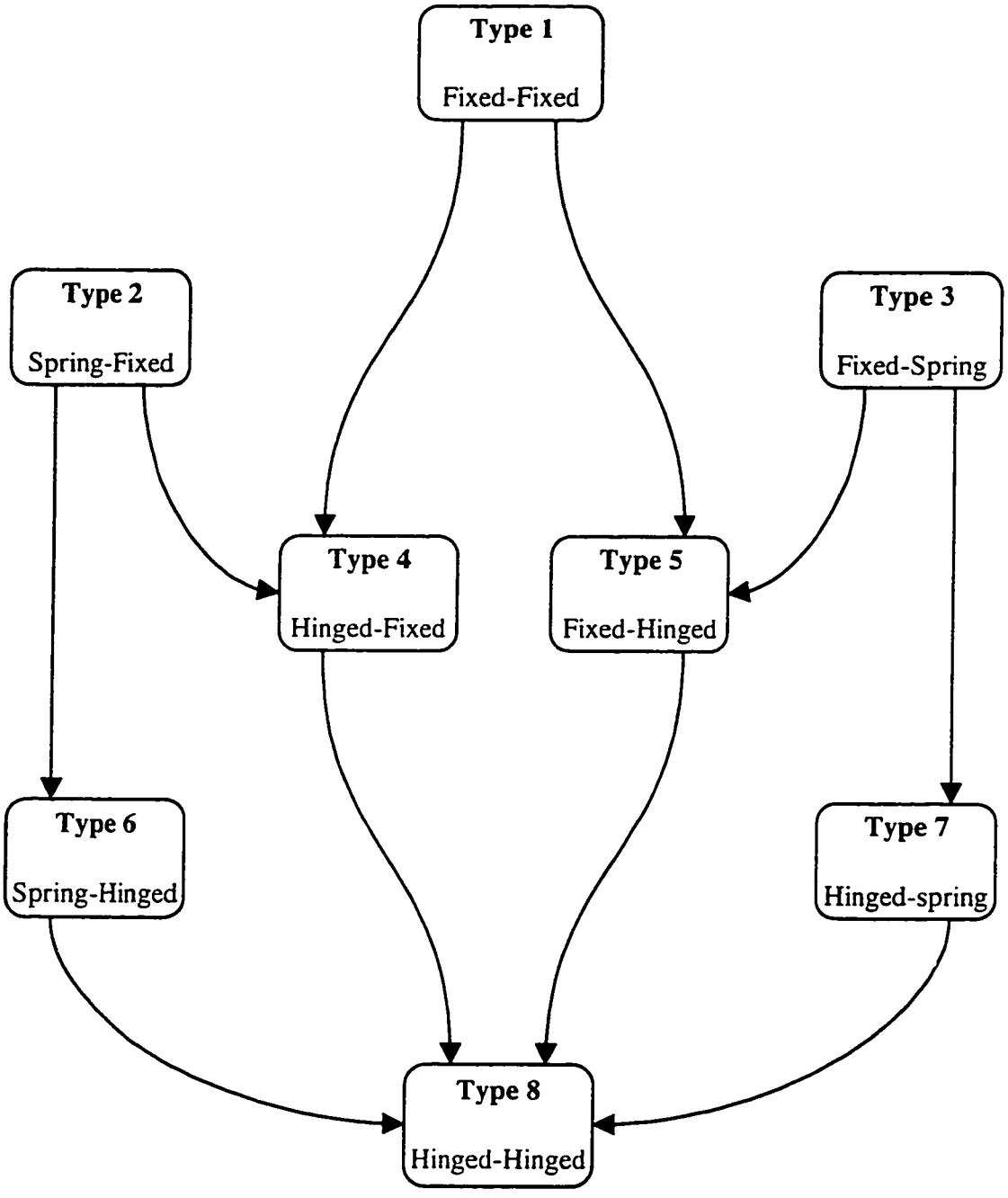

Figure 3.5 Transition Between Different Member Types

to ***plastic collapse***. During the analysis, the stiffness matrix changes continuously due to the effect of axial forces, connection flexibility and the lateral sway. The computerized solution algorithm is presented in Chapter 4.

It is clear that the elements of the matrix K_{ms} can be evaluated only when the axial force P in the member is known. For a given load vector $\{F\}$, the displacement vector $\{\delta\}$ is found by solving the equation

$$\{\delta\} = [K]^{-1}\{F\} \tag{3.43}$$

This equation is a ***nonlinear equation*** and can not be solved directly at a load level. The nonlinearity comes from two sources: (a) the nonlinear spring stiffness and (b) the second-order effects due to the member axial force P. Since the problem is highly nonlinear, the solution is achieved in incremental steps. For each step, an incremental load is applied on the structure and the corresponding displacements are found after getting the required tolerance for the convergence on the axial force and the spring stiffness. At the end of each step the total load, total displacements and total actions are calculated.

The iterative solution procedure is summarized in the following steps:

1. Apply an incremental external load $\{\Delta F_1\}$ on the structure.

2. Assume an initial, trial value of axial force $\{\Delta P\}$ in each member in the first cycle, as it is required to construct the member stiffness matrix. These axial forces are updated in each iterative cycle.

3. Using the assumed axial forces and the given initial rotation stiffness R_i of the semi-rigid connections, construct the member stiffness matrix according to the member type.

4. Construct the global stiffness matrix $[K]$ by assembling the individual member stiffness matrices.

5. Solve the system of equations $\{\Delta F_i\} = [K]\{\Delta \delta_i\}$ for the unknown displacements corresponding to $\{\Delta F_i\}$.

6. Obtain the displacements $\{\Delta \delta\}$ and the new axial forces $\{\Delta P\}$ in members.

7. After the first cycle, the axial force $\{P\}$ will be equal to $\{\Delta P\}$.

8. Check the convergence on the axial force: if $\sum_{i=1}^{m} \frac{(P_{old} - P_{new})^2}{P_{old}^2}$ is larger than the required tolerance, where m is the number of members, then go to step 3 with the new set of axial forces to obtain a new set of $\{P\}$. The procedure is repeated until the convergence criterion for $\{P\}$ is satisfied. The convergence for $\{P\}$ is very rapid and it requires only few cycles.

9. Obtain the total converged values of $\{\delta_1\}$, $\{P_1\}$ and $\{M_1\}$ corresponding to $\{\Delta F_1\}$.

10. From the spring model, calculate the connection rotation θ_1 at M_1. The connection stiffness at $\{\Delta F_1\}$ is then given as $R_1 = \frac{M_1}{\theta_1}$.

11. Increase the external load by an increment $\{\Delta F_j\}$ where j is the new cycle number. The total applied load becomes $\{F_j\} = \{F_{j-1}\} + \{\Delta F_j\}$.

12. Construct the stiffness matrix $[K]$ which is a function of $\{P_{j-1}\}$ and R_{j-1} obtained from the previous cycle (cycle j-1).

13. Check if the determinant of the stiffness matrix $[K]$ is less than or equal zero, then the failure load is obtained by buckling mode and stop the analysis.

14. Apply the external force $\{\Delta F_j\}$ and solve the system of equations $\{\Delta F_j\} = [K]\{\Delta \delta_j\}$.

15. Obtain $\{\Delta \delta_j\}$ then $\{\Delta P_j\}$ for all members and ΔM_j at the semi-rigid connection.

16. Calculate the total axial forces $\{P_j\} = \{P_{j-1}\} + \{\Delta P_j\}$.

17. Check the convergence on $\{P_j\}$ then calculate the total moments $\{M_j\}=\{M_{j-1}\}+\{\Delta M_j\}$.

18. Compute $R_{j+1}=\dfrac{M_j-M_{j-1}}{\theta_j-\theta_{j-1}}$ for the semi-rigid connection.

19. If the ratio $\dfrac{R_{j+1}-R_j}{R_{j+1}}$ is greater than the required tolerance then go to step 12 using the new connection stiffness $R_j = R_{j+1}$.

20. After the convergence is obtained, apply the interaction equation $\dfrac{P_j}{P_y}+\dfrac{M_j}{1.18M_p}\le 1.0$ at each joint. With the development of a hinge, the member stiffness and hence the code number will change.

21. If no failure is detected, go to step 11 and continue until the collapse load is obtained.

22. Check the total number of the plastic hinges, and if a mechanism is formed, stop the program and the failure is obtained by plastic mechanism collapse mode.

The above solution procedure is coded in a computer program EPASF to readily analyze a single bay portal frame. The details of the program EPASF are given in Chapter 4.

CHAPTER 4

COMPUTER PROGRAM

4.1 GENERAL

A computer program (EPASF) has been developed for the elastic plastic analysis of semi-rigid plane frames using the stiffness method presented in Chapter 3 with a general description of its features. EPASF is written in FORTRAN code. It consists of several subprograms which are part of the main program. The program is written in the same format described by Weaver [61] and Hinton and Owen [84] for the first order analysis of rigid frames. The program takes into consideration the non-linearity resulting from the second-order effects and the connection flexibility. The program works in double precision for the accuracy of the obtained results. The units of output results are consistent with the input data units. It can be either in SI units (kilonewtons, meters and radians) or US units (kips, inches and radians).

4.2 FLOW CHART

A schematic flow chart of the main and the subprograms is shown in Fig. 4.1.

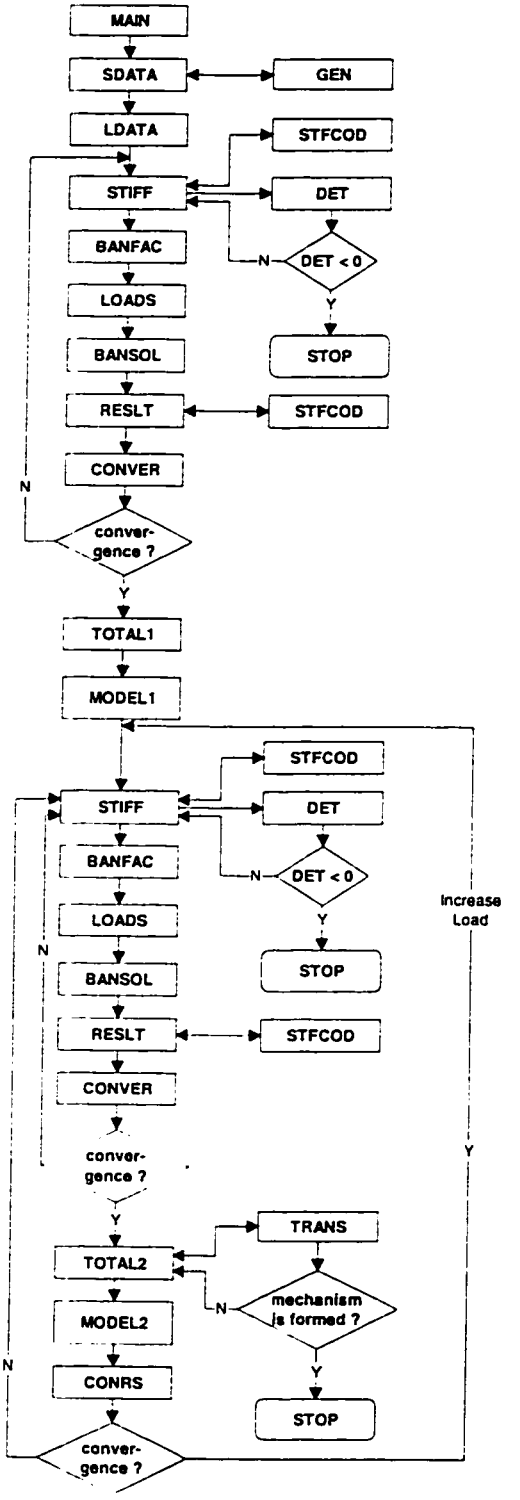

Figure 4.1 Flow Chart

4.3 MAIN PROGRAM AND SUBPROGRAMS DESCRIPTION

4.3.1 Main Program

In the main program all the used variables and arrays with their sizes are listed in COMMON declaration to be used in all the subprograms. The main program calls a series of subprograms. The arrays initialization is given in their appropriate places in the subprograms. A brief description of every subprogram is given in the following sections. A control statement is given in the program to stop the execution when the determinant of the structural stiffness matrix is equal to or less than zero or when a failure by the formation of sufficient number of plastic hinges.

4.3.2 Subprogram SDATA

In subprogram SDATA, the problem description is identified, then it reads and writes the following structural data: (a) the structural parameters composed of number of members, number of joints, number of support restraints, number of restrained joints, modulus of elasticity of the used material and initial rotational stiffness of the connections, (b) joint coordinates data for each joint consisting of the joint number as well as its x and y coordinates in structural system, (c) member information for each member which are: the member number, its incidences, member cross-section area, moment of inertia and a member code depending on the initial member type, (d) joint restraint list indicating the restrained direction for each restrained joint.

4.3.3 Subprogram GEN

Subprogram GEN generates the joints numbers and members properties with their codes, since not all of the data have to be input in subprogram SDATA to reduce the size of the input data file.

4.3.4 Subprogram LDATA

This subprogram reads and writes the load parameters which are the number of loaded joints the load intensity and its direction in the structural global system. The load is applied in incremental steps, since the solution is iterative because of the nonlinearity of the stiffness matrix.

4.3.5 Subprogram STIFF

The subprogram STIFF constructs the overall structural stiffness matrix for the frame to be analyzed. The member stiffness matrix for each member is constructed first by calling the subprogram STFCOD to calculate the corresponding stiffness matrix depending on the element type. From the direction cosines, the rotational stiffness matrix is constructed for each member. The member stiffness matrix is then multiplied by its rotation matrix to obtain the member stiffness matrix in the global direction. Depending on the numbering of joints, the overall structural stiffness matrix is constructed by placing every member stiffness matrix in its appropriate location in the global one. The global stiffness matrix is stored in the computer in a banded form

to save storage space and execution time. The program calls the subprogram DET to calculate the value of the determinant of the structural stiffness matrix.

4.3.6 Subprogram BANFAC

The factorization method is more efficient for solving a system of equations in a banded matrix form than for a filled matrix because no calculations need be made for elements outside of the band. The subprogram BANFAC factors the upper band of a symmetric matrix stored in a rectangular array. The subprogram uses the modified Cholesky method for the solution of the equation system in the banded form.

4.3.7 Subprogram LOADS

Subprogram LOADS constructs the load vector matrix from the incremental joint loads given previously in subprogram LDATA.

4.3.8 Subprogram BANSOL

It accepts the upper band of the matrix U from subprogram BANFAC and solves for the unknowns in the original system of equations by the modified Cholesky method.

4.3.9 Subprogram RESLT

This subprogram is responsible for the output of the results. It calls subprogram STFCOD then calculates and writes the following results: (a) joint displacements and support reactions in global system (b) member end actions in local system, resulting from an incremental applied load.

4.3.10 Subprogram CONVER

The convergence of the solution over the members axial forces is calculated in this subprogram. The subprogram iterates by calculating the difference of the axial forces between every two successive cycles for each member. If the ratio of the force difference to the previous axial force is less than the required tolerance limit, then the convergence is obtained.

4.3.11 Subprogram TOTAL1

It calculates the displacements, moments and axial forces by the application of the first increment of external load after the convergence on the axial force in the members. The subprogram works with the initial rotation stiffness of the connection.

4.3.12 Subprogram MODEL1

The suggested model for the non-linear moment-rotation relationship is introduced in this subprogram. The connection rotation θ is calculated as a function of the moment connection and from it the rotation stiffness R is calculated.

4.3.13 Subprogram TOTAL2

This subprogram calculates the total moments and displacements after each iteration cycle, by adding the incremental moments ΔM and displacements $\Delta\delta$ from each cycle to the total obtained from all the previous cycles. The subprogram works with the updated rotation stiffness of the connection.

4.3.14 Subprogram MODEL2

From the connection model and depending on the total moments at the connection, the relative rotation is obtained and the value of the connection stiffness changes from the initial value and a new one is obtained. The solution proceed with the new value for the next cycle.

4.3.15 Subprogram CONRS

In this subprogram, the convergence over the rotational stiffness is calculated until reaching the required accuracy by subtracting the old value from the new value and dividing by the new one as described in Chapter 3.

4.3.16 Subprogram STFCOD

In this subprogram, the member stiffness matrix is calculated in local axis system depending on the member type from the code number given for each member. This stiffness matrix is a function of the member axial force and the connection flexibility if a semi-rigid connection exist.

4.3.17 Subprogram TRANS

In subroutine TRANS the element type is modified during the execution of the program depending on the member boundary conditions. A plastic hinge can develop depending on the interaction between the moments and the axial force at the member ends. If a plastic hinge is formed at a joint after a load level, then it can not carry any additional bending moment and the boundary condition is modeled as a hinge in the

following cycles. The program stops if the number of hinges develop a mechanism and the failure is by the collapse mechanism mode.

4.3.18 Subprogram DET

It calculates the determinant of the structural stiffness matrix. The program stops when the instability is introduced by getting a vanishing determinant. At this stage the critical buckling load is reached.

CHAPTER 5

EXPERIMENTAL WORK

5.1 GENERAL

The experimental program for this research work has been designed to examine the behavior of the cap plate connection which is widely used in steel frames. Tests were conducted on ***six*** different beam-column connections with different configurations to measure the joints rotation, the beams strains and the forces in tension bolts at different load levels. The moment-rotation relationship of cap plate connections is recorded using the traditional cantilever test setup. The moment applied to the connection was calculated at the center-line of the column using static equilibrium equations.

The main parameters of the tests are the cross section of the beam, the bottom flange thickness of the beam and the bolt size. The influence of different parameters on the rotational stiffness and strength was investigated. The main objectives of the experimental work are:

(a) To develop the moment-rotation curves for the cap plate connection.

(b) To measure the force in bolts acting in tension.

(c) To examine the stress distribution in the beam at the connection.

Experimental results obtained would add valuable information to the available test data in the steel connection research area, since no data is available in the literature for this type of connection. A detailed description of the experimental program including the setup design, fabrication, instrumentation and test procedure is given in this chapter.

5.2 TEST SPECIMENS

The test specimen selected in this experiment is a cantilever subassemblage of a beam and a column, representing a portion of moment-resisting frame. The typical cantilevered beam specimen used is shown in Fig. 5.1. The size of the members were chosen in due consideration of the available test facility and to have reasonable proportions. A total of six assemblies with different beam and column section and bolt diameters were used.

5.2.1 Specimen Details

The dimensions of the six tests specimens were chosen such that the used cross-sections were compact to eliminate the effect of any local buckling during testing. Typical details of the connection assembly are shown in Fig. 5.2 and the sizes of the flange plates and web plates for the beam and column for each test are shown in Table

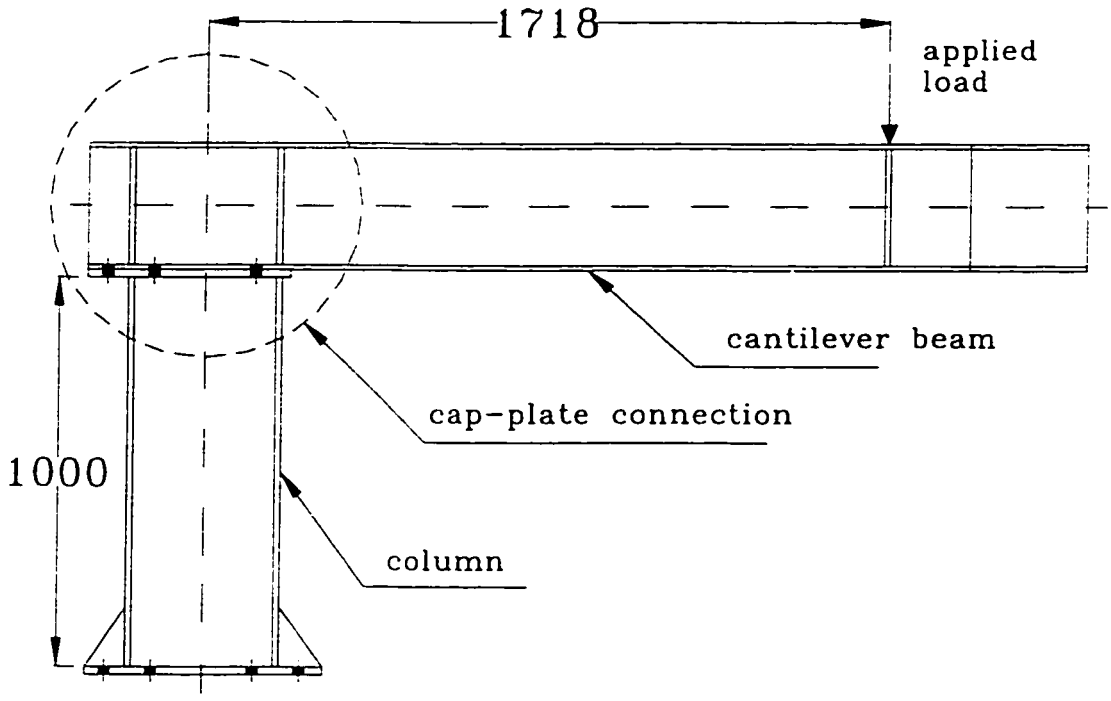

Figure 5.1 Cantilever Beam Specimen

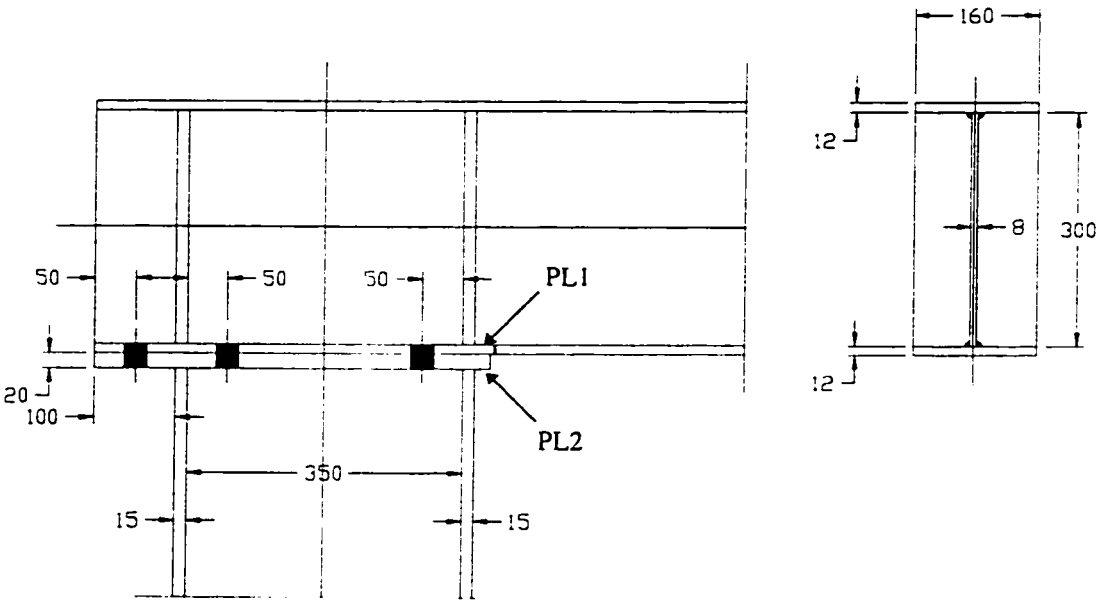

Figure 5.2 Typical Specimen Dimensions

TABLE 5.1 Specimens Description (Dimensions in mm)

	Beam			Column			
Test No.	**Flange**	**Web**	**Plate PL1**	**Flange**	**Web**	**Cap-Plate PL2**	**Bolt Diam.**
C1	160x12	300x8	160x12	200x15	350x10	200x20	19
C2	160x15	300x10	160x20	200x15	350x10	200x25	25
C3	160x12	300x8	160x20	200x15	350x10	200x25	22
C4	180x15	325x12	180x20	200x15	350x10	200x25	28
C5	180x15	325x12	180x15	200x15	350x10	200x25	28
C6	160x15	300x10	160x15	200x15	350x10	200x20	25

5.1. The members were designed in such a manner that only 3 columns would be needed to test 6 beams so as to reduce the material used for columns. Each specimen consisted of a column 1000 mm height with a cap plate welded at the top of the column. Above the column a cantilever beam 2000 mm length was fixed to the cap plate. The beam was connected to the cap plate by 6 bolts: 4 bolts in the tension side and 2 in the compression side. Vertical stiffeners were welded to the beam to prevent the web local buckling at two locations: (a) at the connection and (b) under the applied load (Fig. 5.1).

5.3 TEST SETUP

As a first part of the experimental work, a test setup was designed, constructed and installed under an existing test frame to support the assembly on the test floor of the Heavy Testing Laboratory at King Fahd University of Petroleum and Minerals (KFUPM).

5.3.1 Existing Test Frame

The existing test frame is a rigid space frame consisting of 4 large columns of 5000 mm height and 700 mm depth as shown in Fig. 5.3. The frame is fixed to a reinforced concrete reaction floor slab of 1000 mm thickness. The floor slab is provided with a grid of holes each 50 mm diameters every 1000 mm in two perpendicular directions. Each column is fixed to the floor with two rods of 50 mm diameter and 1500 mm length passing through the slab thickness. The distance between the columns' center

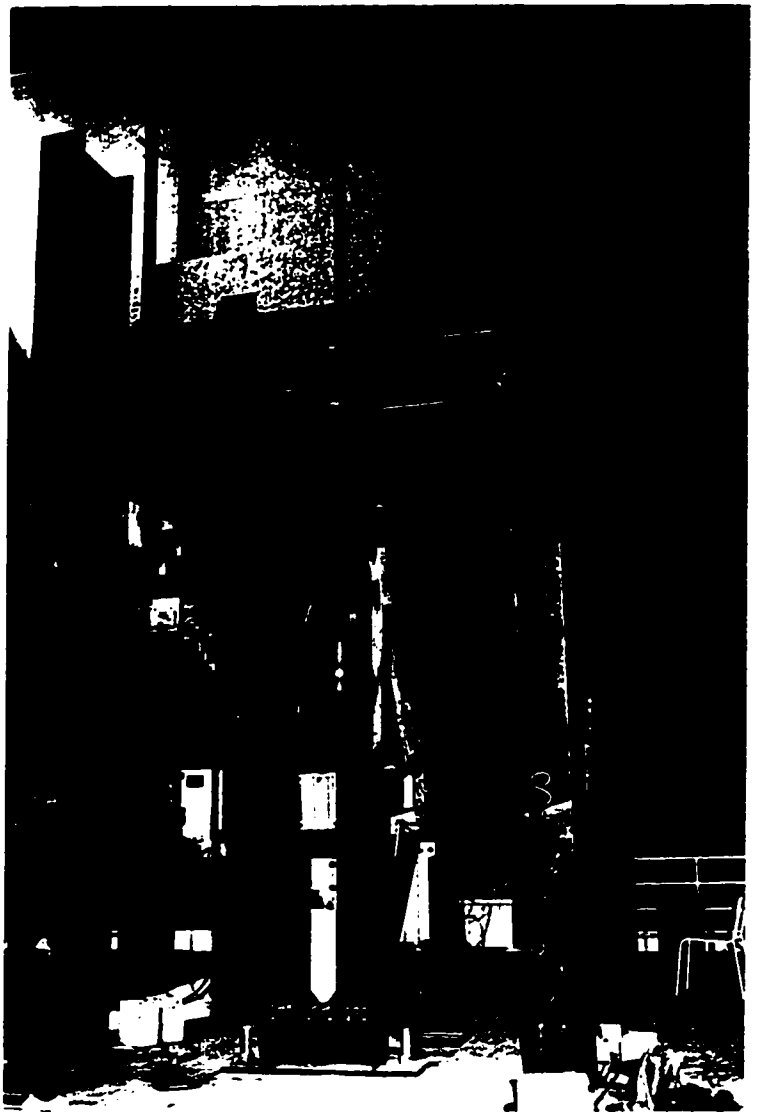

Figure 5.3 Existing Testing Frame

lines is 3000 mm in both directions. The main beams are rigidly connected with extended end plates to the columns at a height of 5000 mm above the top floor slab level. A cross beam 3000 mm length and 700 mm depth is rigidly connected to two parallel main beams. A hydraulic actuator, to apply the load during the test, is mounted on the cross beam.

5.3.2 Setup Design

From several alternatives, the following test setup was chosen to be the suitable one which fits well under the existing testing frame and uses the facilities available in the reaction floor lab. The test setup was designed to resist the applied loads during the tests without any significant deformations.

5.3.3 Support System

A special base (base 1) was designed and fabricated to be used in the test as the support system for the test specimens as shown in Figs. 5.4 and 5.5. The rigid base is built-up of :

- A bottom flange (2500 mm length, 1300 mm width and 50 mm thickness).

- A web plate (2500 mm length, 400 mm depth and 15 mm thickness).

- A top flange (2500 mm length, 400 mm width and 20 mm thickness).

- Flange stiffeners composed of channels cross section (300 mm depth).

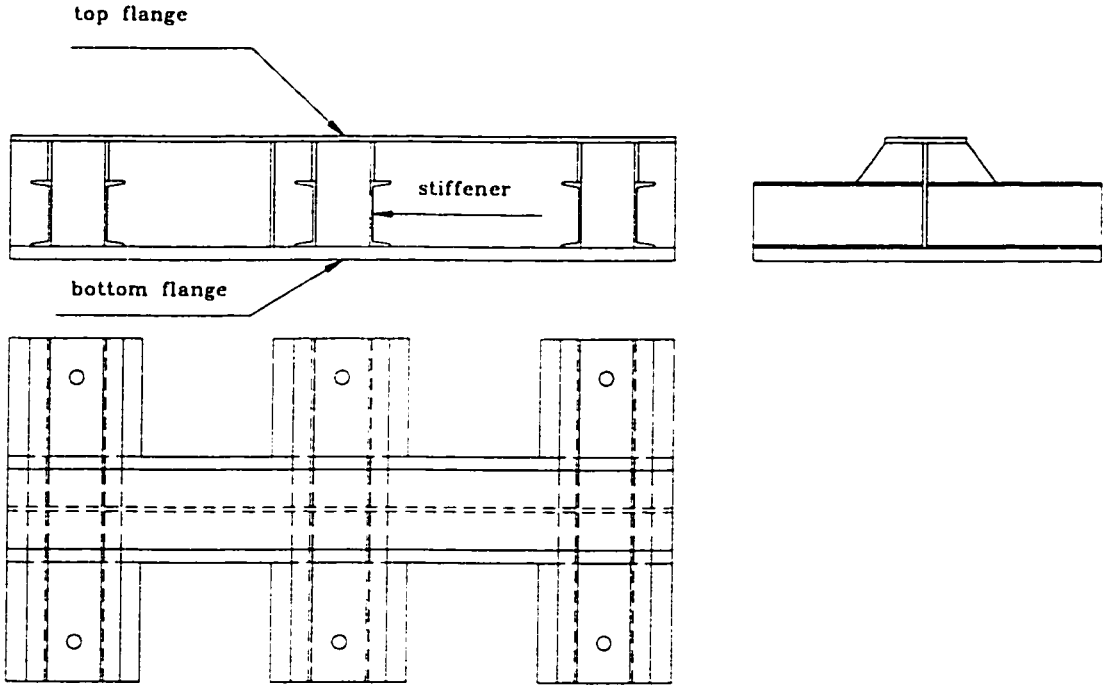

Figure 5.4 Support System (base1)

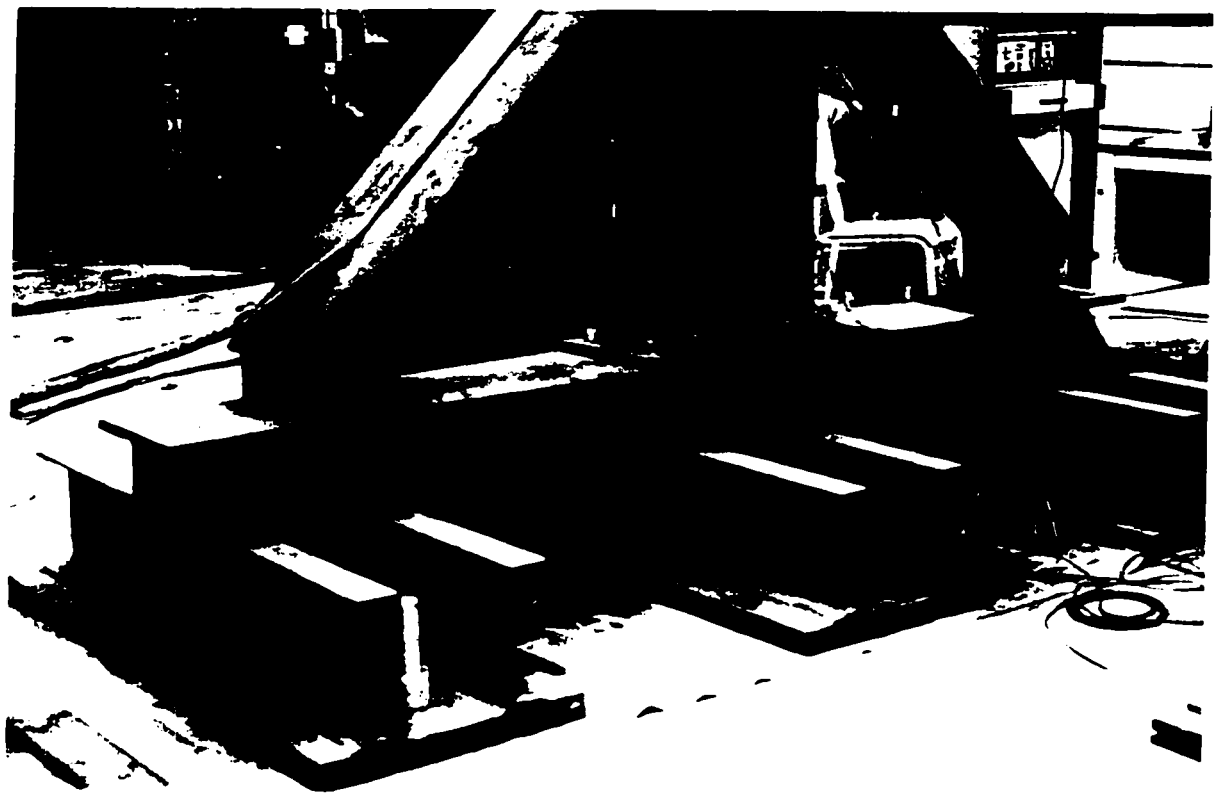

Figure 5.5 Support System (base1)

The base rests on the reaction floor slab. Holes were provided in the bottom flange base to fix it with the floor slab using six rod bolts 50 mm diameter and 1500 mm length. Three plates (1500 mm length, 400 mm width and 20 mm thickness) were installed at the bottom of the floor slab to prevent any slab crushing from the anchor bolt force. The column specimen was fixed at the bottom to the rigid base by means of 8- 25 mm diameter bolts.

The column was laterally supported by inclined double angle bracings 150 x 150 mm back to back as shown in Fig. 5.6 to minimize bending deformation in the column and to prevent the sidesway movement. To prevent the column lateral movement about its minor axis, two horizontal star shaped angles 100 x 100 mm were provided as shown in Fig. 5.6. The bracing system is shown in Fig. 5.7.

5.3.4 Lateral Support at the Beam-End

The free end of the beam is laterally supported to prevent any lateral movement of the beam tip (cantilever end) as shown in Figs. 5.8 and 5.9. A rolling system was designed at the beam tip to allow smooth vertical displacement during the test. The end framing system was built-up of a rigid base (base 2) (1200 mm length, 300 mm width and 300 mm depth) with an I-shaped cross section. Various stiffeners were provided to prevent any local buckling. The base was fixed to the floor slab by the same system described above for the main support system base (base 1).

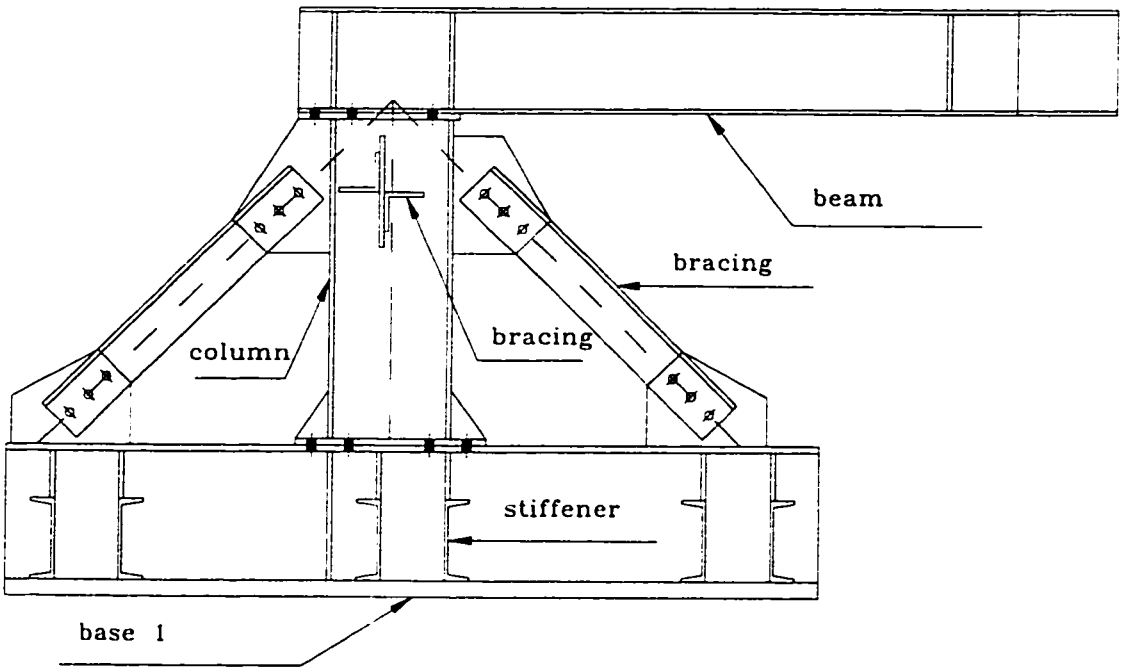

Figure 5.6 Bracing System

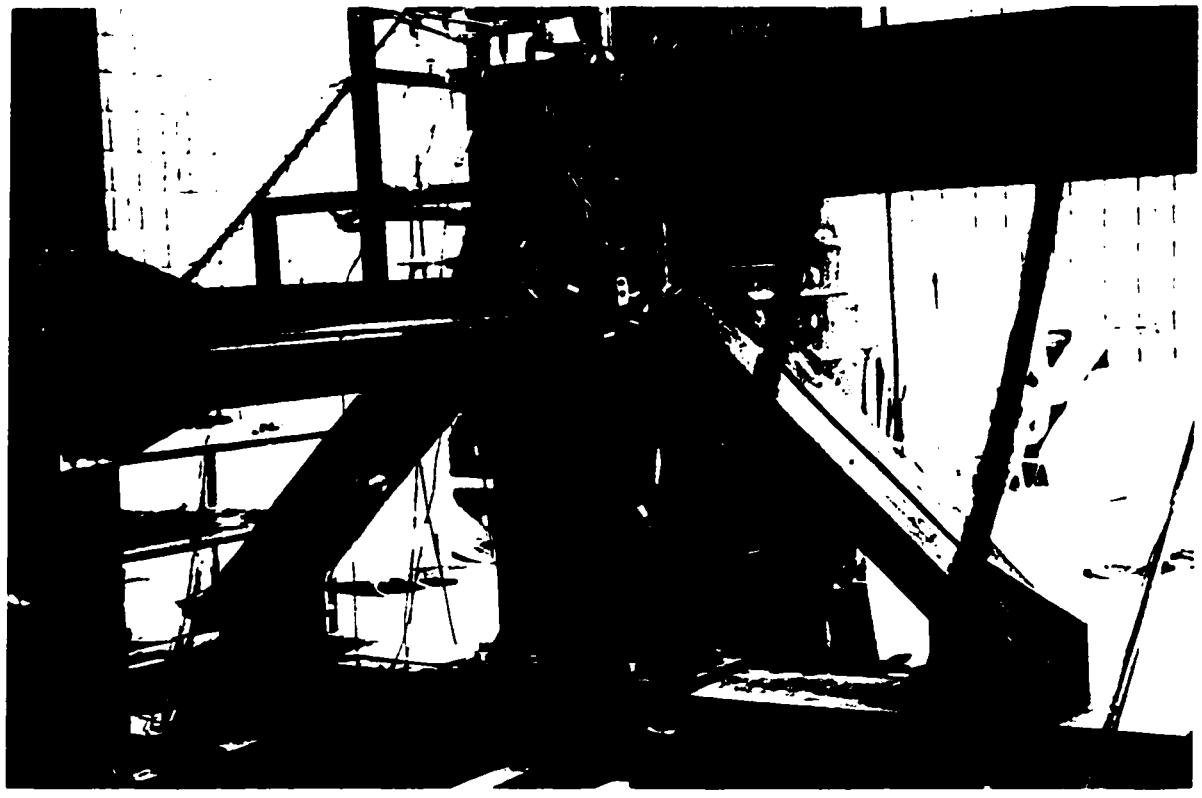

Figure 5.7 Bracing System

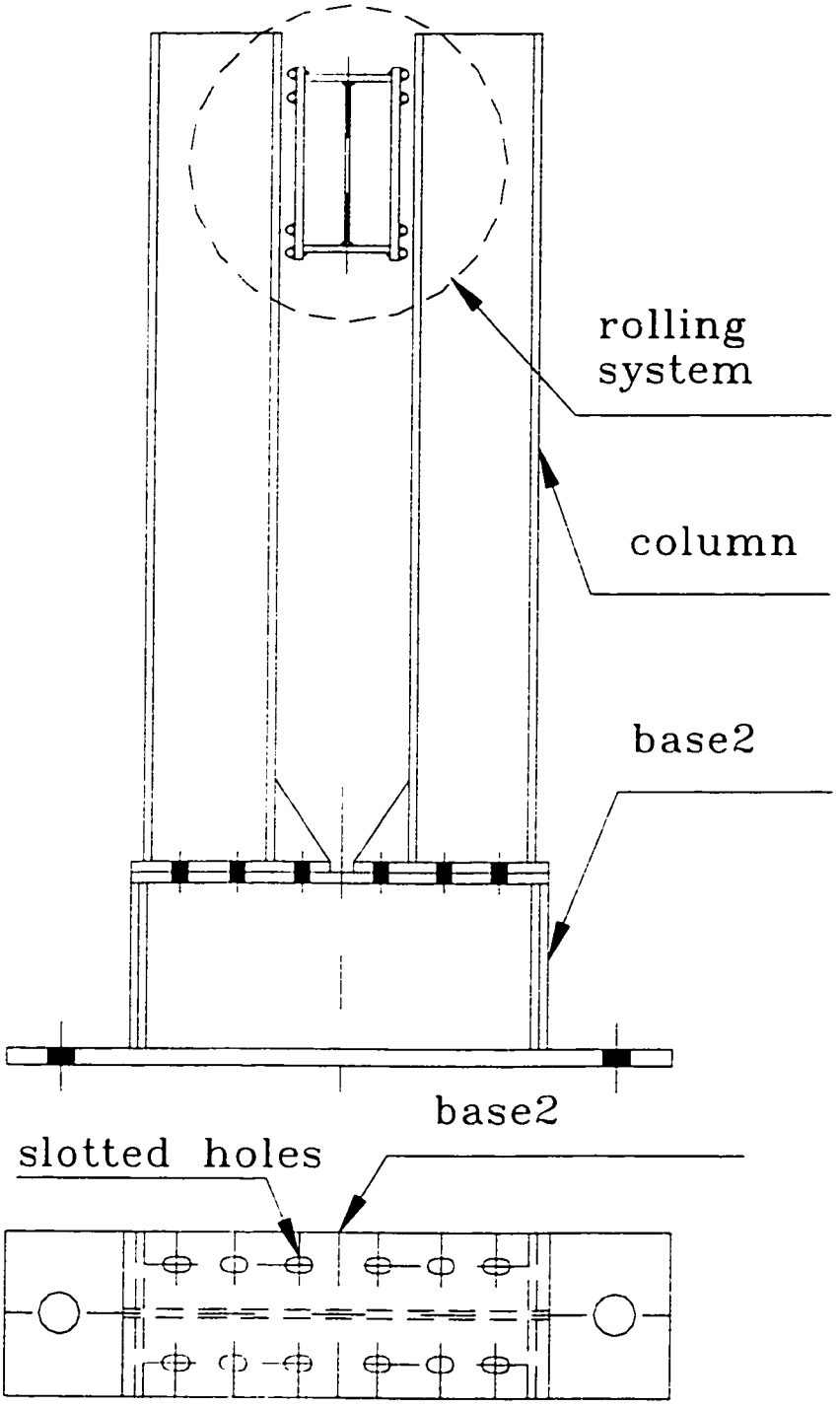

Figure 5.8 End Support System

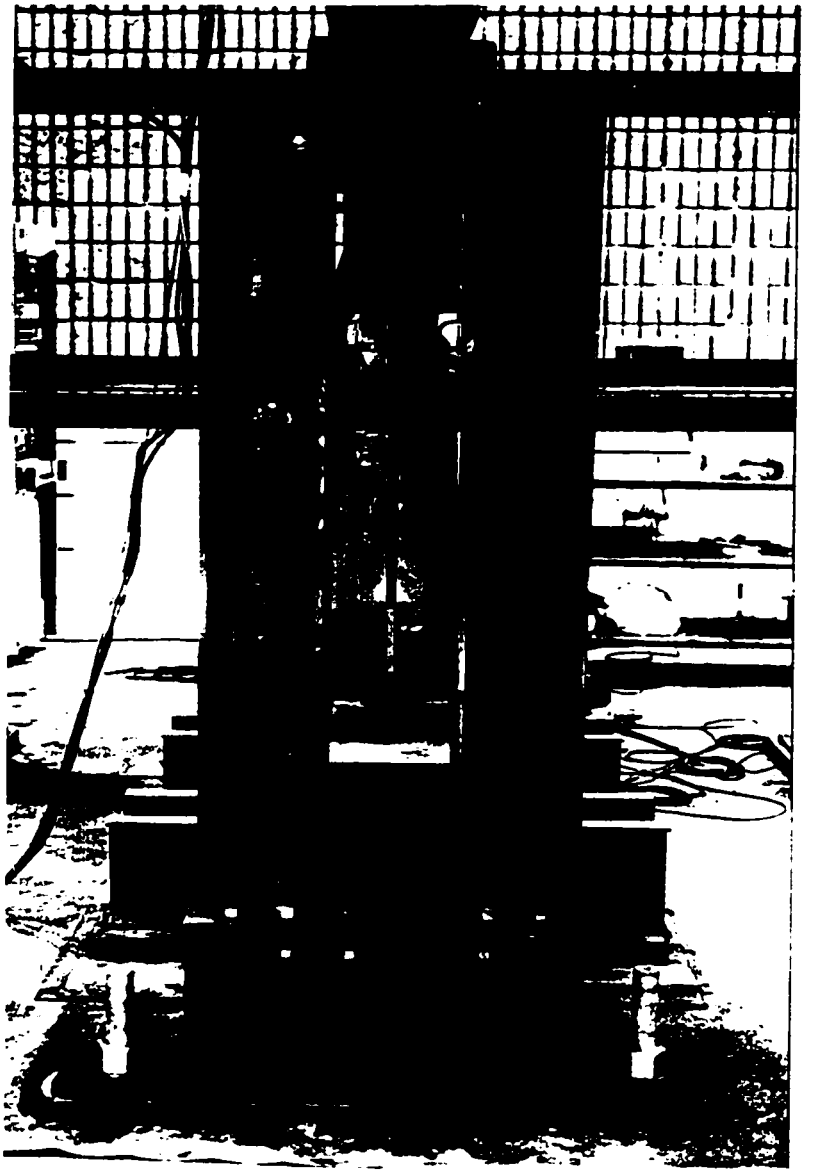

Figure 5.9 End Support System

Two vertical columns were bolted to the base to prevent the beam from any lateral displacement. The holes at the column base were slotted to allow for the columns adjustment to fit in-between different beam widths for different tests as shown in Fig. 5.10.

5.3.5 Materials Properties and Fabrication

The material used for fabricating the specimens components (beams, columns and plates) is high-strength steel (A572) according to AISC Specification. It had a minimum yield strength of 50 ksi (345 MPa) and modulus of elasticity E equal to 29,000 ksi (200,000 MPa). The bolts used for connecting the specimens are high strength bolts (confirming to ASTM A325) which are widely used in steel constructions. Bolt holes were punched 3 mm. larger than the nominal bolt diameters for clearance.

All specimens components were fabricated and supplied by Al-Zamil Steel Company in Dammam. Specimens were fabricated using the standard procedures of the company.

5.3.6 Setup Assembly and Installation

First the support base was tightly anchored to the reaction floor in its designated position under the test frame. Then, the vertical column piece was erected and its base was tightly secured to the support base. The bracings were installed, connecting the column top to the support base. The beam was connected to the column by the cap

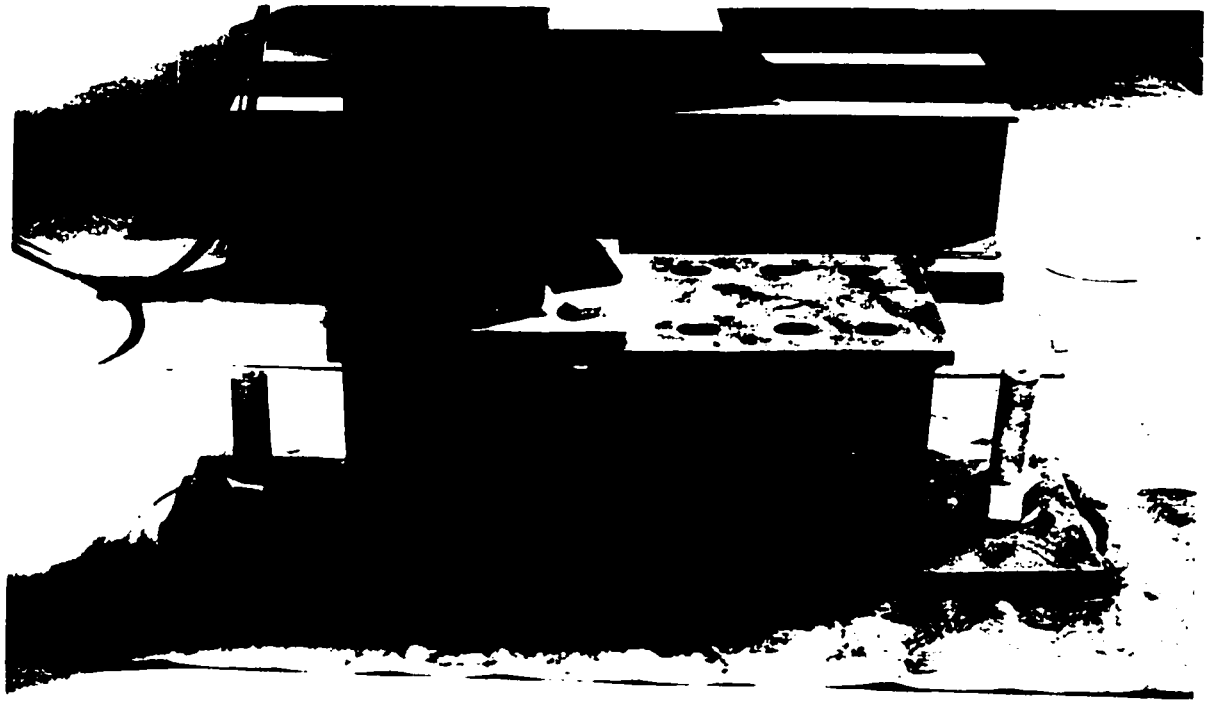

Figure 5.10 Slotted Holes for Column Adjustment

plate connection. At the free end of the beam, the lateral support system was installed, providing a nominal gap between the beam and the two vertical columns. The sides of these columns were well greased to provide a frictionless contact surface.

5.4 INSTRUMENTATION

The main requirements of the instrumentation was to measure the moment-rotation response of the connection, the forces in the tension bolts and the bending stress distribution in the beam at different cross-sections. The following instruments were used for these measurements:

(a) ***Tiltmeters*** to measure the rotation,

(b) ***LVDT***s (Linear Voltage Displacement Transducers) to measure the displacements

(c) ***Electrical Strain gages*** to measure strains.

The results were recorded automatically by multi-channel ***Data logger*** connected to a desktop ***PC***.

5.4.1 Tiltmeters

Two portable tiltmeters (Model 800P) with a resolution of 0.0001 degree were used to calculate the connection rotation directly. The first is placed vertically on the inner column flange and the second placed horizontally on the beam top flange as shown in

Figs. 5.11 and 5.12. The connection rotation is obtained directly as the relative rotation between the beam and the column.

The tiltmeters incorporate a high-precision electrolyte tilt transducer as the internal sensing element, offering resolution and sensibility previously unavailable in measuring instruments. The measured angular movement is referenced to the unchanging vertical gravity vector, eliminating time and expenses of locating an external survey datum. A low-pass filter removes the vibration effects for static measurements.

The tiltmeter operates with the Model 870 Readout Module, which powers the tiltmeter from one internal 9-volt battery. The Model 870 cable has a quarter-turn connector on the end, which mates with the connector on the tiltmeter. The tiltmeters are fixed by means of stainless steel tilt plates which are bounded to the mounting surface using steel filled epoxy adhesives.

5.4.2 Linear Voltage Displacement Transducers (LVDT)

LVDTs (CDP-25) with 25 mm travel length and a sensitivity of $500*10^{-6}$ / mm were used to measure the displacements at several locations on the beam column connection. Locations of LVDTs were indicated in Figs. 5.12 and 5.13. The measured displacements are divided by the distance between the LVDTs to calculate the rotation indirectly.

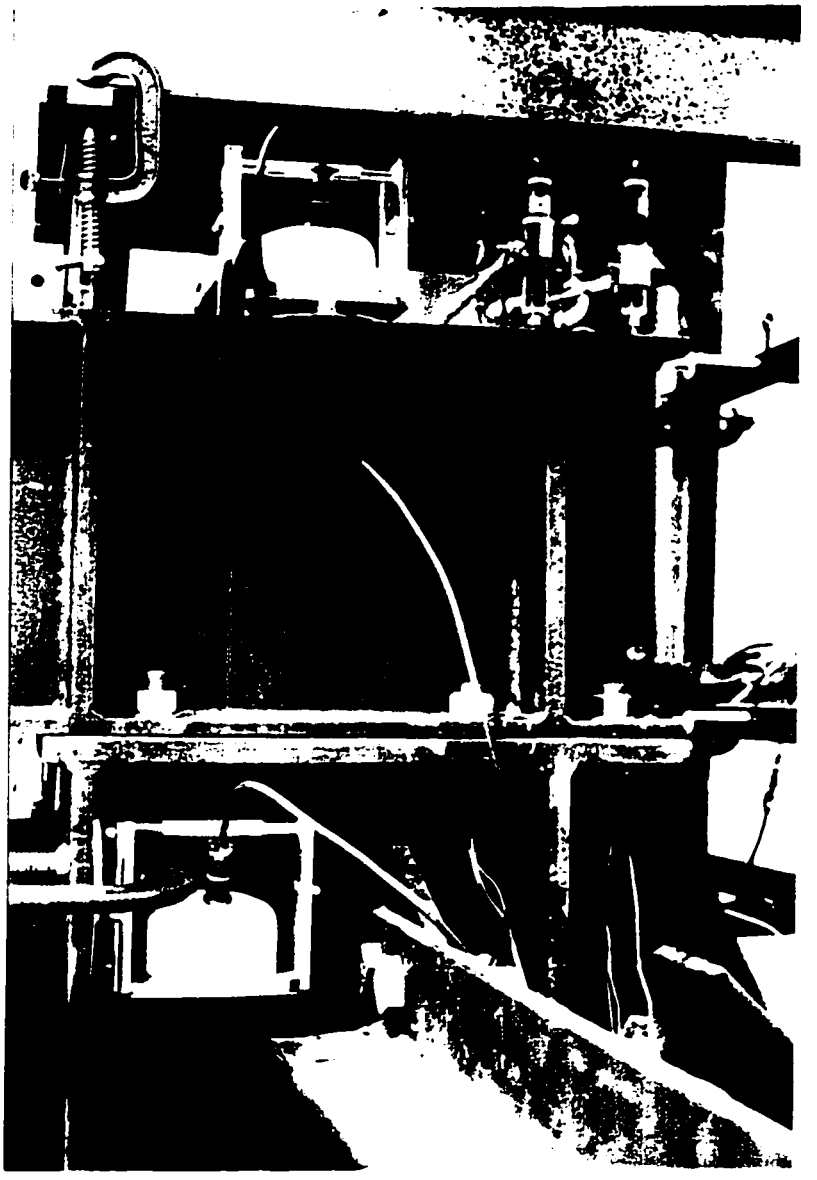

Figure 5.11 Tiltmeters Locations

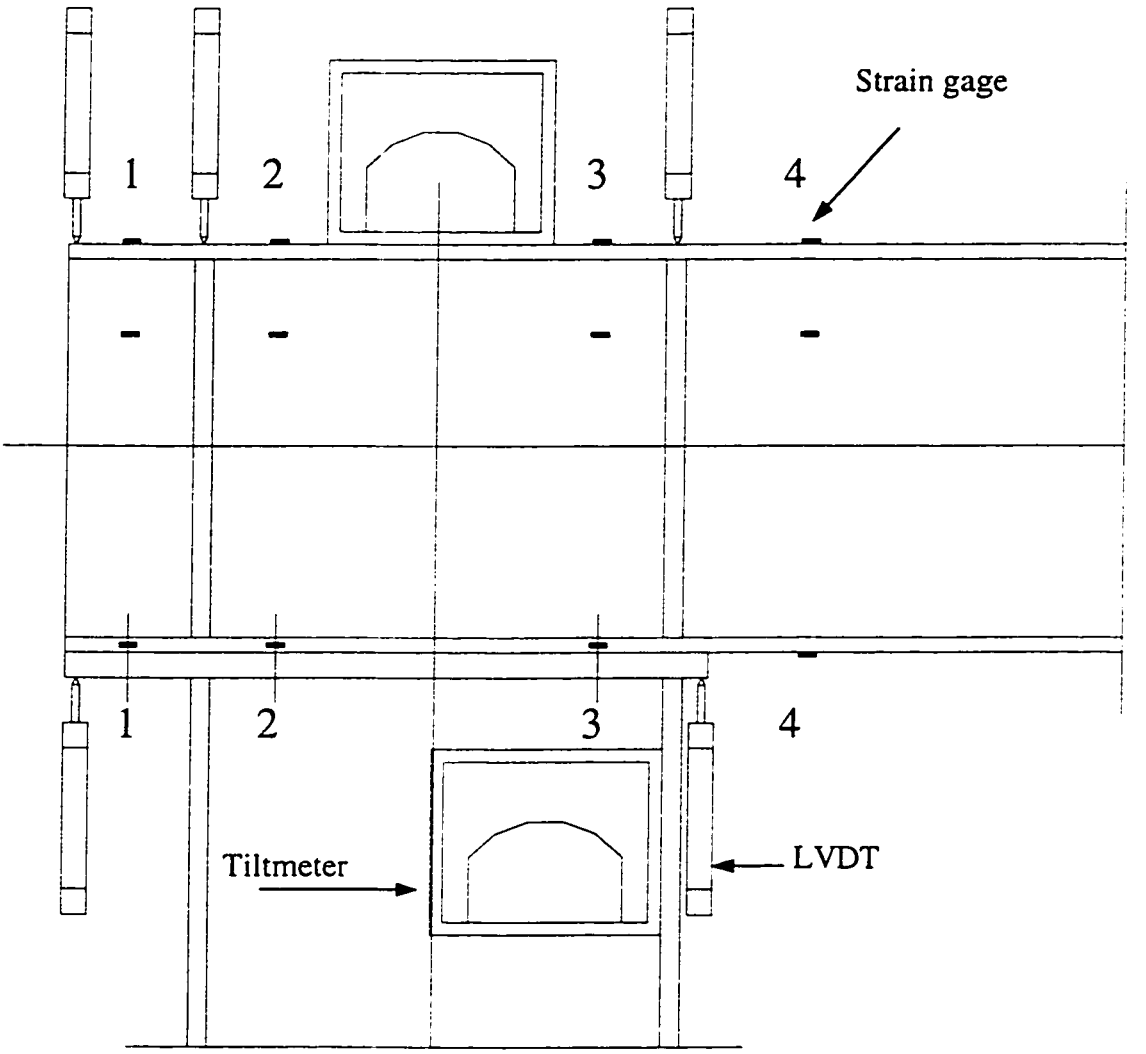

Figure 5.12 Instrumentation Locations

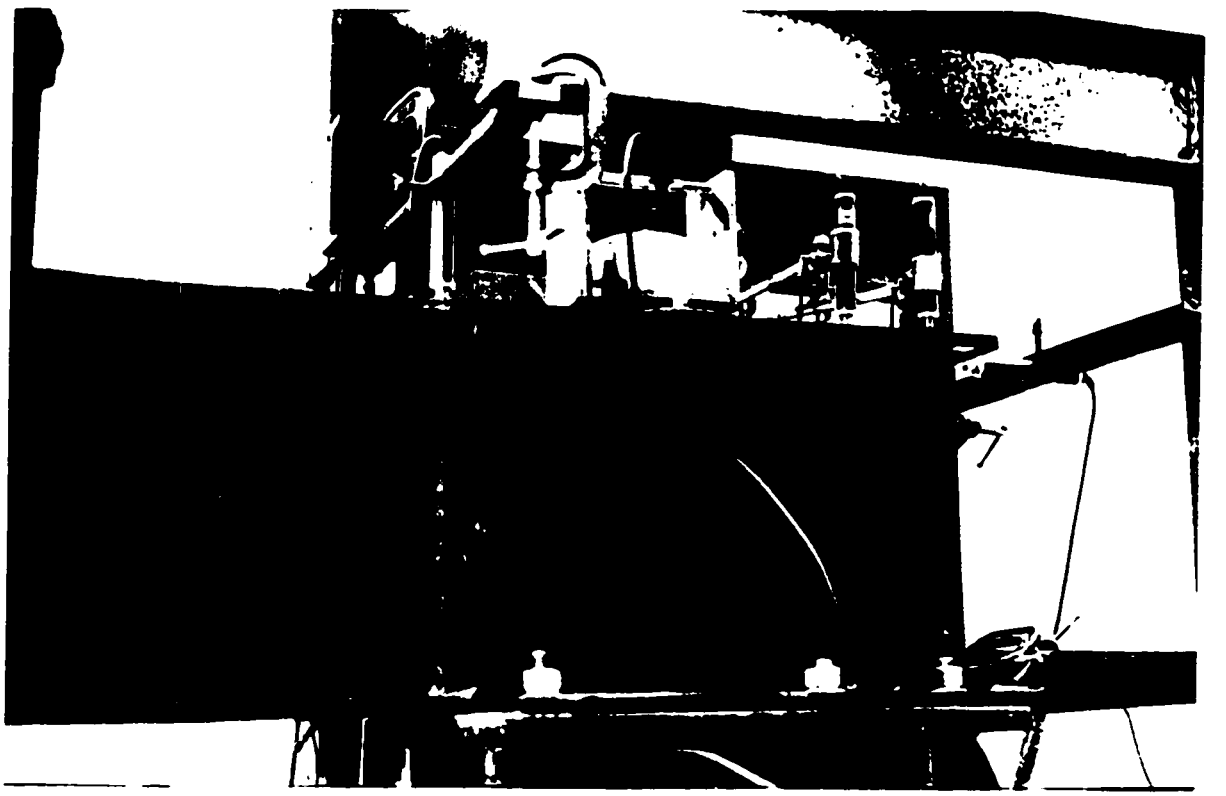

Figure 5.13 LVDTs Locations

5.4.3 Strain Gages

Normal strains were measured at several cross sections along the beam using 120 Ohm strain gages 12.5 mm long as shown in Fig. 5.14. The recorded bending strains were used to plot the bending strain distribution along the depth of beam.

The bolts strains were measured using 120 Ohm strain gages 6.25 mm long fixed to the 4 tension bolts. Two opposite gages are pasted on each bolt to eliminate the effect of bolts bending by taking the average of the two readings. For the passage of the connecting lead wires, two small holes 2 mm diameter each were drilled through the bolt head. A typical gauged bolt is shown in Fig. 5.15. The recorded strains were used later to evaluate the bolts forces.

5.5 TEST PROCEDURE

For each test, the following procedure was followed step-by-step:

5.5.1 Checking Test Assembly and Instrumentation

First, the strain gages were accurately located on their position on the specimen after carefully cleaning and removing the steel protective paint. After mounting all the strain gages, electric wires were prepared with suitable lengths for connecting the strain gages to the data logger. After the specimen preparation, the column is mounted first on the support system. Then, the inclined and lateral bracings were fitted in position to fix the column. The beam was lifted and adjusted on the column. The vertical columns of the end support system were installed after greasing them to have

Figure 5.14 Strain Gages Locations

Figure 5.15 Typical Gauged Bolt

a smooth vertical displacement of the beam tip during loading as shown in Fig. 5.16. Then, the connection bolts were installed and those at the compression side are strongly tightened. A special care was taken for the tension bolts to avoid any damage of the bolt gages during the erection process.

A special framing system was fabricated at the KFUPM workshop as shown in Fig. 5.17. The system is supported by the main test frame to be independent of any movement of the specimen during loading. All LVDTs are mounted on this system in their appropriate locations. Two tiltmeters were installed on the tilt plates and clamped one to the beam and the other to the column to ensure a high fixation.

The wires from all the strain gages, the cables from the LVDTs and the tiltmeters are connected using the appropriate channels numbering to the data logger as shown in Fig. 5.18.

5.5.2 Bolt Pretensioning

Tension bolts are preloaded to ensure the full contact between the beam lower flange and the column cap plate. After checking the instrumentations and before the beginning of the test, all the data logger channels are initialized except those related to the bolts strain gages because of initial pretensile strains in bolts.

5.5.3 Load Application

A small load was applied as a check and records were taken from all the instrumentations to ensure that they were functioning as required. A vertical load was

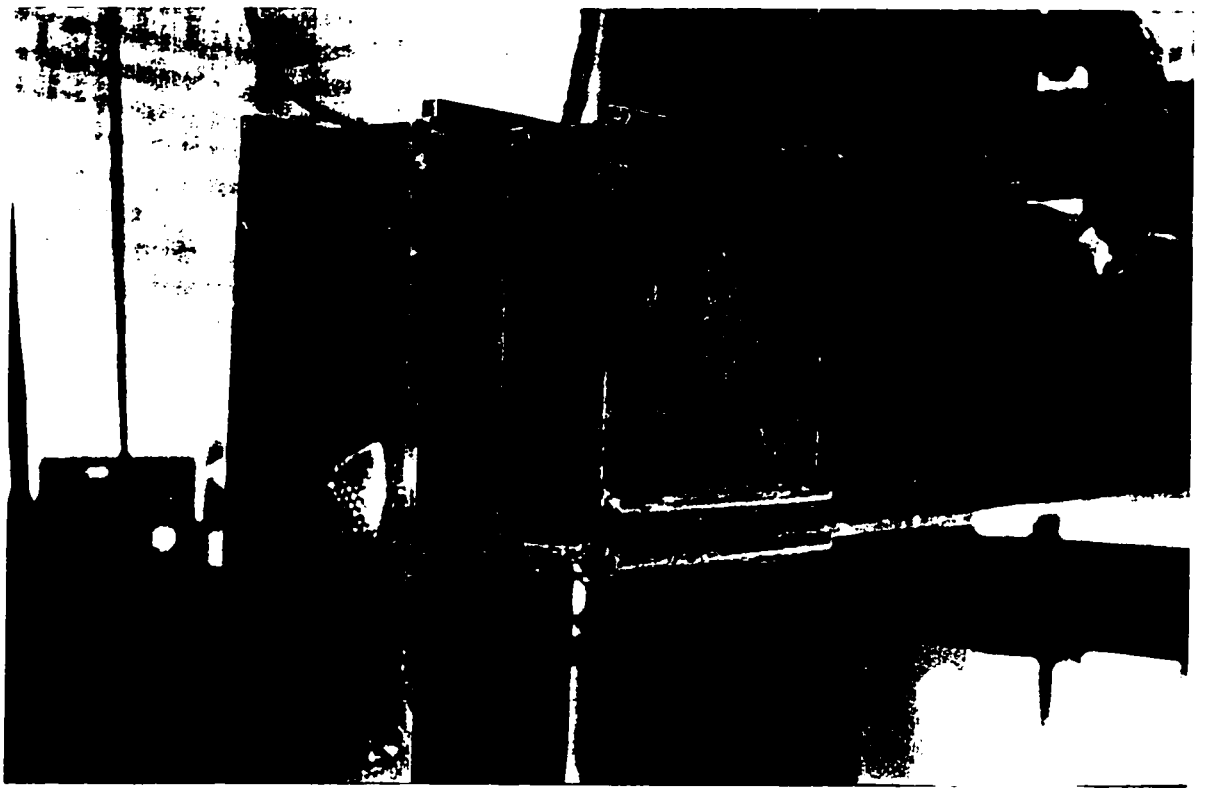

Figure 5.16 Vertical Rolling System

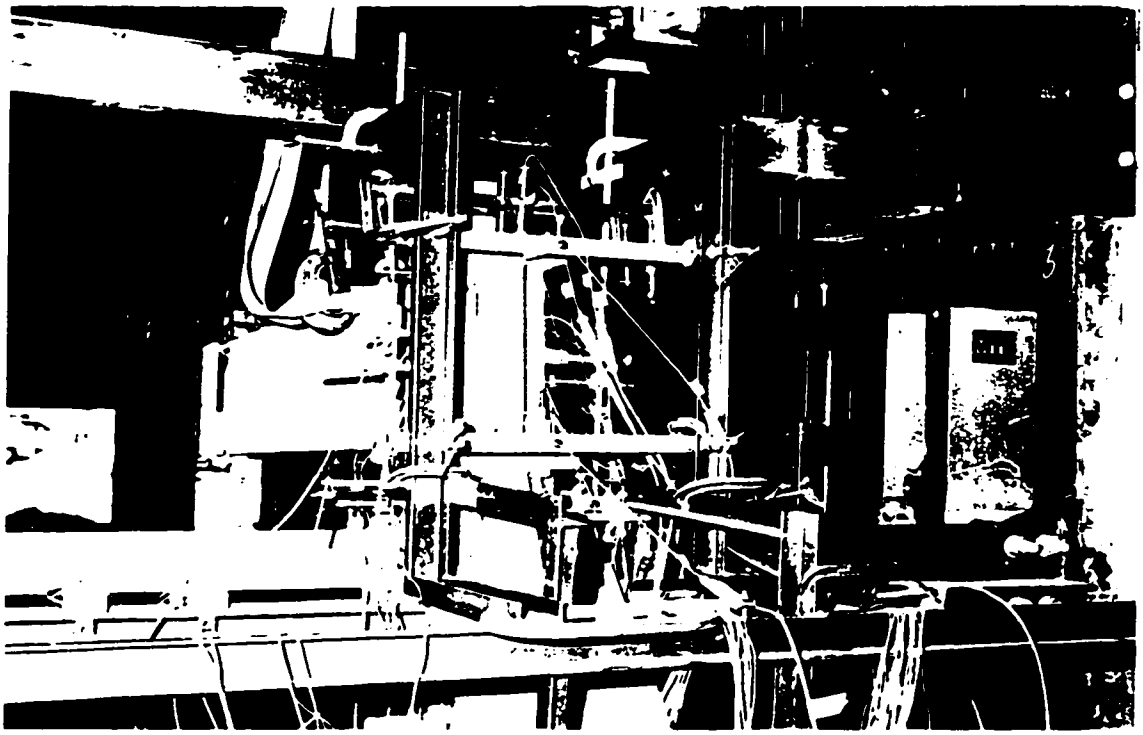

Figure 5.17 LVDTs Framing System

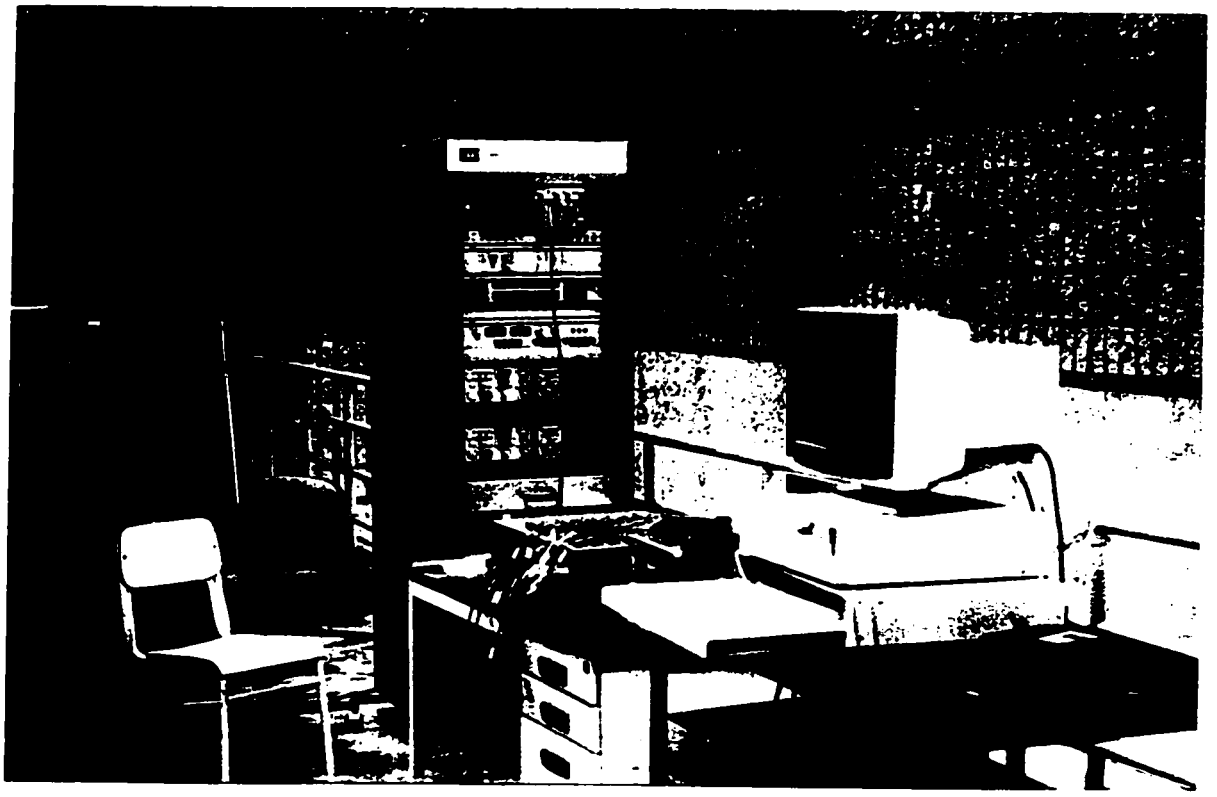

Figure 5.18 Data Logger and Testing System

applied monotonically to the beam tip by a 500 kN hydraulic actuator (MTS 810 Material Testing System) having a stroke length of 150 mm. The testing system is shown in Fig. 5.18. The applied load was monitored by connecting the MTS system to a data logger to automatically record the applied load.

The load was applied at a slow rate and was incremented in steps. At each step of loading, the readings from all instrumented devices were recorded using the data logger. The loading was stopped at the incipient of failure, as judiciously observed from the deformation of the beam and the connection. Admittedly, as the complete collapse was not reached due to safety reasons, the exact collapse load was not recorded. However, the measured ultimate load, which was close to actual failure load, can be referred to as the 'pseudo critical' load.

5.5.4 Record of Test Data

Each specimen was loaded at a slow rate and equal incremental steps up to the pseudo failure of the connection. At different load levels, the readings were taken from all the instruments at the end of each load increment. All readings from testing machine, tiltmeters, strain gages and LVDTs were recorded using a PC and also on paper tape to provide a backup copy for processing, analysis and plotting of test results. At the end of each test, the tested specimen was removed to prepare for the testing of a new connection.

5.6 TEST OBSERVATIONS

The examination of the bolts after the tests indicated that bolts had developed some permanent deformation without fracture. Also, no permanent bearing deformations of bolt holes were observed. It was observed from the test results that the rotations obtained from the tiltmeters are almost identical to those computed using the LVDTs which proves the effectiveness of the test procedure and instrumentation setup. The tests were completed successfully without any major setbacks.

CHAPTER 6

RESULTS AND DISCUSSIONS

6.1 GENERAL

In this chapter, both theoretical and experimental results are presented and discussed. In the theoretical part, the program developed in Chapter 4 is used in a parametric study, to calculate the critical load of plane frames, to show the effect of the connection flexibility on the frame behavior and to determine the mode of failure of the frame. The experimental part presents the analysis of the obtained test results with the main observations.

6.2 THEORETICAL RESULTS

The developed program (EPASF) for the elastic plastic analysis of portal frames with semi-rigid connections, taking into consideration the second-order effects and the connection flexibility, is used to solve several examples. These examples show the program capability and the effect of the non-linear rotational stiffness of connection on the analysis.

6.2.1 Analysis of Frames with Linear Connections

The program was used in the analysis of the semi-rigid plane frame shown in Fig. 6.1. It has a height of 4m and a span = 4m with the following member properties: the cross sectional area A = $1.5*10^4$ mm^2 , the second moment of area I = $4.0*10^8$ mm^4 and the modulus of elasticity E = 200 GPa. The discretization of the frame with numbering of nodes and members is given in Fig. 6.2. The connection flexibility is modeled by a rotational spring as shown in the same figure. Each member is given a code number depending on its type corresponding to its end conditions, as discussed in Chapter 3. To begin with, member 5 is of Type 2, member 8 is of Type 3 and all the remaining members are of Type 1. The program updates the members types, if there is a change in their end conditions after every step of incremental load analysis.

6.2.1.1 Critical Buckling Load

The program has the capability to determine the critical load of semi-rigid frames. The critical load is reached when the determinant of the global stiffness matrix becomes zero. The analysis automatically stops at this load level. To present a solution of the critical buckling load of the described frame, it was analyzed with the application of a concentrated force of intensity P on each column as shown in Fig. 6.3. A small horizontal force of intensity 1/100 of the applied vertical force was applied to introduce the primary bending moments. The loads were increased in steps, keeping the same proportions. The displacements and moments were recorded at each

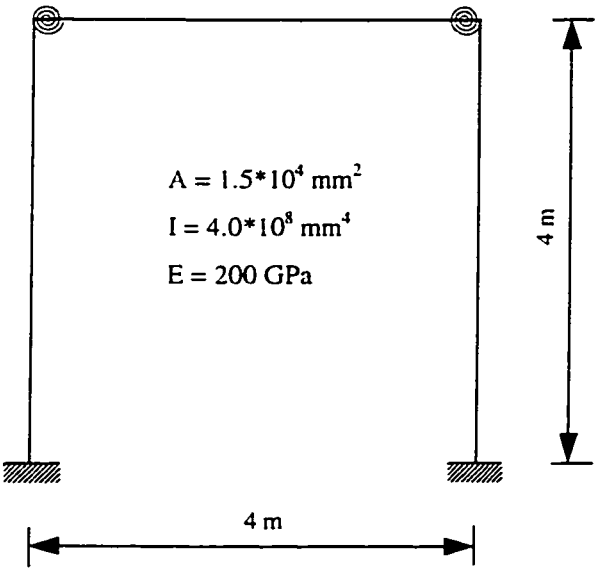

Figure 6.1 Frame Dimensions and Properties

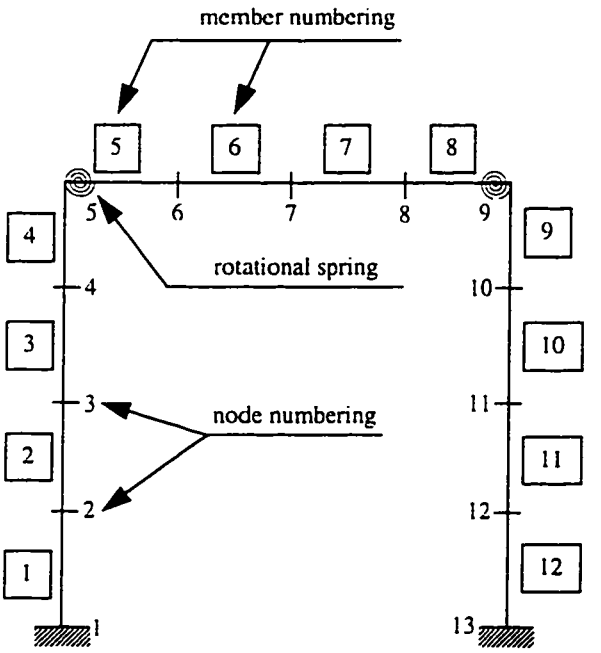

Figure 6.2 Frame Discretization and Numbering

load step. The buckling load was determined when the determinant of the global stiffness matrix approached a null value.

To simulate the case of ***rigid connections***, a very stiff joint was taken with a high value of rotation stiffness $R_k = 1.0*10^{10}$ kNm/rad (Fig. 6.3). The moment at joint 5 is equal and opposite to the moment at joint 9 due to symmetry. The bending moments and displacements of joint number 5 are shown for each load step in Fig. 6.4 which also show the plot of the determinant of the structural stiffness matrix. The results show that the moment and deflection increase rapidly as the critical load is approached. Also the determinant decreases progressively as the load is increased and the plot crosses the zero value at 36,000 kN which is the critical load given by the program. The exact solution for this problem as given by Chajes [63] is $P_{cr} = \frac{7.34EI}{L^2}$ which equals 36,700 kN. This indicates the high accuracy of the iterative solution scheme adopted in the program.

For the case of a ***hinged connection***, the joint is modeled by a very soft spring of small rotational stiffness. For this case, the rotational stiffness of the connection was taken as $R_k = 1.0*10^{-4}$ kNm/rad, which is almost negligible as shown in Fig. 6.5. The analytical results for this frame presented in Fig. 6.6 show that a much lower buckling load of 12,200 kN was obtained. Figure 6.6 also shows that as the buckling load is approached, the deflection increases rapidly and becomes asymptotic. The moment at the connection is very small ($2.4*10^{-5}$ kNm) which is practically zero. The

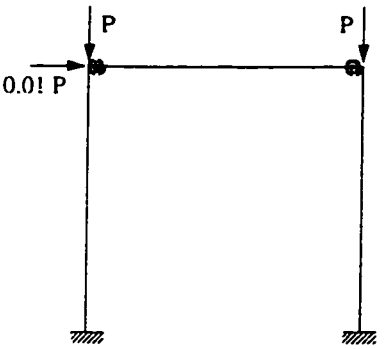

Figure 6.3 Applied Loads on a Frame with Very Stiff Connections

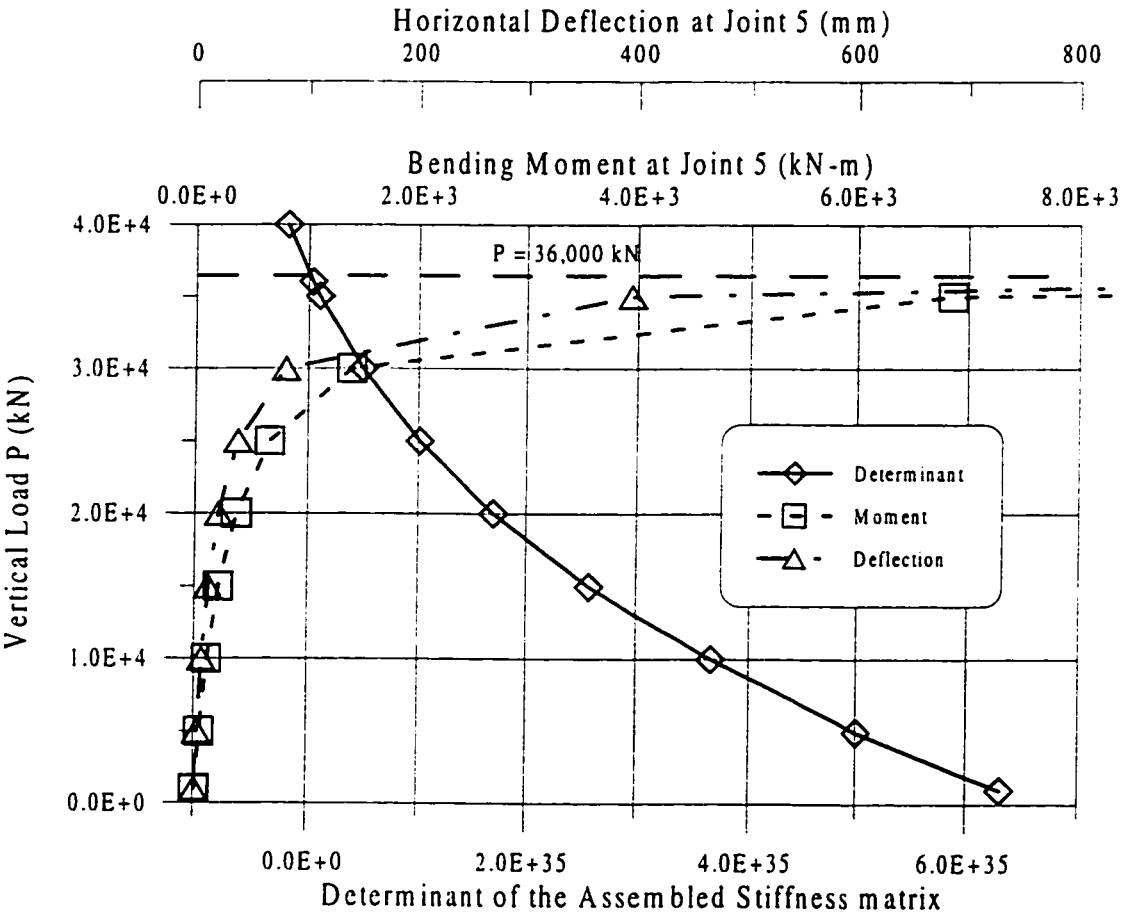

Figure 6.4 Critical Buckling Load of a Frame with Very Stiff Connections

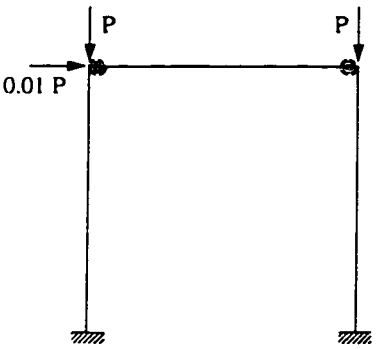

Figure 6.5 Applied Loads on a Frame with Very Soft Connections

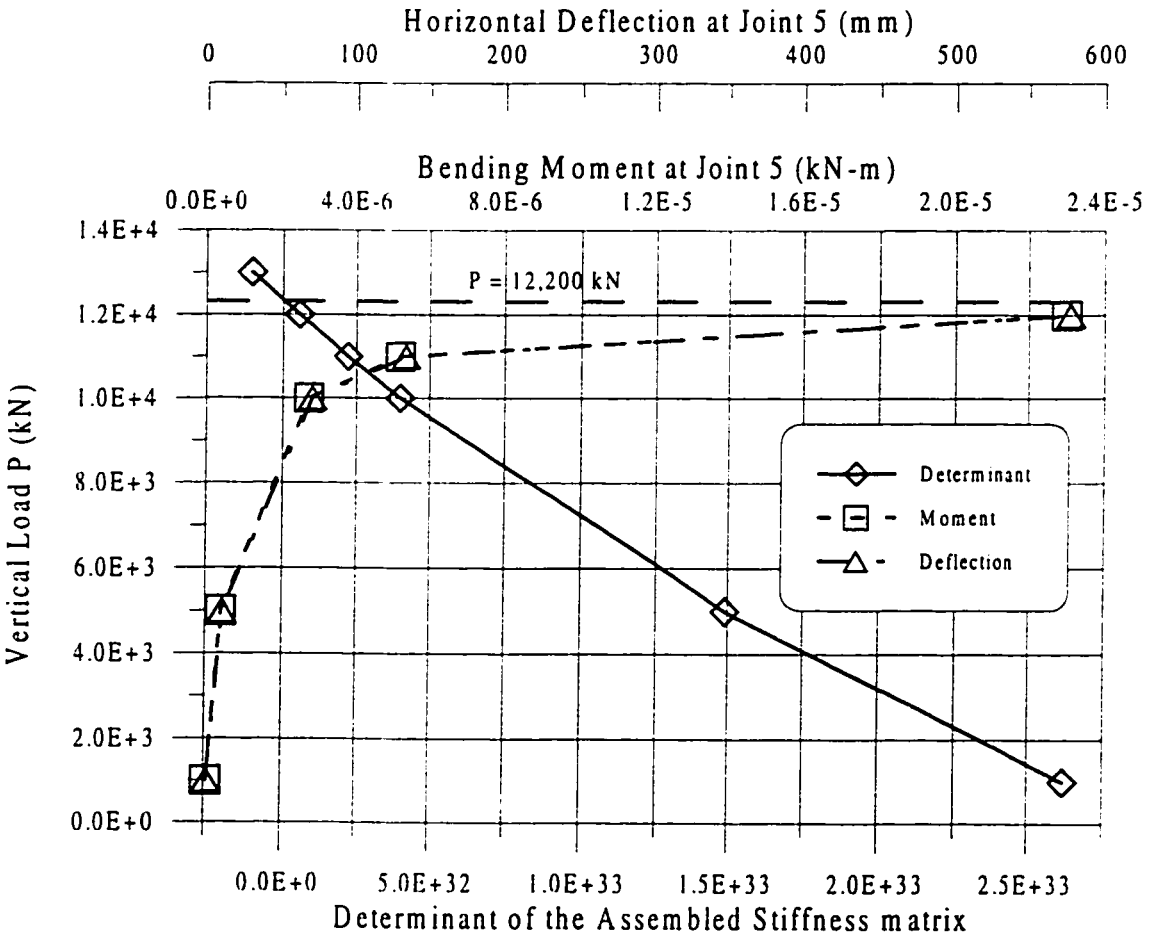

Figure 6.6 Critical Buckling Load of a Frame with Very Soft Connections

obtained value of the critical buckling load can be compared with that of an axially loaded column fixed at one end and free at the other end (due to large sway) which is given as [80] $P_{cr} = \frac{\pi^2 EI}{(2L)^2}$ = 12,340 kN.

A comparison of the two extreme cases of the connection idealization (Figs. 6.4 and 6.6), shows that at the same load level, higher deflection exists with lower moment values for frame with very soft connection. This indicates the significant effect of connection flexibility on the frame behavior and a proper connection response must be considered in the analysis and design of such frames. These two examples show the capability of the program to determine an accurate value of the critical buckling load for a portal frame.

6.2.1.2 Effect of Connection Flexibility

To get a better idea about the effect of the connection flexibility on the frame behavior, a geometrically unsymmetrical frame shown in Fig. 6.7 was analyzed. The frame discretization is shown in Fig. 6.8. The loads are shown in Fig. 6.9. For this case of study, the frame was analyzed with several constant values of the connection rotational stiffness varying from R_k=1.0 kNm/rad (very soft) to R_k=1.0*10^8 kNm/rad (very stiff). The results of the analysis are shown schematically in Fig. 6.10 on a semi-log scale.

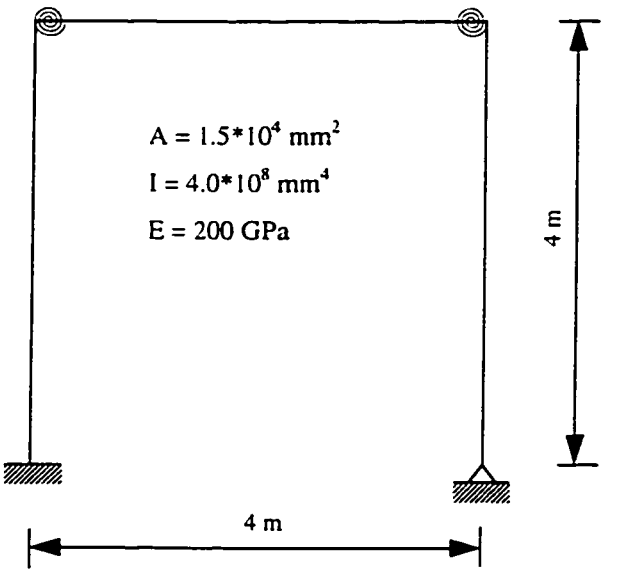

Figure 6.7 Frame Dimensions and Properties

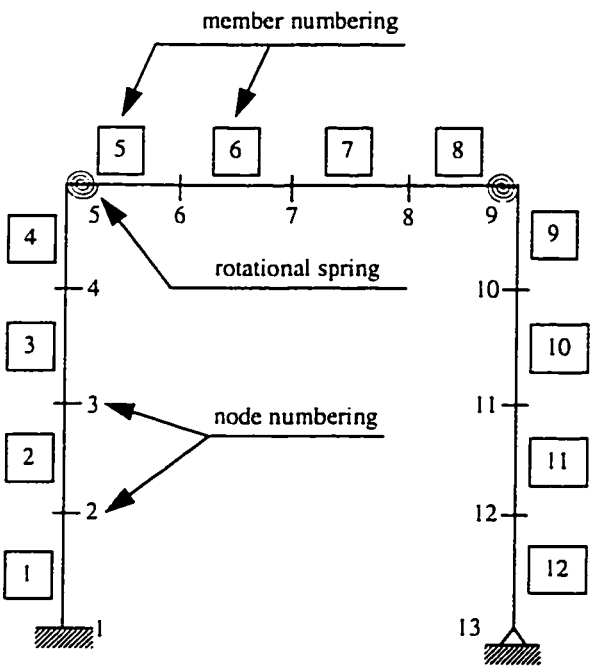

Figure 6.8 Frame Discretization and Numbering

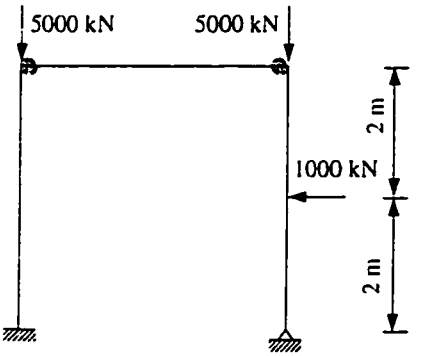

Figure 6.9 Applied Loads on a Frame with Variable Connection Spring Stiffness

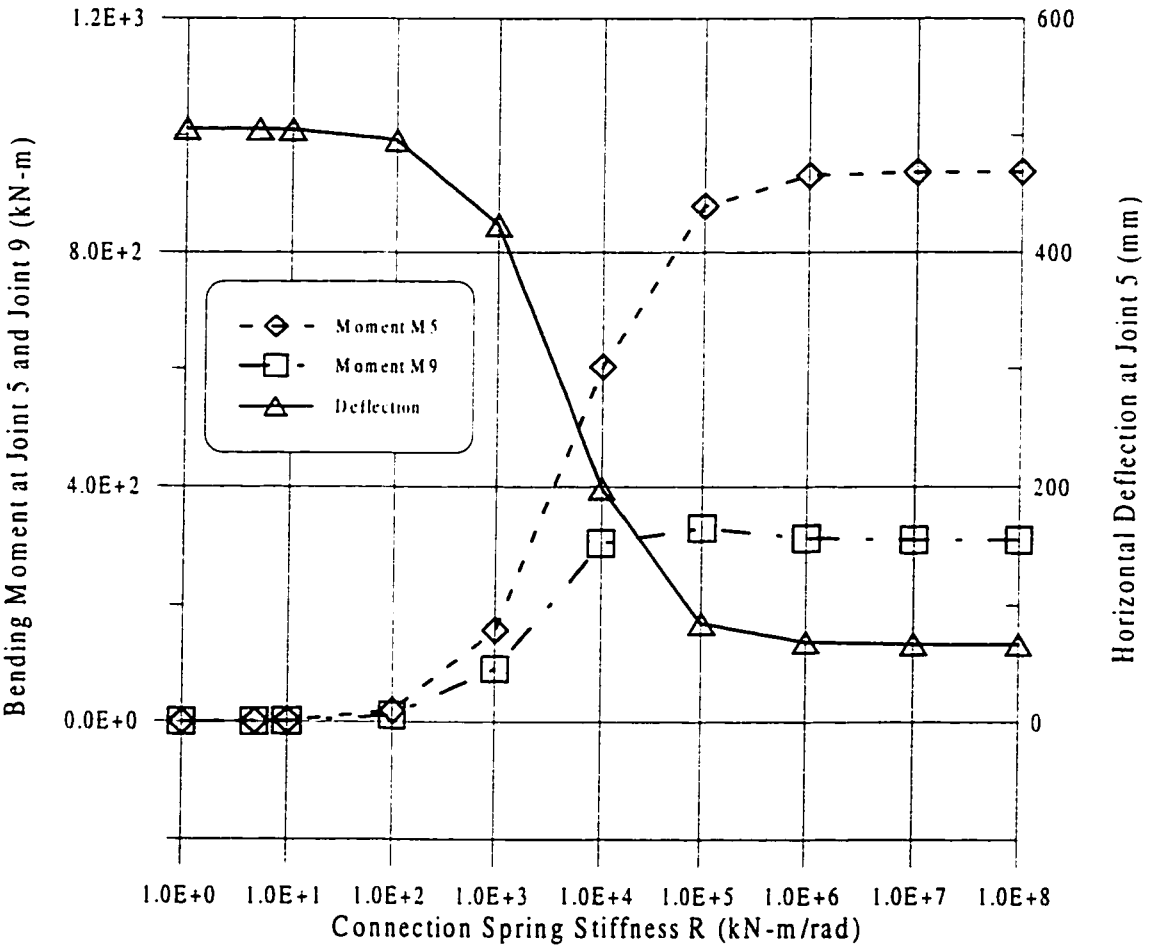

Figure 6.10 Effect of Variation of Connection Spring Stiffness on a Frame

For this case, the moment obtained at joint 9 is different than the one at joint 5 due to unsymmetry. For a very soft connection with R_k=1.0 to R_k=10 kNm/rad, moments at joints 5 and 9 are almost zero and the frame behaves essentially like a frame with a hinged connection between beam and column. At higher connection stiffness R_k >1.0*10^6 kNm/rad, the moment at joint 5 is about 3 times the moment at joint 9. Also, the lateral deflection of the frame is very small for a frame with a stiff connection and relatively high for a soft connection as expected. For this particular frame geometry and loading case, it can be concluded that the connection flexibility has an effective range which is $10 < R_k < 1.0*10^6$ kNm/rad. For $R_k < 10$ kNm/rad, the connection can be considered practically as hinged and for $R_k > 1.0*10^6$ kNm/rad, the connection can be assumed practically as fixed since the three curves shown in Fig. 6.10 are asymptotic beyond this range. A value of R_k within the range $10 < R_k < 1.0*10^6$ kNm/rad represents a case of flexible connection (semi-rigid connection).

6.2.2 Analysis of Frames with Nonlinear Connections

In the previous examples, the connection was modeled as a linear spring having a constant rotational stiffness for all load levels. The effect of connection non-linearity is discussed in the following example. Consider the frame shown in Fig. 6.1 with a lateral force only applied at joint 5 (Fig. 6.11). This frame was analyzed 3 times with 3 different non-linear connections models. The connection non-linearity was modeled

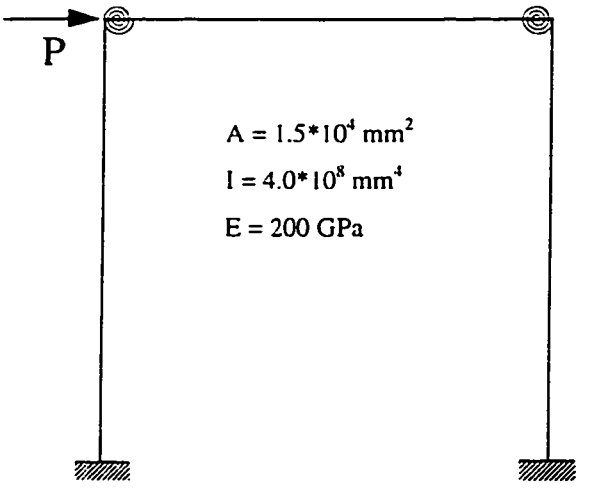

Figure 6.11 Applied Loads on a Frame with Nonlinear Connection Stiffness

TABLE 6.1 Description of the Three Connection Polynomial Models

	Moment-rotation ($M-\theta$) equation	**Initial rotational stiffness (R_{ki})**	**Ultimate moment (M_u)**
Model 1	$M = 5.0*10^3\theta - 1.5625*10^5\theta^2$	$5.0*10^3$	40
Model 2	$M = 5.0*10^4\theta - 1.5625*10^6\theta^2$	$5.0*10^4$	400
Model 3	$M = 5.0*10^5\theta - 1.5625*10^7\theta^2$	$5.0*10^5$	4,000

by a second degree polynomial equation representing the moment-rotation relationship. The moment-rotation equations and properties for each model are given in Table 6.1, the corresponding plots are given in Fig. 6.12. Model 1 represents a soft connection, Model 2 represents an intermediate connection and the stiff connection is given by Model 3. For Model 1, the load P was increased in step of 5 kN, for Model 2, the load step was increased to 25 kN and for Model 3, the load step was further increased to 150 kN. At each load step the connection stiffness changes. The moments recorded after each incremental load cycle are shown in Fig. 6.13 for joint 5. A comparison of the moments at joint number 5 for the three models shows that at the same load level, the value of the moment increases with the increase of the connection stiffness as expected. The nonlinearity in Fig. 6.13 is small because of the load configuration where no vertical load is applied. In the absence of large axial force in members, the effect of axial force in the stiffness matrix is considerably small. The relationship between the applied load and the frame lateral displacement is shown in Fig. 6.14. The behavior in this case is similar to that of a linear frame, since the second-order effects are negligible (small axial forces) and the only nonlinearity arises from the connection flexibility. Again, for the same load level, higher deflection are observed with soft connections.

6.2.3 Modes of Failure

The frame shown in Fig. 6.1 with the discretization shown in Fig. 6.2 was analyzed under the load configuration shown in Fig. 6.15. The load was applied in incremental

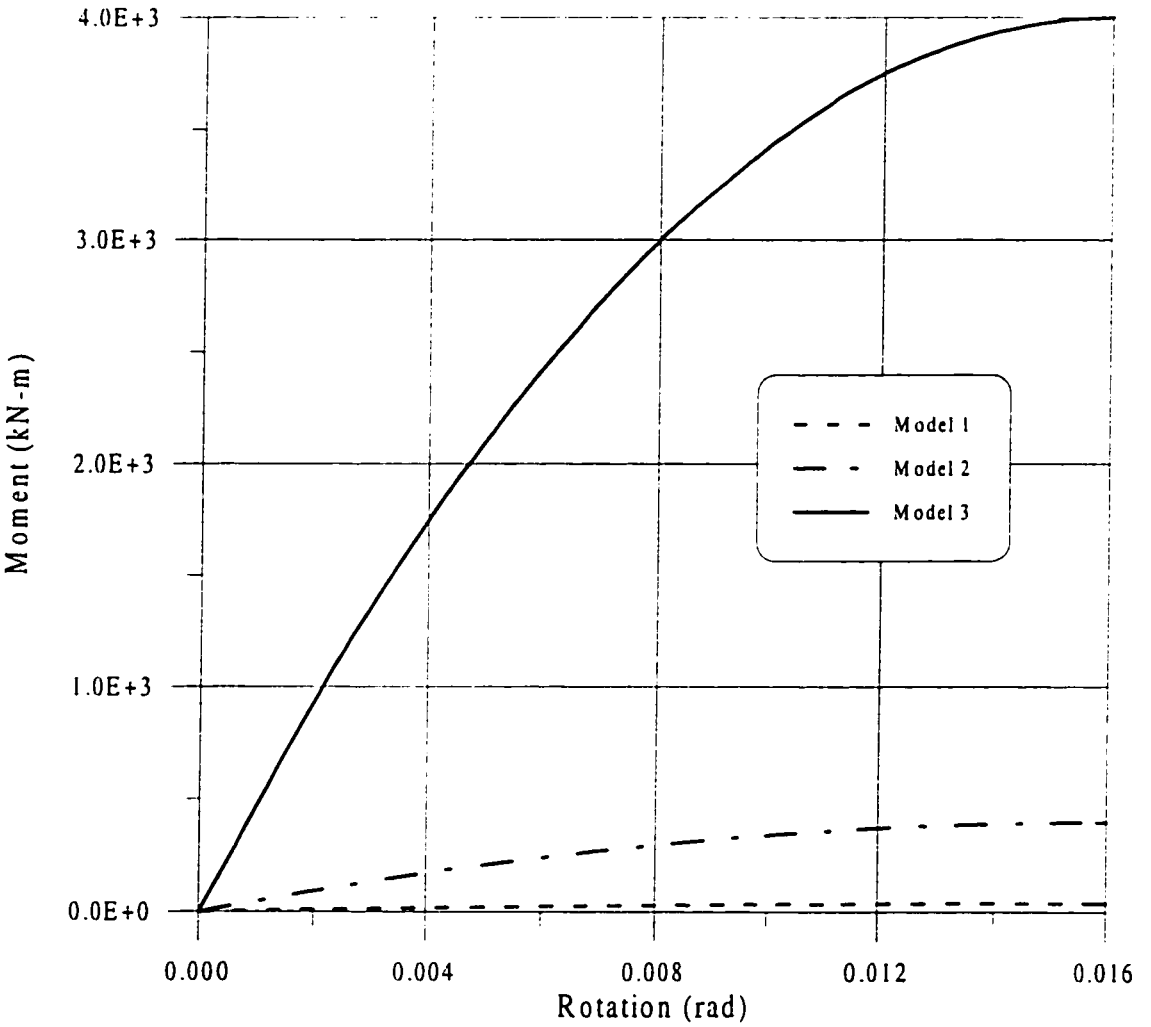

Figure 6.12 Moment Rotation Relationship for Polynomial Models

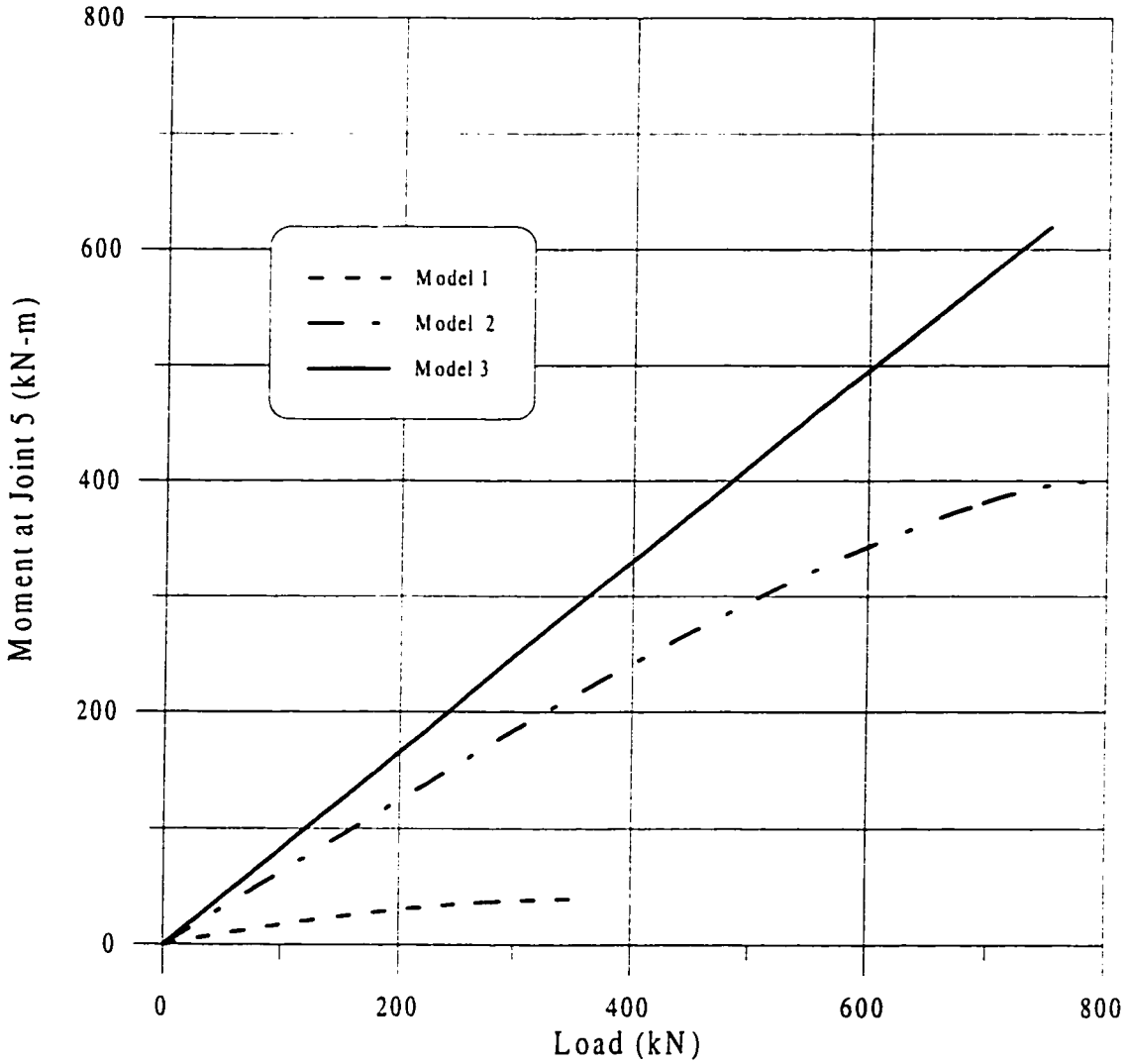

Figure 6.13 Effect of Connection Flexibility on Load-Moment Relationship

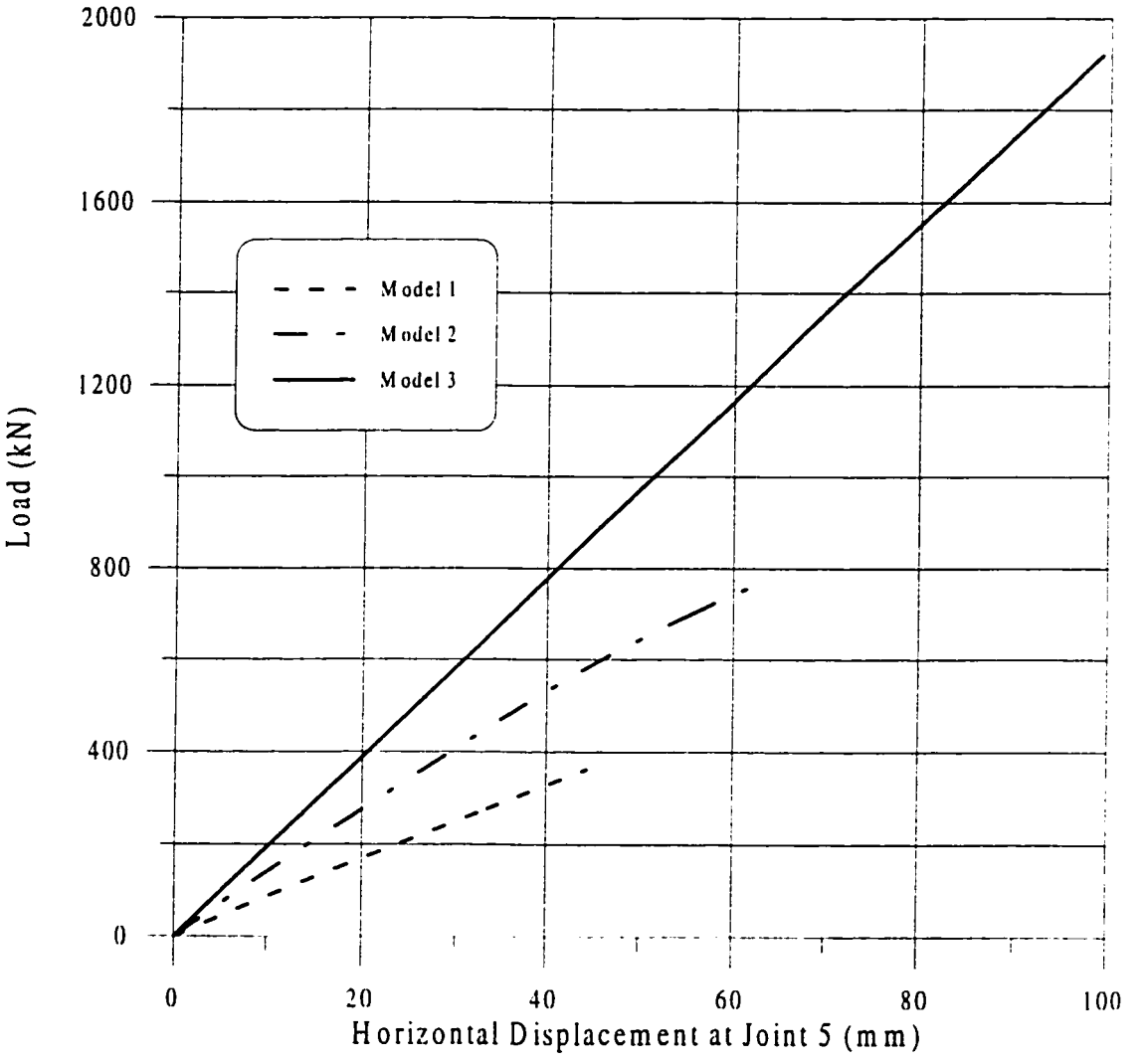

Figure 6.14 Effect of Connection Flexibility on Load-Displacement Relationship

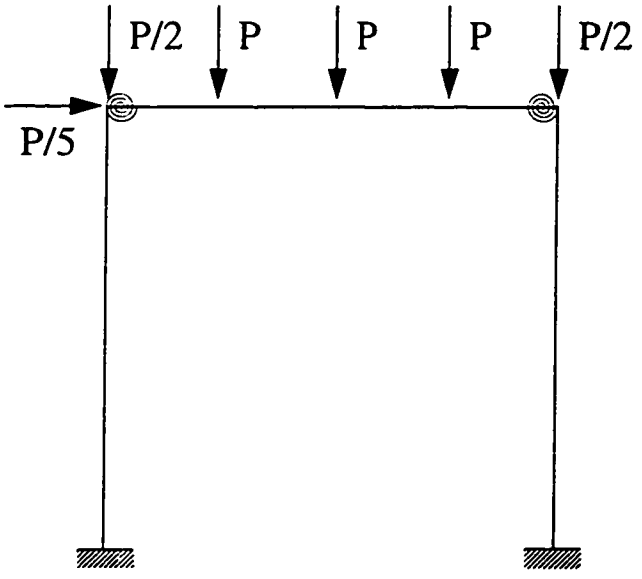

Figure 6.15 Applied Loads on a Frame with Nonlinear Connection Stiffness

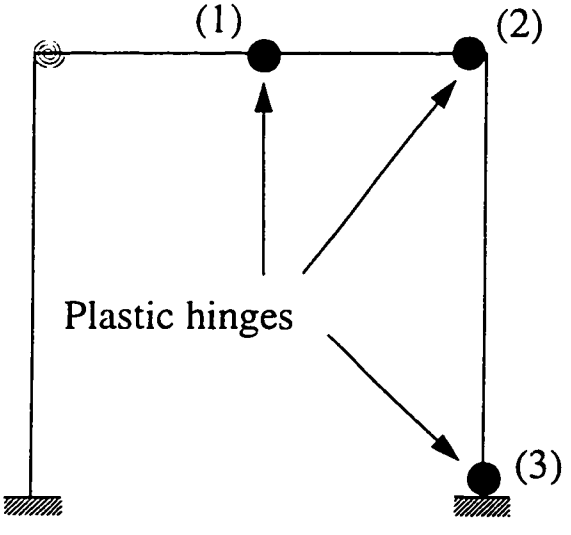

Figure 6.16 Sequence of Plastic Hinges Formation

steps with P = 50 kN for every load step. The initial rotational stiffness of the connection was taken as $R_{ki} = 6*10^4$ kNm/rad, the plastic moment M_p = 800 kNm and the axial plastic capacity of the member was taken as $P_u = 5*10^3$ kN. The connection spring was modeled by the power model

$$\theta = \frac{M}{\left[1 - \left(\frac{M}{M_p}\right)^n\right]^{\frac{1}{n}}} \tag{6.1}$$

where n was taken as 1.5. The interaction equation between the moment at the connection and the axial force was given as

$$\frac{P}{P_u} + \frac{M}{1.18M_p} = 1.0 \tag{6.2}$$

The load was applied in steps and after 11 increments, the first plastic hinge was formed at joint 7. The second plastic hinge was developed after one increment at joint 9 followed by the third plastic hinge at joint 13 to give the partial collapse of the frame by formation of plastic hinges as shown in Fig. 6.16. The lateral deflection of the frame is shown in Fig. 6.17. The relationship between the load increments and the lateral deflection as seen from the figure is approximately linear up to the ninth load increment, this behavior is due to the small axial forces in the members giving negligible second-order effects. After the ninth load increment, the curve becomes non-linear with the formation of plastic hinges in the frame.

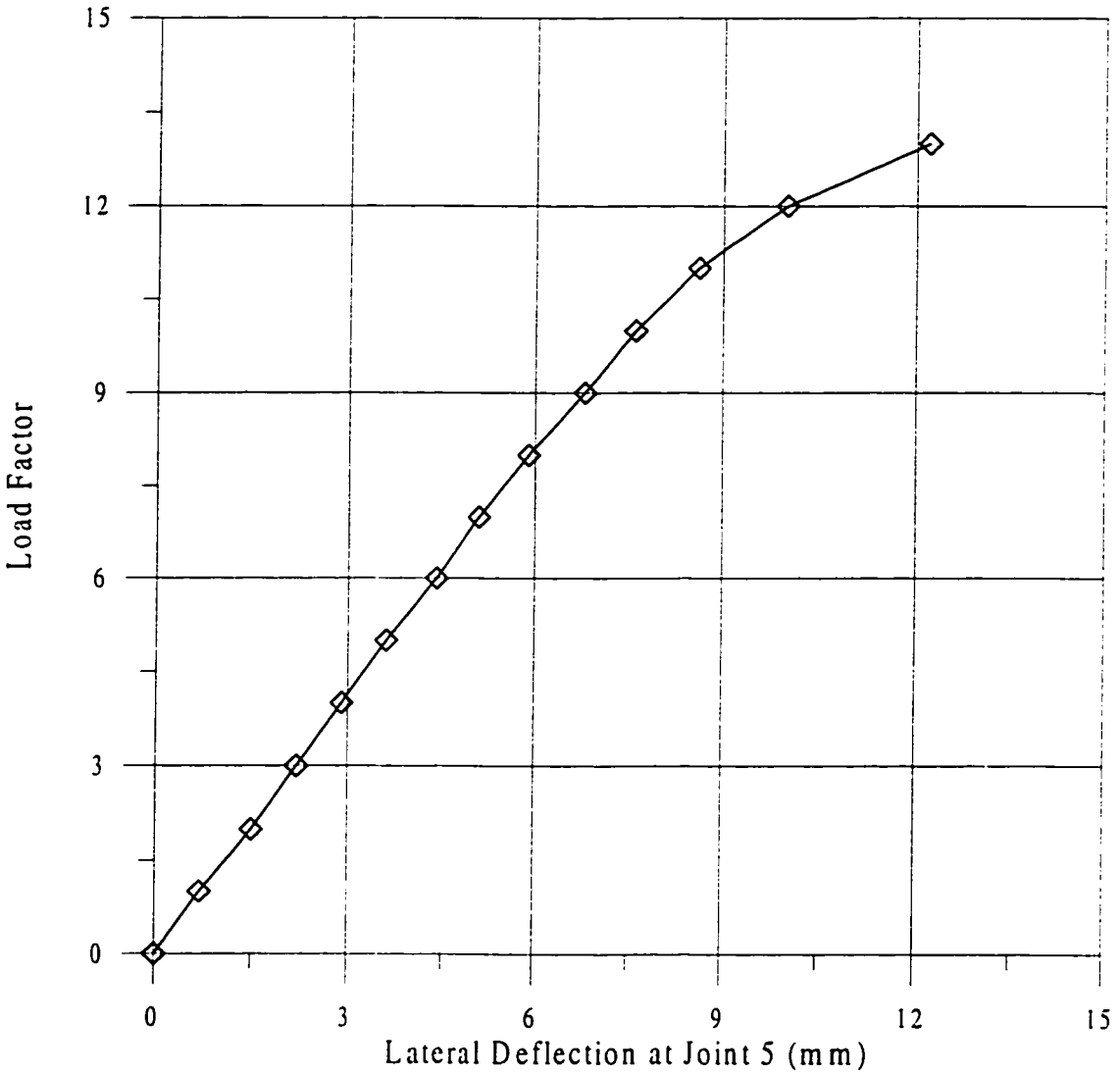

Figure 6.17 Effect of Plastic Hinges Formation on the Load-Deflection Relationship

The same frame was analyzed once again by taking high axial forces on the columns by replacing the column loads of P/2 by 10P so as to initiate elastic buckling failure prior to plastic collapse. The ultimate plastic moment was increased to $8*10^4$ kNm and the axial plastic capacity was taken as $5*10^5$ kN to ensure the failure of the frame by buckling of columns. The same model was used for the spring connections. The load was applied incrementally, and the failure was reached after 26 increments. The lateral deflection of the frame was shown in Fig. 6.18 where the nonlinearity of the curve starts from the beginning of the application of the loads which indicates the effect of the second-order effects on the deflection of the frame.

The results of several frames analyzed by the program EPASF, which are presented here clearly demonstrates the general applicability and accuracy of the method of solution. The iterative scheme adopted in this program for the elastic-plastic analysis of frames yields accurate results and capture the response of a frame with semi-rigid connections at any load level.

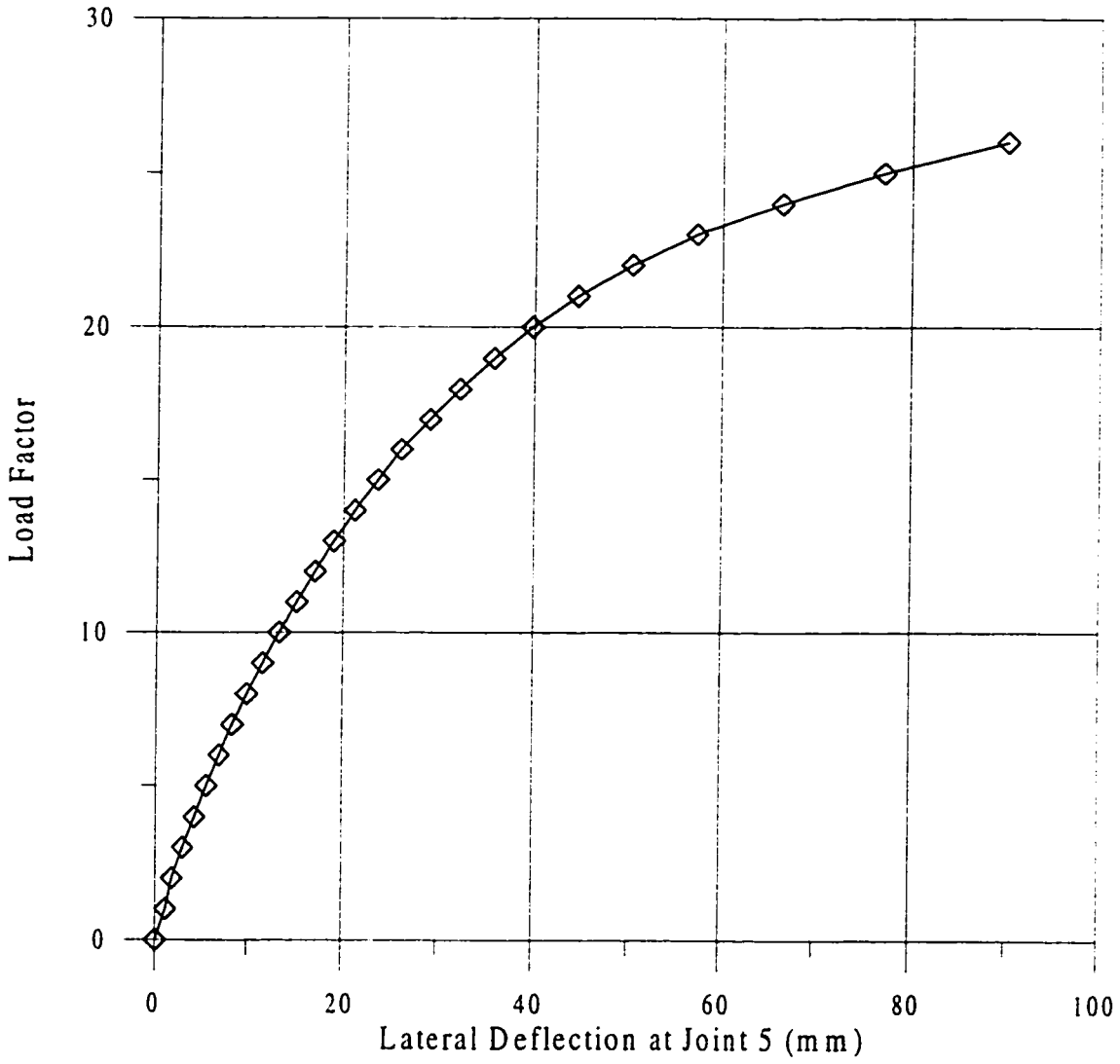

Figure 6.18 Second-Order Effects on Load-Deflection Relationship

6.3 EXPERIMENTAL RESULTS

The experimental results from the six tests are covered in this section with a discussion of the observations obtained from the results. The specimens dimensions are given in Table 5.1. The experimental results are presented and discussed here test by test including a commentary on the following items of interest:

(a) **moment rotation curve** which is plotted using the recorded values of the tiltmeter readings and the LVDTs readings, with a comparative study of the plots from different sets of tests.

(b) **bolt strains** for the outer and the inner bolts on the tension side of the connection. For each bolt, the average of the two strain gages attached to the bolt was considered to be the normal strain by eliminating the effect of possible bending. The average of the two outer bolts and the average of the two inner tension bolts constituted the tensile strains at the outside and the inside bolt line. The measured strains are then compiled to their equivalent forces.

(c) **normal stress distributions** along the connection at four locations (vertical sections) on the beam at the connection panel (Fig. 5.12).

(d) **mode of failure:** It should be noted that in all tests, the loading was stopped at a value when the member and the connection showed visible sign of distress, so as to avoid actual collapse which could have been dangerous. The maximum moment, to which a connection was subjected to, was close to the ultimate value.

For all the following figures, the moments levels are calculated at the center line of the connection which is greater than the moments near the face of the column at Sec. 4-4 by 20%.

Depending on the specimen dimensions, given in Table 5.1, they were divided into three groups. Group A consists of specimens C1 and C3; they had the same cross section of the beam but C3 has thicker beam flange plate (PL1) and larger bolt diameter. Group B comprises specimens C2 and C6, as they had the same cross section with the same bolt diameter but C6 had a thicker beam flange plate. Group C consists of specimens C4 and C5, also with the same cross section and same bolt diameter but C5 had thicker beam flange plate. The moment of inertia and the cross sectional area of the beam sections increased from Group A to Group B but with the same depth and width. Group C had the largest cross-section, inertia, depth and width. The yield and plastic moments for the six beams, which were calculated using a value of yield stress of 345 MPa, are given in Table 6.2.

Three tensile tests were conducted on rods (20 mm diameter and 200 mm long) of the same bolts material to obtain the stress strain relationship for such material (Fig. 6.19). The rod was used to ensure a sufficient grip length in the testing machine. The three tests show similar behavior with almost identical yield strength and fracture strength. A typical curve is shown in Fig. 6.20. The stress strain relation is linear up to the yield strength of 750 MPa with its slope equal to modulus of elasticity of steel which is $200*10^3$ MPa. After yielding a large plateau is observed up

TABLE 6.2 Yield and Plastic Moments for Different Beams

Specimen No.	Beam yield moment kNm	Beam plastic moment kNm
C1	237	269
C2	296	338
C3	237	269
C4	370	426
C5	370	426
C6	296	338

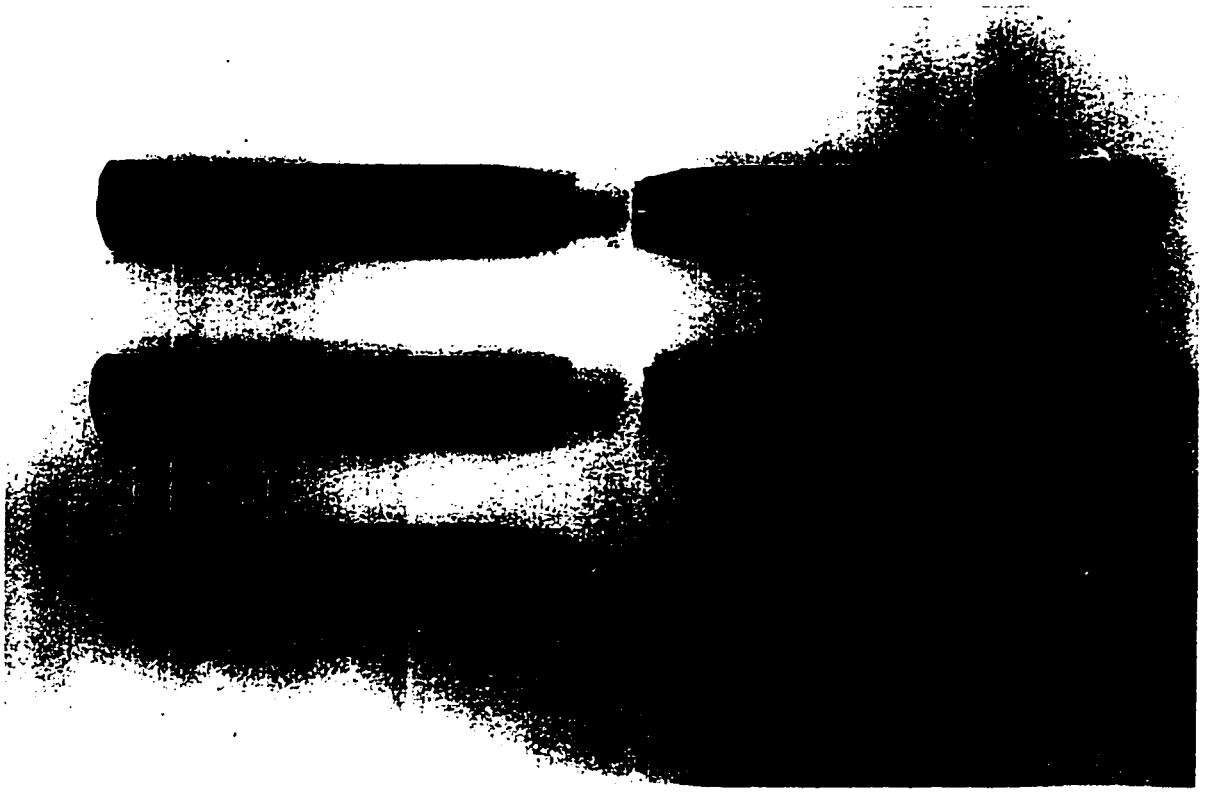

Figure 6.19 Tested Bolts Specimens

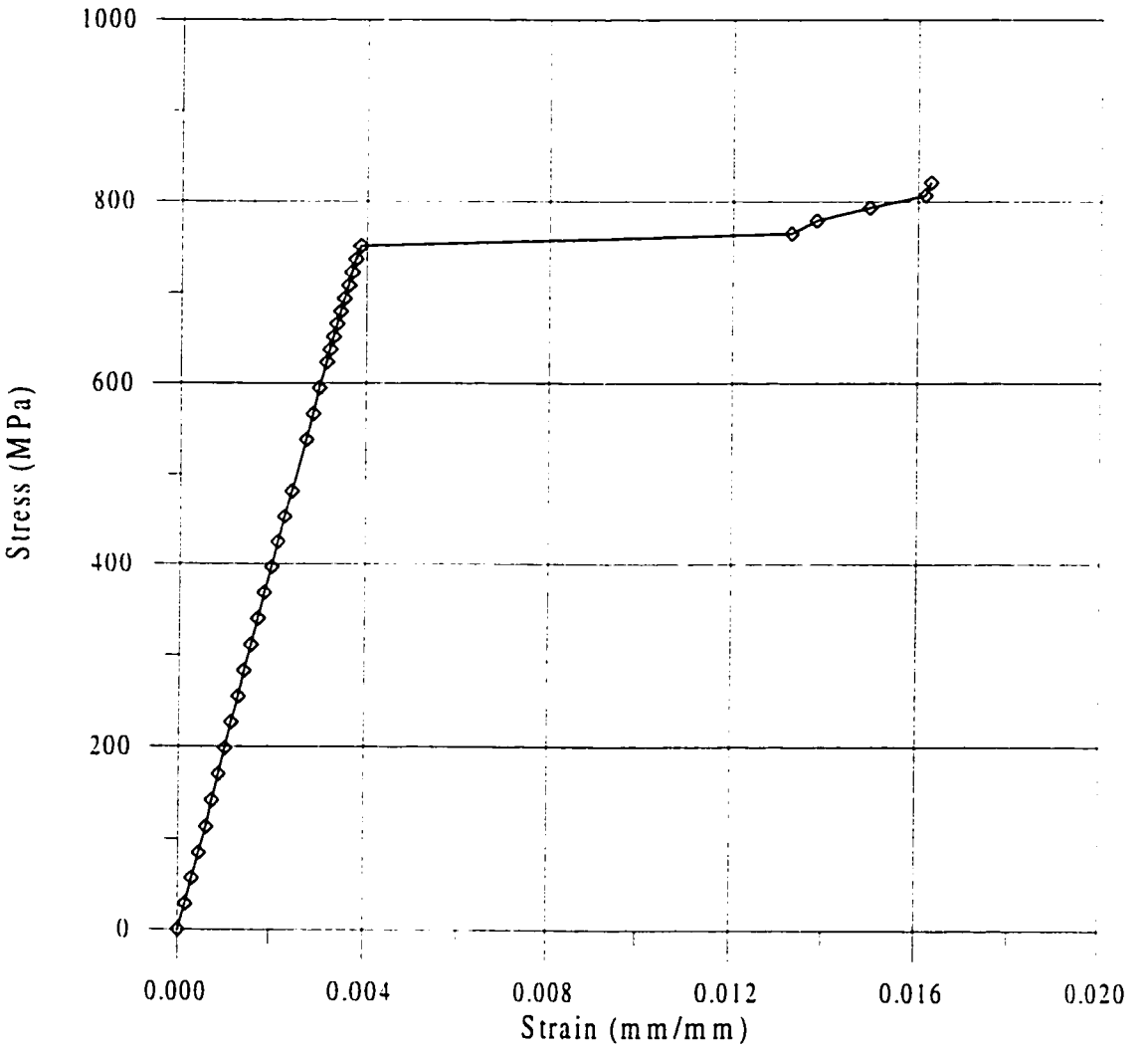

Figure 6.20 Typical Bolt Stress-Strain Relationship

to the fracture strength of 800 MPa. This value was taken as the tensile strength of the bolts.

6.3.1 Specimen C1

For this test, both the bolt diameter (19 mm) and the bottom flange thickness (12 mm) of the beam have the smallest sizes compared to other tests. Figure 6.21 shows the plot of the moment-rotation relationship which is approximately linear up to a moment level of 150 kNm. Thereafter, the $M-\theta$ plot becomes nonlinear up to the maximum moment when test was stopped. This non-linearity indicates a degradation in the connection stiffness represented by the slope of the curve. Also, the unloading path as shown in Fig. 6.21 has a stiffness almost equal to the initial stiffness of the connection. The area under the $M-\theta$ curve represents the high ductility of the specimen C1.

The tension bolts were preloaded at the start of the test and therefore there were initial strains before a moment was applied. As shown in Fig. 6.22, both of the outer and the inner bolts had nearly the same strain at different load levels from 50 kNm up to the maximum moment, which means that they had the same tensile force. The reason attributable to this similar force in both inner and outer bolts is the relatively thin beam flange plate thickness of 12 mm. The maximum recorded value reached 3750 μ and permanent yield was observed in these bolts after removing the specimen. The strain plot is approximately linear up to about 1500 μ and thereafter, the plot becomes nonlinear. Although the yield strain of bolt is close to 3500 μ, nonlinearity begins at much earlier level due to bending of bolts. Although for each bolt, the average normal strain at the two opposite faces has been taken, at high load

level with increased bending of bolts, the average does not truly nullify the bending strains at high load level. This was apparent from the observation of highly different readings of strain from two gages fixed to each tension bolt.

The normal strain distributions are shown in Figs. 6.23 - 6.25 for three levels of the applied moment. For sec. 3-3 and 4-4, the normal strain distribution is linear up to a connection moment level of about 200 kNm with a neutral axis approximately at the mid depth as shown. After this level, some non-linearity appear from the deformation of the connection itself. For section 1-1 and 2-2, which are at the connection ends, the neutral axis is no longer at mid depth and high strains were recorded at the bottom flange especially at the maximum load. At moment level of 298 kNm strains exceed the yield strains in the beam bottom flange at Sec. 1-1, 2-2 and 3-3 indicating the yield of the beam flange plate as shown in Fig. 6.25. By reducing the connection center line moment (298 kNm) by 20%, we obtain the actual moment at the face of the column equal to 245 kNm which lie between the range of the yield moment (237 kNm) and the plastic moment (269 kNm) given in Table 6.2. The normal strain at Sec. 1-1 at the top of the beam remains almost zero for all moment levels as seen from Figs. 6.23 - 6.25, clearly indicating that at Sec. 1-1, the top part of the beam does not participate in the bending action. The deformation of the connection C1 is shown in Fig. 6.26. The force transfer takes place predominately through the bottom part. Near the top of the column the recorded strains were very small.

The beam deflection was high at the end of the test as shown in Fig. 6.27. Excessive flange deformations were observed with a gap between the beam flange and the cap-plate (Fig. 6.26), indicating the apparent yielding of the tension bolts. The behavior of this specimen indicated that the tensile force at the tension zone resulting from the applied moment is equally distributed on the four tension bolts due to the excessive deformation of the thin beam flange plate. No significant deformation was visible at the column cap-plate because of its high thickness (20 mm) compared to the beam bottom flange thickness (12 mm).

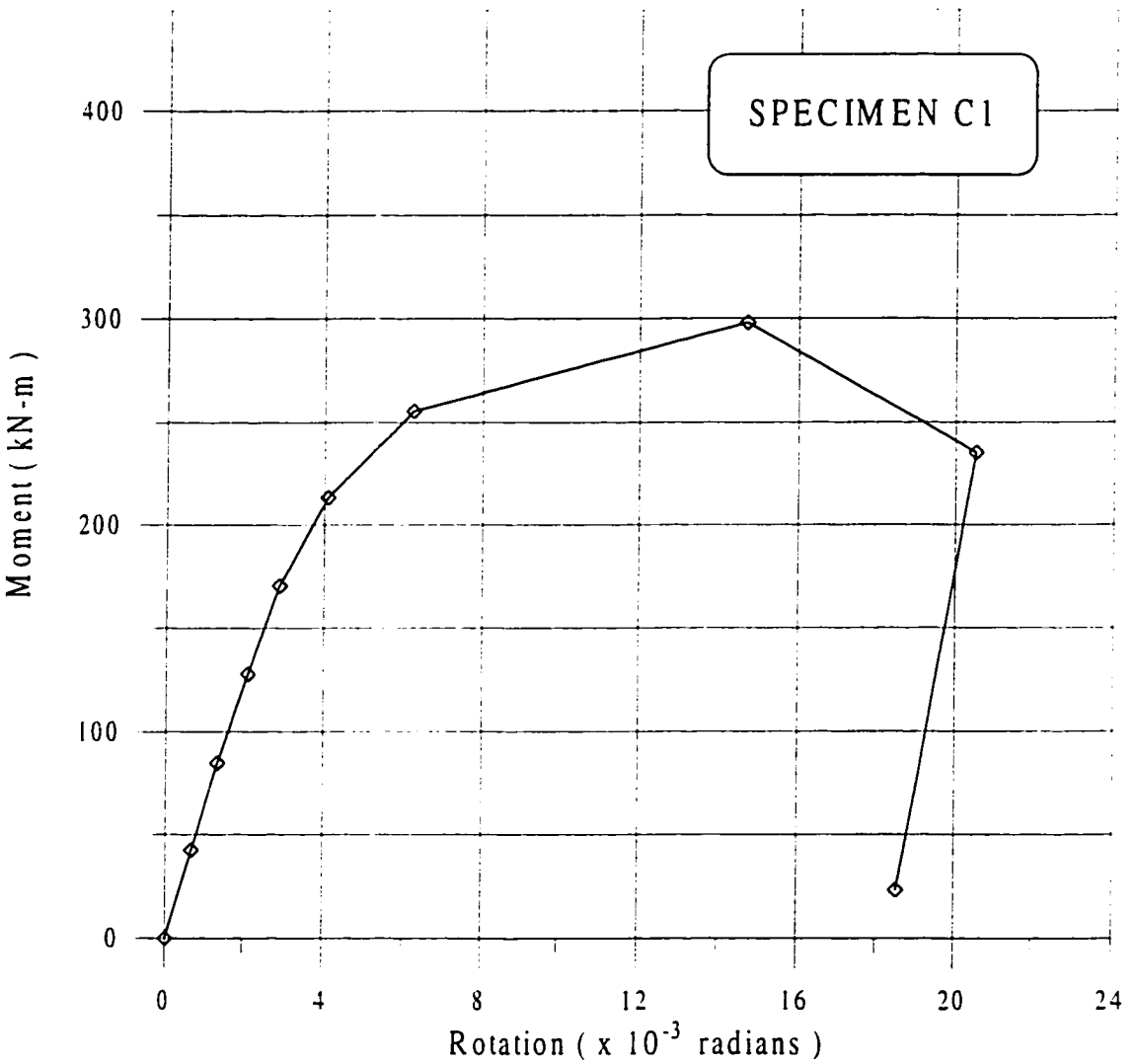

Figure 6.21 Moment-Rotation Relationship for Specimen C1

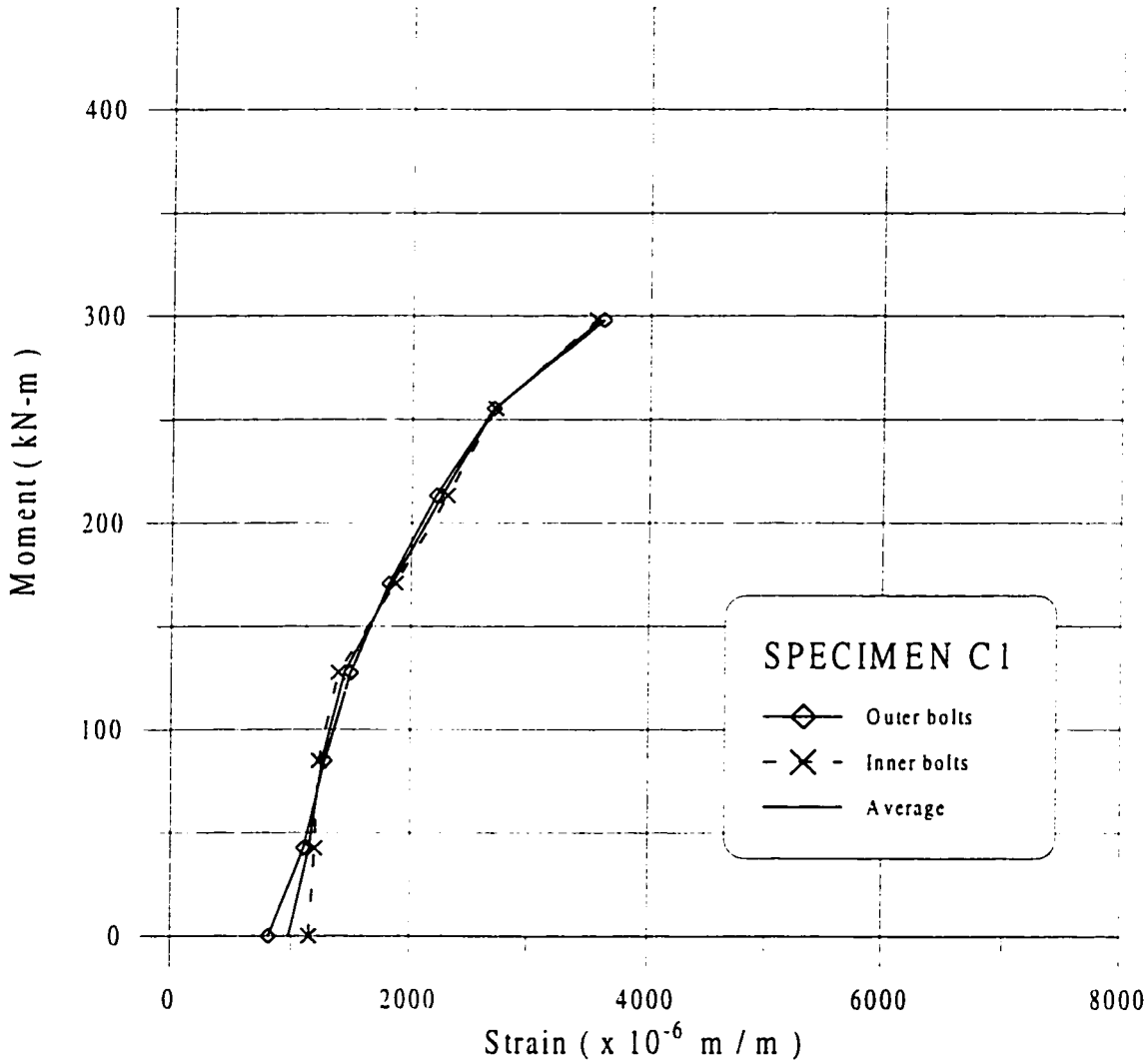

Figure 6.22 Bolts Strains for Specimen C1

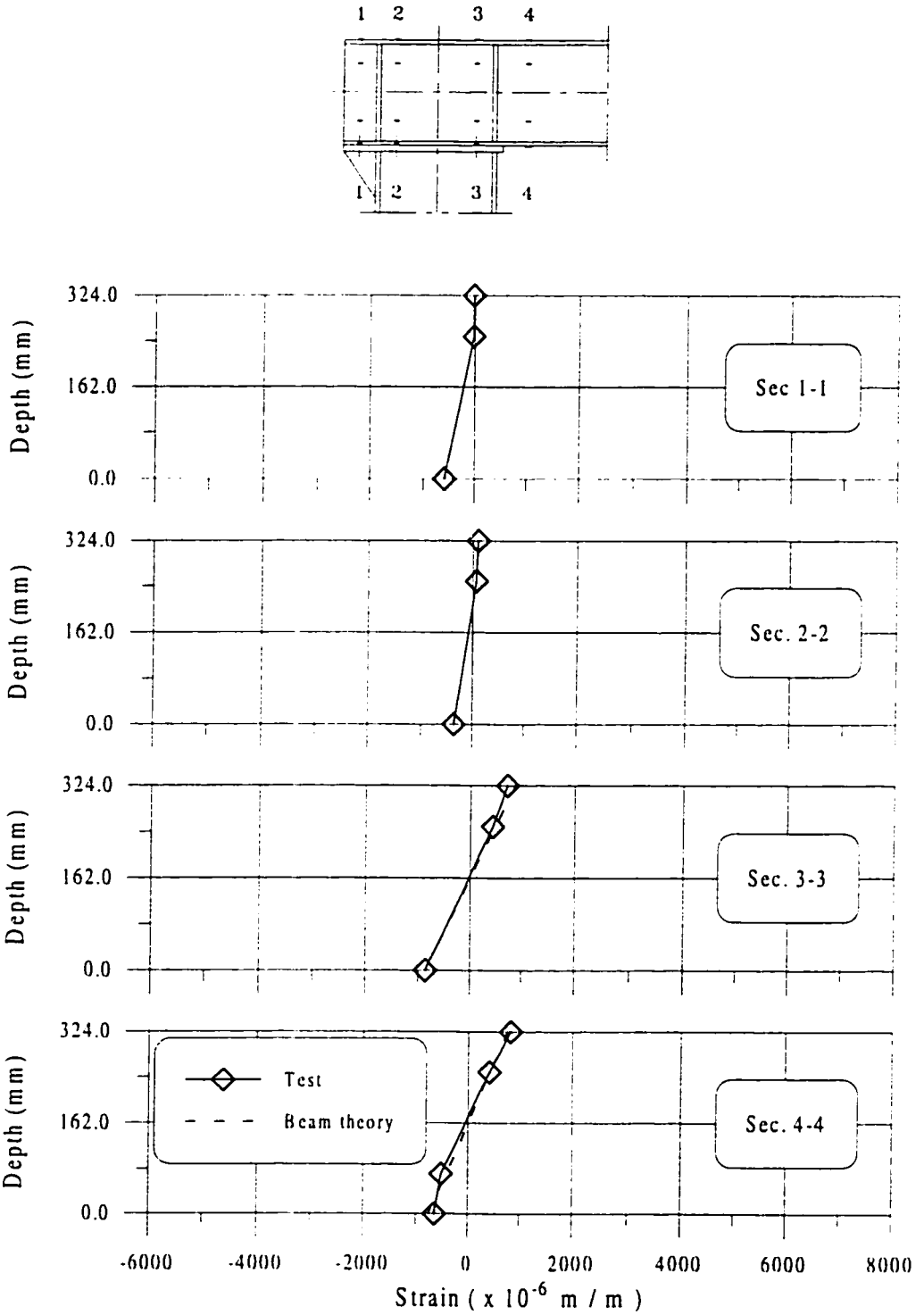

Figure 6.23 Normal Strain Distribution for Specimen C1 at M = 127 kNm

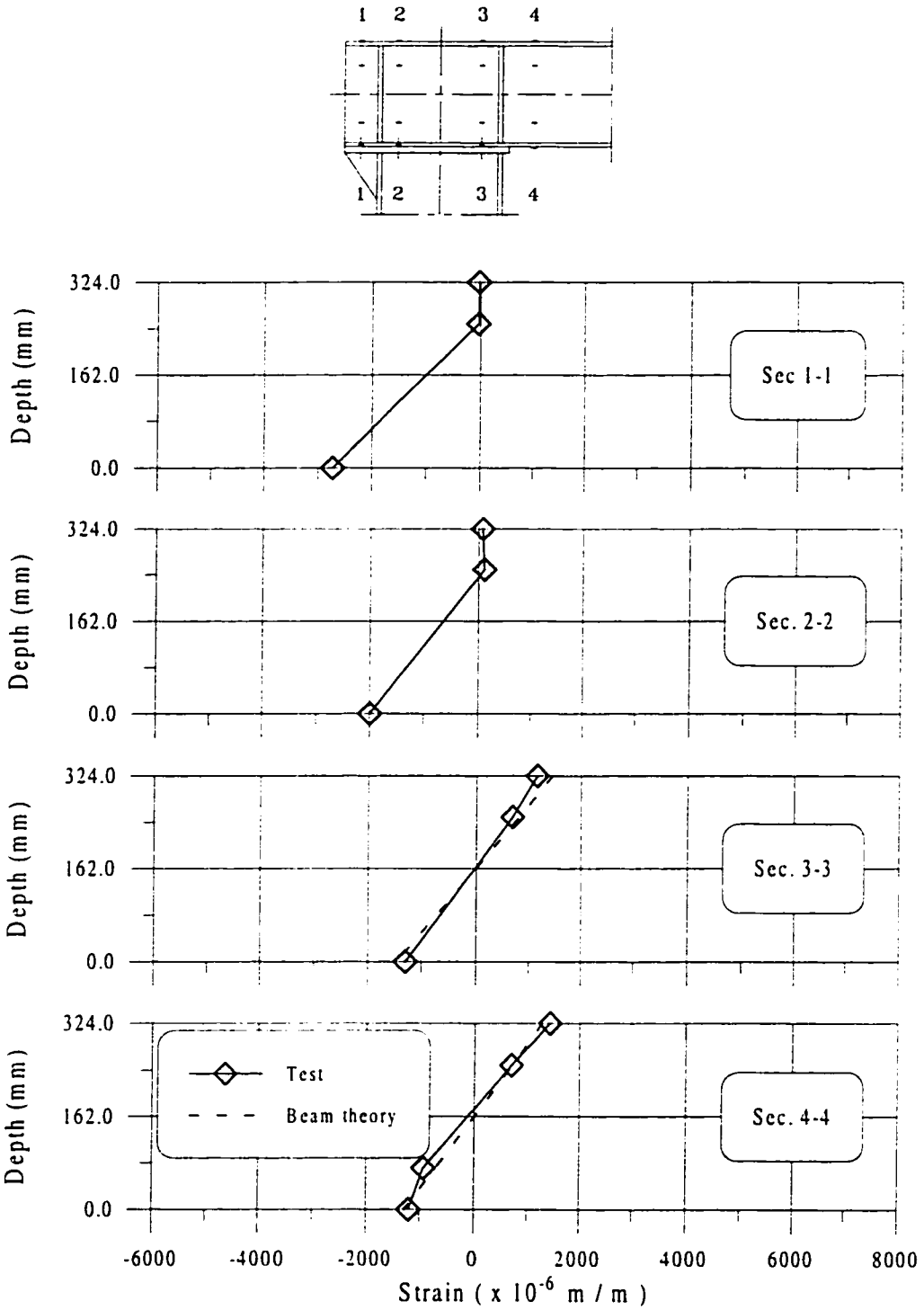

Figure 6.24 Normal Strain Distribution for Specimen C1 at M = 213 kNm

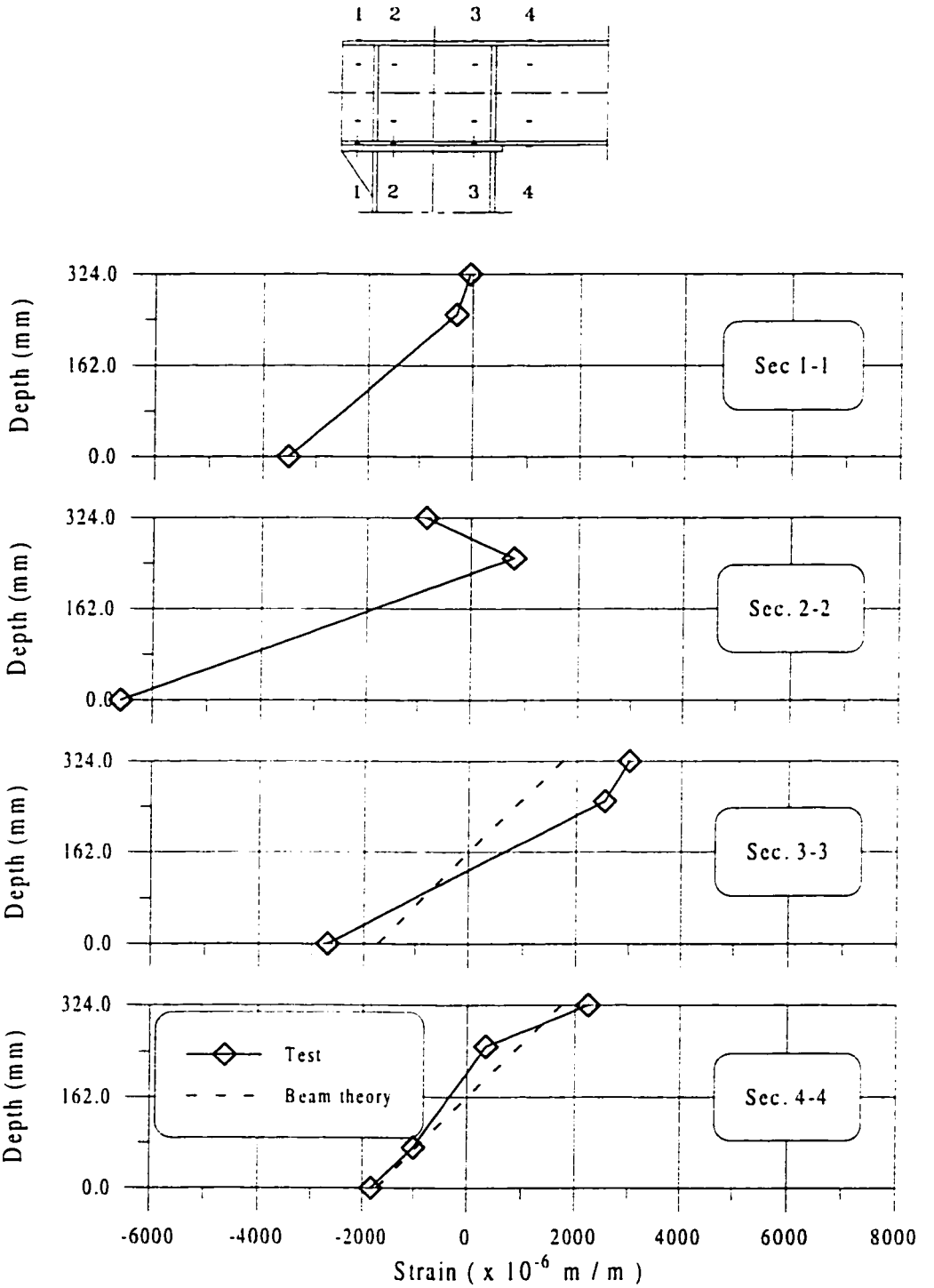

Figure 6.25 Normal Strain Distribution for Specimen C1 at M = 298 kNm

Figure 6.26 Lower Flange Deformation for Specimen C1

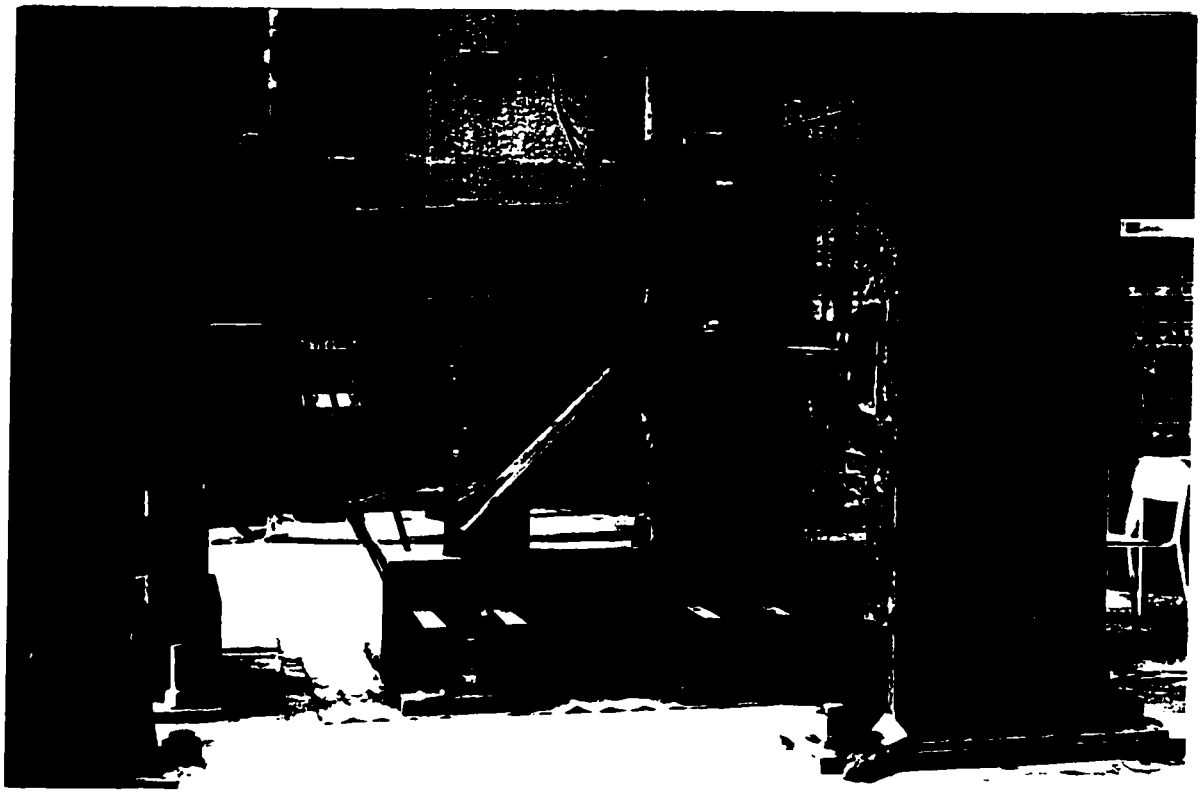

Figure 6.27 Typical Beam Deflection for Specimen C1

6.3.2 Specimen C2

In test number 2, the moment rotation curve plotted in Fig. 6.28 shows that the elastic part of the curve is up to about 300 kNm. The non-linear part extends from 300 kNm and continues up to the maximum value of 400 kNm reached in this test. The unloading path shows approximately the same slope as that of the elastic loading path.

In Fig. 6.29, the outer and the inner bolts strains are plotted. The strain plots, unlike test C1, shows that the bolt strains in the outer bolts are significantly higher than the inner bolts. The outer bolts showed nonlinearity after about 2000 μ, whereas the inner bolts remained linear throughout. The discrepancy between the two lines of bolts indicates that the tensile force in the outer bolt is much higher than the tensile force in the inner bolt, even at high moment. Although the outer bolts were approaching yielding, the inner bolts remain well below the elastic limit. The average strains of the inner and outer bolts are also shown in Fig. 6.29 to represent the average tensile force.

From Figs. 6.28 and 6.29, it was observed that the nonlinear part of the $M-\theta$ curve start at a load level of 300 kNm. At the same level, the strains in the inner bolts were reduced which indicated the beginning of deformation in the beam plate, since the moment at the connection as well as its rotation were increasing. As shown in Fig. 6.29, both of the inner and the outer bolts did not exceed the yield strains since the bolt diameter (25 mm) is relatively large compared to the beam flange thickness (20 mm).

The normal strain distributions are shown in Figs. 6.30 - 6.33. At Secs. 3-3 and 4-4, the strain distribution is almost linear. After 300 kNm the strain distribution of Sec. 2-2 is nonlinear because of the stress concentrations at the connection at this local section. The longitudinal distribution of the normal strain at the top beam flange is increasing from Sec. 1-1 to Sec. 4-4 which means that the upper left corner of the connection is not active in transmitting the moment from the beam to the column. The maximum reached moment for the specimen (398 kNm), at centerline of column, gave at Sec. 4-4 a column face moment of 327 kNm which was near to the plastic moment given in Table 6.2. Figure 6.33 shows clearly that Sec. 4-4 was yielding at both the upper and lower flange. The end of this test is due to high deflection at the free beam end.

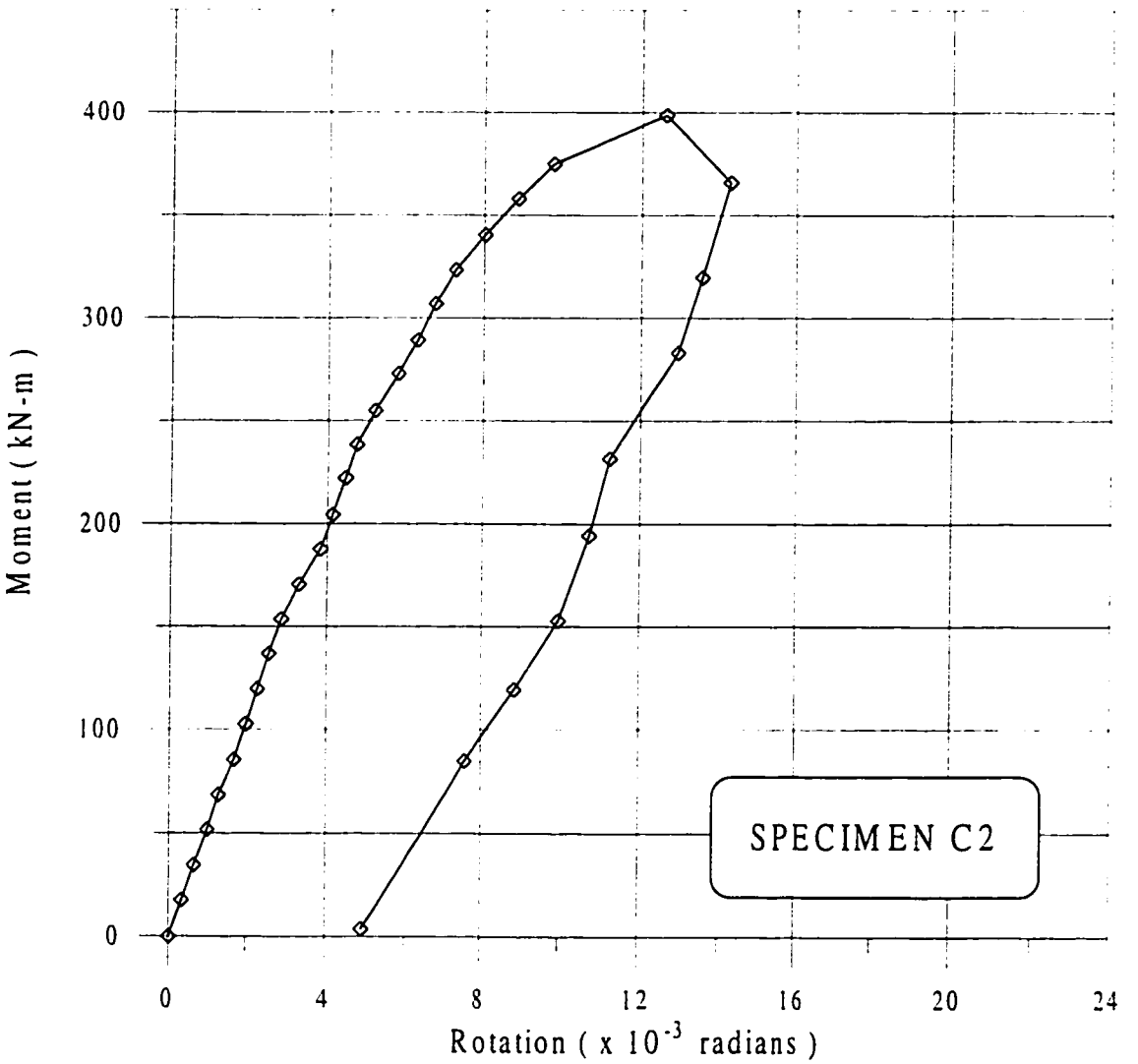

Figure 6.28 Moment-Rotation Relationship for Specimen C2

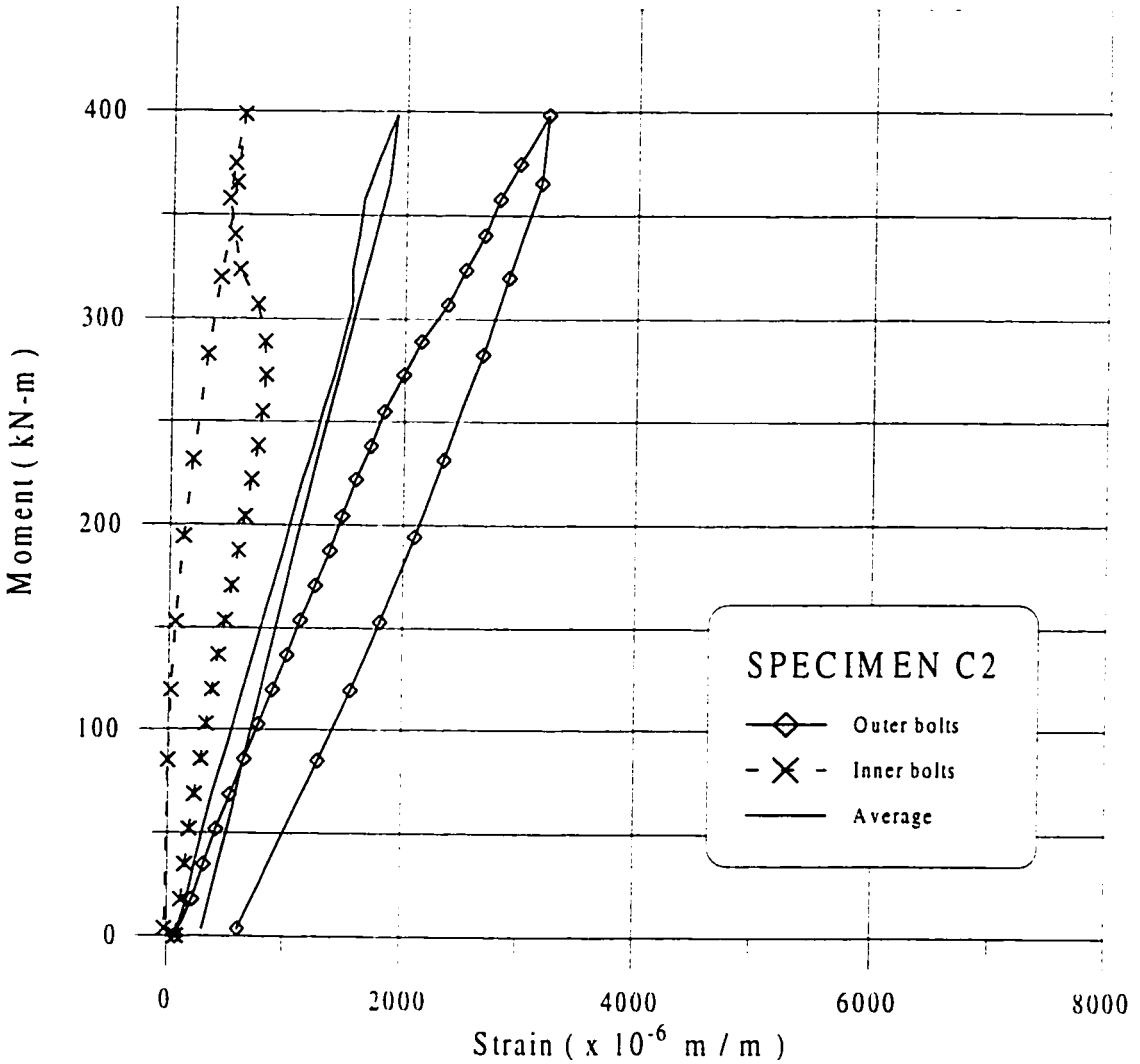

Figure 6.29 Bolts Strains for Specimen C2

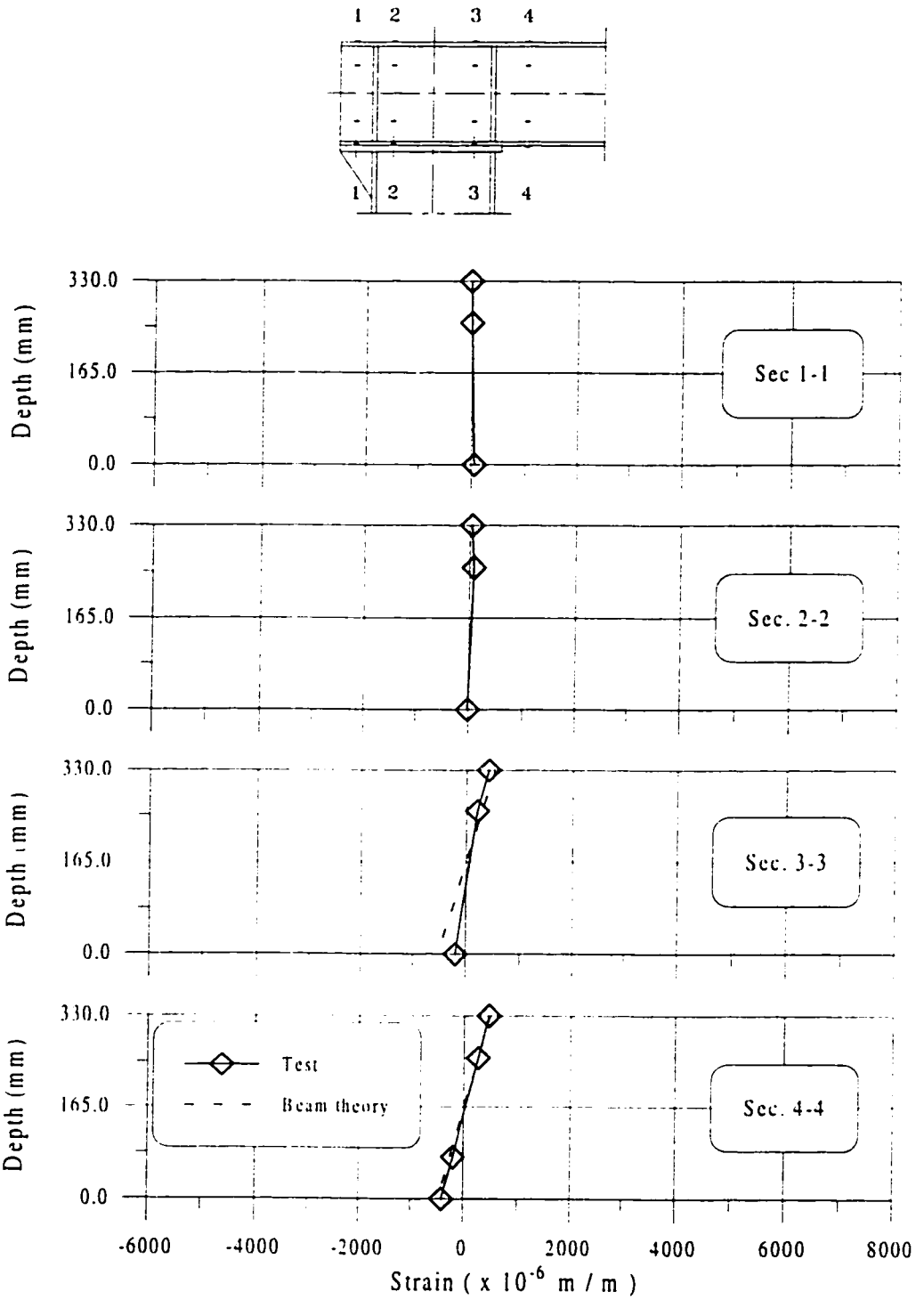

Figure 6.30 Normal Strain Distribution for Specimen C2 at M = 102 kNm

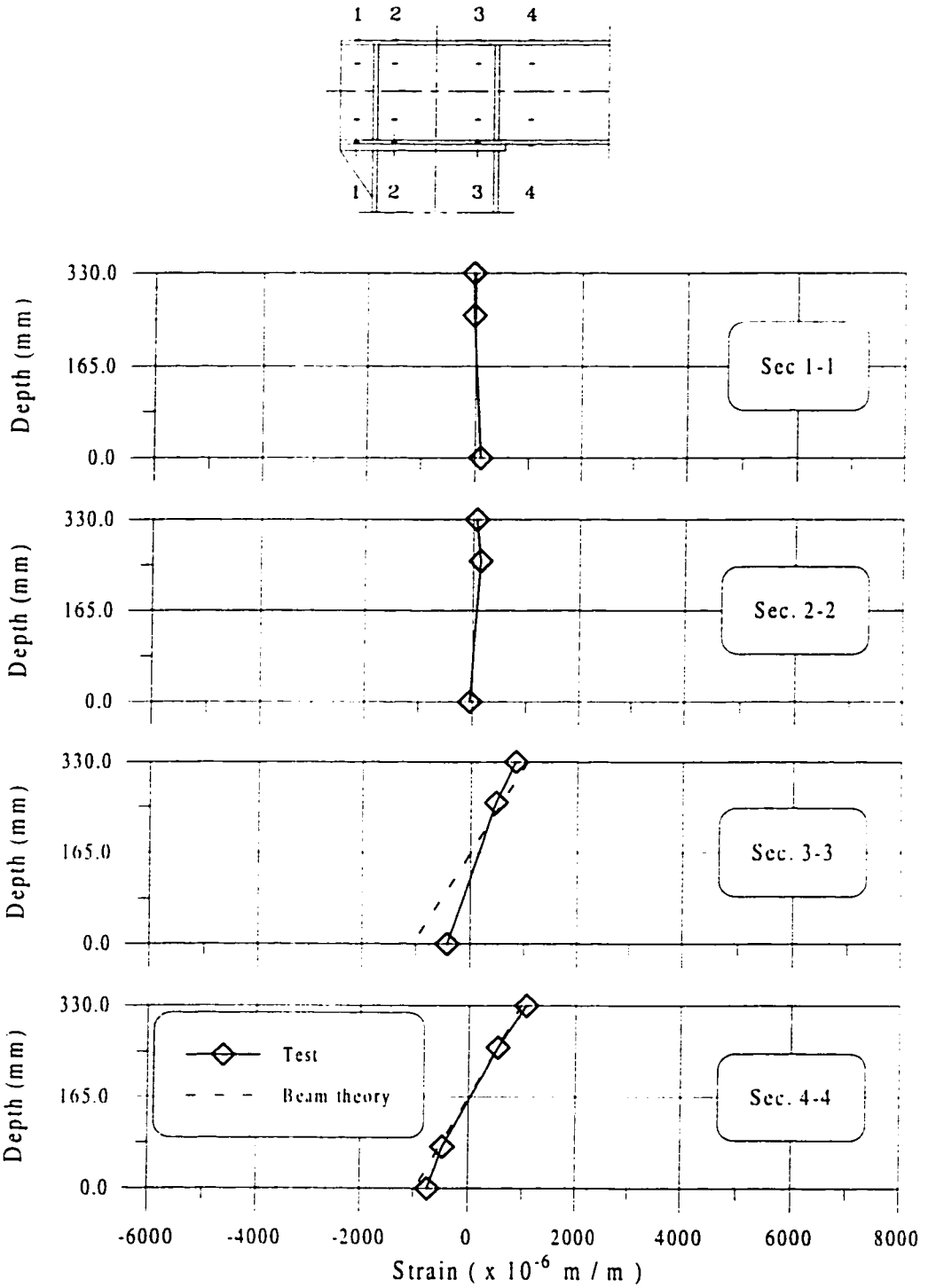

Figure 6.31 Normal Strain Distribution for Specimen C2 at M = 204 kNm

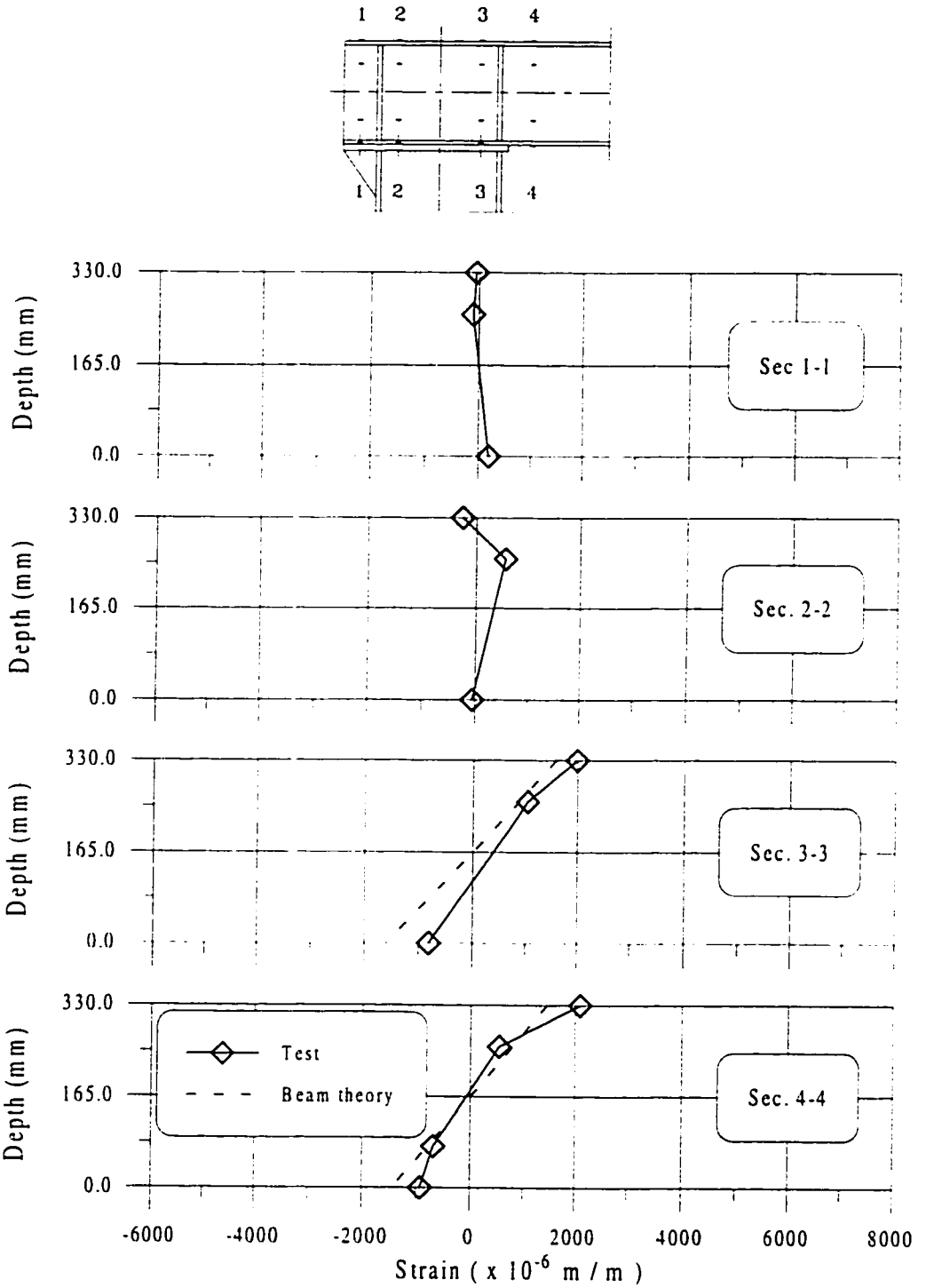

Figure 6.32 Normal Strain Distribution for Specimen C2 at M = 307 kNm

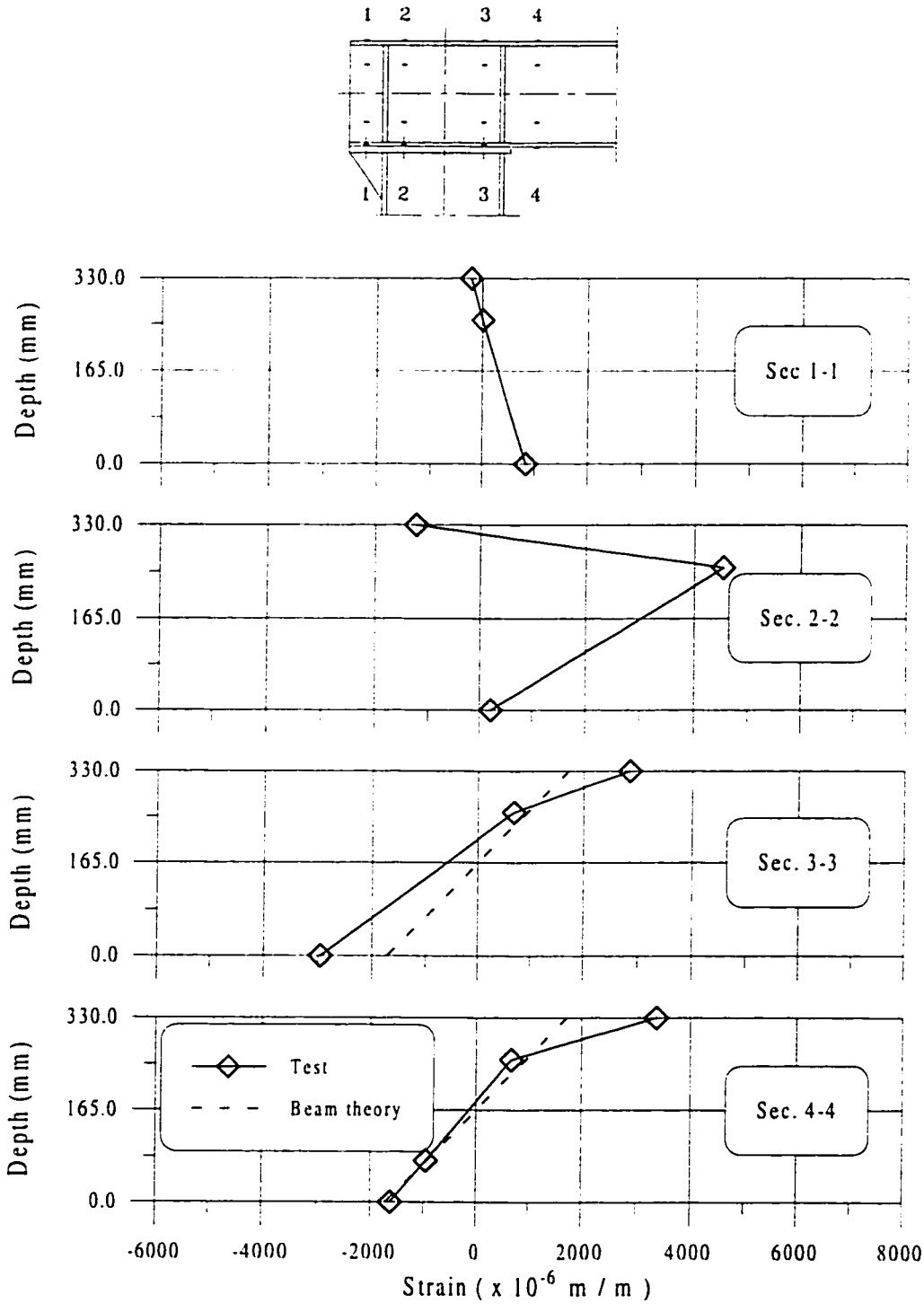

Figure 6.33 Normal Strain Distribution for Specimen C2 at M = 398 kNm

6.3.3 Specimen C3

As stated earlier, C3 and C1 are of the same Group A. The $M-\theta$ curve is shown in Fig. 6.34. A comparison of the $M-\theta$ curves for C1 and C3 (Figs. 6.21 and 6.34), shows that C3 has slightly higher initial stiffness than C1. Also, the maximum moment of C3 is much higher than C1. The reason is that C3 is stiffer than C1 due to the increase of bolt diameter from 19 mm to 22 mm and the beam plate thickness from 12 mm to 20 mm, although the two beams are of the same cross section. The plot in Fig. 6.34 clearly shows that the sufficient inelastic rotation was not captured, as the test was aborted on the incipient of large deformation, avoiding failure of the test.

Two distinct curves for strain distribution are shown in Fig. 6.35 for the outer and inner tension bolts. Compared with Fig. 6.22 for C1, it can be concluded that outer bolts have higher strains than inner ones for C3. The reason of this is the increase in the beam plate thickness.

Referring to Fig. 6.35, it can be shown that the bolts strains are linear up to 200 kNm. Beyond this level, the outer bolts carried more forces with yield strains. At the same time the forces in the inner bolts were released in the range of 200 kNm to 250 kNm, then the force increased up to 350 kNm where the outer bolts had their maximum strains of 7500 μ.

The unloading path for C3 is approximately parallel to the initial loading path for the inner and the outer bolts. After unloading, the inner bolts returned to their initial pretension level, but high deformations are observed for the outer bolts. Although the inner bolts obey a nonlinear path during the test, they were still in the elastic range. Comparing the unloading path with the loading path for the inner bolts of C3 (Fig. 6.35) and C2 (Fig. 6.29), it was observed that both bolts returns to their initial preloading strain. But for C3 the unloading force was higher than the loading force, because the outer bolts exceeded their yield strain.

The normal strain distributions shown in Figs. 6.36 - 6.38 indicate that the elastic distribution exists at low levels of applied moments. Then it becomes nonlinear for high moments due to yielding of the flanges. A comparison of the test strains with the elementary beam strain distribution in Fig. 6.38 shows that the flange strains exceeded the yield strains. The moment at the face of the column for this specimen is 251 kNm by reducing the center line of the connection moment (305 kNm) by 20%. Comparing this moment with the theoretical moments shown in Table 6.2, it can be concluded that the test beam moment pass the yield moment (237 kNm) and is near to the plastic moment (269 kNm). The connection deformation shown in Fig. 6.39 shows clearly the effect of shear deformation due to the relatively small web thickness (8 mm).

For specimens C3, C4, C5 and C6 extra strain gages were added to Sec. 1-1, 2-2, 3-3 and 4-4 on the beam web near the bottom flange. Then, the total number of

strain gages per section became four instead of three, to obtain a better strain distribution over the cross-section. Slight deformation was observed in the beam plate. And the test stopped again at excessive deflection of beam.

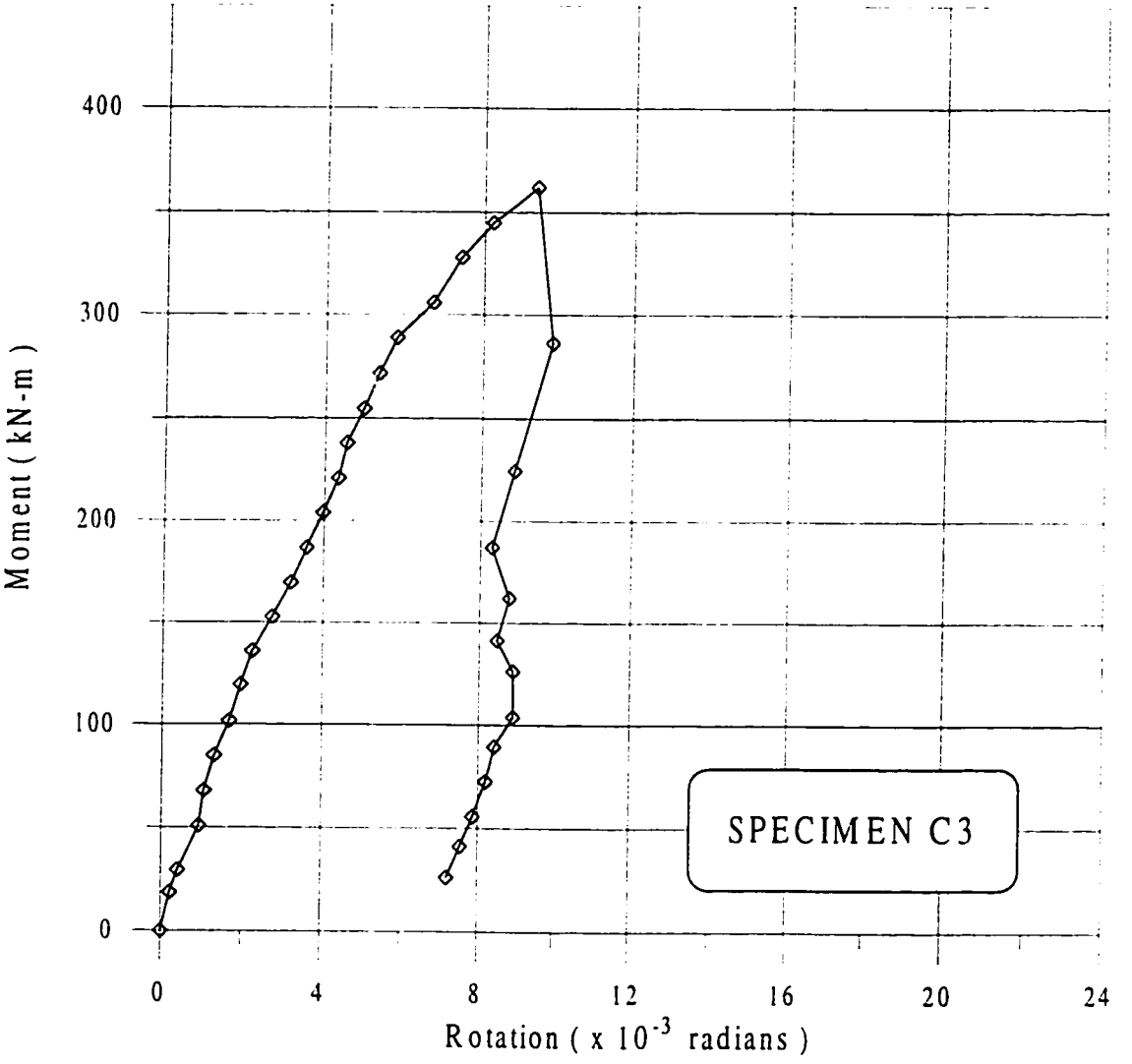

Figure 6.34 Moment-Rotation Relationship for Specimen C3

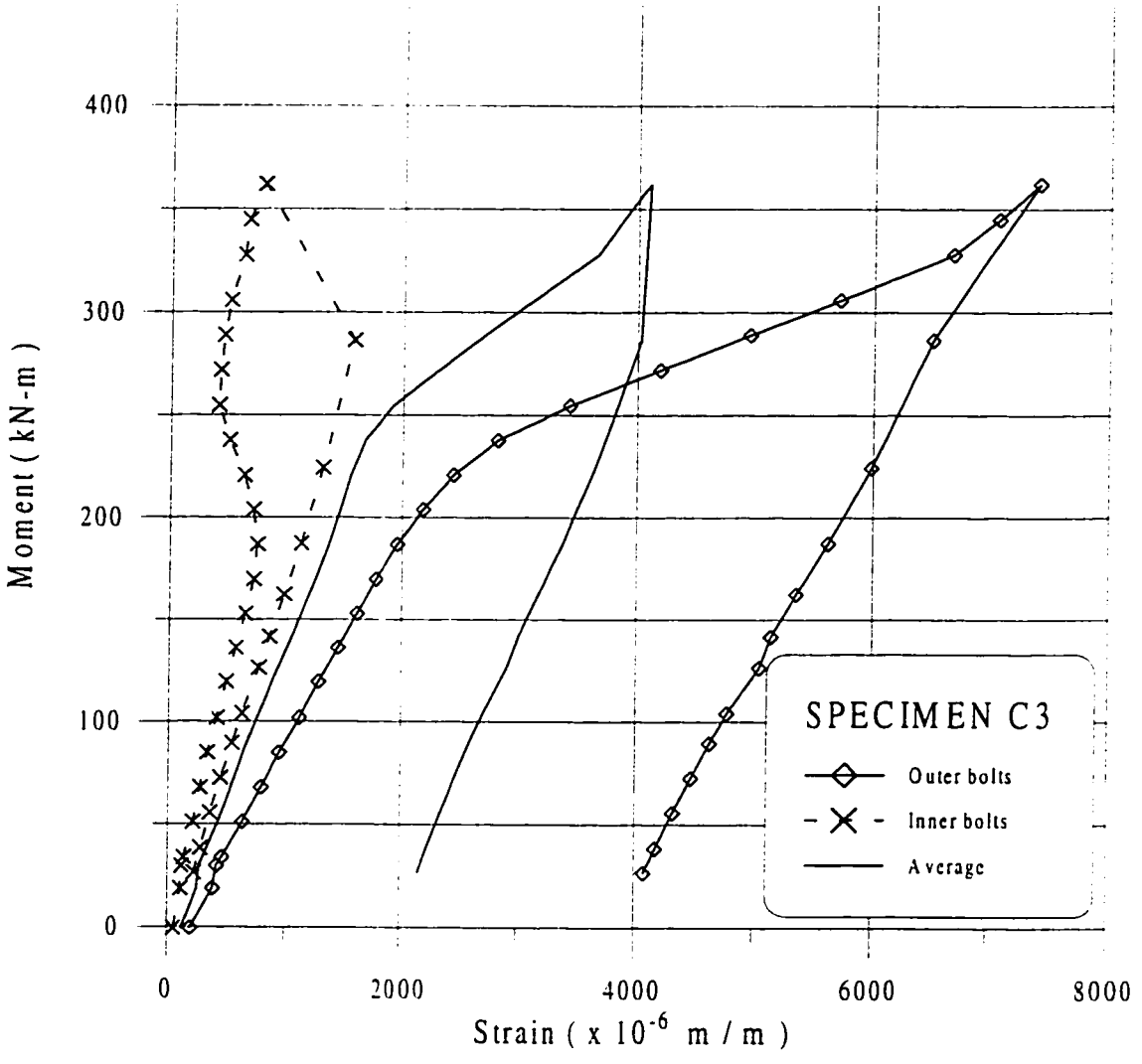

Figure 6.35 Bolts Strains for Specimen C3

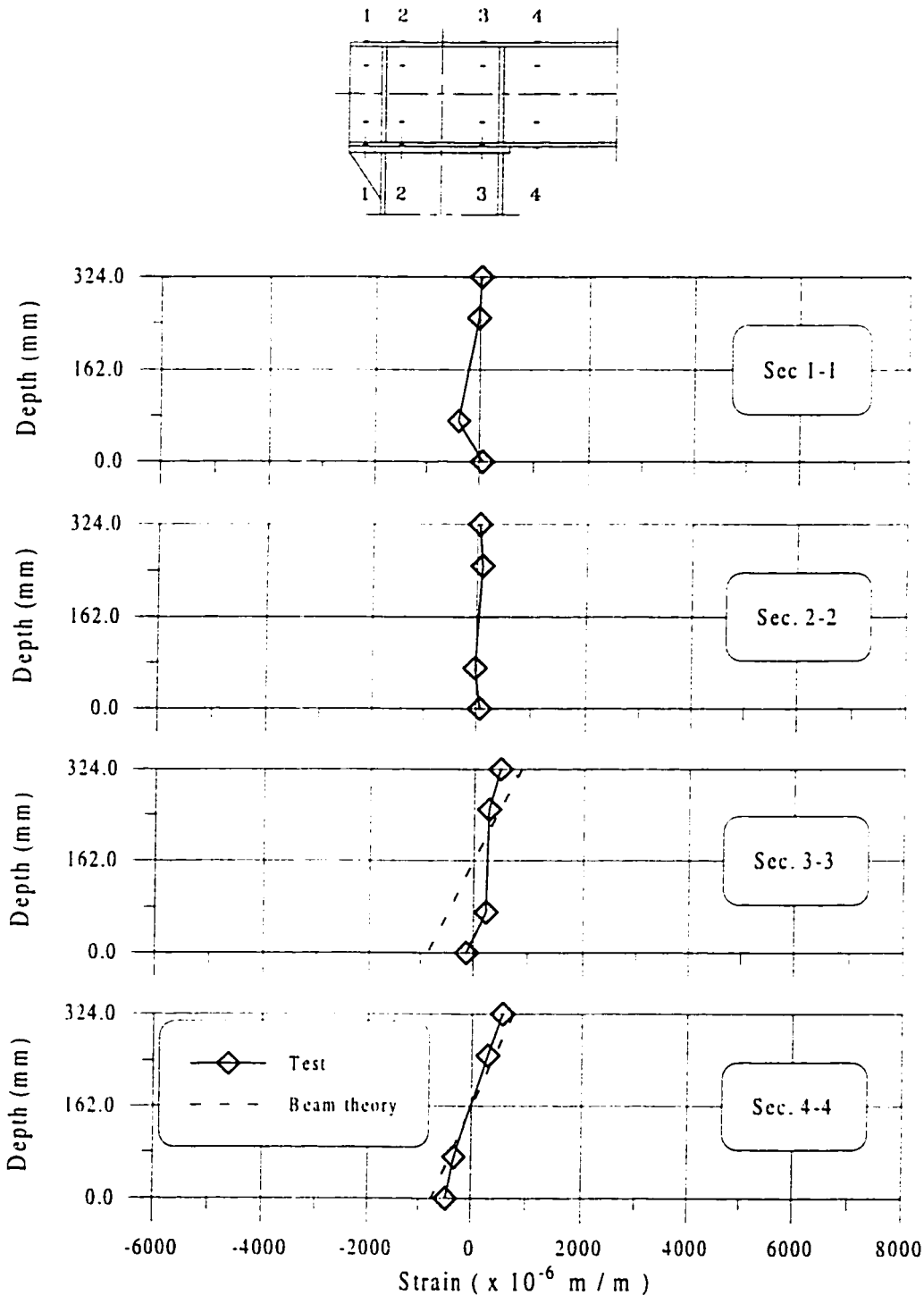

Figure 6.36 Normal Strain Distribution for Specimen C3 at M = 95 kNm

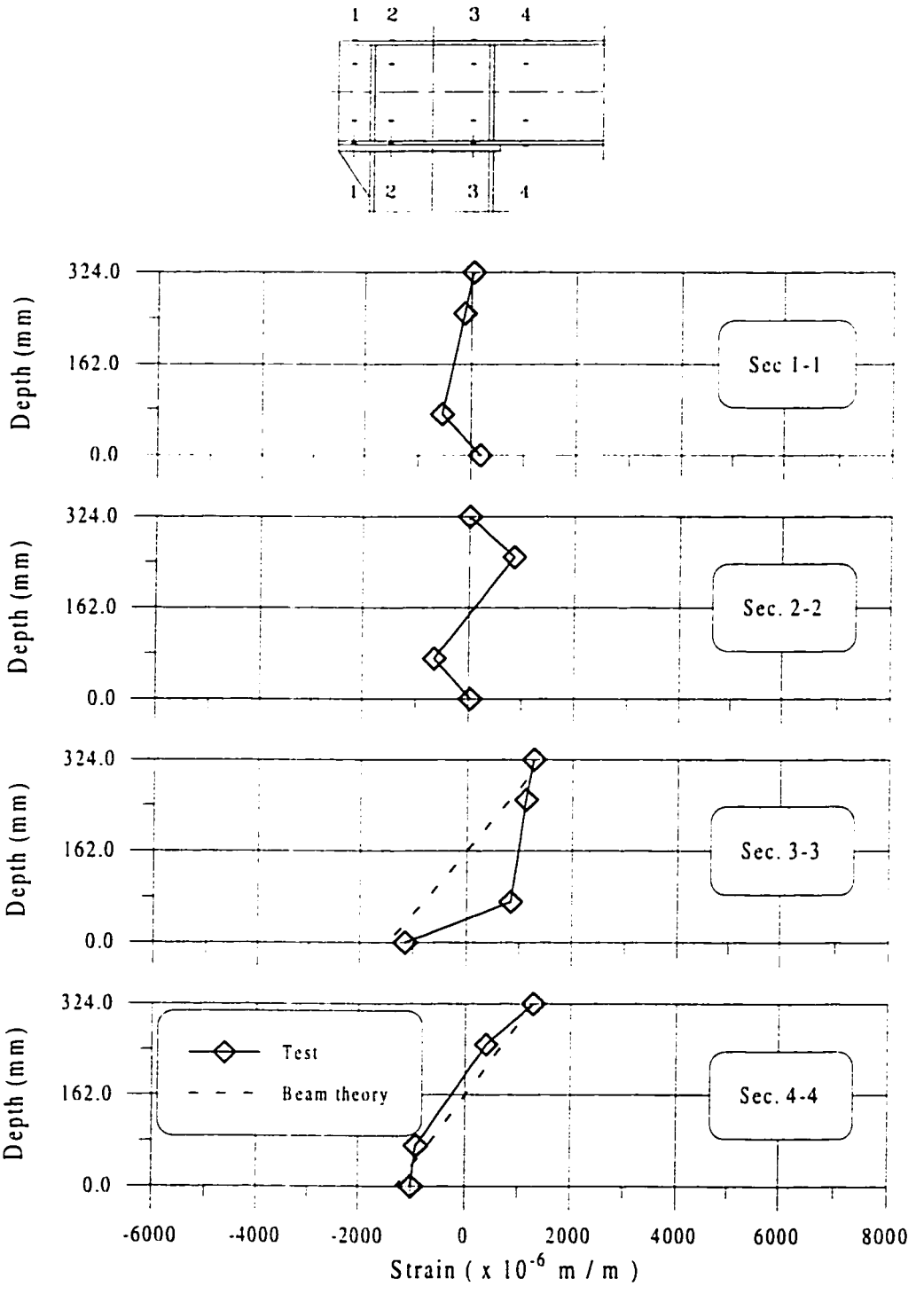

Figure 6.37 Normal Strain Distribution for Specimen C3 at M = 203 kNm

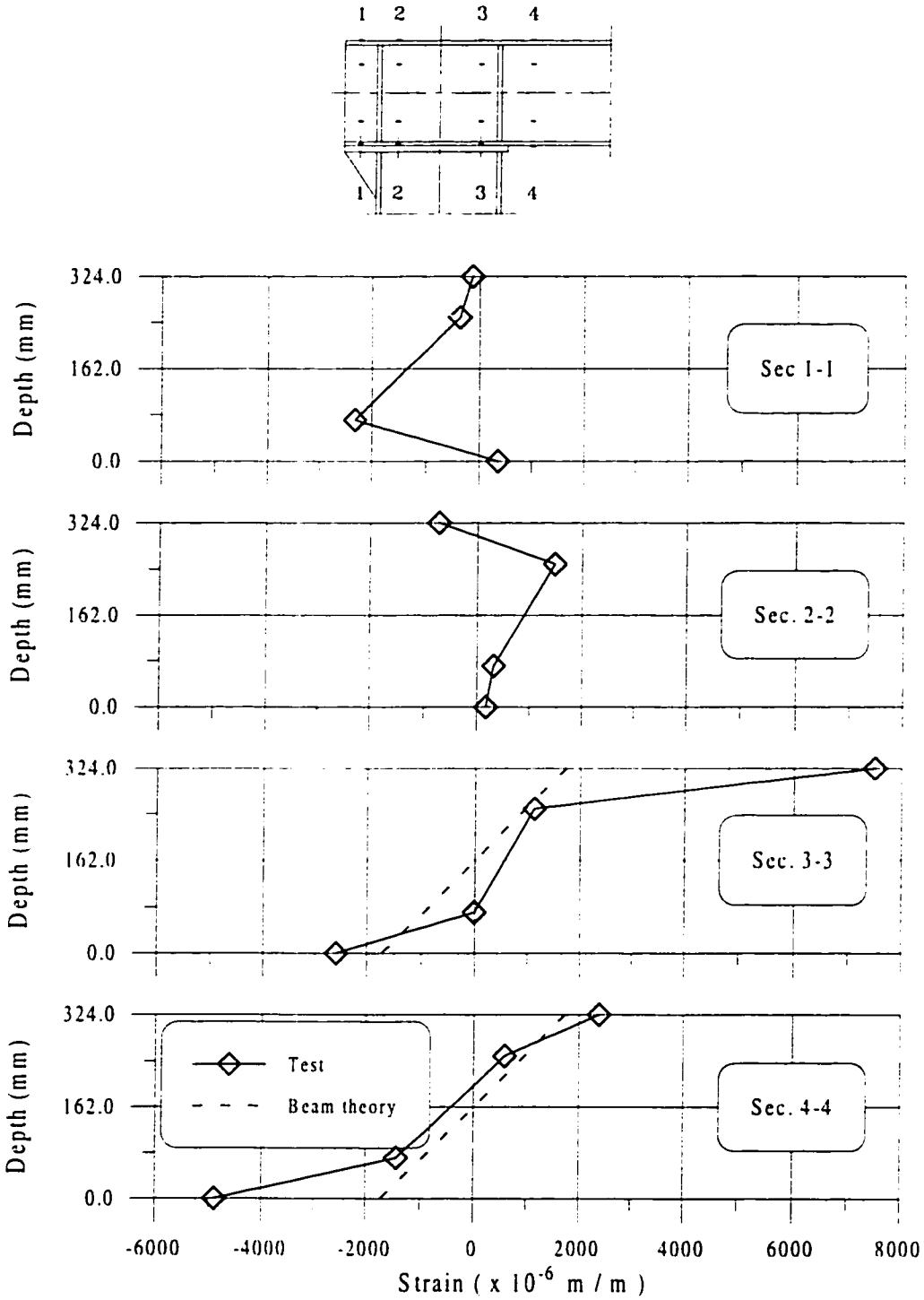

Figure 6.38 Normal Strain Distribution for Specimen C3 at M = 305 kNm

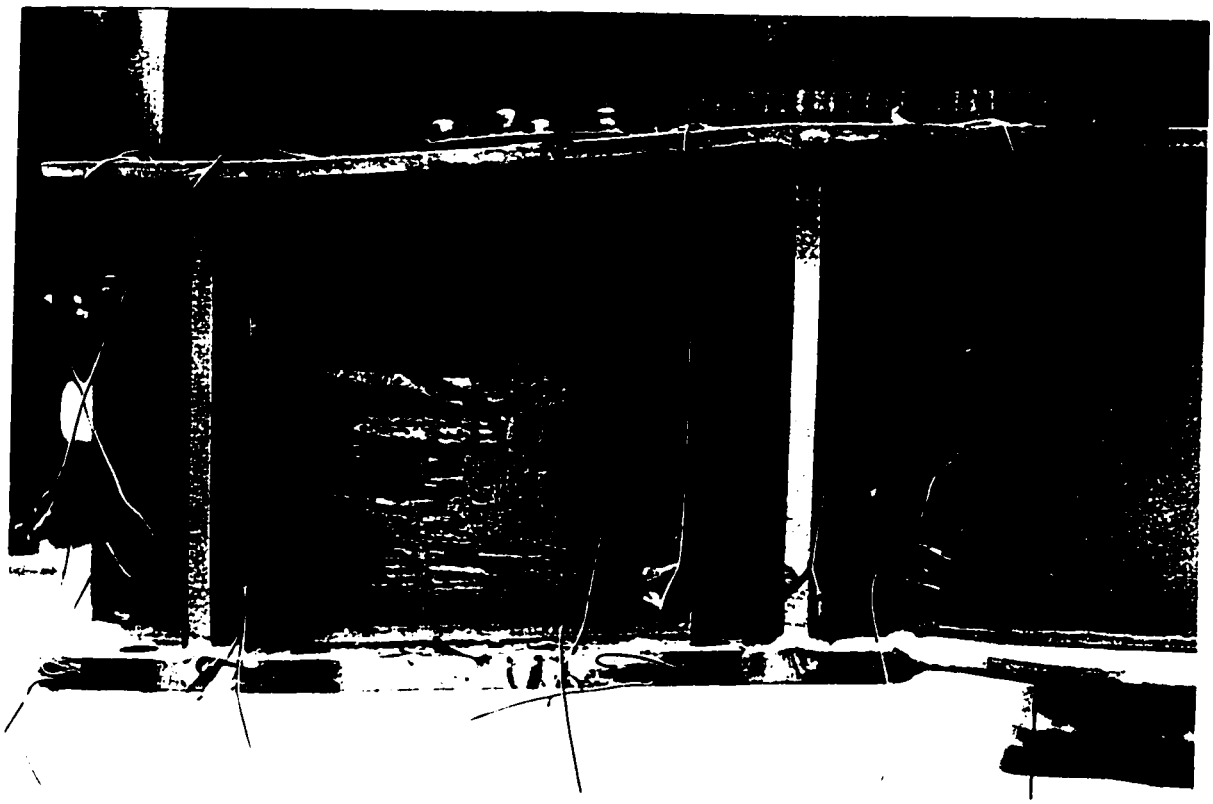

Figure 6.39 Connection Deformation for Specimen C3

6.3.4 Specimen C4

Specimen C4 was the heaviest specimen with the largest plate thickness and the largest bolt diameter. An unexpected brittle failure occur for specimen C4 before reaching the predicted ultimate moment. The failure occur at the beam weld between the web and the bottom flange plate due to inadequate welding size as shown in Fig. 6.40. But the $M-\theta$ curve shown in Fig. 6.41 indicates a good portion of non-linearity before weld fracture.

The sudden failure of the weld in C4 transferred a high value of force to both of the inner and the outer bolts as seen in Fig. 6.42, and both of them yield at this stage. The unloading path shows that permanent deformation is approximately equal for both of outer and inner bolts.

The normal strain distribution for Sec. 3-3, 4-4 show an approximately linear distribution at levels up to 300 kNm (Figs. 6.43 - 6.45). At the moment of weld failure, the strains became very high as shown for Sec. 3-3 in Fig. 6.46 in both of the upper and the lower flanges of the beam exceeding the yield strains. At the failure of the weld the test was stopped. But the maximum reached moment (414 kNm) at the center line of the connection and reduced by 20% at the Sec. 4-4 (340 kNm) indicate that this moment was approaching the beam yield moment (370 kNm) as given in Table 6.2.

Figure 6.40 Weld Failure for Specimen C4

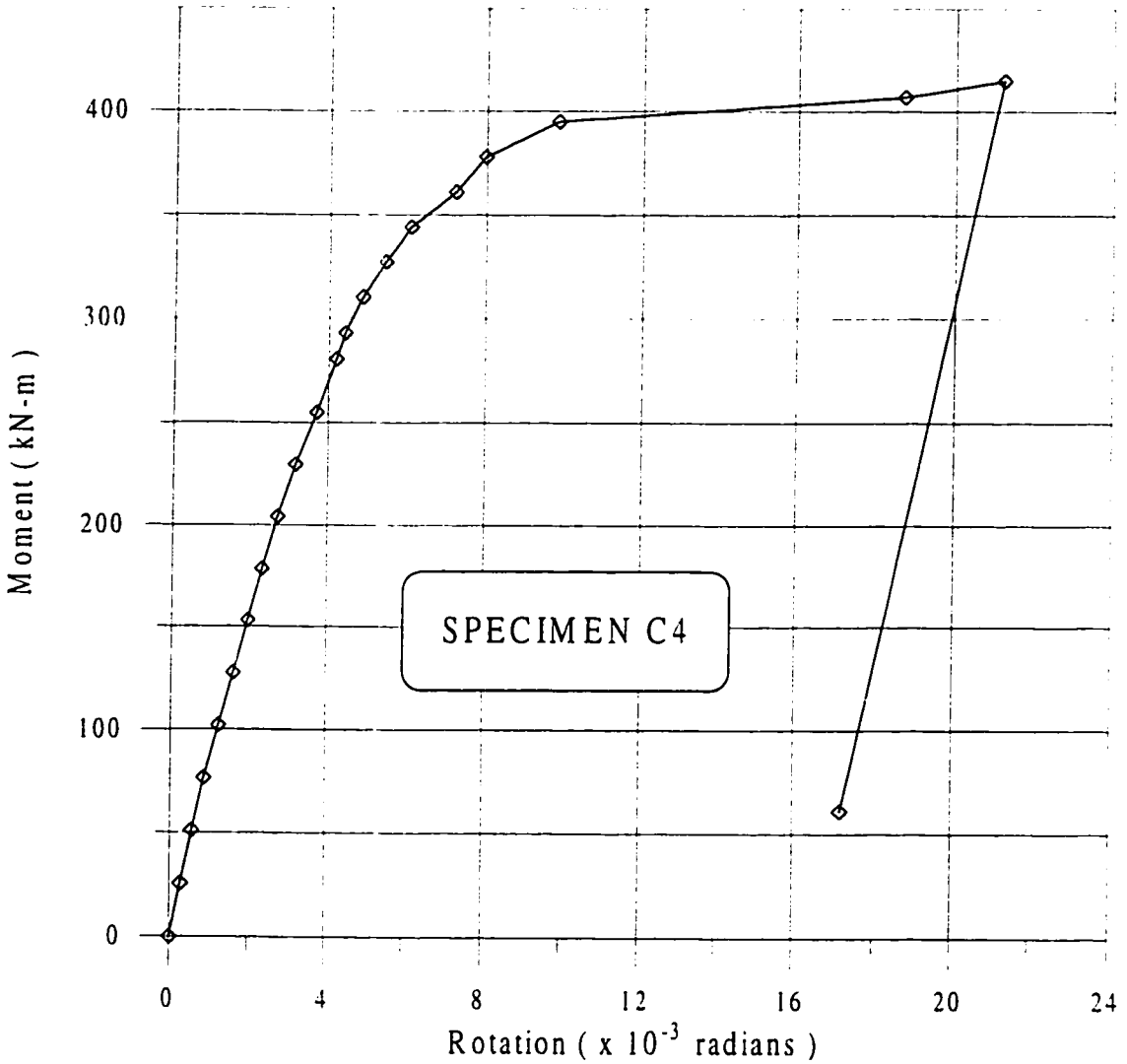

Figure 6.41 Moment-Rotation Relationship for Specimen C4

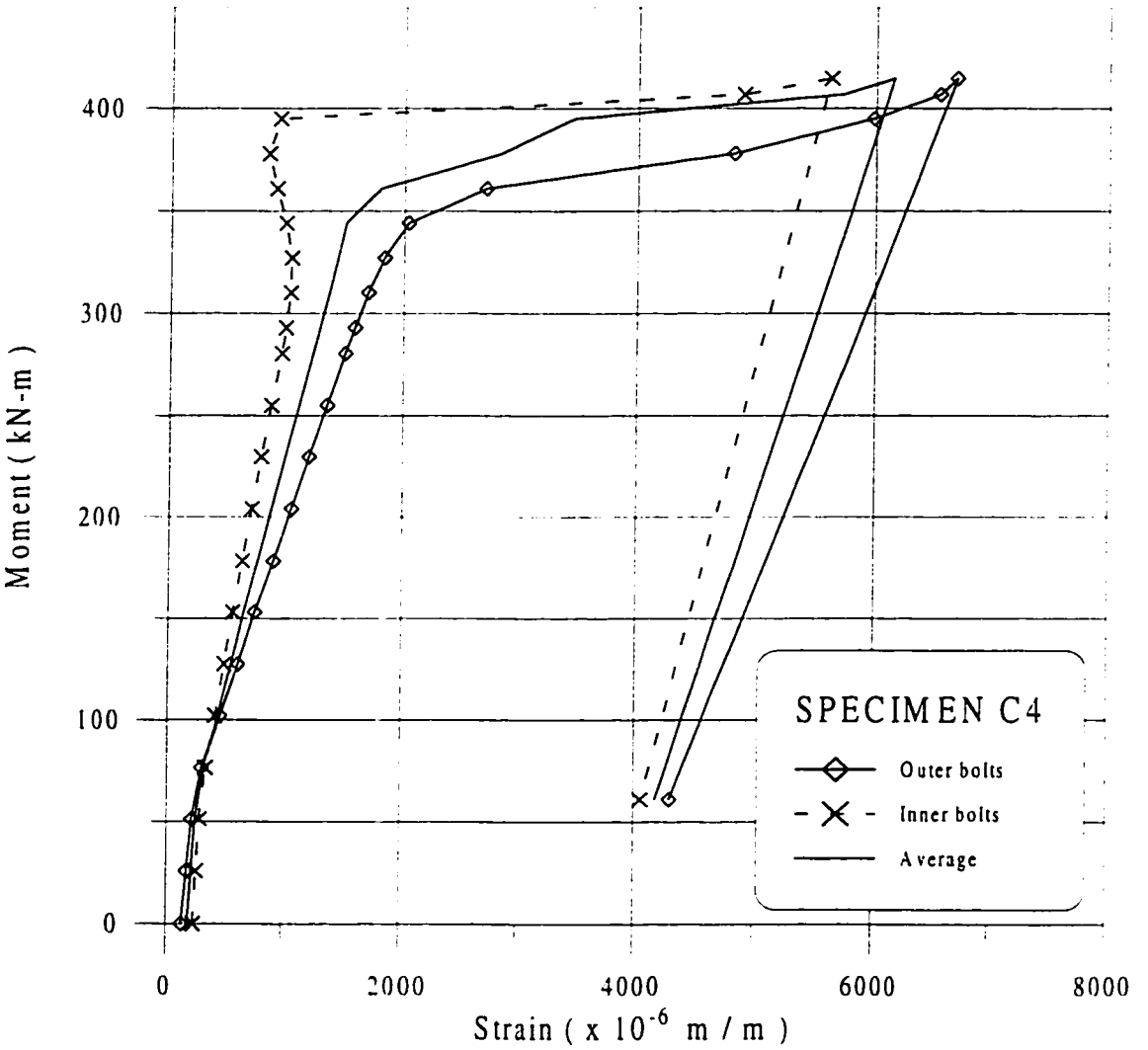

Figure 6.42 Bolts Strains for Specimen C4

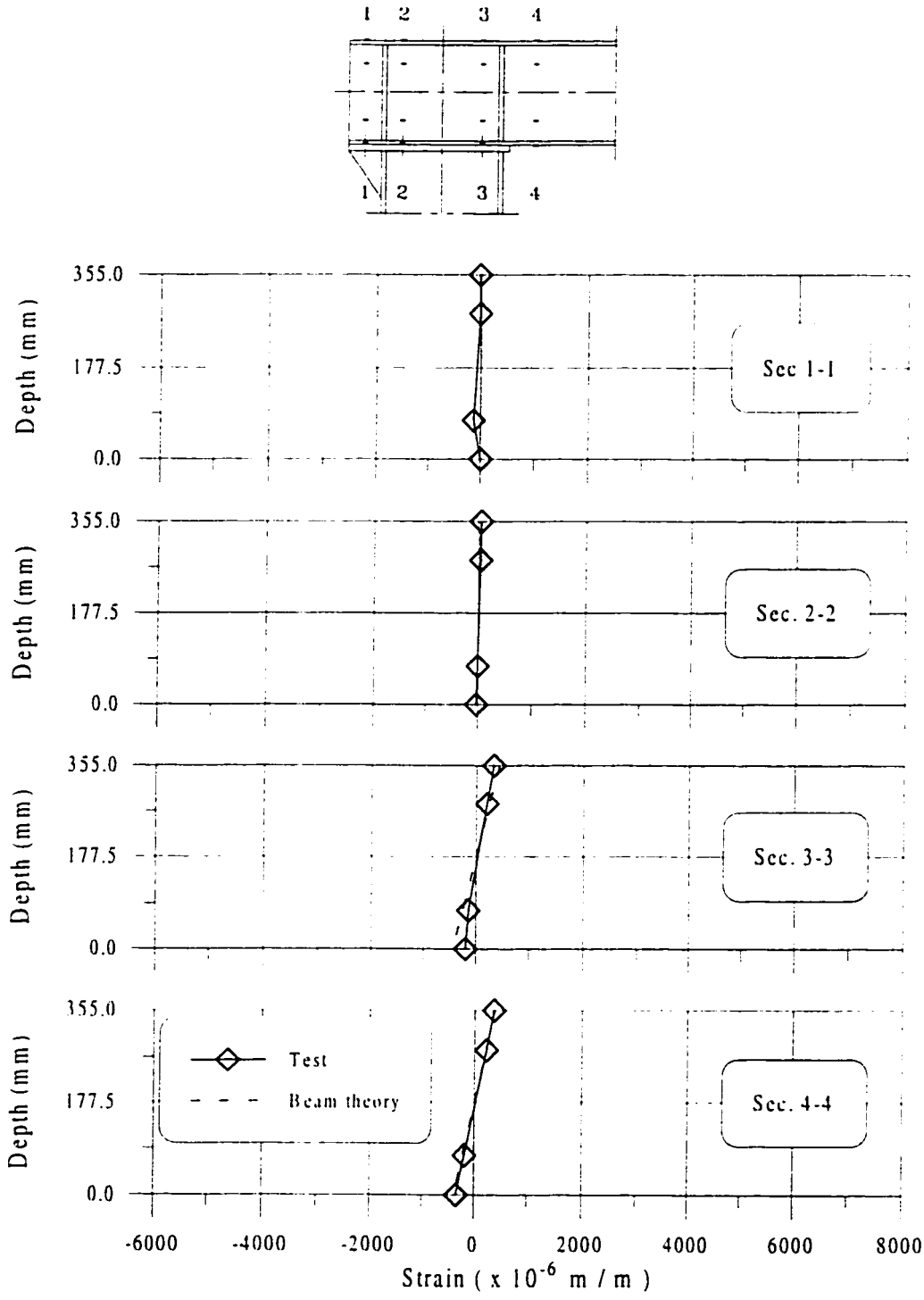

Figure 6.43 Normal Strain Distribution for Specimen C4 at M = 102 kNm

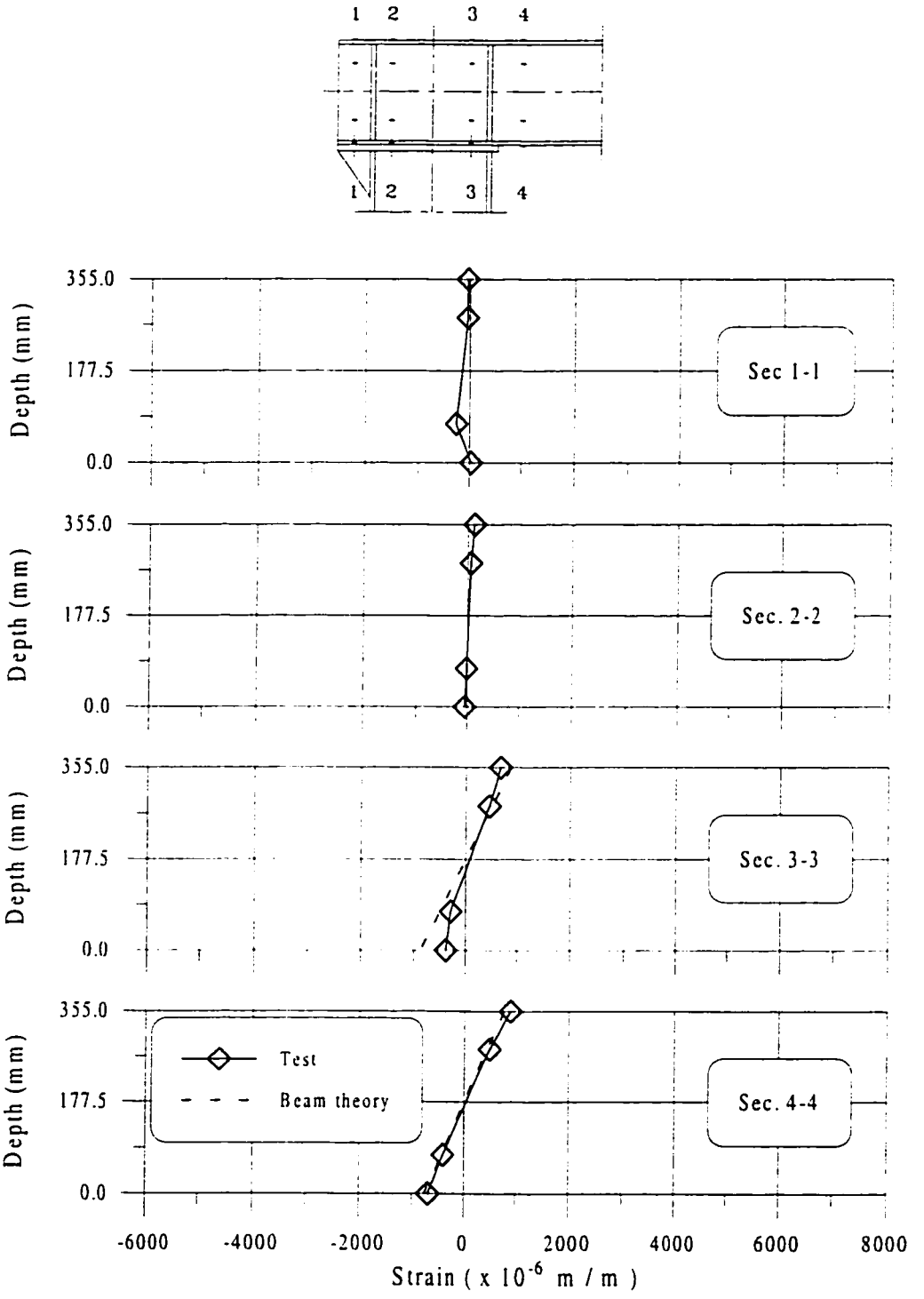

Figure 6.44 Normal Strain Distribution for Specimen C4 at M = 204 kNm

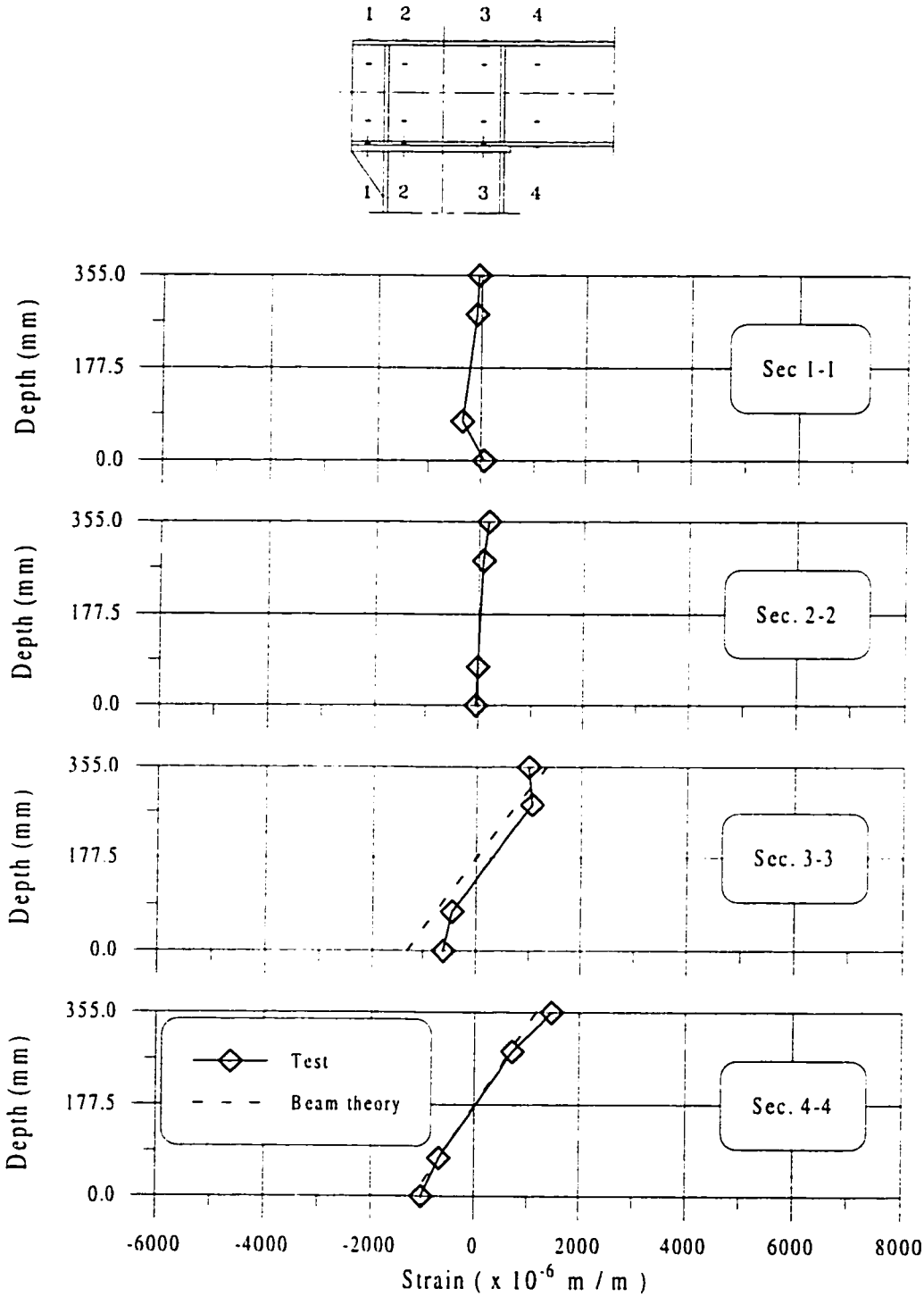

Figure 6.45 Normal Strain Distribution for Specimen C4 at M = 293 kNm

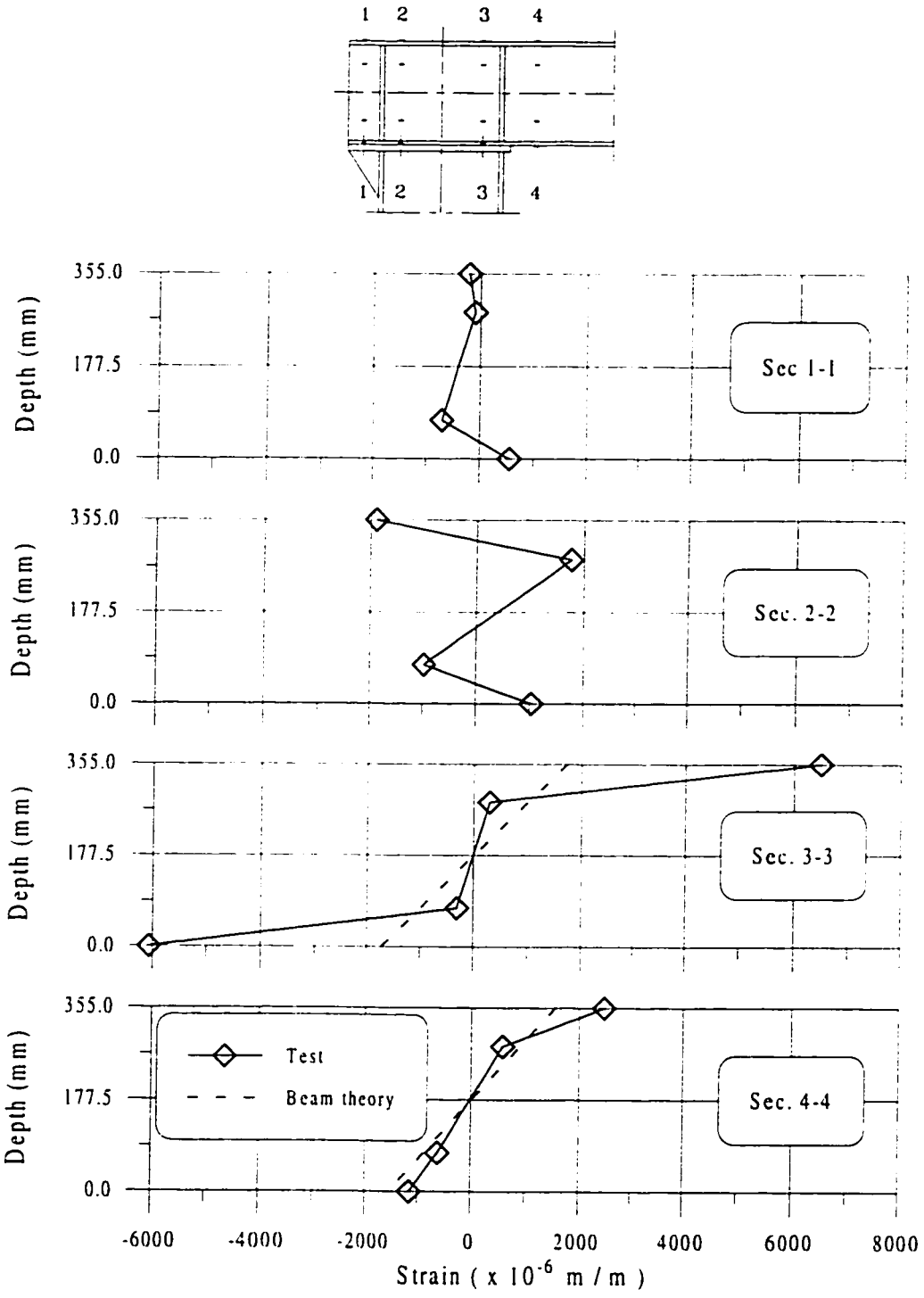

Figure 6.46 Normal Strain Distribution for Specimen C4 at M = 414 kNm

6.3.5 Specimen C5

The two specimens C4 and C5 of Group C had the largest beam cross section with 180 mm flange width and with 355 mm depth. The used bolts are of the same diameter. The failure moment is approximately the same as shown in Figs. 6.41 and 6.47. But the initial stiffness for C5 is lower than that of C4. The difference in the initial stiffness is due to the difference in the beam flange plate thickness (20 mm for specimen C4 and 15 mm for specimen C5).

The bolt strain distribution for Group C shows equal values up to 300 kNm because both of C4 and C5 had relatively thick beam plate (20 mm and 15 mm) which indicates that the effect of plate thickness on the bolt forces above 15 mm is not significant in the elastic range of the connection (Figs. 6.42 and 6.48). Below the level of 300 kNm, the behavior of C4 and C5 show a linear strain distribution for inner and outer bolts with a slope ratio equal approximately to their distances to the compression zone. Beyond the elastic range, the plate thickness has the same effect as discussed for Group B.

The strains distributions for the two tests C4 (Figs. 6.43 - 6.46) and C5 (Figs. 6.49 - 6.52) across different cross-sections show approximately the same trend up to the maximum reached moment (396 kNm). Again the corresponding moment (326 kNm) at Sec. 4-4 was approaching the beam yield moment (370 kNm) given in Table 6.2, and this is clearly shown in Fig. 6.52 for Sec. 4-4 since the lower beam flange did not reach the yield strain.

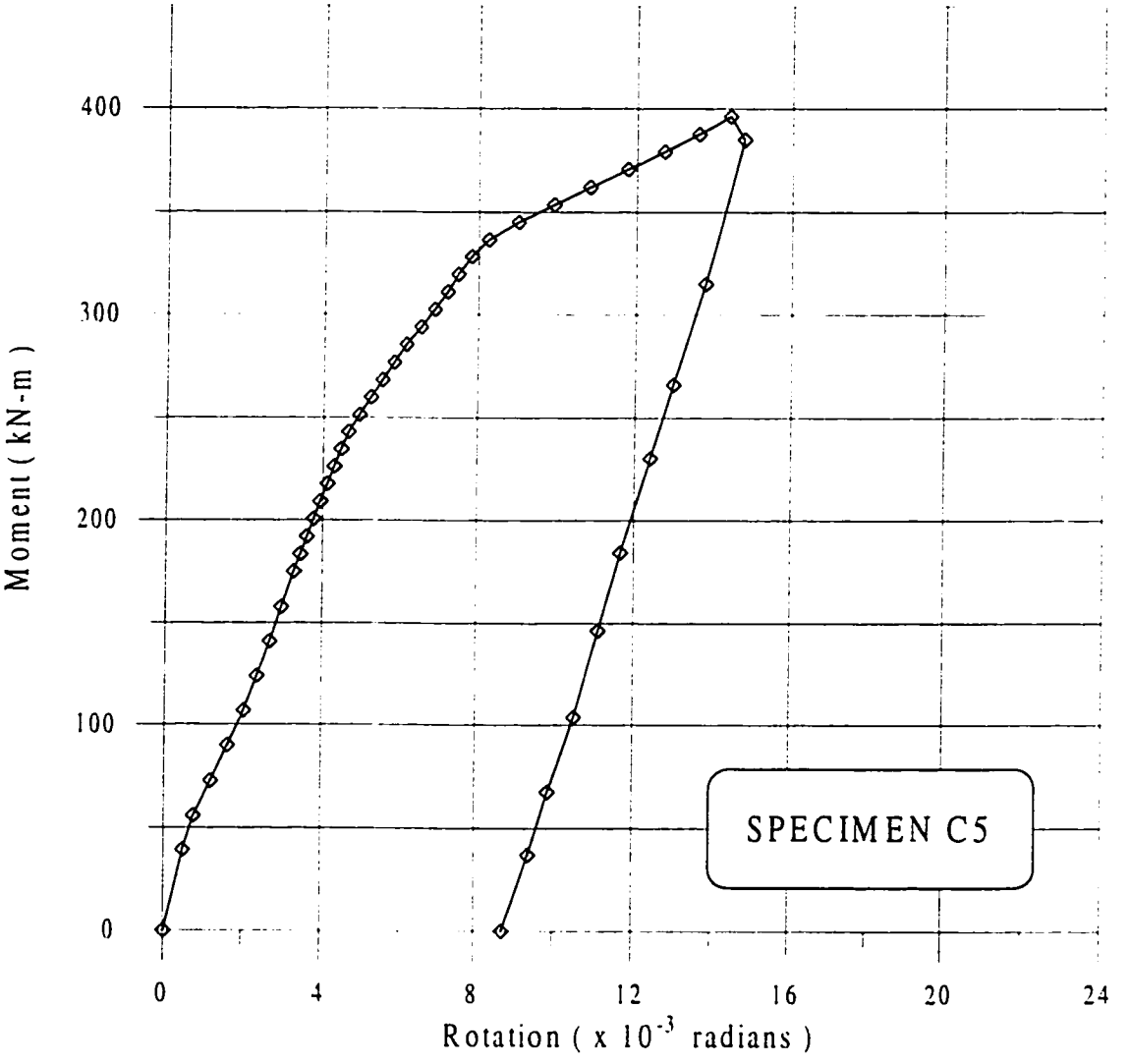

Figure 6.47 Moment-Rotation Relationship for Specimen C5

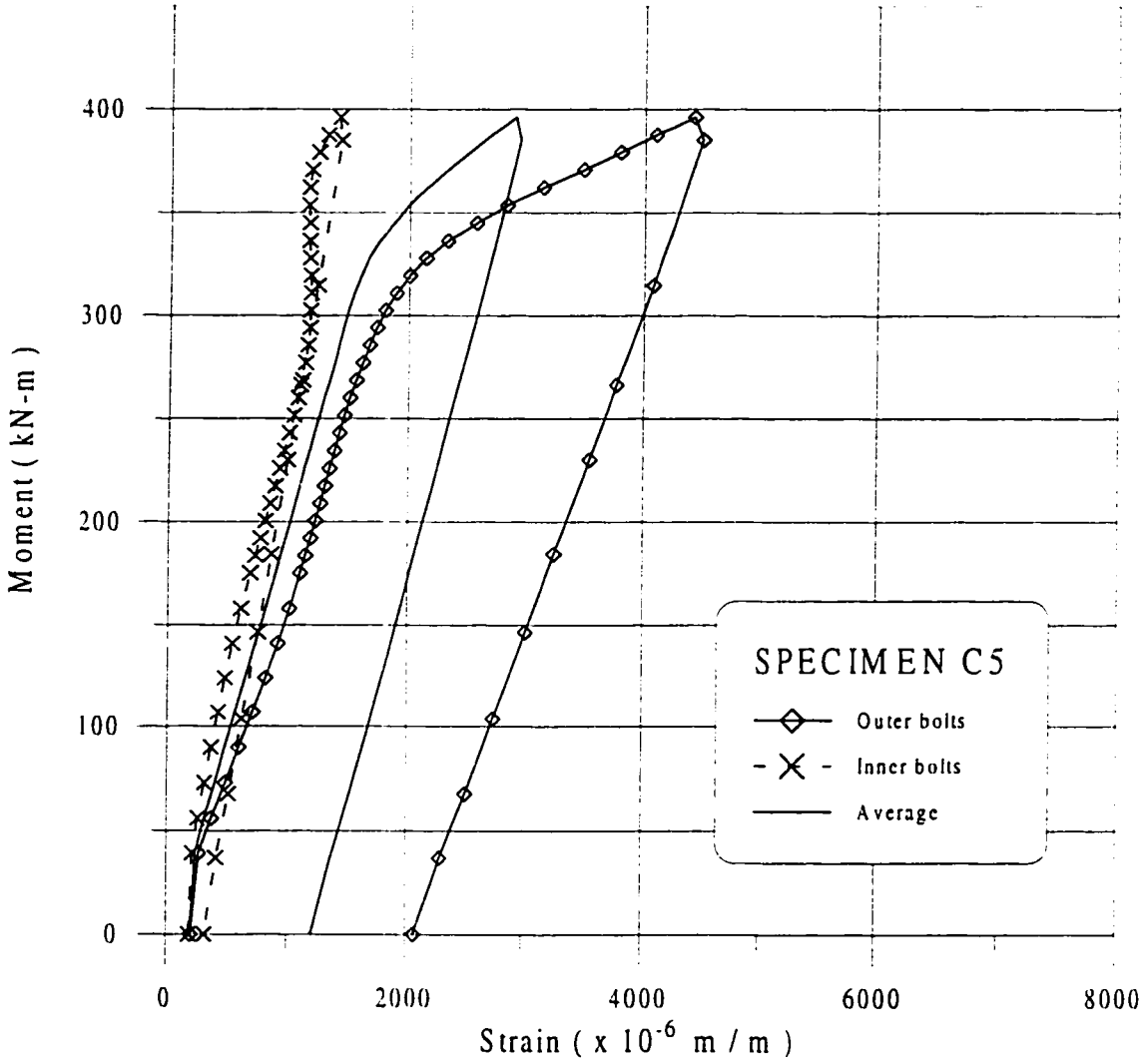

Figure 6.48 Bolts Strains for Specimen C5

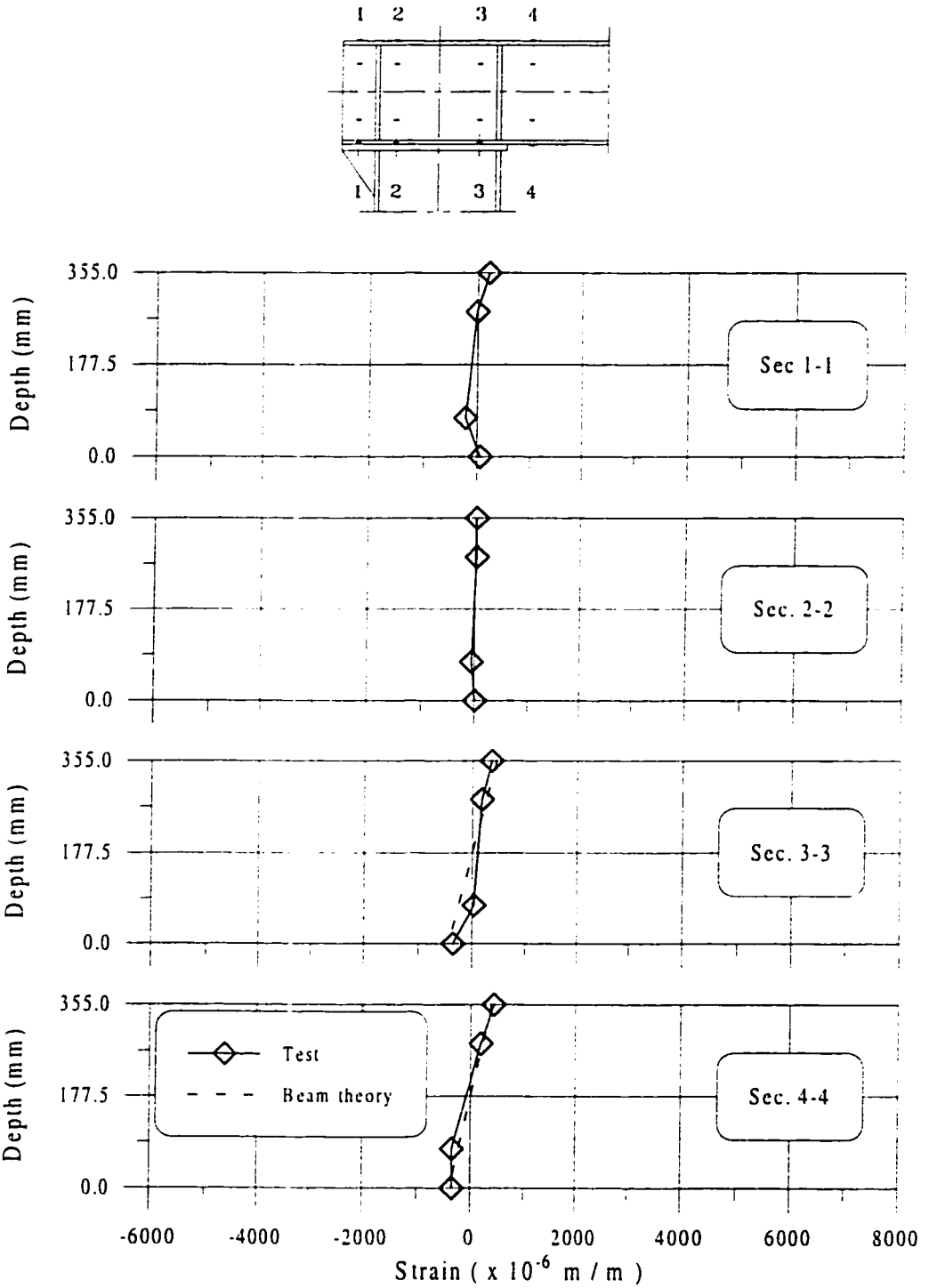

Figure 6.49 Normal Strain Distribution for Specimen C5 at M = 106 kNm

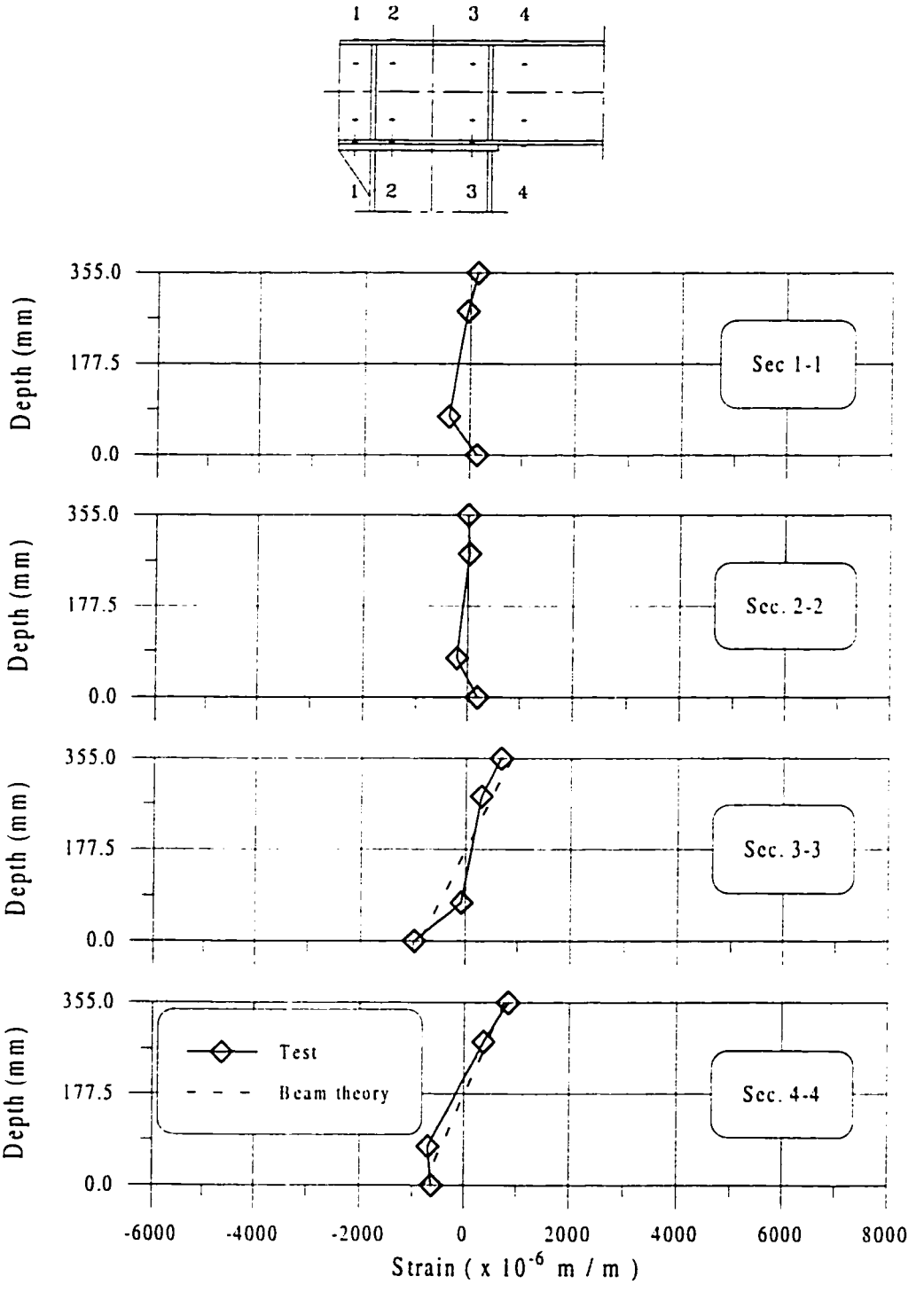

Figure 6.50 Normal Strain Distribution for Specimen C5 at M = 200 kNm

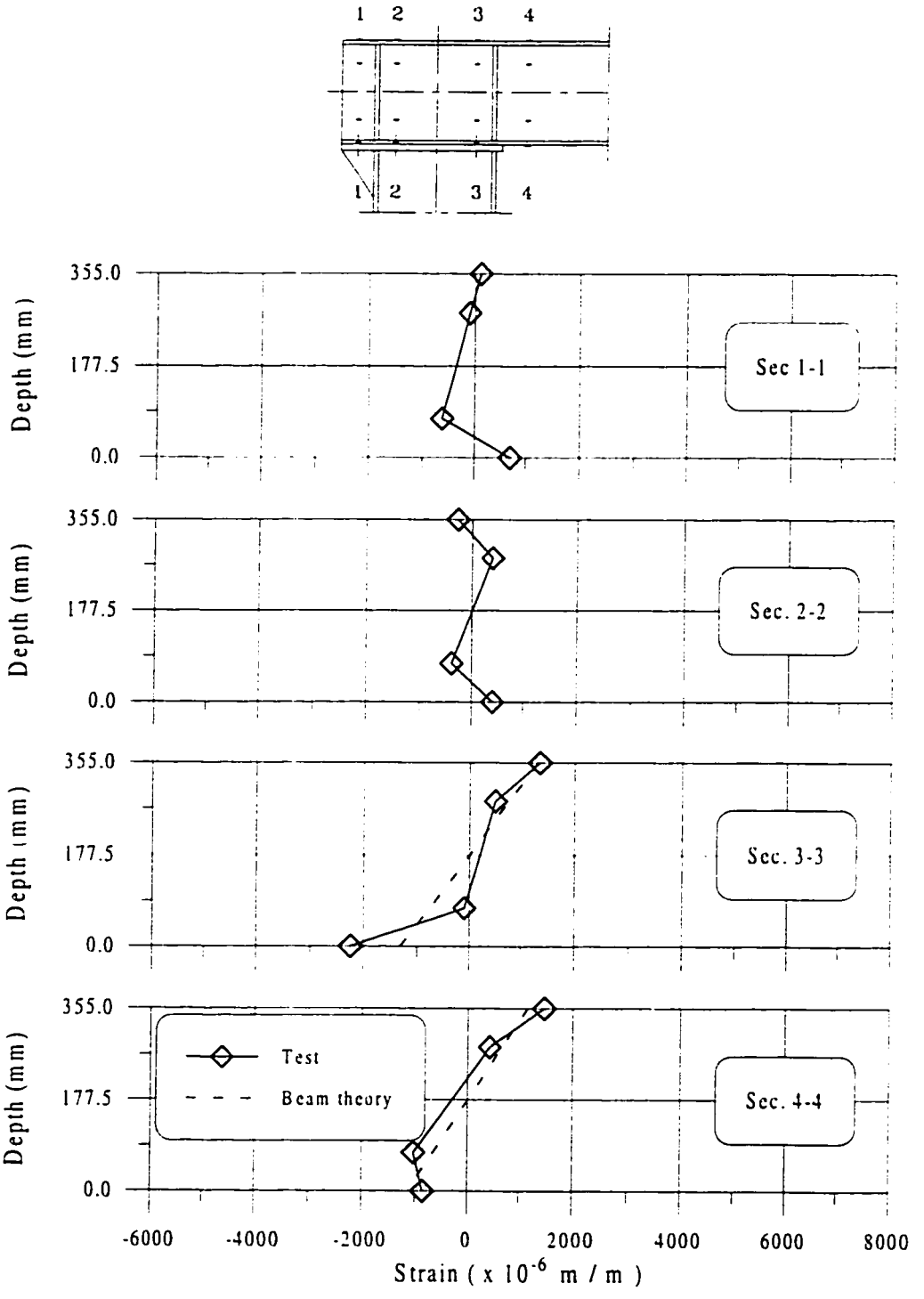

Figure 6.51 Normal Strain Distribution for Specimen C5 at M = 302 kNm

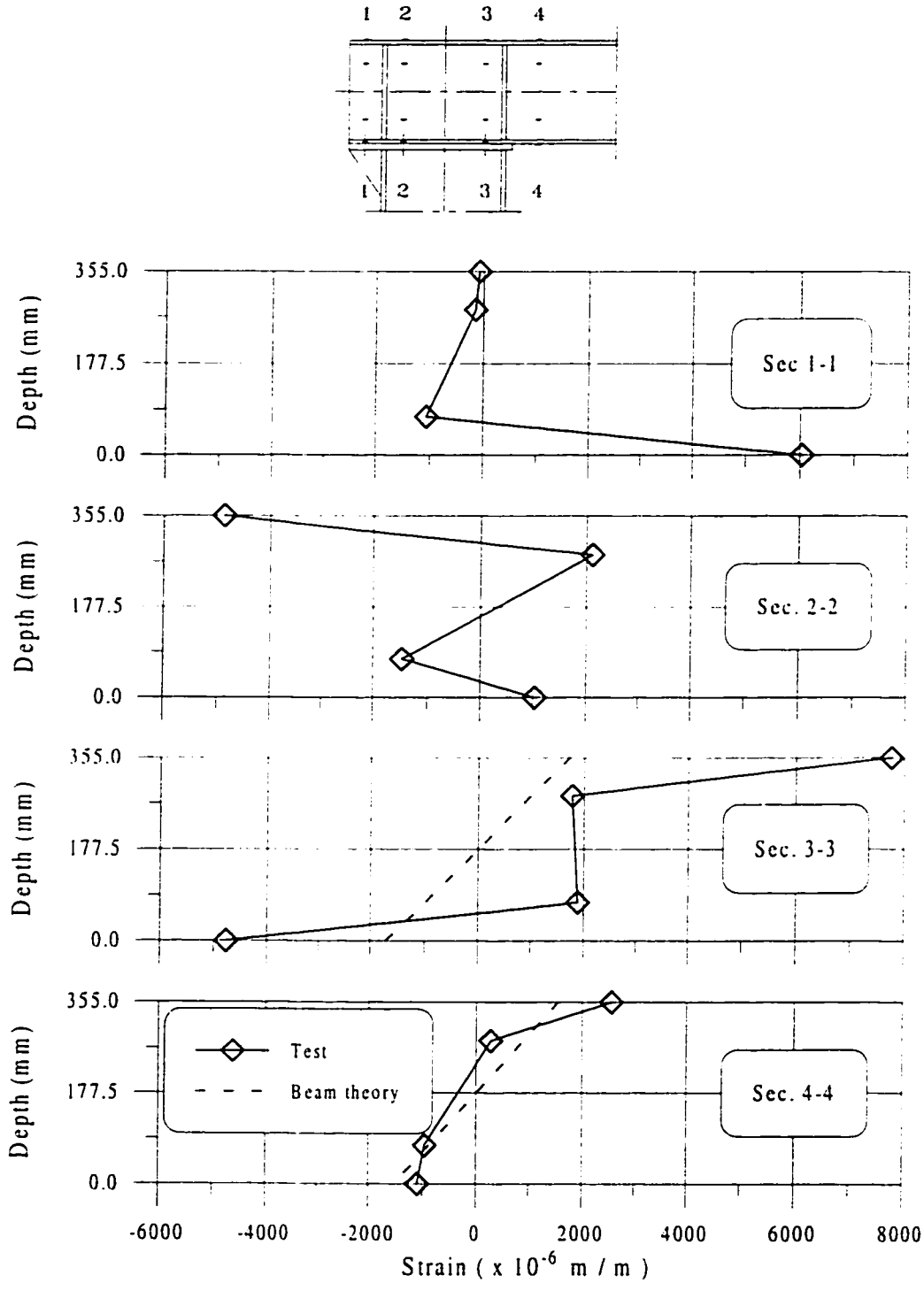

Figure 6.52 Normal Strain Distribution for Specimen C5 at M = 396 kNm

6.3.6 Specimen C6

Specimen C6 had the $M-\theta$ curve shown in Fig. 6.53, which is linear to about 200 kNm. The unloading path is approximately parallel to the initial slope of the curve. The plate thickness for C2 and C6 (Group B) are 20 mm and 15 mm respectively. Comparing their $M-\theta$ curves (Figs. 6.28 and 6.53), it can be observed that their initial rotational stiffness are nearly the same. So, it can be concluded that the effect of beam plate thickness is not significant above 15 mm. The maximum moment for C2 is higher than the maximum moment for C6 as expected.

Referring to Figs. 6.29 and 6.54 for the bolt strains of C2 and C6, it was observed that the bolts forces are almost equal at any level below 200 kNm. Beyond this level, the outer bolts yielded in C6 but they were still elastic in C2 due to the smaller plate thickness of C6.

The normal strain distributions shown in Figs. 6.55 - 6.57 indicate that Specimen C6 had approximately the same behavior of C2 of the same Group B. The maximum reached moment (314 kNm) which is equal to 258 kNm at Sec. 4-4, indicates that the section is approaching to the yield moment (269 kNm) given in Table 6.2.

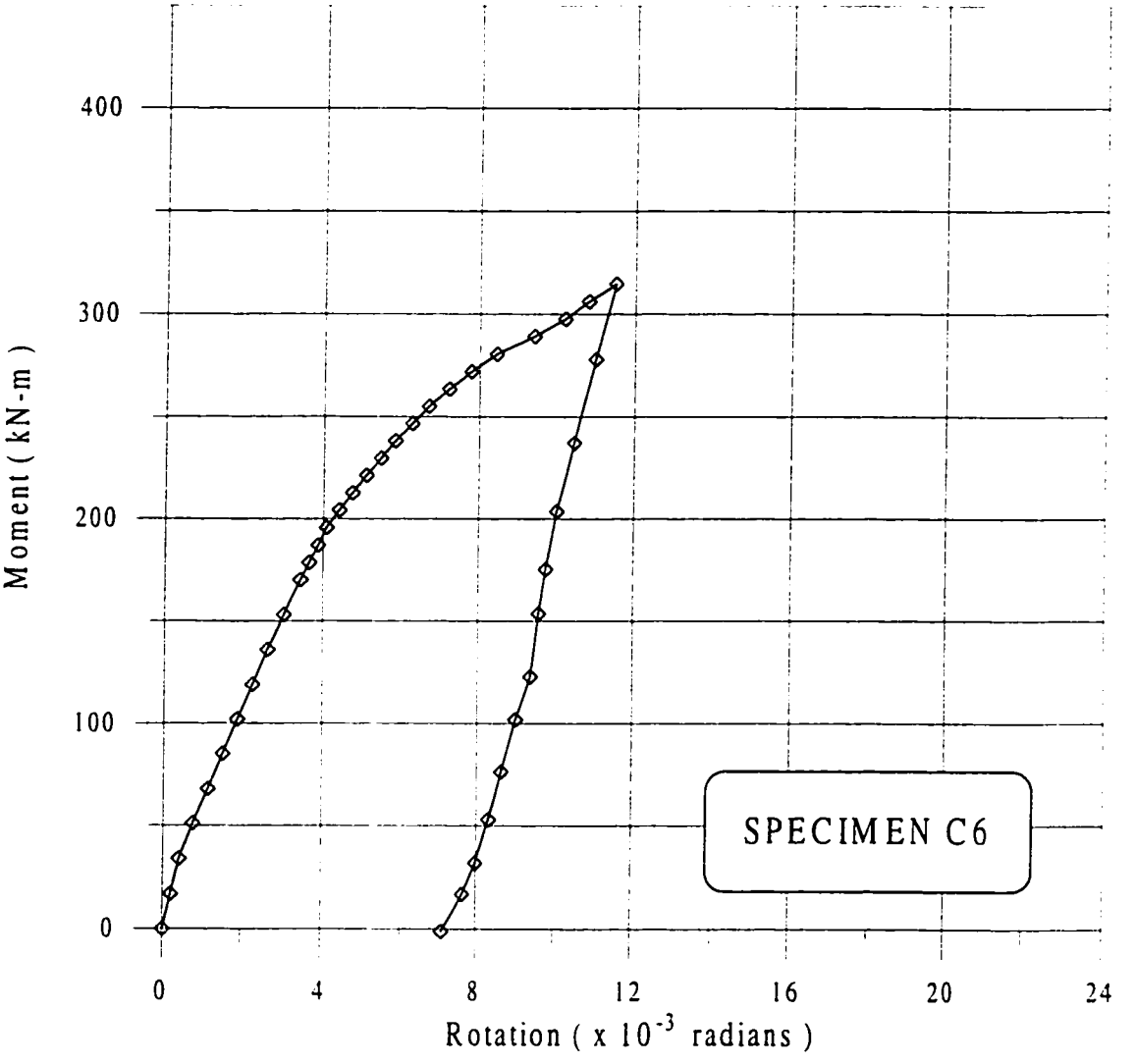

Figure 6.53 Moment-Rotation Relationship for Specimen C6

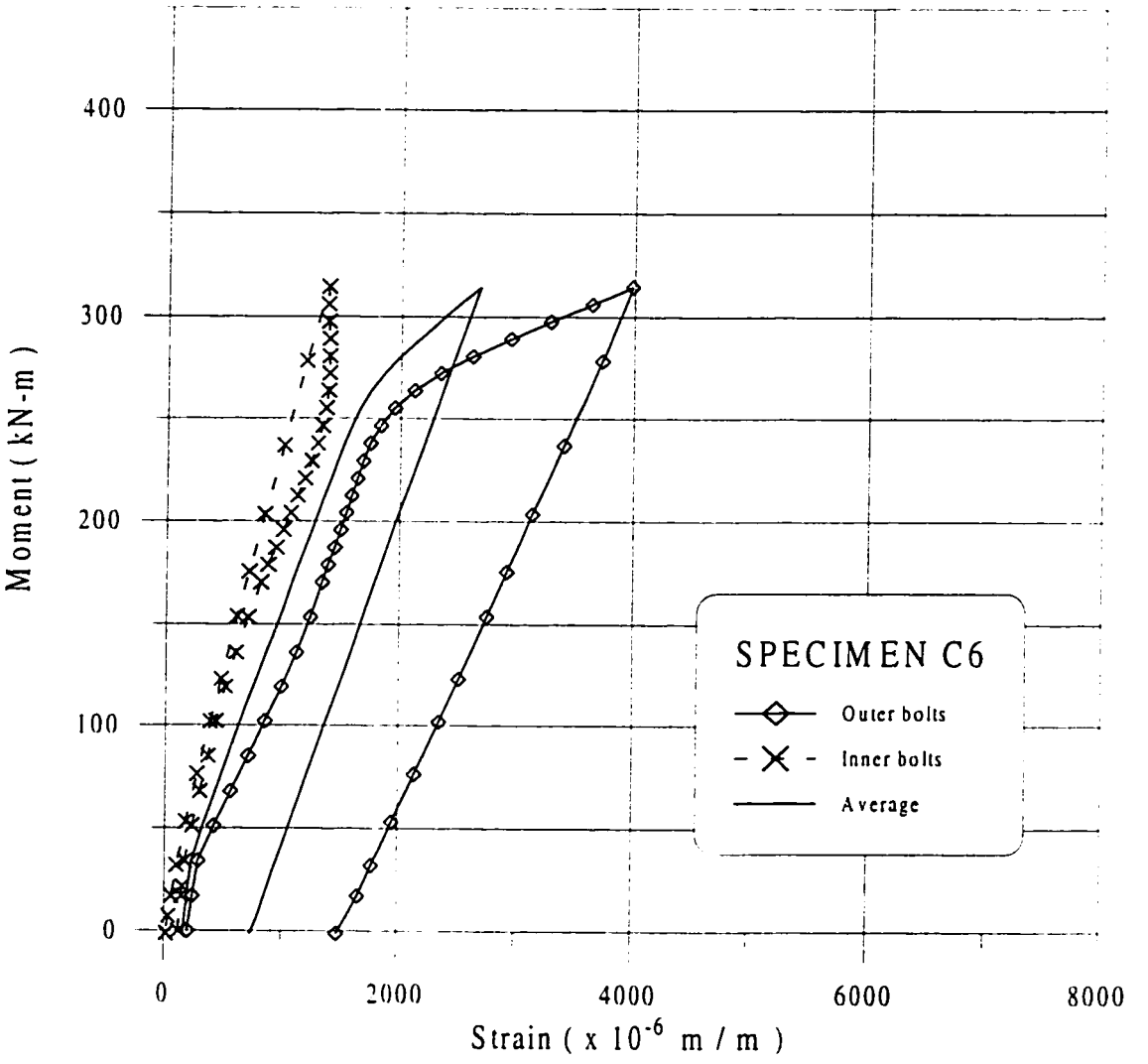

Figure 6.54 Bolts Strains for Specimen C6

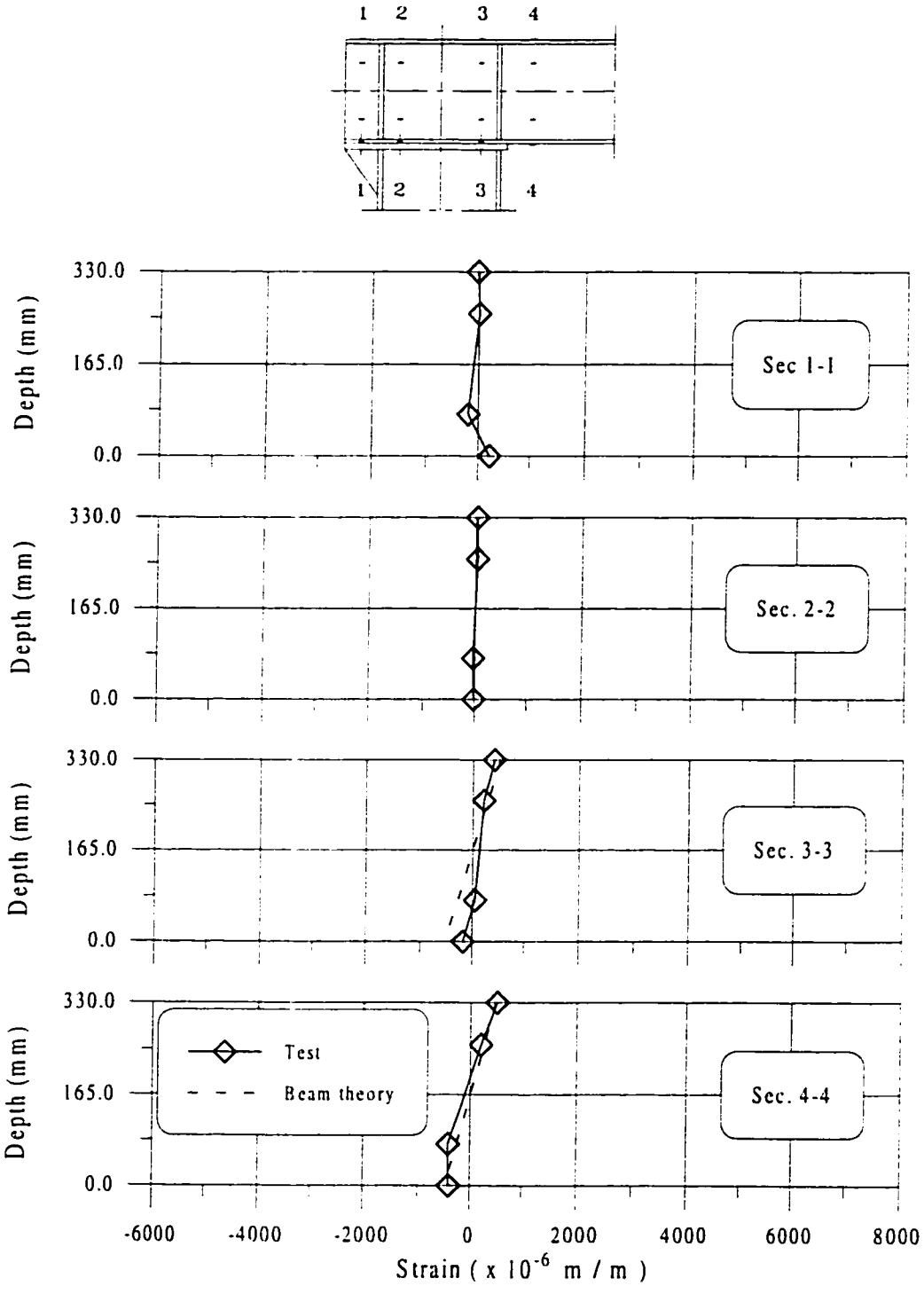

Figure 6.55 Normal Strain Distribution for Specimen C6 at M = 102 kNm

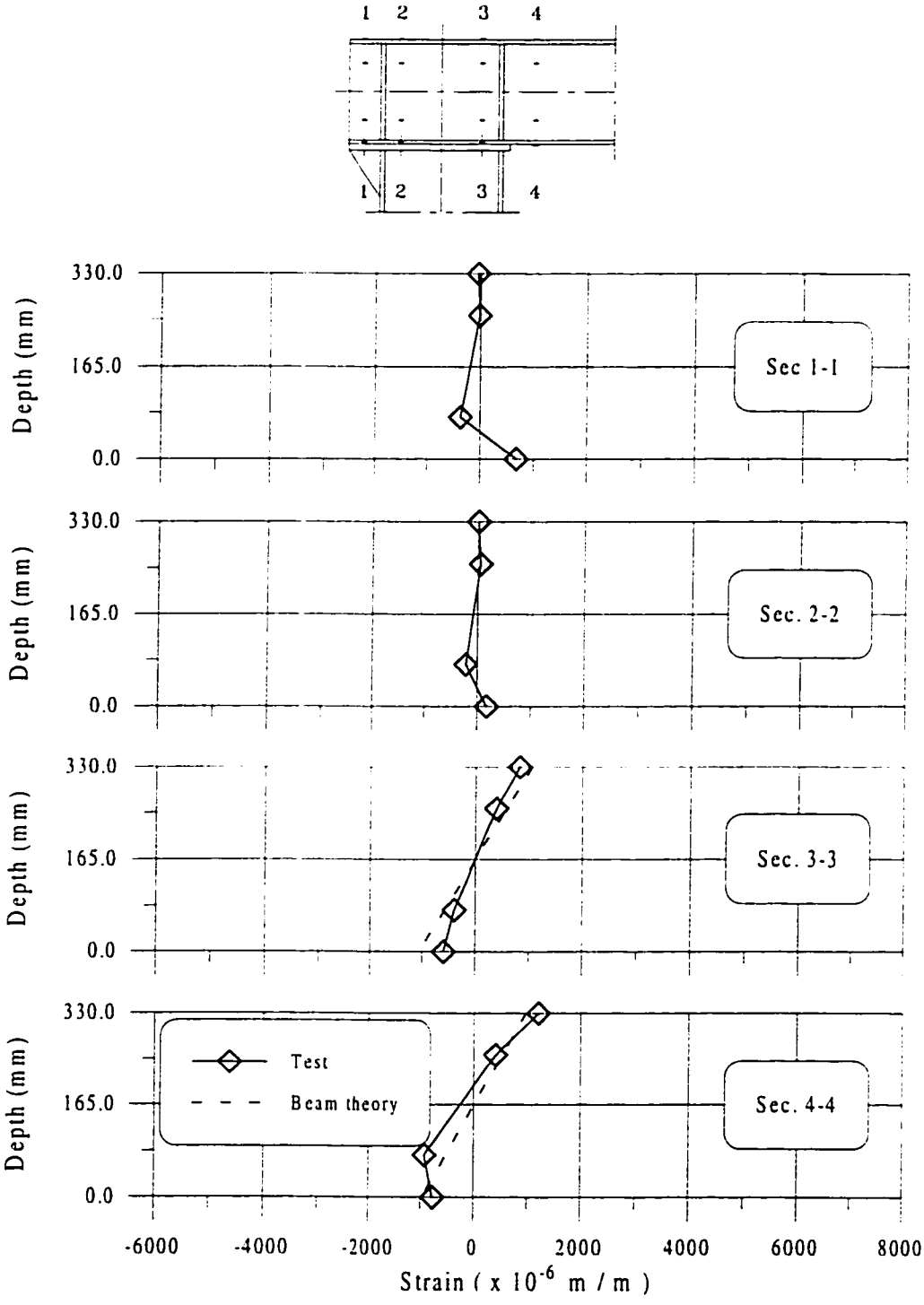

Figure 6.56 Normal Strain Distribution for Specimen C6 at M = 195 kNm

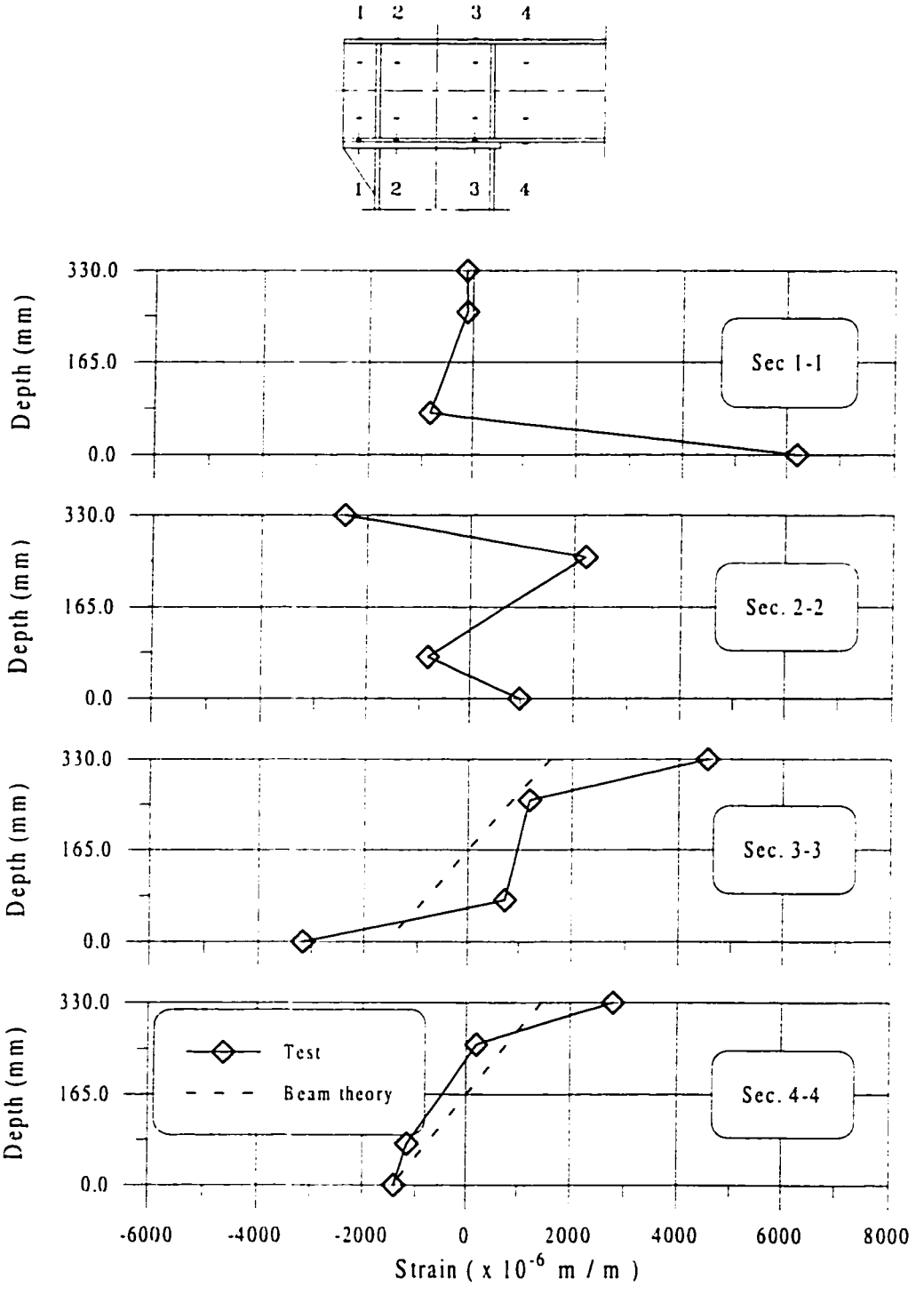

Figure 6.57 Normal Strain Distribution for Specimen C6 at M = 314 kNm

6.3.7 General Observations

The bolts strains results shown previously in Figs. (6.22, 6.29, 6.35, 6.42, 6.48 and 6.54) were used to calculate the bolt forces in the tension side bolts at failure in accordance with Fig. 6.20. In Table 6.3, the maximum bolt forces are given for outer and inner bolts. The yield strength of bolts are shown in the same table to compare with the bolts forces at maximum reached loads. No bolt fracture happened in all the tests, but permanent bolt deformations were observed in many cases.

The loading in each test was stopped at the incipient of apparent failure as observed by excessive deformation of the beam and the connection before the calculated ultimate moments of the beam to avoid dangerous failure and to avoid damage of equipments. All tested connections were unloaded after failure and the readings show that the $M-\theta$ curve of the connection unloads with a slope approximately equal to its initial slope. The permanent deformation of the connection after failure was shown in the plastic bolt elongation and the yield of the beam flange plate. It was also observed that some damage in the protecting steel paint of the shear panel took place and this means that shear strength is affecting the connection behavior.

The strain distributions over several cross-sections of the connection indicate that the elementary beam theory predict the actual strain distribution accurately at Sec. 4-4 and to some approximate values at Sec. 3-3. But the beam theory is not valid at

TABLE 6.3 Maximum Bolt Force Versus Yield Strength

Test No.	Bolt diameter (mm)	Maximum bolt force from test (kN)		Yield bolt strength (kN)
		Outer bolt	Inner bolt	
C1	19	207	207	212
C2	25	320	59	368
C3	22	285	120	285
C4	28	462	462	462
C5	28	462	172	462
C6	25	368	144	368

Sec. 1-1 and Sec. 2-2 where the load path did not pass through the upper left corner of the connection.

CHAPTER 7

MODELING OF CAP-PLATE CONNECTION

7.1 GENERAL

In steel frames, the connection behavior is highly indeterminate as it depends on many factors such as the yield strength, bolt properties, local restraints introduced by stiffeners, prying force and the relative deformations of components. The connection behavior is more complex than the members it joins and a purely theoretical approach is always difficult, if not impossible. An alternative approach for solving this problem is to develop an acceptable model for the connection by studying its response. A connection model should be simple enough and practical for its adoption in structural analysis. It should be capable of generating a non-linear moment-rotation curve that closely corresponds to the observed experimental data.

Cap plate connection and end plate connection are widely used in industrial frames because they are economical to fabricate. Although the cap plate connection has advantages over the end plate connection, ***no design model exists for the behavior of such type of connection***. The use of this connection necessitates the development of simple design model.

As seen from the literature review presented in Chapter 2, the end plate connection has been frequently modeled as a T-stub connection [85, 86], neglecting the stiffening effect of stiffeners used in beams and columns at the joint as shown in Fig. 7.1.

A model is presented in this chapter taking into consideration the bending of the stiffened beam and the column cap plate in a two-way action for the cap plate connection. The proposed model is based on the fundamentals of mechanics. The effects of the horizontal shear and the vertical force on the cap plate connection are ignored and only pure bending is considered.

7.2 PROPOSED MODEL

The experimental data on the connection rotation gathered from limited tests were used to develop a fitting nonlinear relationship between the moment and the rotation of the connection for the cap plate type connection. Different models were attempted for end-plate type connection to express the nonlinear relationship between the applied moment and the rotation. And finally the three-parameter model, proposed by Chen [30] was found suitable to closely model the moment-rotation characteristics of the connection. It has the form:

$$\theta_r = \frac{|M|}{R_{ki}\left[1-\left|\frac{M}{M_{cu}}\right|^n\right]^{\frac{1}{n}}} \tag{7.1}$$

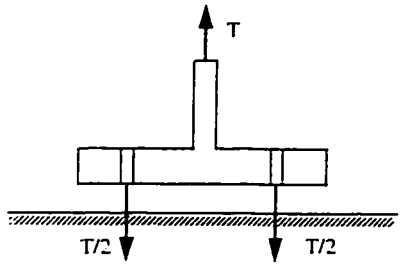

Bolt failure (thick plates / weak bolts)

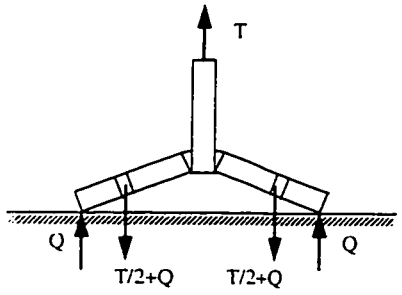

Bolt failure with flange yielding

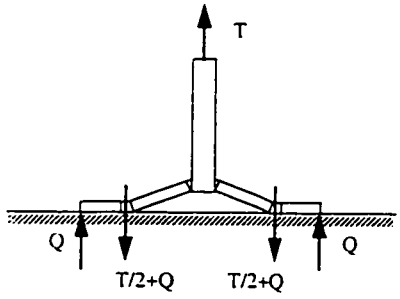

Complete flange yielding (thin plates / strong bolts)

Figure 7.1 Tee-Stub Failure Modes

where the three parameters are:

R_{ki} = the initial stiffness of the connection

M_{cu} = the ultimate moment capacity of the connection

n = a shape parameter

Of the three parameters, R_{ki} and M_{cu} must be calculated for a connection as they would vary from connection to connection and the shape parameter n controls essentially the shape of the moment rotation curve and its value can be established from the numerical adjustment to properly fit the experimental values.

7.3 INITIAL STIFFNESS

The initial stiffness of the connection R_{ki} is the ratio of the applied moment to the rotation of the connection at the early stage of loading when the response is essentially linear. With reference to Fig. 7.2 which shows a typical cap plate connection subjected to an end moment, the connection rotation takes place due to the following factors:

1. elongation of tension bolts due to tensile forces
2. local bending of beam flange plate
3. local bending of column cap-plate

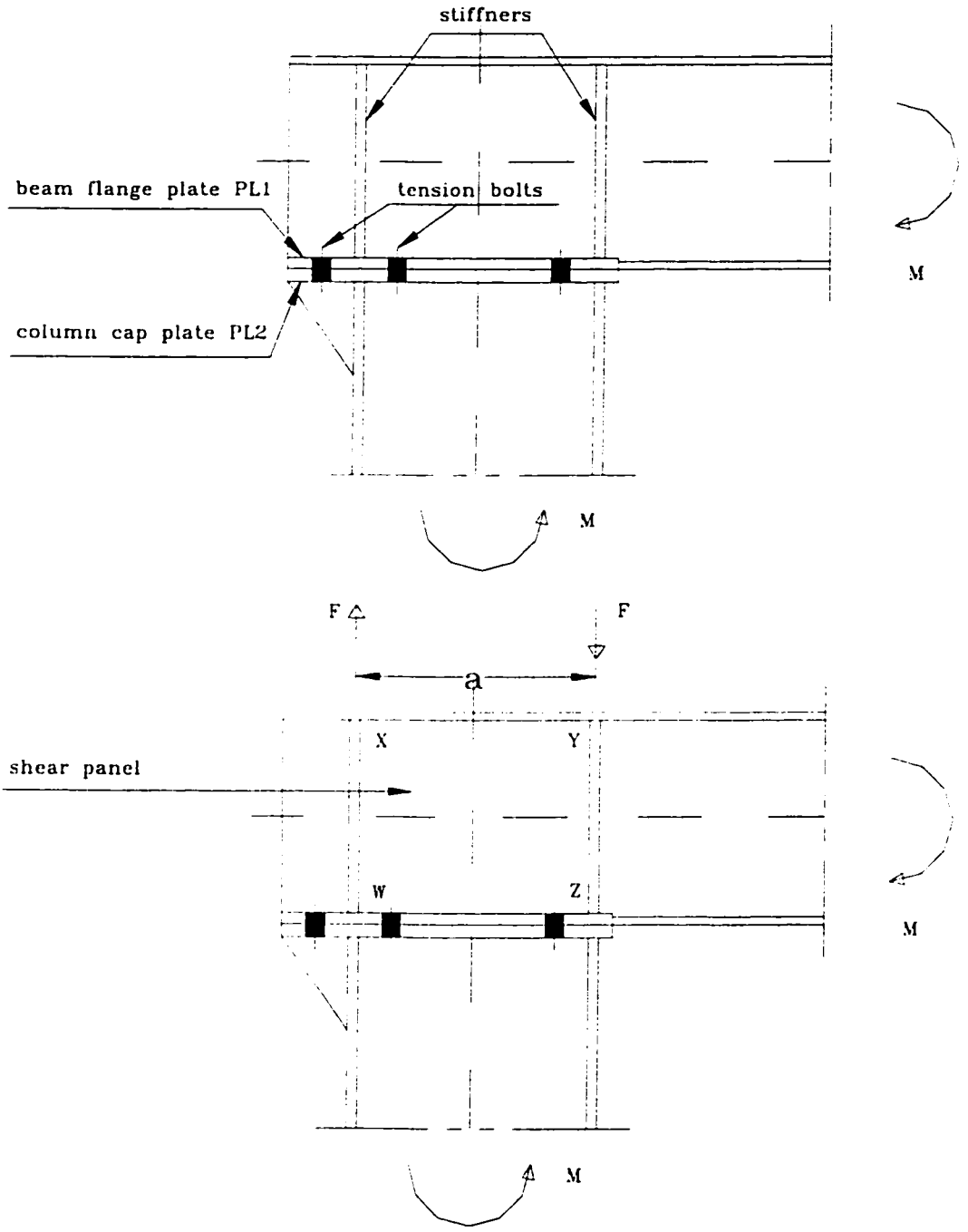

Figure 7.2 Typical Cap-Plate Connection

4. shear deformation of the beam panel WXYZ (Fig. 7.2).

The cumulative effect of the first three actions can be attributed to bending of the connection. The fourth action is due to high shear action in the panel. The deformation at the connection is shown schematically in Fig. 7.3. The small angle of rotation θ of the beam is calculated with respect to the column head. This rotation angle consists of two components: one due to bending and the other due to shear.

7.3.1 Rotation Due to Bending

First, the deflection δ_b due to bending is calculated by using a finite element analysis of the connection assembly. The available GT STRUDL software package was used to analyze an idealized assembly.

The most difficult part of the structural idealization arises from the contact pressure of the two deformed plates (the beam flange plate and the cap-plate) which is unknown and must be accounted for. This plate contact pressure is often referred to as the result of 'prying action' of the tension bolts. As this contact area and the contact force (prying force) is unknown, the analysis has been carried out on a trial basis to obtain a compatible solution.

7.3.1.1 GT STRUDL Program

GT STRUDL program is a powerful structural analysis and design software [87]. It permits the use of elements (members and finite elements) of different types to be mixed in the same problem solution, whether they have the same or different number

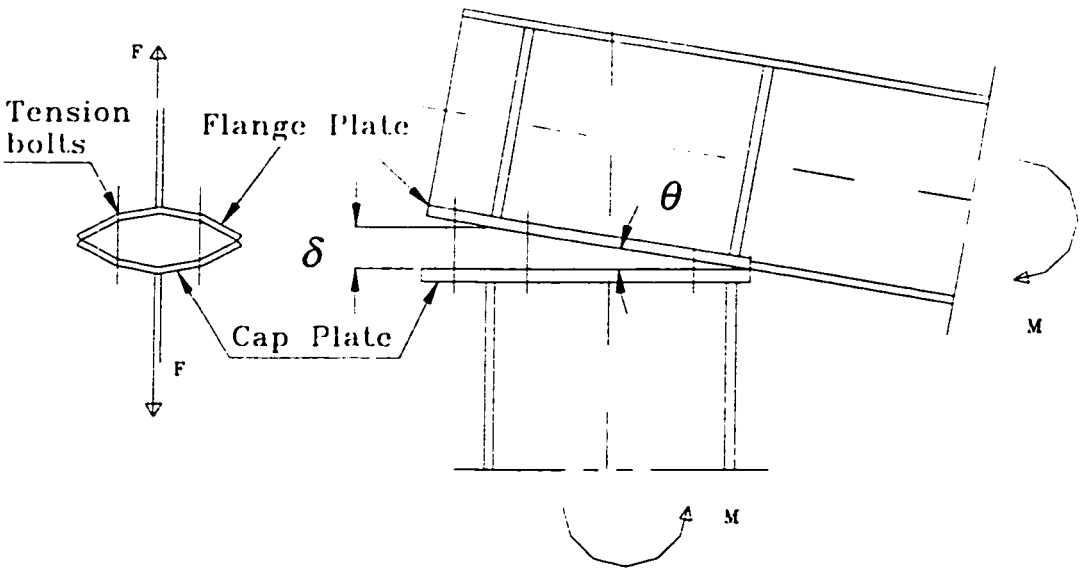

Transverse deformation Longitudinal deformation

Figure 7.3 Typical Cap-Plate Connection Deformation

of degrees of freedom per joint. The program is used to model the cap plate connection and to find its initial stiffness. To benefit from the symmetry of the connection assembly, only half of the connection is modeled. The idealized connection showing the different types of elements and members is illustrated in Fig. 7.4.

7.3.1.2 Element and Members Types

The elements used, to represent the cap plate A-C-L-J (Figs. 7.4 and 7.5), and the lower beam flange A'-C'-F'-D' (Figs. 7.4 and 7.6), are the four nodes ***plate bending elements*** SBHQ6. They are defined as a Stretching and Bending Hybrid Quadrilateral with six degrees of freedom at each of the four corner nodes. The aspect ratio of the used elements is 1.1. The element thickness varies among 12, 15, 20 and 25 mm. depending on the test configuration. The mesh discretization, nodes, elements and members numbering are shown for the column cap plate in Fig. 7.5 and for the beam bottom flange in Figs. 7.6 and 7.7.

The web of the beam is modeled by ***space frame members*** with half of its cross-sectional properties because of symmetry along edge A'-C'. The beam stiffeners also are defined by the same member type along edge B'-E'.

The bolts are represented by ***space truss members*** type. The member length equals the sum of plates thicknesses which the bolt joins plus half the head depth and

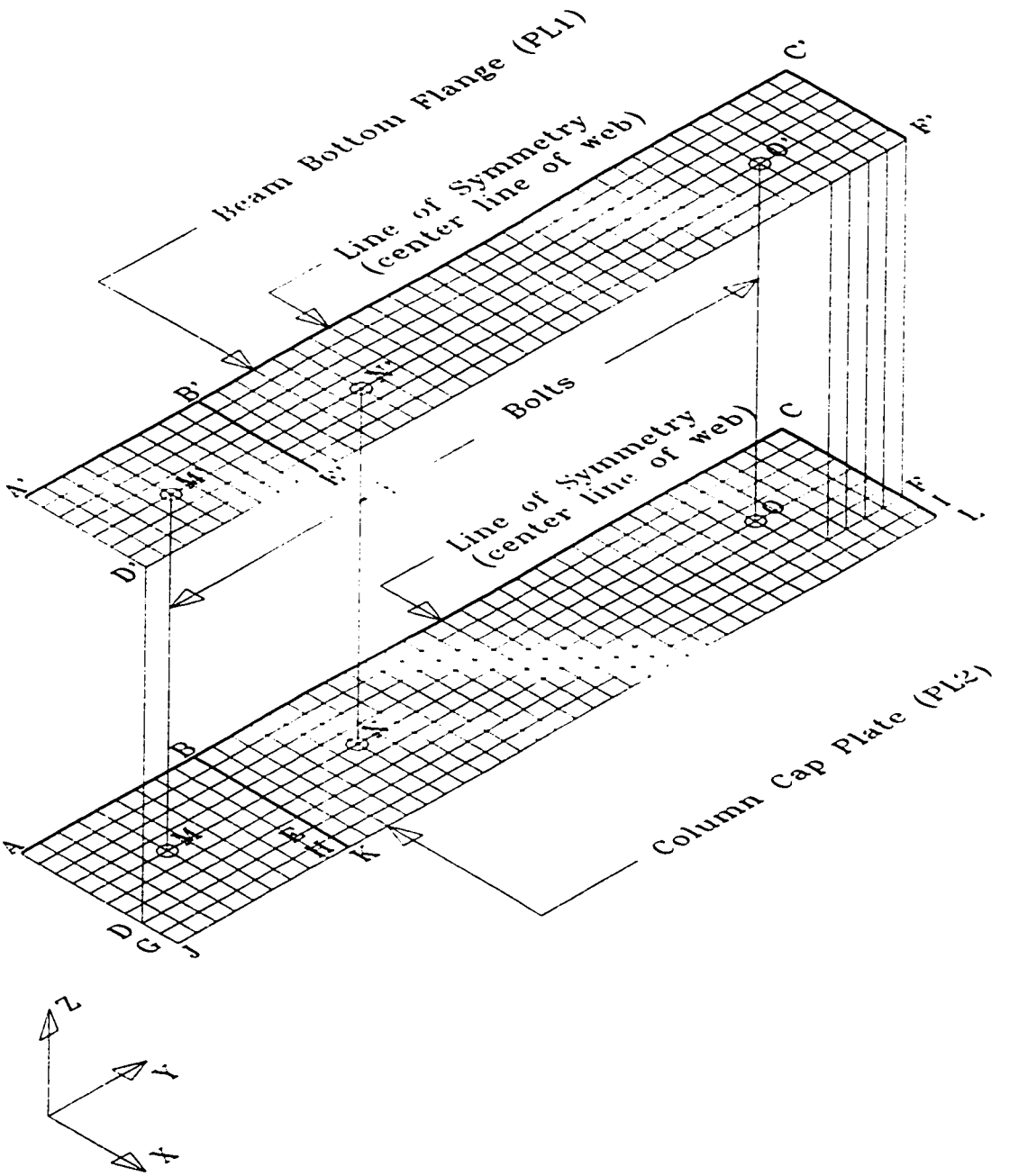

Figure 7.4 Finite Element Model Discretization

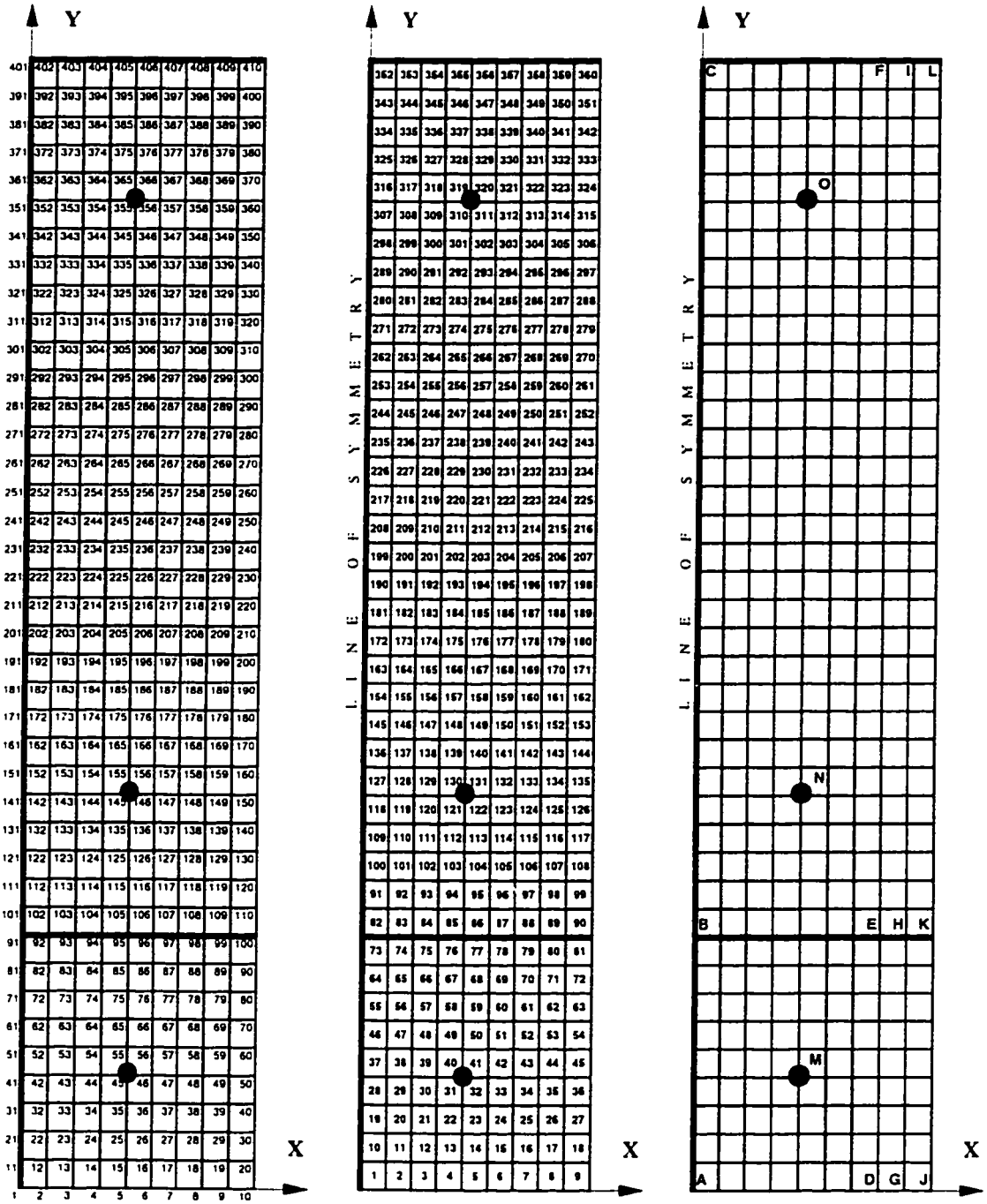

Figure 7.5 Finite Element Mesh for Cap Plate PL2 (Width = 200 mm)

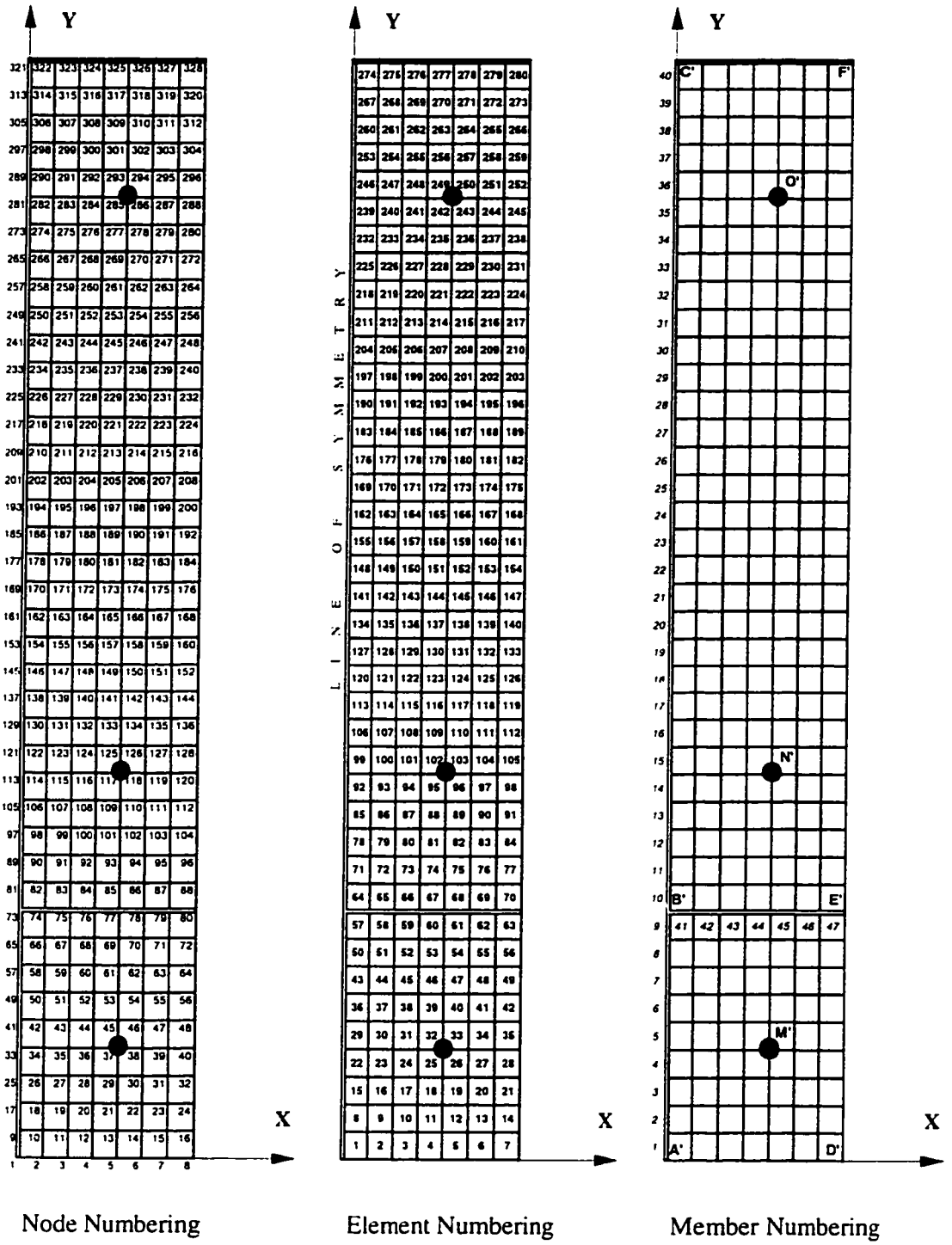

Figure 7.6 Finite Element Mesh for Beam Bottom Flange PL1 (Width = 160 mm)

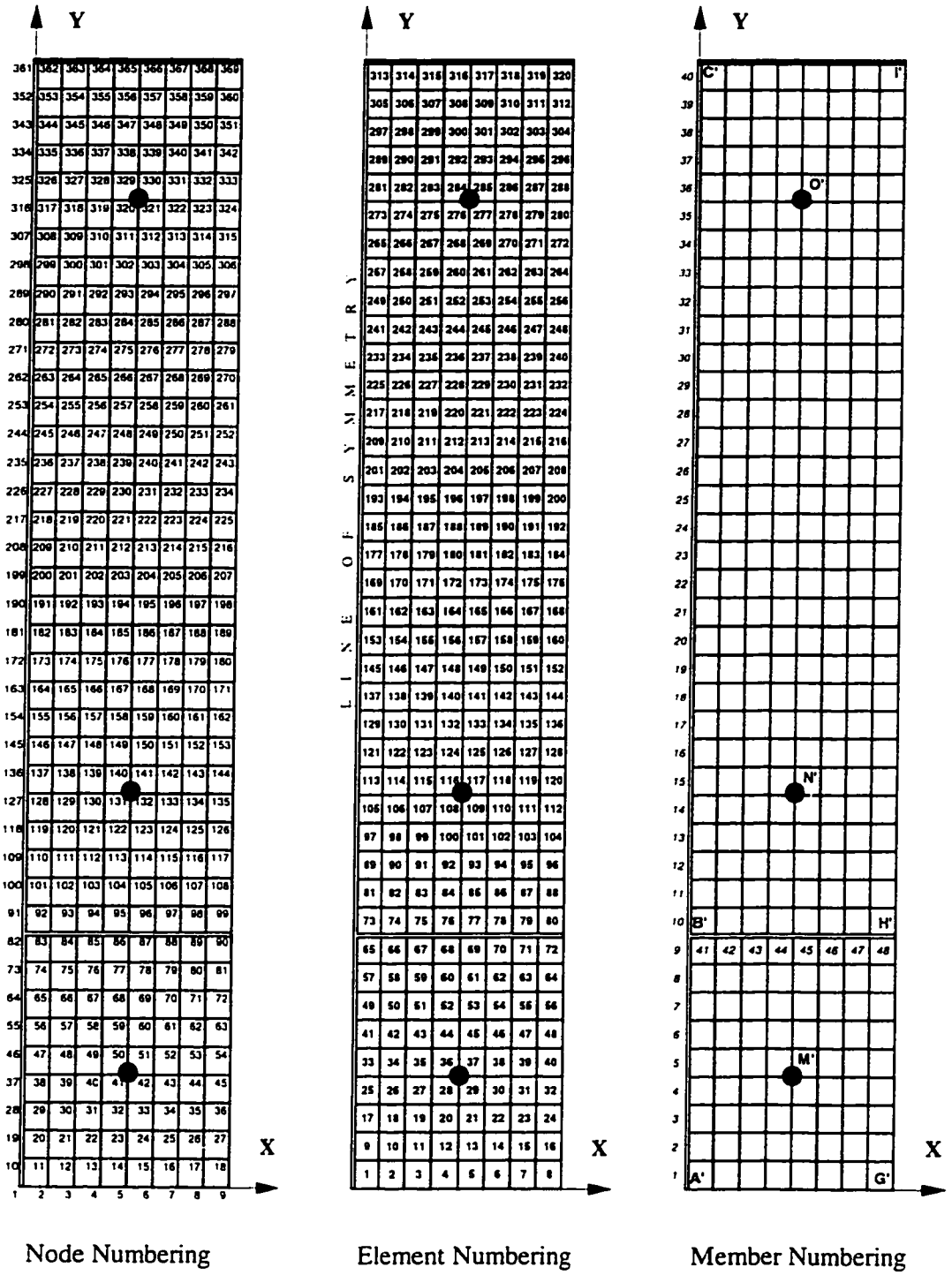

Figure 7.7 Finite Element Mesh for Beam Bottom Flange PL1 (Width = 180 mm)

half the nut depth. The member area is the cross-section area of the bolt. The two tension bolts are M-M' and N-N'. The bolt in the compression side is O-O'.

The contact area due to prying force is modeled by ***space truss members*** connecting between the two edges D-F and D'-F' which are only active in compression and are inactive when subjected to tensile force. These special elements have large areas so as to have virtually no deformation in compression. Also these members can move in space as rigid bodies if subjected to compression during the loading.

7.3.1.3 Analysis

The material properties of steel are taken as: modulus of elasticity $E = 29 * 10^6$ psi, shear modulus $G = 11 * 10^6$ psi and Poisson's ratio $v = 0.3$. The boundary conditions for the two plates are defined in Table 7.1 in accordance with Fig. 7.4.

The applied moment at the connection is idealized by two concentrated forces (Fig. 7.2) applied at points B' and C' (Fig. 7.4). The force intensity F is taken as:

$$F = \frac{M}{a} \tag{7.2}$$

where :

M = applied moment

a = distance between the two vertical stiffeners

TABLE 7.1 Boundary Conditions for Cap-Plate Connection Model

Edge	Actual edge status	Assumed boundary condition
A-C	Cap-plate (PL2) welded to the column web	Fixed
B-K	Cap-plate (PL2) welded to the column flange	Fixed
A-J , J-L	Free edge of cap-plate (PL2)	Free
A'-D' , D'-F'	Free edge of beam flange plate (PL1)	Free
A'-C'	Beam flange plate (PL1) welded to the beam web	Fixed but released in Fy, Fz, Mx directions
C-L	Cap-plate (PL2) welded to the column flange	Fixed but released in Mx, My, Mz directions
C'-F'	Beam flange plate (PL1) welded to the beam stiffener	Fixed but released in Mx, My, Mz directions

The applied moment is divided by two since only half of the connection is modeled due to symmetry. It was found that no significant difference exist if the force is applied at point B' as a concentrated load or along the line B'-E' as line load. For the analysis, a moment M = 146 kNm was used which yields a force F = 400 kN with distance a = 365 mm. Half of the value of F which equals $\frac{1}{2}$F = 200 kN was used in the analysis due to symmetry.

From analysis, the relative displacement between the two points B and B' is calculated as δ_b which includes the effect of plate bending and the extension of the bolts. The typical deflected shape and contour of deformations for plates PL1 and PL2 are shown in Figs. 7.8 and 7.9 respectively.

The rotation due to bending is given as

$$\theta_b = \frac{\delta_b}{a} \tag{7.3}$$

The values of θ_b calculated for the six tests are shown collectively in Table 7.2

7.3.2 Rotation Due to Shear

The rotation due to shear results from the deformation of the thin web panel bounded by the top and bottom flanges and the two vertical stiffeners as shown in Fig. 7.2. This deformation is calculated using simple shear deformation formula for beams. Referring to the loading in Fig. 7.2 the shear deformation in the panel between W-X and Y-Z is given as:

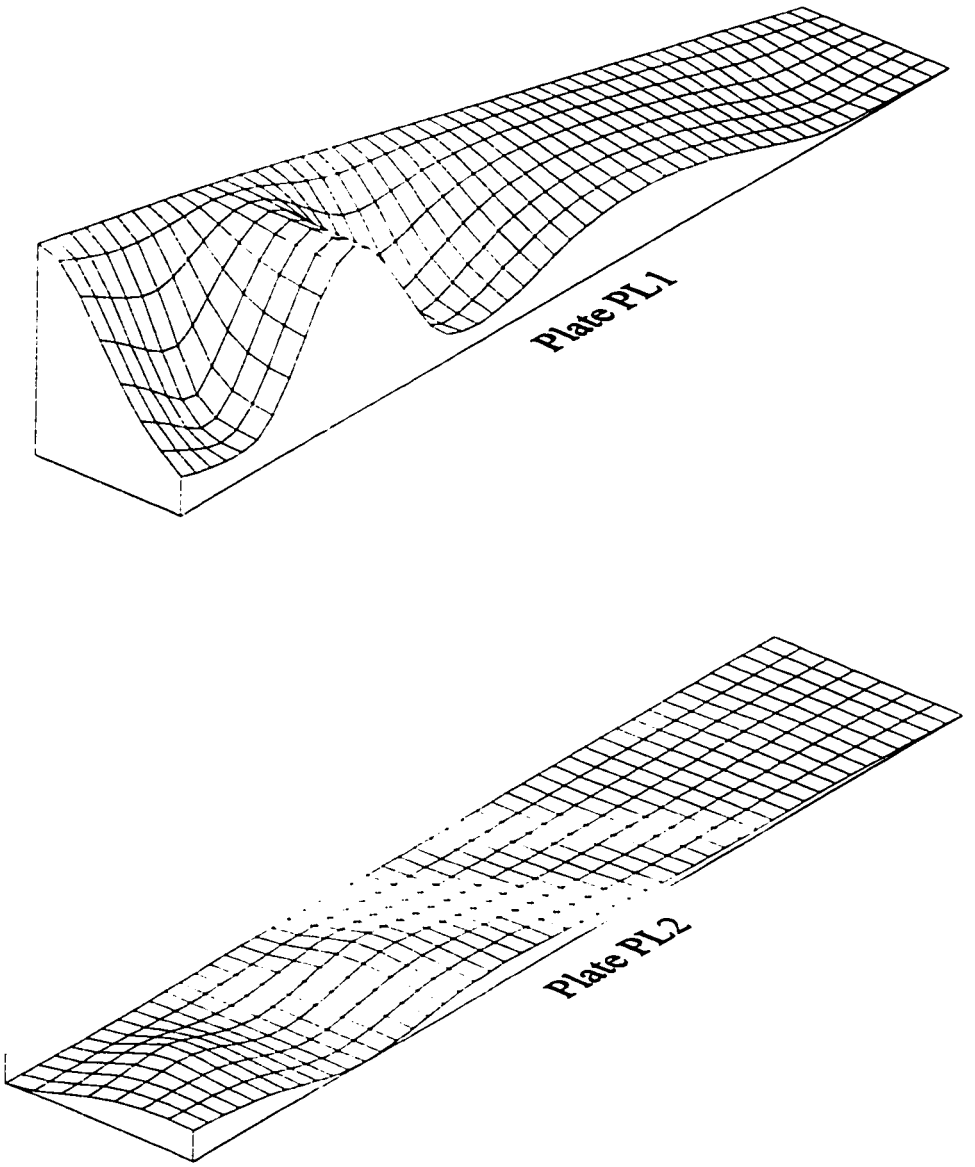

Figure 7.8 Deflected Shapes for Plates PL1 and PL2

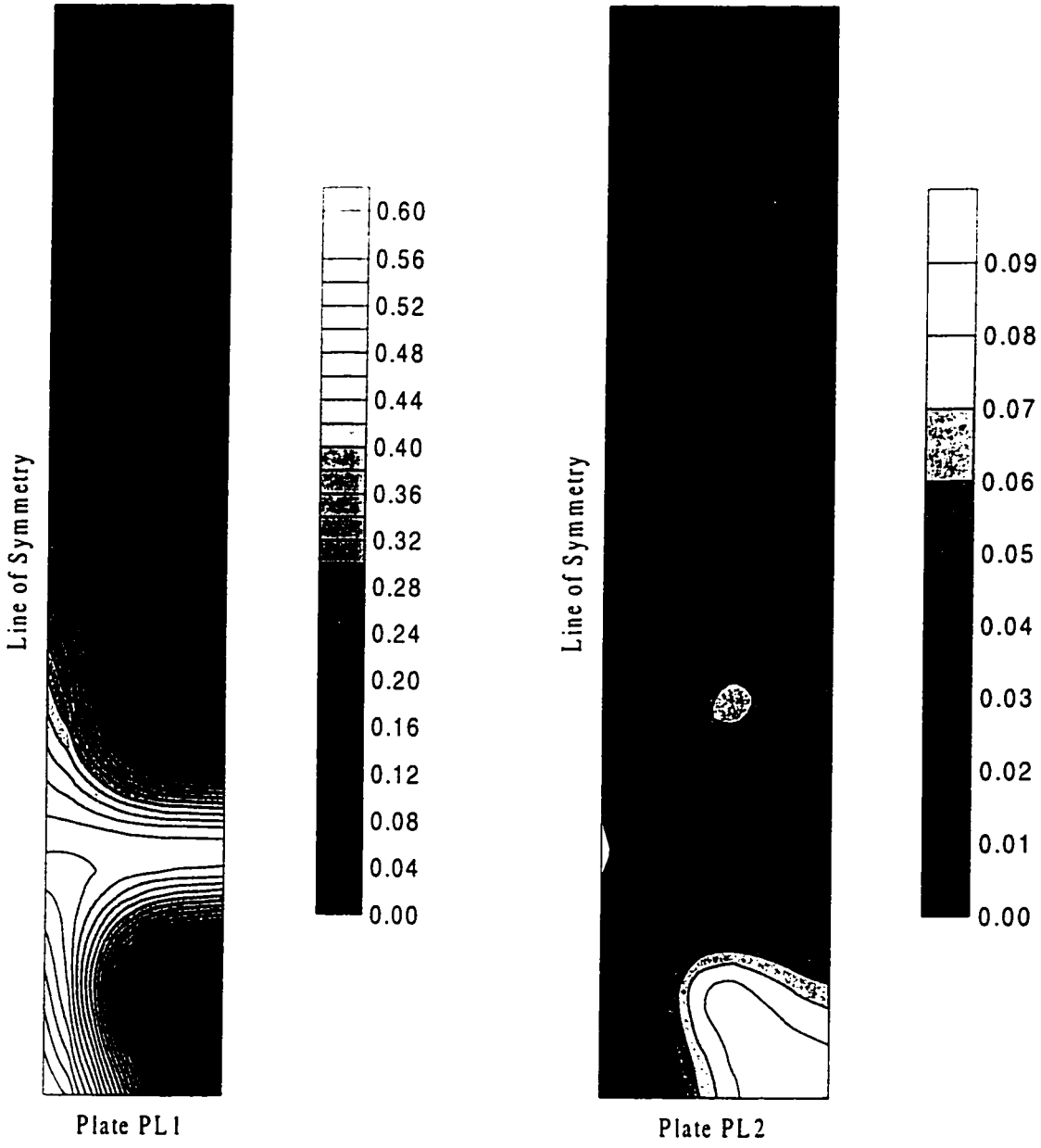

Figure 7.9 Deformation Contour Lines for Plates PL1 and PL2

TABLE 7.2 Comparison of Initial Stiffness Calculated from the Model

Test No.	Rotation due to bending θ_b (rad)	Rotation due to shear θ_{sh} (rad)	Total rotation θ_t (rad)	Initial stiffness from model R_{ki} (kNm/rad)
C1	1.34×10^{-3}	1.81×10^{-3}	3.14×10^{-3}	47×10^{3}
C2	0.59×10^{-3}	1.44×10^{-3}	2.03×10^{-3}	72×10^{3}
C3	0.65×10^{-3}	1.81×10^{-3}	2.46×10^{-3}	59×10^{3}
C4	0.46×10^{-3}	1.11×10^{-3}	1.57×10^{-3}	93×10^{3}
C5	0.73×10^{-3}	1.11×10^{-3}	1.84×10^{-3}	79×10^{3}
C6	0.81×10^{-3}	1.44×10^{-3}	2.25×10^{-3}	65×10^{3}

$$\theta_{sh} = \frac{F}{\alpha A_w G} \tag{7.4}$$

where:

α = shape factor taken as 1.2

A_w = area of the web

G = shear modulus

The calculated values of θ_{sh} for six tests are given in Table 7.2.

7.3.3 Evaluation of Initial Stiffness

The total rotation θ_t is the contribution of bending and shear rotations:

$$\theta_t = \theta_b + \theta_{sh} \tag{7.5}$$

Using the calculated value of θ_t from Eq. 7.5, the initial stiffness of the connection is computed as

$$R_{ki} = \frac{M}{\theta_t} \tag{7.6}$$

7.3.4 Comparison Between Theoretical and Experimental Values of R_{ki}

The value of initial stiffness R_{ki} computed from Eq. 7.6 for each test specimen is shown in Table 7.3 along with the experimental values determined from the initial slope of the $M-\theta$ diagram. A comparison of the two sets of values shows that there

TABLE 7.3 Comparison of Predicted and Actual Test Values

for the Initial Stiffness and the Ultimate Moment

TEST No.	Initial Stiffness		Ultimate Moment	
	Predicted	Test	Predicted	Test*
C1	47×10^3	60.0×10^3	278	300
C2	72×10^3	60.0×10^3	575	420
C3	59×10^3	63.0×10^3	445	400
C4	93×10^3	90.0×10^3	658	450
C5	79×10^3	70.0×10^3	465	420
C6	65×10^3	66.0×10^3	452	360

* Projected (extrapolated) failure values

is a good agreement between the two sets of values. This affirms that the proposed analytical method to evaluate R_{ki} of a connection is sufficiently accurate.

7.4 ULTIMATE MOMENT

The ultimate moment capacity of a connection is the theoretical maximum moment which a connection can resist at failure. As a connection is an assembly of plates and bolts, several failure mechanisms are possible and each mechanism must be investigated to determine the smallest load which can cause the failure.

7.4.1 Failure Mechanisms

The possible failure mechanisms are identified as:

1. failure of the column cap plate in bending
2. failure of the beam bottom flange plate in bending
3. yielding and fracture of the connecting bolts in tension
4. the tearing of the beam web from the flange due to inadequate welding

Depending on the cap plate thickness, beam flange thickness, the bolt diameter and the presence of stiffeners, any of the above mentioned failure mechanisms can take place. If the beam web is adequately welded to the flange for built-up section, as is normally the case, the tearing of web can be excluded.

Referring to Fig. 7.1, an additional edge force, known as prying force, results because of the effects of plate deformation. When prying occurs, the bolt force is increased. This increase has been reported to be up to 30 to 40% [85, 86] for end-plate connections. In design, prying action should therefore be accounted for by estimating the prying force and adding this to the primary loads in the bolts, or the allowable bolt strength may be reduced in order that the effect of prying does not overload the bolt [3, 4].

Depending on the relative values of the plate thickness and the bolt diameter, any of the first three causes of failures can occur. The deformation of the cap-plate is usually negligible compared to the beam bottom flange plate because of the difference in their thickness (Table 5.1). Thus one of the following three modes of failure can take place:

1. Thick-plate mode of failure (Mode 1)

2. Thin-plate mode of failure (Mode 2)

3. Intermediate-plate mode of failure (Mode 3)

7.4.1.1 Thick-Plate Mode of Failure (Mode 1)

The failure of the connection by Mode 1 occurs by fracture of the tensile bolts (when these bolts reach their tensile capacity). Failure happens when both the cap-plate and the flange plate are thick and the bolts are relatively small in diameters. As the plates are considered thick and no plate deformation would occur, therefore no prying force

will exist. For this mode of failure the plate is rigid enough to ensure that the ultimate strength of the connection is reached before yielding of the plates can occur. It can be classified as ***the thick plate mode of failure***.

This mode of failure is illustrated in Fig. 7.10. The applied moment M is converted to two vertical concentrated forces F as given in Eq. 7.2, where M is half of the actual moment because of symmetry. In this case, the bolts in the tension side reach their ultimate tensile capacity having forces equal to B_u given as:

$$B_u = \sigma_{ub} A_b \tag{7.7}$$

where

σ_{ub} = ultimate tensile strength of bolts = 800 MPa (from bolt test)

A_b = bolt cross sectional area

The applied force F will be equal to:

$$F = \sum_{j=1}^{s} B_u \tag{7.8}$$

where:

s = number of bolts in tension side

The ultimate moments calculated by failure mode 1 for the six tests are given in Table 7.4.

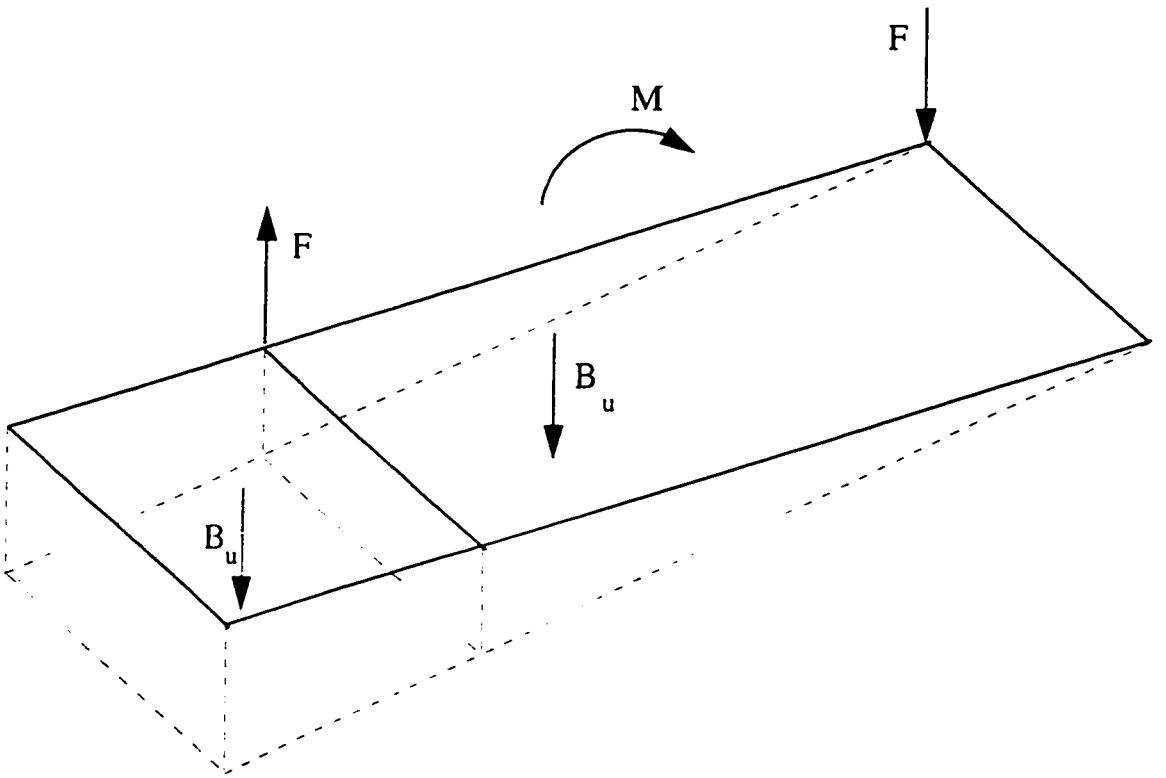

Figure 7.10 Thick-Plate Mode of Failure (Mode 1)

TABLE 7.4 Comparison of Failure Moments from Different Modes

Test No.	Bolt Diam. mm	Beam bottom flange plate (PL1)	Mode 1 moment kNm	Mode 2 moment kNm	Mode 3 moment kNm
C1	19	160 x 12	331	290	278
C2	25	160 x 20	575	806	606
C3	22	160 x 20	445	806	546
C4	28	180 x 20	721	827	658
C5	28	180 x 15	721	465	518
C6	25	160 x 15	575	452	459

7.4.1.2 Thin-Plate Mode of Failure (Mode 2)

The failure mode 2 is characterized by the yielding failure of the plate through bolts with a large value of prying force. It can occur when thin plates are used in conjunction with relatively large bolt diameter. The plate is considered flexible and significant deformation of the plate can take place, producing appreciable amount of prying force. As the bolts are strong enough, the failure occurs by yielding of bottom flange plate without any significant bolt deformation.

To obtain the ultimate moment capacity of the cap plate connection, the yield line method was applied. The yield line method of analysis is a limit state design method and is an upper bound solution for the ultimate load capacity. This method equates the work done by the external loads to the energy absorbed in a series of yield lines associated with an assumed failure mechanism. The yield line method was used by Wheeler *et al.* [88] to determine the ultimate moment capacity of the end plate connection joining rectangular hollow section. The difficulty of the yield line analysis lies with the proper selection of the yield lines which, if not identified properly, the estimated capacity would be much overestimated.

By suggesting the deformed shape shown in Fig. 7.11 with a displacement δ_0 just below the force F, a suitable yield pattern for Mode 2 failure can be drawn. The displacement at different locations can be found by geometry as a function of the virtual displacement δ_0. The prying force reaches its maximum value Q_{max} as the

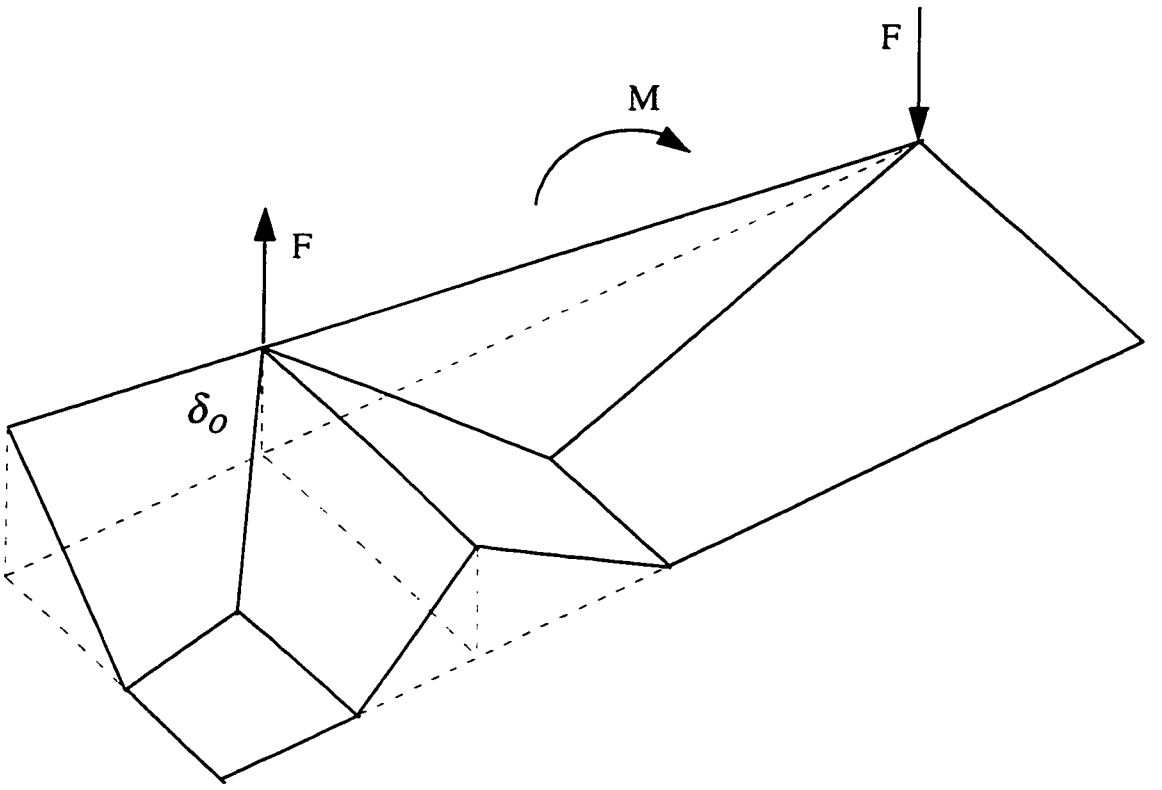

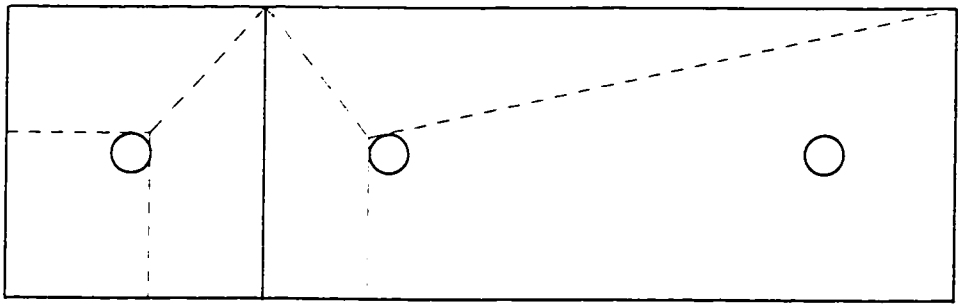

positive yield line

negative yield line

Figure 7.11 Thin-Plate Mode of Failure (Mode 2)

bolts are assumed to be very stiff with forces much less than their tensile strength. The internal work W_I is expressed as:

$$W_I = \sum_{i=1}^{n} m_i l_i \theta_i \tag{7.9}$$

$$m_i = m = \frac{\sigma_{yp} t_{pl}^2}{4} \tag{7.10}$$

where:

m_i = the plate yield moment

l_i = yield line length

θ_i = corresponding yield line rotation

σ_{yp} = plate yield stress

t_{pl} = plate thickness

n = number of yield lines

and the external work done is given by:

$$W_E = F\delta_0 \tag{7.11}$$

By equating the internal work to the external work, the connection ultimate moment for Mode 2 can be calculated. The ultimate moment values calculated in this manner are shown in Table 7.4.

7.4.1.3 Intermediate-Plate Mode of Failure (Mode 3)

Failure Mode 3 falls between the previous two modes, where bolt and plate are yielding simultaneously. It happens for intermediate plate thickness with intermediate bolt diameter, so it can be named as the intermediate plate mode. As shown in Fig. 7.12 the yield pattern is accompanied by the bolt elongation (yielding). In this case, the bolt forces were taken as the yielding forces B_y and the existing prying forces Q did not reach their maximum values.

$$W_I = \sum_{i=1}^{n} m_i l_i \theta_i + \sum_{j=1}^{r} B_{yj} \delta_{bj} \tag{7.12}$$

and

$$B_y = \sigma_{yb} A_b \tag{7.13}$$

where

σ_{yb} = yield tensile stress of bolts = 750 MPa (from bolt test)

δ_b = bolt elongation

Mode 1 is the simplest mode of failure but it is a brittle mode. Mode 2 is complex than the first mode due to the presence of prying force and yield line pattern. Mode 3 is the most complex mode of failure, but it leads to an economical and ductile connection. The computed values of the ultimate moment M_u obtained from three different modes of failure are shown collectively in Table 7.4. The minimum of the

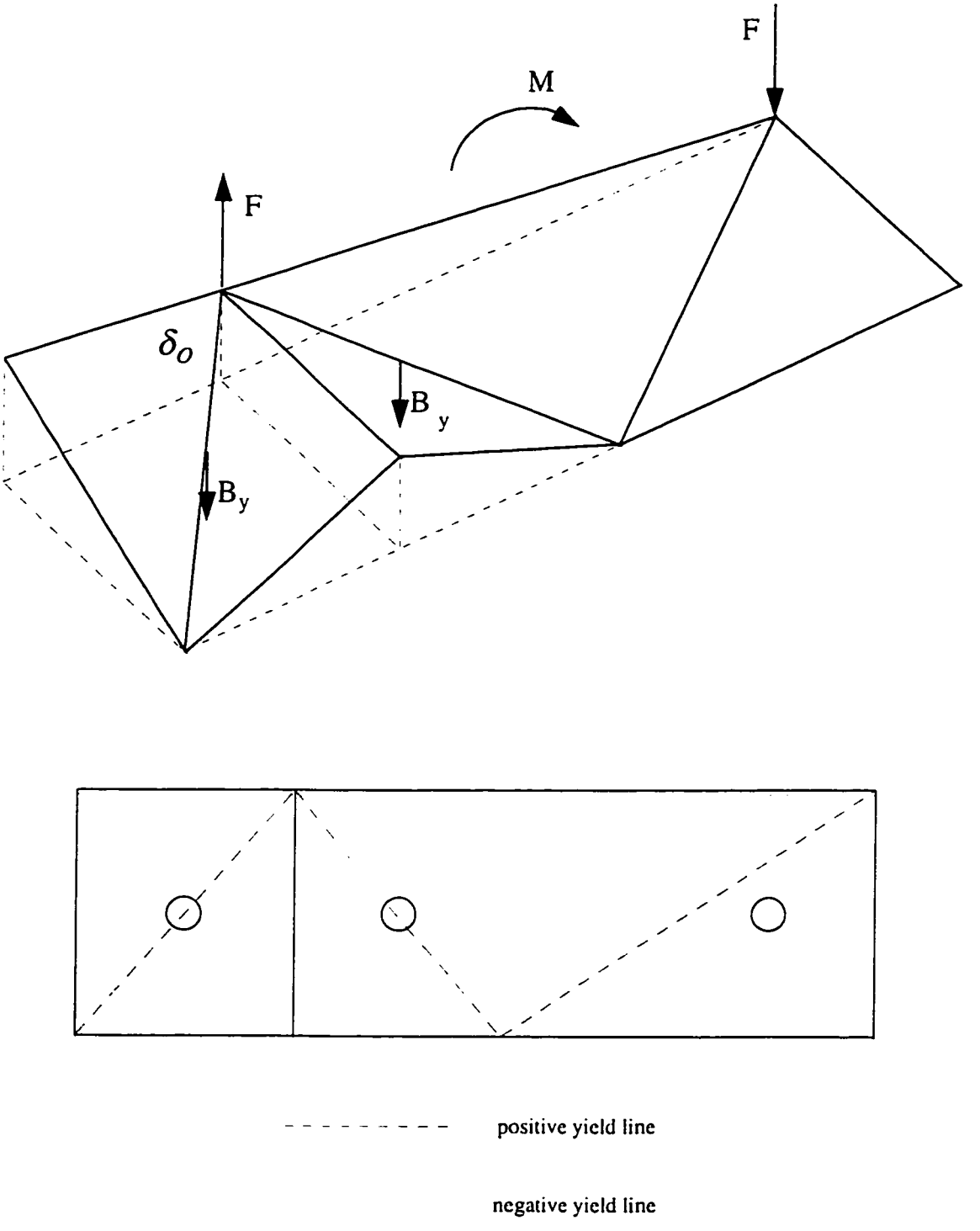

Figure 7.12 Intermediate-Plate Mode of Failure (Mode 3)

three values for each connection represent the ultimate moment strength of the connection.

7.4.2 Comparison Between Theoretical and Experimental Values of M_u

In Table 7.5, the maximum moment capacity as deduced from the $M-\theta$ plot of each test are shown. As the tests were not carried out to the failure, due to safety reasons, the ultimate or the collapse moment were not obtained in the experiment. The values of M_u shown are the projected (extrapolated) values. They are indicative values and are close to the actual M_u values. Results show that there is an agreement between the two sets of values. When the failure occurs through fracture of bolts, the computed moment capacity is highly accurate. The yield line analysis is an upper bound solution and therefore values from such an analysis are expected to be higher than the actual.

TABLE 7.5 Comparison of Predicted and Tests Moments

Test No.	Predicted moment kNm	Moment to C.L. of connection from test kNm	Moment at face of the column from test kNm
C1	278	300	264
C2	575	420	370
C3	445	400	353
C4	658	450*	397*
C5	465	420	370
C6	452	360	318

* Premature failure due to failure of weld

7.5 MODELING OF THE MOMENT-ROTATION RELATIONSHIP

The experimental $M-\theta$ curves as obtained from the six connection tests were shown in Chapter 6. Common observations are found for the six tests: (a) the curves are approximately linear at early stage of loading and (b) they become non-linear at high level of loading up to the failure of the connections. This proves the existing non-linearity of the cap-plate connections and they can not be assumed in both the analysis and design as rigid connection. Furthermore, the assumption of rigid connection will lead to underestimation of the frame deflection and overestimation of the connection resisting moment.

From the observation of test results, it was found that the three main parameters characterizing the $M-\theta$ curves are: (a) the initial rotational stiffness of the connection R_{ki} representing the slope of the $M-\theta$ curve at the beginning of application of load, (b) the ultimate moment M_u of the connection just at failure and (c) the shape of the curve itself between the previous two parameters. For this reason it was suggested to use the three-parameter model described in chapter 2.

Table 7.3 shows the comparison between the predicted values taken from the connection model and the actual test values for both of the initial stiffness R_{ki} and the ultimate moment M_u.

The proposed model was superimposed on the moment-rotation curves in Figs. 7.13 - 7.18 with the predicted value of R_{ki} and M_u. The shape parameter n is determined by a regression analysis to obtain the best fit with the actual data set of M and θ. It was found that the value of n varies between n = 1.3 to n = 3.5 for the tests considered in this study. Using all test data for the six tests, an attempt was made to determine the value of n through a regression analysis which would have the best fit. A value of n = 1.6 appears to fit reasonably well with all plots, though not as good as the individual values of n, as seen through Figs. 7.13 - 7.18. Thus it appears that the value of n for a particular connection depends upon some parameters which would include among others initial stiffness and ultimate moment capacity. Due to the limited number of tests, it was not possible to suggest a value of n which would be valid for any cap-plate connection.

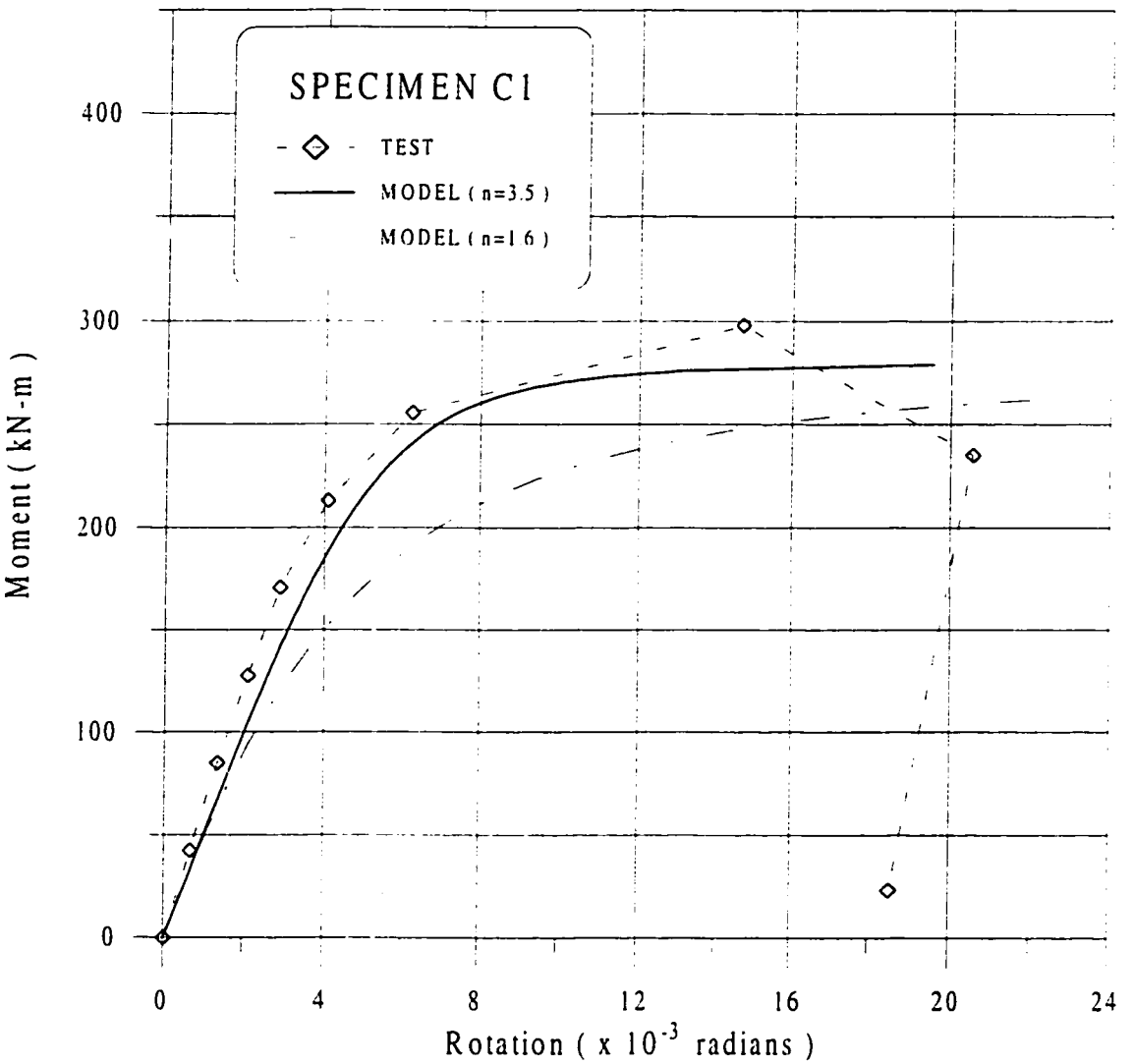

Figure 7.13 Moment - Rotation Model for Specimen C1

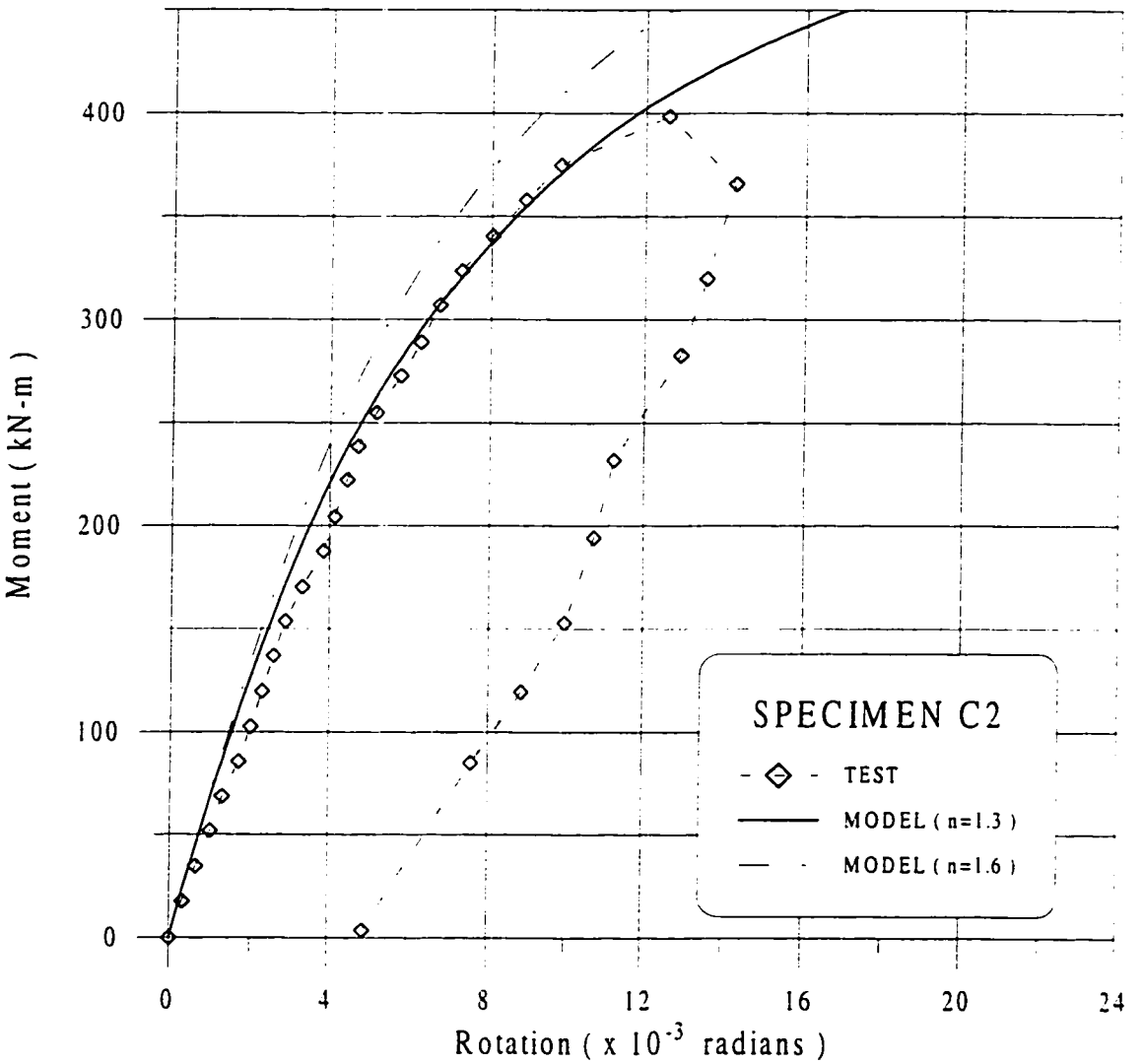

Figure 7.14 Moment - Rotation Model for Specimen C2

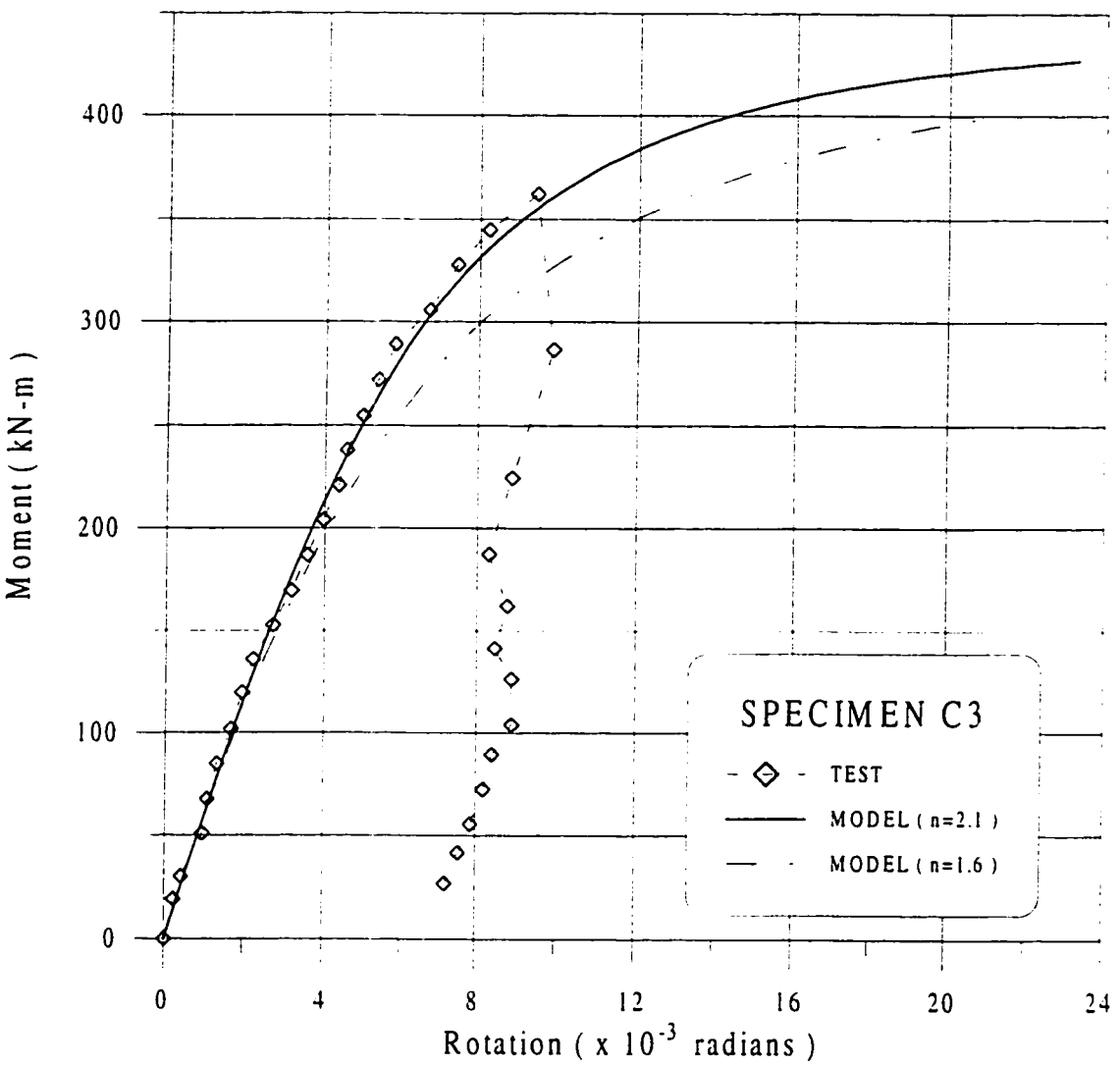

Figure 7.15 Moment - Rotation Model for Specimen C3

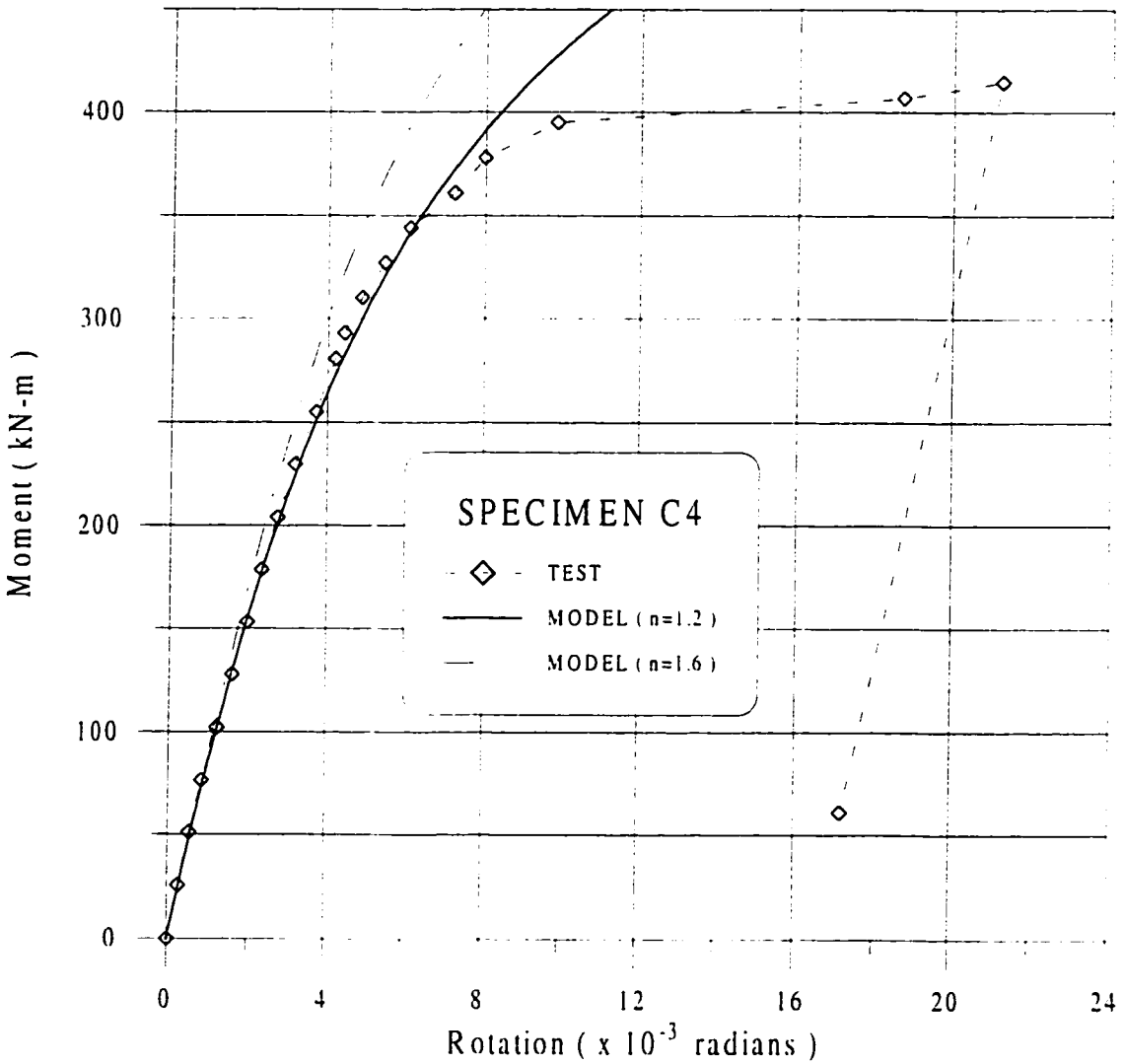

Figure 7.16 Moment - Rotation Model for Specimen C4

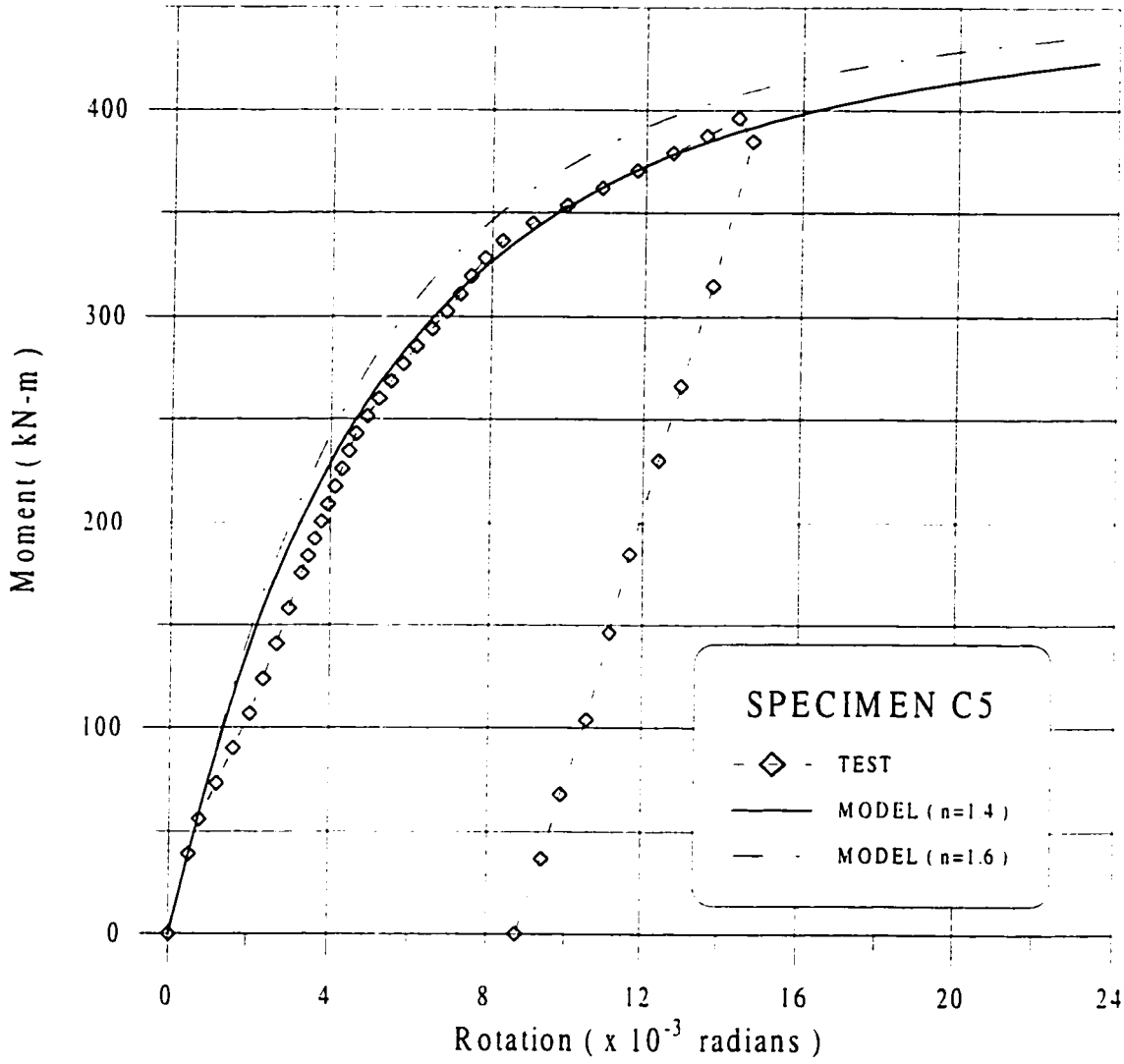

Figure 7.17 Moment - Rotation Model for Specimen C5

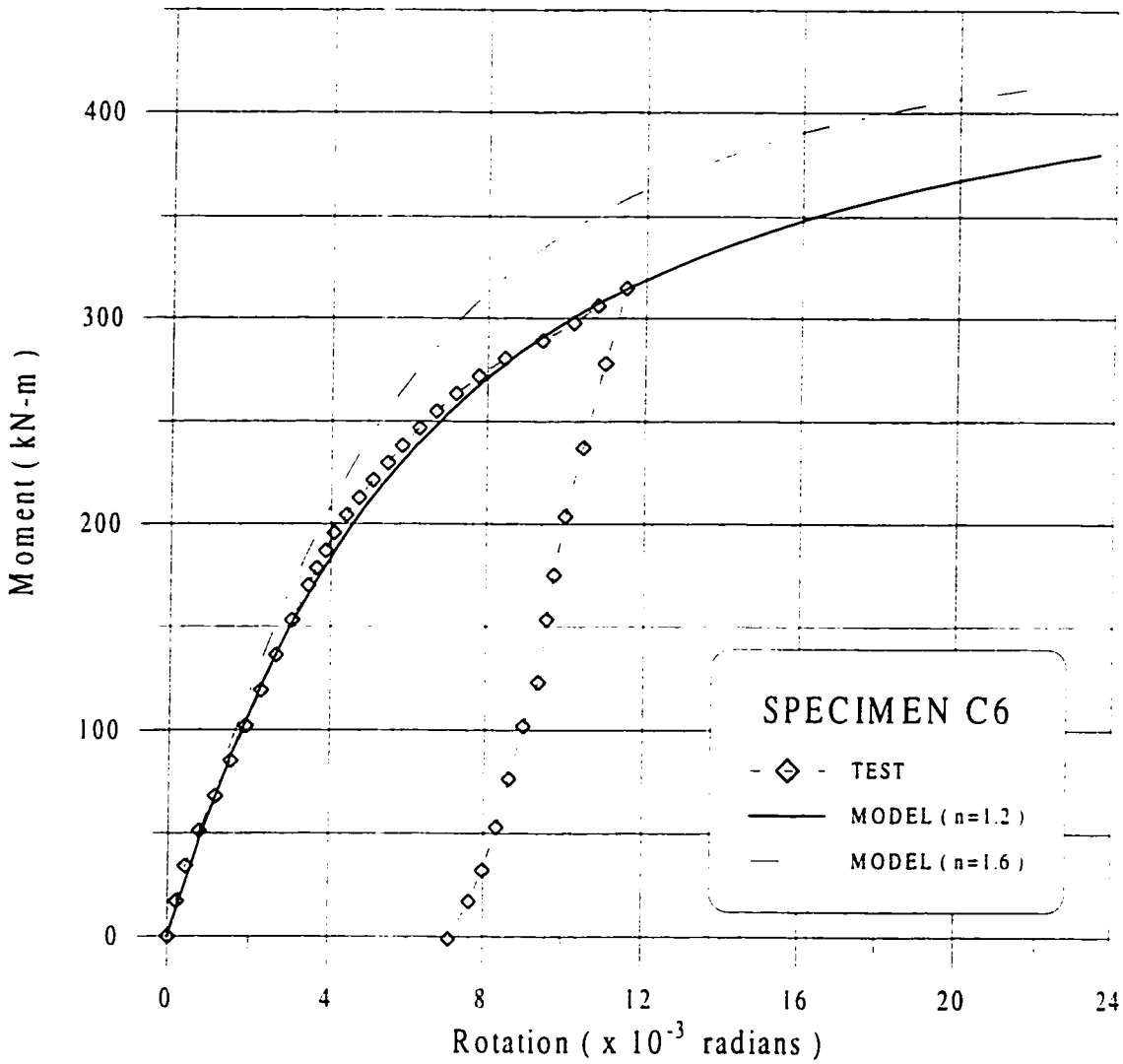

Figure 7.18 Moment - Rotation Model for Specimen C6

CHAPTER 8

SUMMARY, CONCLUSIONS AND RECOMMENDATIONS

8.1 SUMMARY

A study was made on the behavior of cap-plate connections which are widely used in industrial steel frames since adequate information about this type of connection was found lacking. The study contains a literature review on the available data for building connections type. A computer program was developed for the analysis of semi-rigid frames taking into consideration the second-order effects and the connection flexibility with some examples.

Six full scale tests were conducted on cap-plate connection type with varying cross-section, bottom beam plate thickness and different bolt sizes. The test results were presented and discussed with the observations obtained from the plots. A proposed model was suggested to simulate the moment-rotation behavior of the cap-plate connection. A comparison was made between the proposed model and the obtained results from tests.

8.2 CONCLUSIONS

Based on this study, the following conclusions are drawn:

1. A computer program for elasto-plastic analysis of semi-rigid frames has been developed by taking into consideration the connection flexibility and the second order effects. The program accurately performs the nonlinear frame response at any load level and predicts the collapse load and the deformation at collapse. The incremental load analysis, which requires moment-rotation response of the connection, captures the failure of frames dictated either by elastic stability or by plastic collapse.

2. The connection flexibility has a significant effect on the behavior of the frame and it must be considered in the analysis and design. Neglecting the built-in flexibility of a connection and assuming it as a rigid joint will lead to an overestimate of the connection moment and an underestimate of the frame deflection.

3. An analytical model to represent the nonlinear response of the cap-plate type connections has been proposed. The model requires the calculated values of the initial stiffness of the connection and its predicted ultimate moment capacity. The finite element methodology was used to determine the initial stiffness of the connection and its ultimate moment capacity was calculated by the yield line

theory. The proposed connection model shows a good agreement with the experimental results, lending confidence in the proposed modeling.

4. The suggested analytical methods for computing the initial stiffness of a cap-plate connection and its ultimate moment capacity appears to yield satisfactory results as evidenced from a comparison of the theoretical values with those from the experiment.

5. The typical cap-plate connection used in industrial buildings typifies a semi-rigid connection due to its characteristic joint flexibility which arises from the connection being made only by connecting the bottom flange of the beam to the column cap-plate. This behavior is shown clearly in moment-rotation curves obtained from experimental test results.

6. The thickness of the beam bottom flange plate at the connection location influences both the initial rotation stiffness and the ultimate moment capacity of the connection which increase with the increase of plate thickness by preventing high plate deformation (failure Mode 2).

7. The distribution of the normal forces in the tension bolts at below critical load level is greatly influenced by the beam bottom flange thickness. A thicker plate produces more disparity between the tensile forces in the outer bolts and the inner bolts. The outer bolts reaches the yield stress much faster than the inner bolts for thick plates since the plate rotates rigidly about the compression zone. As a

thinner plate deforms more, the disparity between the outer and the inner bolt tension becomes lesser as shown from bolt strains values of connections with same cross-section and different beam bottom flange thickness.

8. The normal strain distribution in the beam can be predicted at the connection using the elementary beam theory only at a section near the face of the column as observed from the experimental results. The normal strains are approximately null at the upper flange near the corner due to the path of the moment from the beam to the column which is dependent on the bolts and the plates in contact between the beam and the column.

9. The web thickness of the beam at the connection location affect the initial stiffness of the connection due to shear deformation in the unstiffened panel. The initial stiffness decreases with thinner webs due to increased shear deformation as shown from the developed analytical model of the connection.

10. The use of vertical web stiffeners in beams at the connection increases the connection stiffness. In the absence of such stiffeners the flange may fail prematurely due to bending. Also, the existence of the vertical web stiffeners changes the behavior of the beam flange from one way (T-stub) action to two way action which reduces significantly the flange deformation.

8.3 DESIGN RECOMMENDATIONS

Based on the observations of the experimental behavior of test specimen, the following suggestions can be made for the design of cap-plate type connection:

1. In order to increase the stiffness of such a connection, the bottom flange plate of the beam should be thicker at the connection.

2. The column cap-plate should be at least equal to or thicker than the increased bottom flange plate thickness of the beam at the connection to avoid excessive deformation of the cap-plate.

3. For very thin web, it would be required to stiffen the web by a diagonal stiffener in the connection to prevent web buckling as recommended by design codes.

The basic problem in designing semi-rigid frames is the evaluation of exact stiffness of the connection, a design approach can be summarized in the following steps:

1. Analyze the frame first as a rigid frame and get its actions

2. Design the connection bolts using Mode 1 failure

3. Use stiffeners to reduce the connection shear deformation

4. Calculate the flange plate thickness at the connection using Mode 2 and Mode 3 so that yielding of plate will not occur before bolt failure

5. Calculate the initial rotational stiffness of the connection

6. Develop the connection moment-rotation curve using initial stiffness, ultimate moment and suggested shape parameter

7. Reanalyze the frame as a semi-rigid frame using the developed moment-rotation curve of the connection and get its new actions

8. Check the adequacy of members

9. Check the members and frame deflection based on the connection response

8.4 FUTURE WORK

More tests are required to be conducted on cap-plate connections to increase the data base for such connection since only six test data are presently available. From future tests the proposed cap-plate model can be improved. Also full scale tests on frames need to be conducted to obtain the response and the overall behavior of the frame which is affected by the cap-plate connection. A study is needed to see the effect of bolt rows number on the behavior of the connection.

REFERENCES

1. Bose B. and Hughes A. F. (1995). "Verifying the performance of standard ductile connections for semi-continuous steel frames." *Proc. Inst. Civ. Engrs. Structures and Buildings*, Vol. 110, pp. 441-457.

2. Jones S. W., Kirby P. A. and Nethercot D. A. (1983). "The analysis of frames with semi-rigid connections - A state-of-the-art report." *Journal of Constructional Steel Research*, Vol. 3, No. 2, pp. 2-13.

3. AISC (1989), Manual of Steel Construction, Allowable Stress Design, Ninth Edition, American Institute of Steel Construction, Chicago, IL.

4. AISC (1986), Manual of Steel Construction, Load and Resistance Factor Design, First Edition, American Institute of Steel Construction, Chicago, IL.

5. Salmon C. G. and Johnson E. J. (1990). "Steel Structures, Design and Behavior.", Third Edition, Harper Collins

6. Bose B. Youngson, G. K. and Wang, Z. M. (1996). "An appraisal of the design rules in Eurocode 3 for bolted end-plate joints by comparison with experimental results." *Proc. Inst. Civ. Engrs. Structures and Buildings*, Vol. 116, pp. 221-234.

7. Liew, J. Y. R., White, D. W. and Chen, W. F. (1993). "Limit states design of semi-rigid frames using advanced analysis: Part 2: Analysis and design." *Journal of Constructional Steel Research*, Vol. 26, pp. 29-57.

8. Chen, W. F. (1993) (Ed.). "Semi-rigid connections in steel frames." *Council on Tall Building and Urban Habitat*, McGraw-Hill.

9. Lipson S. L. and Antonio M. E. (1980). "Single angle welded-bolted beam connections." *Canadian Journal of Civil Engineering*, Vol. 7, pp. 315-324.

10. Chen, W. F. and Kishi, N. (1989). "Semi-rigid steel beam-to-column connections: Data base and modeling." *Journal of Structural Engineering*, ASCE, Vol. 115, No. 1, pp. 105-119.

11. Richard, R. M., Kriegh, J. D. and Hormby, D. F. (1982). "Design of single plate framing connections with A307 bolts." AISC *Engineering Journal*, Vol. 19, No. 4, pp. 209-213.

12. Richard, R. M., Gillett, P. E., Kriegh, J. D. and Lewis, B. A. (1980). "The analysis and design of single plate framing connections." AISC *Engineering Journal*, Vol. 16, Second quarter, pp. 38-52.

13. Hormby, D. F., Richard, R. M. and Kriegh, J. D. (1984). "Single-plate framing connections with grade-50 steel and composite construction." AISC *Engineering Journal*, Vol. 21, No. 3, pp. 125-138.

14. Moore, D. B. and Owens, G. W. (1992). "Verification of design methods for finplate connections", *The Structural Engineer*, Vol. 70, No. 3/4, pp. 46-53.

15. Astaneh, Abolhassan and Nader, Marwan N. (1990). "Experimental Studies and design of steel tee-shear connections." *Journal of Structural Division*, ASCE, Vol. 116, No. 10, pp. 2882-2902.

16. Bose, B. (1981). "Moment rotation characteristics of semi-rigid joints in steel structures." *Journal of Institution of Engineers* (India), Part CI, Civil Engineering Division, Vol. 62, Part 2, pp. 128-132.

17. Bjorhovde, R. (1984). "Effect of end-restraint on column strength-Practical Applications." AISC *Engineering Journal*, Vol. 20, No. 1, First quarter.

18. Maxwell, S., Howlett, J., Jenkins, W. and Bose, B. (1981). "A realistic approach to the performance and application of semi-rigid joints in steel structures." in *Joints in Structural Steelwork*, J. H. Howlett, W. M. Jenkins and R. Stainsby, (Eds.) Wiley, New York, N. Y., pp. 271-298.

19. Van Dalen, K. and Godoy, H. (1982). "Strength and rotational behavior of composite beam-column connections." *Canadian Journal of Civil Engineers*, Vol. 9, No. 2, pp. 313-322.

20. Aggarwal, A. K. (1990). "Behavior of flexible beam-to-column connections." The Institution of Engineers Australia Structural Engineering Conf. pp. 462-467.

21. Zoetemeijer, P. (1974). "A design method for the tension side of statically loaded beam to column connections." *Heron*, Vol. 20, No. 1.

22. Altman, W., Azizinamini, A., Bradburn, J. and Radziminski, J. (1982). "Moment rotation characteristics of semi-rigid steel beam-to-column connections." Report of Investigation, Department of Civil Engineering, University of South Carolina.

23. Sommer, W. H. (1969). "Behavior of welded header plate connections." Masters Thesis, University of Toronto, Ont. Canada.

24. Owens G. W. and Moore D. B. (1992). "Steelwork connections: The robustness of simple connections." *The Structural Engineer* Vol. 70, No. 3/4, pp. 37-46.

25. Van Dalen K. and Mac Intyre J. (1988). "The rotational behavior of clipped end plate connections." *Canadian Journal of Civil Engineering*, Vol. 15, pp. 117-126.

26. Aggarwal, A. K. (1990). "Behavior of flexible end plate beam-to-column joints." *Journal of Constructional Steel Research*, Vol. 16, pp. 111-134.

27. Abdalla, K. M. and Chen, W. F. (1995). "Expanded database of semi-rigid steel connections." *Computers and Structures*, Vol. 56, No. 4, pp. 553-564.

28. Jenkins, W. M., Tong, C. S. and Prescott, A. T. (1986). "Moment-transmitting endplate connections in steel construction, and a proposed basis for flush endplate design." *The Structural Engineer* Vol. 64A, No. 5, pp. 121-132.

29. Aggarwal, A. K. and Coates, R. C. (1988). "Moment-rotation characteristics of bolted beam-column connections." *Journal of Constructional Steel Research*, Vol. 6, pp. 303-318.

30. Chen W. F. and Lui E. M. (1991). "Stability design of steel frames." *CRC Press*, Boca Raton, Florida, U.S.A.

31. Rathbun, J. C. (1936). "Elastic properties of riveted connections." ASCE *Transactions*, Vol. 101, pp. 524-563.

32. Monforton G. R. and Wu T. S. (1963). "Matrix analysis of semi-rigidly connected frames." *Journal of Structural Division*, ASCE, Vol. 89, No. ST6, pp. 13-42.

33. Lightfoot, E. and Le Messurier, A. P. (1974). "Elastic analysis of frameworks with elastic connections." *Journal of Structural Division*, ASCE, Vol. 100, No. ST6, pp. 1297-1309.

34. Jones, S. W., Kirby, P. A. and Nethercot, D. A. (1983). "The analysis of frameworks with semi-rigid connections: A state-of-the-art report." *Journal of Constructional Steel Research*, Vol. 3, No. 2, pp. 2-13.

35. Romstad, K. M. and Subramanian, C. V. (1970). "Analysis of frames with partial connection rigidity." *Journal of Structural Division*, ASCE, Vol. 69, No. 11, pp. 2283-2300.

36. Sugimoto, H. and Chen, W. F. (1982). "Small end restraint effects on the strength of H-columns." *Journal of Structural Division*, ASCE, Vol. 108, No. ST3, pp. 661-681.

37. Moncarz, P. D. and Grestle, K. H. (1981). "Steel frames with nonlinear connections." *Journal of Structural Division*, ASCE, Vol. 107, No. ST8, pp. 1427-41.

38. Razzaq, Z. (1983). "End restrained effect on steel column strength." *Journal of Structural Division*, ASCE, Vol. 109, No. ST2, pp. 314-334.

39. Frye, M. J. and Morris, G. A. (1975). "Analysis of flexibly connected steel frames." *Canadian Journal of Civil Engineering*, Vol. 2, No. 3, pp. 280-291.

40. Morris, G. A. and Packer, J. A. (1987). "Beam to column connections in steel frames." *Canadian Journal of Civil Engineering*, Vol. 14, No. 1, pp. 68-76.

41. Jones, S. W., Kirby, P. A. and Nethercot, D. A. (1982). "Columns with semi-rigid joints." *Journal of Structural Division*, ASCE, Vol. 108, No. ST2, pp. 361-372.

42. Krishnamurthy, N., Huang. H. T., Jeffrey, P. K. and Avery, L. K. (1979). "Analytical $M-\theta$ curves for end-plate connections." *Journal of Structural Division*, ASCE, Vol. 105, No. ST1, pp. 133-145.

43. Goldberg, J. E. and Richard, R. M. (1963). "Analysis of nonlinear structures." *Journal of Structural Division*, ASCE, Vol. 89, No. ST4, pp. 333.

44. Kishi, N. and Chen W. F. (1990). "Moment-rotation relations of semi-rigid connections with angles." *Journal of Structural Engineering*, ASCE, Vol. 116, No. 7, pp. 1813-1834.

45. Ang, K. M. and Morris, G. A. (1984). "Analysis of three-dimensional frames with flexible beam-column connections." *Canadian Journal of Civil Engineers*, Vol. 11, No. 2, pp. 245-254.

46. Lui, E. M. and Chen W. F. (1986). "Analysis and behavior of flexibly-jointed frames." *Engineering Structures*, Vol. 8, pp. 107-118.

47. Yee, Y. L. and Melchers, R. E. (1986). "Moment-rotation curves for bolted connections." *Journal of Structural Engineering*, ASCE, Vol. 112, No. 3, pp. 615-635.

48. Wu, F. S. and Chen W. F. (1990). "A design model for semi-rigid connections." *Engineering Structures*, Vol. 12, No. 2, pp. 88-97.

49. Chasten, C. P., Lu, L. W. and Driscoll, G. C. (1992). "Prying and shear in end plate connection design." *Journal of Structural Engineering*, ASCE, Vol. 118, No. 5, pp. 1295-1311.

50. Bahaari, M. R. and Sherbourne, A. N. (1994). "Computer modelling of an extended end plate bolted connection." *Computers and Structures*, Vol. 52, No. 5, pp. 879-893.

51. Sherbourne, A. N. and Bahaari, M. R. (1994). "3D simulation of end-plate bolted connection." *Journal of Structural Engineering*, ASCE, Vol. 120, No. 11, pp. 3122-3136.

52. Bahaari, M. R. and Sherbourne, A. N. (1996). "Structural behavior of end-plate bolted connections to stiffened columns." *Computers and Structures*, Vol. 122, No. 8, pp. 926-935.

53. Choi, C. K. and Chung, G. T. (1996). "Refined three-dimensional finite element model for end-plate connection." *Journal of Structural Division*, ASCE, Vol. 122, No. 11, pp. 1307-1316.

54. Goverdhan, A. V. (1983). "A collection of experimental moment-rotation curves and evaluation of prediction equations for semi-rigid connections." Thesis, Vanderbilt University, Nashville, Tennessee.

55. Nethercot, D. A. (1985). "Steel beam-to-column connections-A review of test data and its applicability to the evaluation of joint behavior in the performance of steel frames." CIRIA Project Record, RP 338, London.

56. Kishi, N. and Chen W. F. (1986). "Steel connection data bank program." Structural Engineering Report no. CE-STR-86-11, School of Civil Engineering, Purdue University, West Lafayette, Ind.

57. Kishi, N. and Chen W. F. (1986). "Data base of steel beam -to-column connections." Vols. I and II. Structural Engineering Report no. CE-STR-86-26, School of Civil Engineering, Purdue University, West Lafayette, Ind.

58. Gutkowski, R. M. (1981). "Structures: Fundamental theory and behavior." Van Nostrand Reinhold Company, New York.

59. Wang C. K. (1983). "Intermediate structural analysis." McGraw Hill, U.S.A.

60. Chajes, A. (1990). "Structural analysis." Second Edition, Prentice Hall, Englewood Cliffs, New Jersy.

61. Weaver W. and Gere J. M. (1990). "Matrix analysis of framed structures." Third Edition, Van Nostrand Reinhold, U.S.A.

62. Ghali A. and Neville A. M. (1979). "Structural Analysis: A unified classical and matrix approach." Second Edition, Chapman and Hall, New York.

63. Chajes, A. (1974). "Principles of structural stability theory." Prentice-Hall International, Inc., London.

64. Chajes, A. and Churchull, J. E. (1987). "Nonlinear frame analysis by finite element methods." *Journal of Structural Engineering*, ASCE, Vol. 113, No. 6, pp. 1221-1235.

65. Chen, W. F. and Lui, E. M. (1987). "Structural stability: Theory and Inplementation." Elsevier Science Publishing Co., Inc.

66. Gaiotti, R. and Smith, B. S. (1989). "P-delta analysis of Building structures." *Journal of Structural Engineering*, ASCE, Vol. 115, No. 4, pp. 755-770.

67. Abu-Yasein, O. A. and Fredrick, G. R. (1994). "Elastic second-order analysis for frame design." *Computers and Structures*, Vol. 52, No. 6, pp. 1161-1168.

68. Mourad, S. A. (1987). "Stability of steel frames with semi-rigid connections." M. Sc. Thesis, Cairo University, Egypt.

69. Lui, E. M. (1988). "A practical P-delta analysis method for Type FR and PR frames." AISC *Engineering Journal*, Vol. 25, Part 3, Third quarter, pp. 85-98.

70. Barakat, M. and Chen, W. F. (1990). "Practical analysis of semi-rigid frames." AISC *Engineering Journal*, Vol. 27, No. 2, pp. 54-68.

71. Al-Mashary, F. and Chen W. F. (1990). "Elastic second-order analysis for frame design." *Journal of Constructional Steel Research*, Vol. 15, pp. 303-322.

72. Li, T. Q., Choo, B. S. and Nethercot, D. A. (1995). "Connection element method for the analysis of semi-rigid frames." *Journal of Constructional Steel Research*, Vol. 32, pp. 143-171.

73. Lo. D. S. K. and Stiemer, S. F. (1995). "A practical method for incorporating flexible connections in plane frame analysis." *Canadian Journal of Civil Engineering*, Vol. 22, pp. 871-882.

74. Rashed, A., Machaly, B. and Niaz, A. S. (1990). "Stability of space frames with semi-rigid connections." *Computers and Structures*, Vol. 36, No. 4, pp. 613-622.

75. Galal, G. M. H. (1992). "Plastic design of steel frames with rigid and semi-rigid joints." Ph. D. Thesis, Suez Canal University, Egypt.

76. Patodi, S. C. and Patel, J. S. (1993). "A modified elastic-plastic analysis including graphical processing of plane framed structures." *Computers and Structures*, Vol. 47, No. 1, pp. 155-161.

77. Liew, J. Y. R., White, D. W. and Chen, W. F. (1993). "Second-order refined plastic-hinge analysis for frame design. Part I." *Journal of Structural Engineering*, ASCE, Vol. 119, No. 11, pp. 3196-3216.

78. Scholz, H. (1991). "Plastic design of sway frames with semi-rigid connections using allowable slenderness ratio." *Journal of Constructional Steel Research*, Vol. 19, Part 1, pp. 19-32.

79. Gaylord, E. H., Gaylord, C. N. and Stallmeyer, J. E. (1992). "Design of steel structures." Third Edition, New York: McGraw-Hill.

80. Galambos, T. V. (Ed.) (1988). "Guide to stability design criteria for metal structures." Fourth Edition, New York: John Wiley & Sons.

81. Aristizabal-Ochao, J. D. (1996). "Braced, partially braced and unbraced columns: complete set of classical stability equations." *Structural Engineering and Mechanics*, Vol. 4, No. 4, pp. 365-381.

82. Neal, B. G., (1977). "The plastic methods of structural analysis" Third Edition, Chapman and Hall (London).

83. Horne, M. R. and Morris, L. J. (1981). "Plastic design of low-rise frames." Granada, London.

84. Hinton, E. and Owen, D. R. J. (1979). "An introduction to finite element computations." Pineridge Press Limited, Swansea, U. K.

85. Packer, J. A. and Morris, L. J. (1977). "A limit state design method for the tension region of bolted beam-column connections." *The Structural Engineer*, Vol. 55, No. 10, pp. 446-458.

86. Packer, J. A., Bruno, L. and Birkemoe, P. C. (1989). "Limit analysis of bolted RHS flange plate joints." *Journal of Structural Engineering*, ASCE, Vol. 115, No. 9, pp. 2226-2242.

87. GTSTRUDL Software, Version 9601 PC (1995), Georgia Tech Research Corporation, Georgia Institute of Technology, Atlanta, Georgia, U.S.A.

88. Wheeler, A. T., Clarke, M. J., Hancock, G. J. and Murray, T. M. (1998). "Design model for bolted moment end plate connections joining rectangular hollow sections." *Journal of Structural Engineering*, ASCE, Vol. 124, No. 2, pp. 164-173.

VITA

Mahmoud Hassan El-Boghdadi was born in Cairo, Egypt in February 1963. He finished his high school degree in Cairo form College De La Salle in June 1980. In June 1985, he received his Bachelor of Science Degree in Civil Engineering with Honors from Ain Shams University, Cairo, Egypt. In May 1991, he received his Master of Science Degree in Civil Engineering from Ain Shams University, Cairo, Egypt. In November 1992, he joined the Department of Civil Engineering at King Fahd University of Petroleum and Minerals (KFUPM), Dhahran, Saudi Arabia, as a graduate student. In June 1998, he received his Doctor of Philosophy Degree in Civil Engineering from King Fahd University of Petroleum and Minerals.

IMAGE EVALUATION TEST TARGET (QA-3)

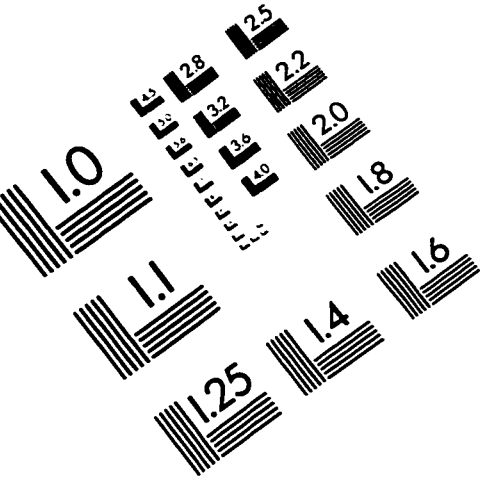

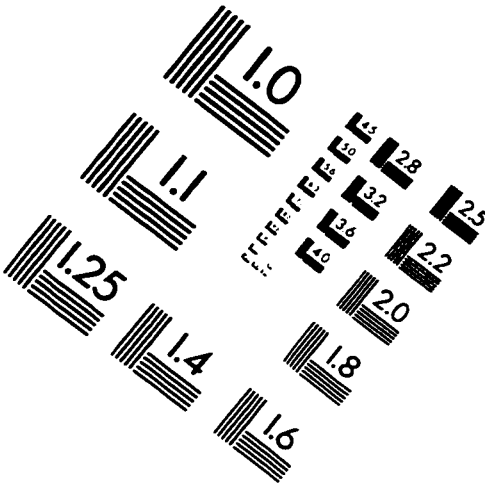

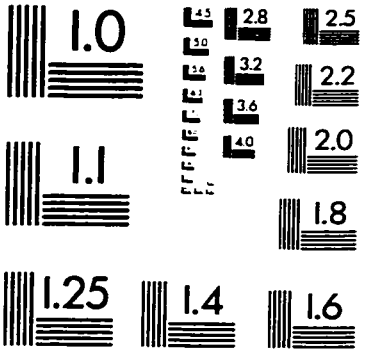

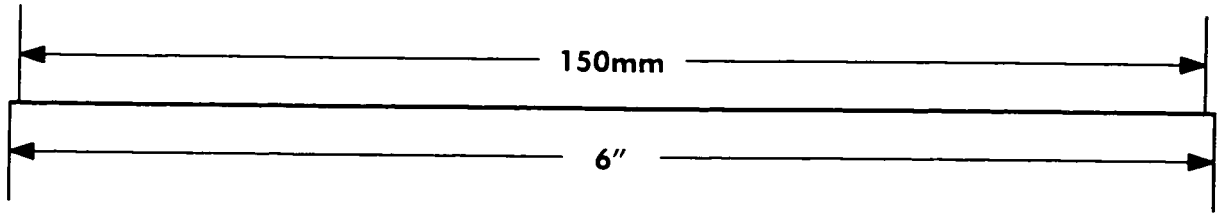

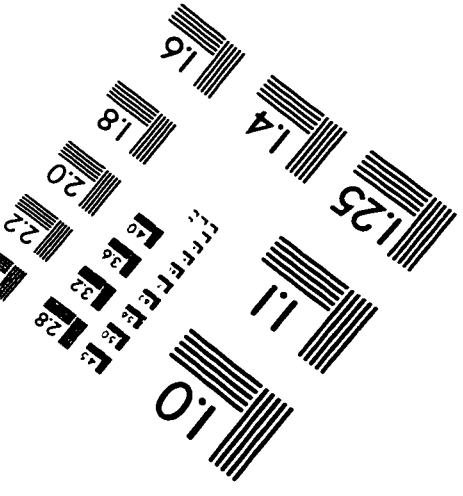

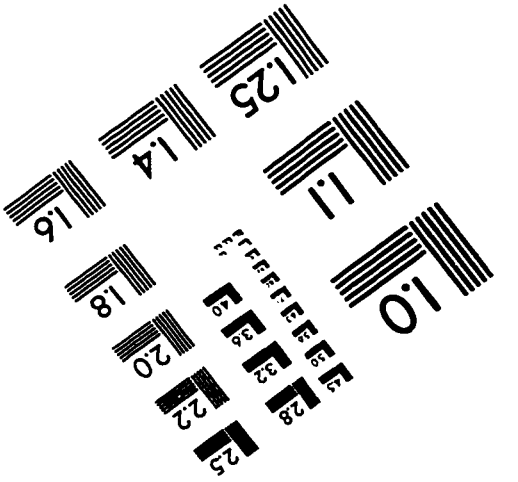

APPLIED IMAGE, Inc
1653 East Main Street
Rochester, NY 14609 USA
Phone: 716/482-0300
Fax: 716/288-5989